MUTATIONAL STUDY OF INTRACELLULAR SCALING MECHANISMS IN *TETRAHYMENA THERMOPHILA*

by

YU-YANG JIANG

(Under the Direction of Jacek Gaertig)

ABSTRACT

In biology, size control (or scaling) is a fundamental property at all levels of organization, from polymeric protein complexes to tissues, organs and organisms. This thesis addresses the mechanisms of scaling at the intracellular level using the ciliate *Tetrahymena thermophila* as a model. *Tetrahymena* carries a polarized cortical pattern of organelles including hundreds of cilia, on the cell surface. This cortical pattern can be used to study the intracellular scaling with high resolution. We developed a genetic pipeline for identification of causal variants in *Tetrahymena* mutants by comparative whole genome sequencing, with unusually high accuracy. In Chapter 3, I focused on the scaling at the organelle level, using cilium length as a model. We developed a genetic interactor screen based on a hypermorphic allele of the conserved kinase, LF4/MOK, that acts as negative regulator of cilium length. We identified another conserved cilium length kinase, LF2/CCRK/DYF-18, as an upstream regulator of LF4/MOK abundance. We adapted total internal reflection microscopy for imaging inside cilia, to show that LF4 is a ciliary protein that is distributed uniformly along cilia, mostly immobile and likely microtubule-bound. We also found that LF4 affects the intraflagellar transport (IFT), a motility mechanism that distributes components inside cilia.

Most cells double their size prior to cell division to produce two daughters of equal size. In Chapter 4, I studied a *Tetrahymena* mutant, *cdaI-1,* that during cell division produces daughters of unequal size. I found that *cdaI-1* results from a mutation in CdaI, an ortholog of the Hippo/Mst kinases, components of the highly conserved Hippo signaling, which in diverse eukaryotes regulate cell growth and cell division, and in animals affect embryo polarity and organ size. We conclude that in *Tetrahymena,* the Hippo pathway maintains the equatorial placement of the division plane. In summary, this dissertation delivers new powerful genetic and imaging tools to *Tetrahymena,* a large single-cell eukaryote that is highly amenable for studies of intracellular scaling. We dissected the principles of size control inside the single cell across multiple levels of organization and identified specific proteins and interactions that affect intracellular size control.

INDEX WORDS: organelle size, intracellular scaling, cilium length regulation, LF4, IFT, genetic screen, LF2, intracellular pattern

MUTATIONAL STUDY OF INTRACELLULAR SCALING MECHANISMS IN *TETRAHYMENA THERMOPHILA*

by

YU-YANG JIANG

B. S., ZHEJIANG UNIVERSITY, CHINA, MAY 2009

A Dissertation Submitted to the Graduate Faculty of The University of Georgia in Partial Fulfillment of the Requirements for the Degree

DOCTOR OF PHILOSOPHY

ATHENS, GEORGIA

2017

MUTATIONAL STUDY OF INTRACELLULAR SCALING MECHANISMS IN *TETRAHYMENA THERMOPHILA*

by

YU-YANG JIANG

Major Professor:	Jacek Gaertig
Committee:	Edward T. Kipreos
	Marcus Fechheimer
	Scott T. Dougan

Electronic Version Approved:

Suzanne Barbour
Dean of the Graduate School
The University of Georgia
May 2017

ACKNOWLEDGEMENTS

I would like to express my highest gratitude to my major professor Jacek Gaertig. He has created a lab environment that encourages free thinking and communication, allowing the students to think independently and critically while helping each other in a friendly and cheerful manner. As one of the lab children, I feel I am always at the receiving side of the warm encouragement, thoughtful advices and sometimes much needed persuasions from him as well as former and current lab members: Dorota, Shilpa, Krishna, Sally, Mayukh and Penny. My lab family is my reliable source of critiques and creativity that have helped me greatly.

I must also thank our fantastic collaborators including: Karl Lechtreck and his lab members, Wolfgang Maier, Ralf Baumeister, Gregory Minevich, Ewa Joachimiak, Dorota Wloga, Zheng Ruan, Natarajan Kannan, Eduardo Orias and Joseph Frankel. I am amazed how they bring in thoughts and ideas that we would not be able to imagine, and provide data and work above and beyond our expectations.

I own deep gratitude to my committee members: Scott Dougan, Marcus Fechheimer and Edward Kipreos. They devoted precious time and effort giving me much needed advice on my research and professional development. In addition, I appreciate the honor to work with Karl Lechtreck at several projects and in the process, his passion and persistence in pursuing the truth inspired me to reach beyond my expectation of myself.

Finally, I would like to thank my parents who have been patient and supportive. I know I can always trust them to wish the best of me, do their best for me and push me to the best I can be.

TABLE OF CONTENTS

Page

CHAPTER 1

INTRODUCTION AND LITERATURE REVIEW

A eukaryotic cell consists of organelles, compartments that perform specific functions, and the correct size of organelles relative to the overall size of the cell is essential for vital cellular activities. Various mechanisms exist that control organelle scaling that in principle amounts to the measuring and adjusting of the size of the organelle. For example, nuclear scaling involves adjusting the nucleus size according to the cytoplasmic volume (reviewed in (Levy and Heald, 2012)). The cilium is one of the most actively studied models of organelle scaling. Cilium length is easily quantifiable making it an ideal experimental model to study organelle sizing. The length of cilia varies greatly and does not strictly correlate with the cell size, but rather is cell type (or species)-specific. The green alga *Chlamydomonas reinhardtii* is about 10 µm in diameter and has two equal length cilia of approximately 12 µm. In comparison, the ciliate *Tetrahymena thermophila* is about 30-50 µm in diameter and has 500-1000 cilia of 4-6 µm. The classical "long-short" cilia experiment in the *Chlamydomonas* demonstrates that cilium length is actively monitored and regulated (Rosenbaum et al., 1969a). When one of the two cilia of *Chlamydomonas* is artificially severed, the remaining cilium shortens, until its length matches the length of the remaining cilium, and both cilia elongate at the same rate to achieve equal steady-state length (Rosenbaum et al., 1969a). The mechanism that senses and adjusts cilium length has been extensively studied but the mechanistic principles have been slow to emerge. Furthermore, the length is critical for optimal sensory or motile functions of cilia. In humans, many proteins that are related to cilium length regulation, when mutated, cause a wide range of

cilia-based diseases, or ciliopathies, including developmental disorders (some lethal), blindness, and polycystic kidney disease (Bielas et al., 2009; Castren et al., 2011; Grati et al., 2015; Hakim et al., 2016; Liu et al., 2002; Moon et al., 2014; Oud et al., 2016; Ozgul et al., 2011; Slaats et al., 2016; Stone et al., 2011; Tammachote et al., 2009; Taylor et al., 2015; Thiel et al., 2011; Upadhya et al., 2000). Studying cilium length regulation fulfills curiosity in basic cell biology as well as the motivation to improve human health.

CILIUM STRUCTURE

Cilium is a structurally and functionally conserved organelle consisting of a microtubule-based core, or axoneme, wrapped by the plasma membrane, making the cilium a cell extension. Cilia support important motile and sensory functions. Motile cilia beat to move the cell (for example animal sperm cells, and protists such as *Chlamydomonas* and *Tetrahymena)*, or propel fluids around the cells (e.g. epithelium in the respiratory tract) (Amelar et al., 1980; Satir, 1980; Vincensini et al., 2011). Nonmotile, so-called, primary cilia and some motile cilia are important for sensory functions including chemosensation, photoreception and mechanosensation (Berbari et al., 2009; Falk et al., 2015; Mohieldin et al., 2016; Prasad et al., 2014; Shah et al., 2009; Winyard and Jenkins, 2011).

The axoneme is composed of nine outer doublet microtubules arranged into a circle of ~250 nm in diameter. Most motile cilia have additional two central singlet microtubules (central pair apparatus) that are important for the coordination of the activities of motor complexes (dynein arms) during ciliary beating (Lechtreck et al., 2008). In motile cilia, large protein complexes, including radial spokes and dynein arms, are distributed in regularly spaced repeats along the length of the axoneme, where they function in generating ciliary bending (Oda et al., 2014; Satir et al., 2014). The axonemal microtubules are nucleated from a conserved centriole-like structure,

the basal body (BB), that is usually composed of 9 triplet microtubules and has a pinwheel organization. The BB transits into axoneme at the transition zone (TZ) where the distal end (+ end) of the triplet microtubules are anchored. The TZ is defined by the presence of several structures including transition fibers and Y-links (Fisch and Dupuis-Williams, 2011; Reiter et al., 2012), and is believed to be the "gate" of the ciliary compartment as it restricts entry of non-ciliary proteins into cilia (Basiri et al., 2014; Craige et al., 2010; Lim and Tang, 2013; Szymanska and Johnson, 2012; Takao and Verhey, 2016). C-tubules of the BB triplets also terminate around this region, and the nine A and B-tubules extend into the cilium forming the outer doublets of the axoneme that has a 9+0 organization in non-motile cilia or a 9+2 organization in motile cilia owing to the presence of the central microtubules (Fisch and Dupuis-Williams, 2011). Near the ends of cilia, the B-tubules terminate and only the A-tubules are present and form the distal segment. Finally, at the very end of the axoneme, undefined electron-dense structures known as the ciliary caps attach the A-tubules of outer microtubules and the ends of the central microtubules to the plasma membrane at the ciliary tip (Fisch and Dupuis-Williams, 2011; Portman et al., 1987).

The ciliary membrane is continuous with the cell body membrane though it differs in lipid and protein composition. The barrier function at the cilium base is important in controlling the ciliary membrane domain composition, though its regulation and function are less understood (reviewed in (Rohatgi and Snell, 2010)).

INTRAFLAGELLAR TRANSPORT

There is no protein synthesis inside cilia, based on the absence of ribosomes. A specialized transportation system called the intraflagellar transport (IFT) (Kozminski et al., 1993) is required for most proteins to enter and to distribute inside cilia, and for some proteins to exit cilia as well.

IFT is a bidirectional motility that relies on kinesin-2 motors for the anterograde transportation along the B tubules of the outer doublet, from the BB to the ciliary tip (e.g. - end to + end of the doublet MTs), and cytoplasmic dynein (IFT dynein) motors for retrograde transportation along the A tubules, from the ciliary tip to the BB (Kozminski et al., 1995; Pazour et al., 1999; Signor et al., 1999; Stepanek and Pigino, 2016). These motors move IFT particles or IFT trains, protein complexes that function as cargo-carrying platforms (Cole et al., 1998b; Kozminski, 1995; Piperno and Mead, 1997). IFT particles can be biochemically separated into two large subcomplexes, complex A and complex B (Cole et al., 1998b). IFT complex B is more important for the anterograde IFT, while complex A functions primarily in the retrograde IFT (though not without exceptions) (reviewed in (Taschner and Lorentzen, 2016)). IFT is required for assembly and maintenance of cilia, most likely because it delivers precursors to the tips of cilia where they are incorporated into the growing axoneme (Brown et al., 1999; Cole et al., 1998a; Piperno et al., 1998; Shakir et al., 1993; Walther et al., 1994). Given the importance of the IFT mechanism, a series of questions about it are currently under investigation, that among other topics address the regulation of motility of IFT trains, internal organization of IFT complexes, mechanisms of cargo recognition and loading, as well IFT-related defects that cause diseases (reviewed in (Lechtreck et al., 2017)).

IFT motor proteins

After the initial discovery of IFT in *Chlamydomonas* (Kozminski et al., 1993), kinesin-2 and IFT dynein were soon identified as the motor proteins driving the anterograde IFT and retrograde IFT movement in cilia, respectively (Kozminski et al., 1995; Pazour et al., 1999). FLA10/KIF3A and FLA8/KIF3B form the kinesin-2 motor heterodimer, bind to an accessory subunit KAP (forming a heterotrimeric complex), and are the primary anterograde IFT motor (Brown et al.,

1999; Cole et al., 1998b; Hirokawa et al., 2009; Kozminski et al., 1995; Pan et al., 2006; Wickstead and Gull, 2007). A loss of the heterotrimeric kinesin-2 results in an immediate loss of IFT in *Chlamydomonas, Tetrahymena* and mammals (Brown et al., 1999; Davenport et al., 2007; Kozminski et al., 1995). In addition to the heterotrimeric kinesin-2, there is also a homodimeric kinesin-2 complex, OSM-3/KIF17, but this motor is not required for assembly of cilia in mammals (Jiang et al., 2015; Ou et al., 2005). However, in *Caenorhabditis elegans*, OSM-3 partly compensates for the loss of the heterodimeric kinesin-2 and is required for the anterograde IFT along the most distal part of the axoneme or the distal segment (Ou et al., 2005; Snow et al., 2004) where the outer microtubules are thinner due to the termination of the B-tubule and only the A-tubule is available for both anterograde and retrograde IFT. It needs to be mentioned that the distal segment is particularly long in *C. elegans* in comparison to other organisms (Evans et al., 2006). Thus, the heterotrimeric kinesin-2 may be more adapted for the anterograde IFT along the B-tubules and sufficient in most organisms (Stepanek and Pigino, 2016), while the homodimeric kinesin-2 may be specialized in moving on the A-tubule and more important in organisms with long distal segments where the motor has to use the A-tubule to efficiently deliver the cargo to the ciliary tip.

Retrograde IFT uses cytoplasmic dynein 2 (IFT dynein) (Pazour et al., 1998; Porter et al., 1999; Signor et al., 1999) and drives along the A-tubule from the tip to the base of cilia (Stepanek and Pigino, 2016). A deficiency in the IFT dynein motors reduces the retrograde IFT but does not have an immediate severe impact on the anterograde IFT, except for an accumulation of IFT proteins at the ciliary tip (Engel et al., 2012; Reck et al., 2016). The retrograde IFT is needed for the removal of proteins that are either products of cilium disassembly (see below) or are subject to recycling. For example, when the cilium disassembles,

ciliary proteins undergo massive ubiquitination and the retrograde IFT is needed for the removal of these modified proteins from the cilium (Liang et al., 2016; Long and Huang, 2013; Long et al., 2015).

IFT complexes and cargoes

The structural organization of the IFT particles is actively explored to learn how IFT can transport hundreds of different proteins as cargoes in a proper order and with correct stoichiometries. There are more than 20 IFT complex proteins identified so far (reviewed in (Taschner et al., 2012)). Increasing ionic strength revealed stronger interactions among several IFT-B proteins, dividing them into the core and peripheral IFT proteins (Lucker et al., 2005). A series of recent structural studies has resulted in 3D structures of a number of IFT proteins and a major advance in understanding the overall organization of IFT particles (reviewed in (Taschner and Lorentzen, 2016)). In particular, it is of high interest how IFT transports tubulin, the main component of the axonemal microtubules. Furthermore, the mechanisms of IFT transport of tubulin is highly relevant to understanding cilium length regulation as it seems likely to consider the axoneme as the main stable determinant of the length of the entire cilium. Two IFT-B core proteins, IFT81 and IFT74, form a heterotetramer (Lucker et al., 2005) that interacts with the tubulin dimer through the calponin homology domain of IFT81 and a highly basic domain of IFT74 (Bhogaraju et al., 2013), directly showing the long hypothesized role of IFT proteins as cargo adapters. In addition to the IFT-B and IFT-A complex, the BBSome complex is a peripheral component of IFT specifically responsible for membrane protein trafficking (Goetz et al., 2017; Jin et al., 2010; Nachury et al., 2007), and in particular for removal of membrane proteins from cilia (Lechtreck et al., 2009). The cargo binding rate of IFT proteins could be one

of the main mechanisms of cilium length control mechanism, as the cargo loading of IFT particles is one of the most consistent indicators of the change of cilium length (discussed later).

CILIUM LENGTH REGULATION

Given the physiological importance of cilium length, it is not surprising that this parameter is closely regulated. For example, cilia that have improper length fail to generate proper propulsive forces and show defects in signaling (Thorpe et al., 2017; Tilley et al., 2015). The factors involved in regulating cilium length can be loosely divided into groups: axonemal/structural factors including axonemal structure proteins, IFT proteins, lipid and protein composition of the ciliary membrane, as well as signaling factors including kinases, phosphatases and small signaling molecules in cilia and the cytoplasm.

Axonemal proteins in cilia length regulation

The axonemal microtubules undergo slow turnover even in steady-state cilia and this dynamic property could have some role in the length regulation, albeit the exact mechanism remains unclear (Song and Dentler, 2001). Factors related to microtubule stability and turnover affect the axoneme and the length of cilia. Such factors include tubulin post-translational modifications (PTMs), microtubule-associated proteins (MAPs), and axonemal proteins including dynein arms.

Certain MAPs affect microtubule stability and change cilium length. RP1 and DCDC2 are two members of the doublecortin family that bind to and stabilize microtubules (Coquelle et al., 2006; Reiner et al., 2006). The doublecortin domain is required for overexpressed DCDC2 or RP1 to stabilize the axoneme and increase cilia length (Liu et al., 2004; Massinen et al., 2011; Omori et al., 2010). Structural axonemal components are also known to affect cilia length. Several mutants in *Chlamydomonas* lacking outer dynein arms and/or inner dynein arms have short cilia (Huang et al., 1979; LeDizet and Piperno, 1995). Possibly many proteins that bind to

axonemal microtubules stabilize them and promote microtubule elongation (for example by making the disassembly less likely) and therefore make cilia longer. Recent studies have also implicated certain post-translational modifications of tubulin as regulators of cilium length that interact with the axoneme-binding/stabilizing proteins. Namely, a loss of a tubulin glutamylase TTLL9 (an enzyme that adds polyglutamate side chains to tubulin) suppresses the short cilia length of mutants lacking axonemal microtubule-binding proteins such as dynein arms (Kubo et al., 2015). This indicates that a modification of tubulin, polyglutamylation, has a shortening effect on the axonemal microtubule and consequently shortens the cilium. This effect could be mediated by activation of ciliary microtubule-severing proteins (reviewed in (Wloga et al., 2016)). However, tubulin modifications may also have a cilium-elongating effect. A loss of tubulin glycylase TTLL3 results in shorter cilia (Pathak et al., 2007; Wloga et al., 2009). In addition to the effects of tubulin modifications on severing factors that are thought to have a cilium shortening effect, the same modifications could act in a cilium elongation-promoting manner by regulating IFT (O'Hagan et al., 2011; Sirajuddin et al., 2014). These effects could primarily occur during the anterograde IFT because tubulin is modified strongly on the B-tubule and not on the A-tubule (Lechtreck and Geimer, 2000; Suryavanshi et al., 2010) and the anterograde IFT for most of its length (except for the distal segment) occurs on the B-tubule (Stepanek and Pigino, 2016).

Cilium disassembly is closely related to cell cycle progression

In addition to these modifications and proteins known to affect axonemal stability, many signaling molecules including proteins have been shown to closely associate with cilia disassembly (reviewed in (Liang et al., 2016)). Mostly notably, CNK2, a member of NIMA-related kinase family in *Chlamydomonas*, was shown to prevent extensive elongation of cilia by

increasing the disassembly rate (Hilton et al., 2013). Another NIMA-related kinase, NEK2, phosphorylates kinesin-13 (Kif24), a microtubule depolymerizing motor-like enzyme, thus inhibiting ciliation and encouraging cell cycle progression in breast cancer cells (Kim et al., 2015). Cell cycle progression is a reciprocal regulator of cilium length as a longer cilium causes a delay in G1-S progression (Kim et al., 2011; Li et al., 2011). In mammalian cells that reenter the cell cycle and disassemble the primary cilium, there is activation of Aurora A kinase and PLK1 that promote cilium disassembly, possibly by activating HDAC6 deacetylase which may be involved in deacetylation of tubulin during cilia disassembly (Lee et al., 2012; Pugacheva et al., 2007). In addition, PLK1 also phosphorylates kinesin-13 (KIF2A) and encourages cilium disassembly (Miyamoto et al., 2015). In *Chlamydomonas*, the ratio of phosphorylated Aurora kinase (pT193 of CALK) to the total amount of CALK is a reporter of cilium length (Luo et al., 2011; Pan and Snell, 2014). The initiation of this phosphorylation requires LF5/CDKL5 which is also involved in promoting cell division in *Chlamydomonas* (Hu et al., 2015). Taken together, cilium assembly seems closely related to cell cycle progression (Izawa et al., 2015), although it is not clear whether and how the disassembly is involved in regulating length of cilia that are not programmed to be fully disassembled such as in the *Chlamydomonas* "long-short" experiment. Another example is that overexpression of NRK1 and NRK2 shorten cilia in *Tetrahymena*, while conditional overexpression of a kinase-dead variant of NRK2 elongates cilia, suggesting an activate disassembly regulation by NRKs (Wloga et al., 2006).

IFT affects cilium assembly and cilia length

Except for some special cases where cilia assemble inside the cell body prior to their insertion into the plasma membrane (Kukic et al., 2016; Sorokin, 1962; Sorokin, 1968a; Sorokin, 1968b), in most cell types, the assembly of cilia relies on IFT for the delivery of axonemal proteins,

including tubulin, to the ciliary tip (Kubo et al., 2016; Marshall and Rosenbaum, 2001). A loss of kinesin-2 or other core proteins in the IFT complex causes an immediate arrest in ciliary assembly (Cole et al., 1998b; Fan et al., 2010; Kozminski et al., 1995). IFT activity and cargo loading rate increase in short elongating cilia and subsequently decrease as the cilia lengthen (Craft et al., 2015; Engel et al., 2009b; Ludington et al., 2013). Furthermore, when cilia disassemble (e.g. in cell types where cilia undergo complete disassembly prior to mitosis that results in a release of BBs before their conversion into centrioles), IFT complexes carry little or no cargo (Pan and Snell, 2005). Furthermore in the LF2 (a cilium length kinase, see below) loss of function mutant, the tubulin cargo loading rate is affected (Craft et al., 2015). These observations indicate that a control over the IFT cargo loading rate in the anterograde IFT direction could be critical in cilium length regulation. The role of the retrograde IFT in cilium length regulation is less understood. In some ciliated models, including *Chlamydomonas* and mammals, a loss of the retrograde IFT motor, IFT dynein, results in extremely short cilia with a bulged tip, presumably because the retrograde IFT is needed for recycling of the anterograde IFT components (Engel et al., 2012; Reck et al., 2016; Taylor et al., 2015). Indeed, a conditional fast acting mutation of IFT dynein inhibits both the retrograde as well as the anterograde IFT (Engel et al., 2012). The phenotypes of IFT dynein loss of function mutants do not support an intuitive model that retrograde IFT plays a role in the cilia disassembly pathway, because in such a case a loss of retrograde IFT would be expected to lengthen cilia. Furthermore, in *Chlamydomonas*, cilium disassembly takes place in the absence of IFT (Kozminski et al., 1995; Marshall and Rosenbaum, 2001). Presumably, for the disassembly pathway it is not important to remove the products of axoneme disassembly from the cilium or that diffusion alone is sufficient to provide enough of the removal activity. However, observations in other cell types indicate a link between

the retrograde IFT and cilium length control. For example, in *Tetrahymena*, a loss of the retrograde dynein motor results in fewer cilia that are on average shorter but have a more variable length range, including some that are longer than the wild type (Rajagopalan et al., 2009). Thus, the removal of recycled components including the products of cilia disassembly could contribute to the length regulation as well. However, the major effect of the retrograde IFT appears to be to support the recycling of the components of the anterograde IFT.

Protein phosphorylation in cilia length regulation

In addition to the structural components of axonemal proteins and IFT machinery, published evidence suggests that a dedicated sensing mechanism exists to tightly regulate cilium length. One classical example is the "long-short" cilia experiment in *Chlamydomonas,* where amputating one of the two cilia triggers the other full length cilium to disassemble until the length is equal to the regenerating cilium, indicating a mechanism exists that sets the cilia to equal length and differentially controls the assembly and disassembly rates for each cilium within the same cytoplasm (Rosenbaum et al., 1969b). Furthermore, there is now a direct evidence that in the same *Chlamydomonas* cell, the two cilia are regulated differentially. For example, when only one cilium grows, this cilium has a higher rate of IFT cargo loading (Craft et al., 2015). Thus, the length of each cilium is regulated separately, by independent adjustment of its parameters, such as the rate of IFT cargo loading. *Tetrahymena* represents another perhaps more dramatic example of such individualized regulation, where the cilium length depends on the position within the cell, with cilia being progressively longer toward the posterior end (Wloga et al., 2006). It appears therefore that some unknown mechanisms are in place to sense the length of individual cilia and actively adjust their length using cilium unit-specific mechanisms.

Although the nature of the sensor and feedback mechanism is not known, it is firmly established that protein phosphorylation is one of the key players. Several conserved kinases (e.g. LF2/CCRK, LF4/MOK, DYF-5/ICK/MAK, CALK, NIMA-related kinases, LF4/CDKL5) (Berman et al., 2003; Bradley and Quarmby, 2005; Broekhuis et al., 2014; Burghoorn et al., 2007; Cao et al., 2013; Chaya et al., 2014; Erdmann et al., 2006; Hilton et al., 2013; Lin et al., 2015; Luo et al., 2011; Meng and Pan, 2016; Pan et al., 2004; Tam et al., 2013; Wloga et al., 2006; Yang et al., 2013) have been consistently shown to negatively regulate cilium length in that their loss results in longer cilia (thereafter referred as cilium length kinases). However, there are two exceptions: CDPK1 and CDK5; when these kinases are depleted, cilia get shorter (Husson et al., 2016; Liang et al., 2014; Maskey et al., 2015). Several phosphatases were found inside cilia (Boesger et al., 2009), and PP1 has been implicated in cilium length regulation, based on the observation that an inhibitor of PP1 causes cilia to shorten, indicating that PP1 is a positive regulator while its competing kinase a negative regulator of cilium length (Abdul-Majeed et al., 2012). An irreversible S/T phosphatase inhibitor, sodium pyrophosphate, also induces cilium shortening by an unknown mechanism, presumably via inhibition of PP1, and/or other unknown phosphatases (Lefebvre et al., 1978; Liang and Pan, 2013; Pan et al., 2004).

The discovery and subsequent studies of cilium length kinases have revealed important information about ciliogenesis, cilium assembly and disassembly. However, the nature of the sensor that reports on the length of cilia remains unknown. More work is needed to discover the relevant phosphatases and the phosphorylation targets of the cilium length kinases. Reverse genetic approaches have been fruitful but increasingly less productive as cilium length is entangled with other important cellular functions including cell cycle progression, and developmental contexts in the case of multicellular organisms. In addition, the target proteins of

cilium length kinases may be phosphorylated transiently and possibly at multiple sites, challenging the effectiveness of proteomic studies. Historically, genetic screens have been ground-breaking in the discovery of the several cilia length kinases (Asleson and Lefebvre, 1998; Tam and Lefebvre, 1993; Tam et al., 2013). However, it has been difficult to progress beyond the discovery of the cilium length kinases. In particular, very little is known about the substrates of these kinases. While there is some evidence that cilium length kinases work through both adjustments of IFT and cilium disassembly rates, exactly how these steps are accomplished remains uncertain. One powerful way of the discovery of new components of a biological pathway is by genetic interactor screens. Likely for technical reasons, namely a lack of an approach for selection of appropriate cilium length mutants, the forward genetic approach has not been used to uncover additional interactors of cilium length components. In Chapter 3 we describe a new genetic strategy for isolation of interactors of cilium length kinases by exploring a novel allele of one of the cilium length kinases, LF4, that causes a complete loss of cilia and cell paralysis, a phenotype that can be easily used for isolation of suppressors.

Models of cilia length regulation

Among the most popular models for cilia length regulation is the “balance-point” model (Marshall et al., 2005). This relatively simple model is based on several experimental observations about cilium length and IFT: 1) the IFT velocity and total abundance of IFT trains per cilium do not vary when the cilium length changes; 2) the cilium assembly rate is negatively correlated to cilium length; while 3) the disassembly rate is constant. In order to explain how the assembly rate decreases in a longer cilium, the balance point model postulates that as cilium becomes longer and the travel time for IFT trains between the base and the tip increases, leading to decreased frequency of IFT and reduced delivery of ciliary proteins to the ciliary tip. This

model was later rectified by new observations including that the frequency of IFT entry (mainly anterograde IFT) is in fact not variable with length, but the amount of IFT proteins per entry decreases (smaller trains) as the cilium lengthens (Ludington et al., 2013), and so does the frequency of IFT trains carrying cargoes including DRC4 and tubulins (Craft et al., 2015; Wren et al., 2013). The cilium length-dependent effects on the IFT train organization and cargo loading rate are under investigation as are the mechanism responsible for regulating cilium length. One possibility is that a feedback mechanism that monitors the cilium length directly affects the IFT complexes. The reduction of IFT cargo loading as the cilium lengthens is faster in the *shf2* short cilium mutant, conversely, IFT cargo loading remains higher for an extended duration in the *lf2* mutant, where the cilia are variable in length and often longer than normal (Craft et al., 2015). In addition, the CNK2 mutant of *Chlamydomonas* displays a reduced disassembly rate and longer cilia indicating that in addition to IFT the disassembly pathway also controls cilium length (Avasthi and Marshall, 2013; Hilton et al., 2013). Though as discussed earlier, the main remaining difficulties are the lack of knowledge about the interactions between IFT proteins and cargoes, and even less understanding about the target of the regulatory factors (e.g. the phosphorylation substrates of the cilia length kinases) involved in the regulation of cargo loading.

NOVEL TECHNIQUES IMPROVE UTILITY OF *TETRAHYMENA* AS A MODEL ORGANISM

I used *Tetrahymena thermophila*, a ciliated protist, to study cilium length regulation (Chapter 3) and cell scaling during cell division (Chapter 4). *Tetrahymena* is easy to grow and maintain, and its cultures can reach high cell density (reviewed in Gaertig et al. (2013)). Each cell possesses between 500-1000 of locomotory and about a hundred of oral cilia that can be amputated by a pH shock. The removed cilia can be easily isolated for biochemical studies while

the deciliated cells quickly regenerate a set of new cilia, and thus the process of regeneration can be used to study the mechanism of assembly under conditions where the assembly status is nearly synchronized (Calzone and Gorovsky, 1982; Rosenbaum and Carlson, 1969). Gene targeting by homologous DNA recombination (Orias, 2012) allows for gene knockouts (Dave et al., 2009a), and epitope-tagging at the native loci for localization of gene products at the physiological levels of expression (reviewed in (Gaertig et al., 2013)). It is highly relevant to this thesis that in *Tetrahymena*, hypermorphic alleles can be created by conditionally overexpressing a gene under a heavy metal-dependent promoter (Shang et al., 2002).

Live imaging in *Tetrahymena*

With the help of the versatile genetic tools available in *Tetrahymena*, gene products of interest can be easily detected in fixed cells using fluorescence or electron microscopy. These classical imaging techniques have been proven fruitful in studies of microtubules and cilia (Bregier et al., 2013; Brown et al., 1999; Dave et al., 2009b; Gaertig et al., 2013; Galati et al., 2014; Kushida et al., 2016; Meehl et al., 2016; Pearson et al., 2009; Pigino et al., 2012; Urbanska et al., 2015; Vasudevan et al., 2015; Waclawek et al., 2017; Wloga et al., 2006; Wloga et al., 2008; Wloga et al., 2009). However, the molecules of interest inside cilia are often low in abundance, and their localization sites are transient, making the imaging *in vivo* technically challenging. The lack of a live imaging solution for *Tetrahymena* has also been a limit to investigations of highly mobile ciliary proteins, in particular those in IFT.

In comparison, total internal reflection fluorescence (TIRF) microscopy has greatly facilitated studies of IFT by imaging and measuring the intensity of fluorescence-tagged proteins in *Chlamydomonas* cilia (Collingridge et al., 2013; Engel et al., 2009a; Lechtreck, 2013; Lechtreck et al., 2009; Ludington et al., 2013; Wren et al., 2013). The superb sensitivity of TIRF

microscopy allows for detection of low-abundance ciliary proteins, and tracking of ciliary protein dynamics using techniques such as fluorescence recovery after photobleaching (FRAP). The use of TIRF microscopy has been a unique advantage in studies of cilia in *Chlamydomonas* (Avasthi and Marshall, 2012; Engel et al., 2009b; Lechtreck et al., 2009; Ludington et al., 2013; Pan and Snell, 2014; Wren et al., 2013).

Seeking to introduce TIRF microscopy into *Tetrahymena*, I had the honor to collaborate with Dr. Karl Lechtreck's lab to apply TIRF microscopy for live imaging of IFT and ciliary proteins in *Tetrahymena* (described in Chapter 2). In principle, the use of TIRF in *Tetrahymena* was possible after optimization of conditions for immobilization and paralysis of ciliary beating. We achieved such conditions and the relevant paper forms Chapter 2 of this thesis. This new development facilitated the discovery and study of several projects in the lab. In this study, I used TIRF microscopy to reveal that the cilium length kinase LF4 localizes uniformly along the axoneme and functions as an inhibitor of IFT (Chapter 3). Combined with the existing biochemical, genetic and traditional microscopy capabilities of *Tetrahymena*, TIRF microscopy-based live imaging greatly increases the value of the *Tetrahymena* model for studies of cilia.

Forward genetics in *Tetrahymena*

Genetic screens give researchers a selective handle on the phenotypes of interest yet still allow the benefit of unbiased discovery through a forward genetics strategy. Case in point is the 2016 Nobel Prize in Physiology or Medicine awarded to Yoshinori Ohsumi to honor the discovery of the autophagy mechanism using a genetic screen in yeast. In this case, the autophagy genes were discovered in a screen of protease-defective cells that accumulate otherwise short-lived autophagy bodies (Enserink and Pennisi, 2016; Tooze and Dikic, 2016). *Tetrahymena* is a complex unicellular organism that has many conserved structures of eukaryotic

cells present in animals including mammals. The sequence of the somatic genome (the macronucleus) was published in 2006, revealing the entire set of genes that control the phenotype (Eisen et al., 2006). Most recently, the germline (micronucleus) genome of *Tetrahymena* has been published (Hamilton et al., 2016), allowing for the linkage-based identification of causal mutations that we took advantage of in Chapters 3 and 4. One additional distinct advantage of *Tetrahymena* is the ease of genetic manipulations by homologous DNA recombination, making it possible to generate precise genetic changes, an essential tool for validation of the results of genetics screens. In Chapter 3 of this dissertation, I also used the capability of homologous DNA recombination to create a hypermorphic allele of a cilium length kinase LF4 to enable a genetic screen in *Tetrahymena* that revealed an interactor of the LF4 cilium length kinase. Further potential of this (unsaturated) screen is discussed in Chapter 5.

Recent developments in next generation sequencing and bioinformatics allow for cost-effective and rapid identification of causal mutations, opening exciting possibilities for mutational studies and forward genetic strategy in *Tetrahymena*. Recently, an implementation of comparative whole genome sequencing to *Tetrahymena* led to the identification of the first mutation that affects the cortical pattern in *Tetrahymena*, a mutation responsible for the BB disorientation defect, *disA-1* (Galati et al., 2014). This thesis heavily relies on the use of comparative whole genome sequencing for identification of mutations relevant to biological scaling, namely in the cilium length control (Chapter 3) and equalization of cell division (Chapter 4). In both projects, I used a novel strategy for identification of causal mutations by comparative whole genome sequencing (for details see Chapter 4). The overall strategy is a variation of the bulked segregant approach (Birkeland et al., 2010; Michelmore et al., 1991) where a heterozygote is subject to a number of independent meioses and a genetic link is

identified in the progeny between the phenotype and one or more of the sequence variants. The first innovation that we introduced for *Tetrahymena* is the use of self-crosses instead of standard crosses, that reduce the level of overall genetic variation and facilitates identification of the causal variant(s). The second improvement is the use of variant filtering and subtraction methods that have not been applied to *Tetrahymena* before, including subtractions of variants found in unrelated backgrounds and filtering for types of mutations expected for a particular mutagen. These methods were inspired by the approaches developed earlier for *C. elegans* (Minevich et al., 2012). Finally, we took advantage of the recently published sequence of the germline genome of *Tetrahymena* (the micronucleus) to develop a mapping approach that determines the chromosome interval based on the frequency of variant cosegregation with the mutant phenotype, again also following the footsteps of *C. elegans* (Minevich et al., 2012). While these approaches are not original and have been used in other models, the combination of these approaches in application to *Tetrahymena* has created a powerful pipeline that in our hands identifies causal mutations with an ultimate level of precision – a single variant resolution (see Chapter 4). In practical terms, it means that the "guessing step" (which of the many candidate variants is causative?) is eliminated and researchers can identify a strong candidate for a causal variant without a need for considering the magnitude of the biological effect of the mutation on the gene product or the biological pathway assignment of the gene product. These powerful approaches were used to identify an interactor of the cilium length kinase LF4 in Chapter 3. Chapter 4 in this dissertation is another example in which the outcome of a basic genetic screen informs about the principles of biological scaling using the process of equal cell division.

POLARIZED CELL DIVISION AND CELL SCALING IN *TETRAHYMENA*

Cell division, cell polarization, and scaling of daughter cells are closely related processes. Typically, the mother cell establishes an axis of polarity that enables the correct placement of the division plane. Sometimes the cell divides asymmetrically producing progeny cells of unequal size. Such asymmetric division occurs in the *C. elegans* zygote where the mechanism involves two partitioning-defective (PAR) proteins that mutually exclude each other at the cell membrane. The PAR proteins generate a polarized pattern by either a reaction-diffusion model based on actomyosin flows as diffusion media or a microtubule induced self-organization independent of actomyosin flows (Goehring et al., 2011; Motegi et al., 2011). In this case, the scaling of the mother cell is accomplished by establishing a transient bipolar axis perpendicular to the emerging division plane.

In comparison, *Tetrahymena* has permanent anteroposterior and circumferential axes. The oral apparatus marks the anterior and ventral area while the contractile vacuole pores and the cytoproct are markers of the posterior end. *Tetrahymena* divides by a unique mechanism of "tandem duplication". Unlike in other cell types where there is an underlying bipolar organization that reflects the organization of the bipolar mitotic spindle, in a dividing *Tetrahymena* cortical structures are arranged as a tandem. The best comparable arrangement is seen in planarians that divide by splitting their bodies and the resulting fragments regenerate the missing parts: the anterior fragments regenerate a tail while the posterior fragment regenerates a head and a brain (Salo and Baguna, 1984). Thus, a dividing *Tetrahymena* mother cell splits into two halves and the anterior half develops a new posterior end while the posterior half develops a new anterior end including a new oral apparatus (see Fig. 3.1 in Chapter 4). This extensive remodeling of the mother cell must be precisely coordinated with cytokinesis and scaling

mechanisms must exist to make sure that the two developing daughters are equal in size. Specifically, the emerging division plane establishes a discontinuity at the cell equator called the "cortical subdivision". The regions immediately anterior and posterior to the cortical subdivision undergo different morphogenetic events, and subsequently develop into posterior and anterior poles of the daughter cells, respectively. This newly established polarization is evident as different cortical organelles appear on either side of the division plane (Cole et al., 2008; Frankel et al., 1981; Jerka-Dziadosz, 1981; Kaczanowska et al., 1999; Numata et al., 1995). Meanwhile, two equally-sized daughter cells are generated, indicating a correct scaling despite the "broken ruler". This phenomenon raises interesting questions about the mechanisms of the intracellular scaling. How do *Tetrahymena* cells temporally remodel the cortical pattern from the existing anteroposterior axis during the cell division? And around the same time, how is the division plane established at the mother cell equator so that the two daughter cells are equally sized, despite the vastly different morphogenesis that occur within each? It is not clear if shared conserved regulatory pathways connect the changes in the rulers and the measurements, namely the remodeling of the polarization and the placement of the division plane (Chalker and Frankel, 2014). Chapter 4 attempts to provides some information on this subject.

REFERENCES

Abdul-Majeed, S., B.C. Moloney, and S.M. Nauli. 2012. Mechanisms regulating cilia growth and cilia function in endothelial cells. *Cellular and molecular life sciences : CMLS*. 69:165-173.

Amelar, R.D., L. Dubin, and C. Schoenfeld. 1980. Sperm motility. *Fertility and sterility*. 34:197-215.

Asleson, C.M., and P.A. Lefebvre. 1998. Genetic analysis of flagellar length control in Chlamydomonas reinhardtii: a new long-flagella locus and extragenic suppressor mutations. *Genetics*. 148:693-702.

Avasthi, P., and W.F. Marshall. 2012. Stages of ciliogenesis and regulation of ciliary length. *Differentiation; research in biological diversity*. 83:S30-42.

Avasthi, P., and W.F. Marshall. 2013. Ciliary regulation: disassembly takes the spotlight. *Current biology : CB*. 23:R1001-1003.

Basiri, M.L., A. Ha, A. Chadha, N.M. Clark, A. Polyanovsky, B. Cook, and T. Avidor-Reiss. 2014. A migrating ciliary gate compartmentalizes the site of axoneme assembly in Drosophila spermatids. *Current biology : CB*. 24:2622-2631.

Berbari, N.F., A.K. O'Connor, C.J. Haycraft, and B.K. Yoder. 2009. The primary cilium as a complex signaling center. *Current biology : CB*. 19:R526-535.

Berman, S.A., N.F. Wilson, N.A. Haas, and P.A. Lefebvre. 2003. A novel MAP kinase regulates flagellar length in Chlamydomonas. *Current biology : CB*. 13:1145-1149.

Bhogaraju, S., L. Cajanek, C. Fort, T. Blisnick, K. Weber, M. Taschner, N. Mizuno, S. Lamla, P. Bastin, E.A. Nigg, and E. Lorentzen. 2013. Molecular basis of tubulin transport within the cilium by IFT74 and IFT81. *Science*. 341:1009-1012.

Bielas, S.L., J.L. Silhavy, F. Brancati, M.V. Kisseleva, L. Al-Gazali, L. Sztriha, R.A. Bayoumi, M.S. Zaki, A. Abdel-Aleem, O. Rosti, H. Kayserili, D. Swistun, L.C. Scott, E. Bertini, E. Boltshauser, E. Fazzi, L. Travaglini, S.J. Field, S. Gayral, M. Jacoby, S. Schurmans, B. Dallapiccola, P.W. Majerus, E.M. Valente, and J.G. Gleeson. 2009. Mutations in the inositol polyphosphate-5-phosphatase E gene link phosphatidyl inositol signaling to the ciliopathies. *Nature genetics*. 41:1032-1036.

Birkeland, S.R., N. Jin, A.C. Ozdemir, R.H. Lyons, Jr., L.S. Weisman, and T.E. Wilson. 2010. Discovery of mutations in Saccharomyces cerevisiae by pooled linkage analysis and whole-genome sequencing. *Genetics*. 186:1127-1137.

Boesger, J., V. Wagner, W. Weisheit, and M. Mittag. 2009. Analysis of flagellar phosphoproteins from Chlamydomonas reinhardtii. *Eukaryotic cell*. 8:922-932.

Bradley, B.A., and L.M. Quarmby. 2005. A NIMA-related kinase, Cnk2p, regulates both flagellar length and cell size in Chlamydomonas. *Journal of cell science*. 118:3317-3326.

Bregier, C., L. Krzemien-Ojak, D. Wloga, M. Jerka-Dziadosz, E. Joachimiak, K. Batko, I. Filipiuk, U. Smietanka, J. Gaertig, S. Fabczak, and H. Fabczak. 2013. PHLP2 is essential and plays a role in ciliogenesis and microtubule assembly in Tetrahymena thermophila. *Journal of cellular physiology*. 228:2175-2189.

Broekhuis, J.R., K.J. Verhey, and G. Jansen. 2014. Regulation of Cilium Length and Intraflagellar Transport by the RCK-Kinases ICK and MOK in Renal Epithelial Cells. *PloS one*. 9:e108470.

Brown, J.M., C. Marsala, R. Kosoy, and J. Gaertig. 1999. Kinesin-II is preferentially targeted to assembling cilia and is required for ciliogenesis and normal cytokinesis in Tetrahymena. *Mol Biol Cell*. 10:3081-3096.

Burghoorn, J., M.P. Dekkers, S. Rademakers, T. de Jong, R. Willemsen, and G. Jansen. 2007. Mutation of the MAP kinase DYF-5 affects docking and undocking of kinesin-2 motors and reduces their speed in the cilia of Caenorhabditis elegans. *Proceedings of the National Academy of Sciences of the United States of America*. 104:7157-7162.

Calzone, F.J., and M.A. Gorovsky. 1982. Cilia regeneration in Tetrahymena. A simple reproducible method for producing large numbers of regenerating cells. *Experimental cell*

research. 140:471-476.

Cao, M., D. Meng, L. Wang, S. Bei, W.J. Snell, and J. Pan. 2013. Activation loop phosphorylation of a protein kinase is a molecular marker of organelle size that dynamically reports flagellar length. *Proceedings of the National Academy of Sciences of the United States of America*.

Castren, M., E. Gaily, C. Tengstrom, J. Lahdetie, H. Archer, and S. Ala-Mello. 2011. Epilepsy caused by CDKL5 mutations. *Eur J Paediatr Neurol*. 15:65-69.

Chalker, D.L., and J. Frankel. 2014. Morphogenesis: a Mob rules from the rear. *Current biology : CB*. 24:R700-702.

Chaya, T., Y. Omori, R. Kuwahara, and T. Furukawa. 2014. ICK is essential for cell type-specific ciliogenesis and the regulation of ciliary transport. *The EMBO journal*.

Cole, D.G., D.R. Diener, A.L. Himelblau, P.L. Beech, J.C. Fuster, and J.L. Rosenbaum. 1998a. Chlamydomonas kinesin-II-dependent intraflagellar transport (IFT): IFT particles contain proteins required for ciliary assembly in Caenorhabditis elegans sensory neurons. *The Journal of cell biology*. 141:993-1008.

Cole, D.G., D.R. Diener, A.L. Himelblau, P.L. Beech, J.C. Fuster, and J.L. Rosenbaum. 1998b. Chlamydomonas Kinesin-II–dependent Intraflagellar Transport (IFT): IFT Particles Contain Proteins Required for Ciliary Assembly in Caenorhabditis elegans Sensory Neurons. *The Journal of cell biology*. 141:993-1008.

Cole, E.S., P.C. Anderson, R.B. Fulton, M.E. Majerus, M.G. Rooney, J.M. Savage, D. Chalker, J. Honts, M.E. Welch, A.L. Wentland, E. Zweifel, and D.J. Beussman. 2008. A proteomics approach to cloning fenestrin from the nuclear exchange junction of tetrahymena. *J Eukaryot Microbiol*. 55:245-256.

Collingridge, P., C. Brownlee, and G.L. Wheeler. 2013. Compartmentalized calcium signaling in cilia regulates intraflagellar transport. *Current biology : CB*. 23:2311-2318.

Coquelle, F.M., T. Levy, S. Bergmann, S.G. Wolf, D. Bar-El, T. Sapir, Y. Brody, I. Orr, N. Barkai, G. Eichele, and O. Reiner. 2006. Common and divergent roles for members of the mouse DCX superfamily. *Cell Cycle*. 5:976-983.

Craft, J.M., J.A. Harris, S. Hyman, P. Kner, and K.F. Lechtreck. 2015. Tubulin transport by IFT is upregulated during ciliary growth by a cilium-autonomous mechanism. *The Journal of cell biology*. 208:223-237.

Craige, B., C.C. Tsao, D.R. Diener, Y. Hou, K.F. Lechtreck, J.L. Rosenbaum, and G.B. Witman. 2010. CEP290 tethers flagellar transition zone microtubules to the membrane and regulates flagellar protein content. *The Journal of cell biology*. 190:927-940.

Dave, D., D. Wloga, and J. Gaertig. 2009a. Manipulating ciliary protein-encoding genes in Tetrahymena thermophila. *Methods Cell Biol*. 93:1-20.

Dave, D., D. Wloga, N. Sharma, and J. Gaertig. 2009b. DYF-1 Is required for assembly of the axoneme in Tetrahymena thermophila. *Eukaryotic cell*. 8:1397-1406.

Davenport, J.R., A.J. Watts, V.C. Roper, M.J. Croyle, T. van Groen, J.M. Wyss, T.R. Nagy, R.A. Kesterson, and B.K. Yoder. 2007. Disruption of intraflagellar transport in adult mice leads

to obesity and slow-onset cystic kidney disease. *Current biology : CB*. 17:1586-1594.

Eisen, J.A., R.S. Coyne, M. Wu, D. Wu, M. Thiagarajan, J.R. Wortman, J.H. Badger, Q. Ren, P. Amedeo, K.M. Jones, L.J. Tallon, A.L. Delcher, S.L. Salzberg, J.C. Silva, B.J. Haas, W.H. Majoros, M. Farzad, J.M. Carlton, R.K. Smith, Jr., J. Garg, R.E. Pearlman, K.M. Karrer, L. Sun, G. Manning, N.C. Elde, A.P. Turkewitz, D.J. Asai, D.E. Wilkes, Y. Wang, H. Cai, K. Collins, B.A. Stewart, S.R. Lee, K. Wilamowska, Z. Weinberg, W.L. Ruzzo, D. Wloga, J. Gaertig, J. Frankel, C.C. Tsao, M.A. Gorovsky, P.J. Keeling, R.F. Waller, N.J. Patron, J.M. Cherry, N.A. Stover, C.J. Krieger, C. del Toro, H.F. Ryder, S.C. Williamson, R.A. Barbeau, E.P. Hamilton, and E. Orias. 2006. Macronuclear genome sequence of the ciliate Tetrahymena thermophila, a model eukaryote. *PLoS biology*. 4:e286.

Engel, B.D., H. Ishikawa, K.A. Wemmer, S. Geimer, K. Wakabayashi, M. Hirono, B. Craige, G.J. Pazour, G.B. Witman, R. Kamiya, and W.F. Marshall. 2012. The role of retrograde intraflagellar transport in flagellar assembly, maintenance, and function. *The Journal of cell biology*. 199:151-167.

Engel, B.D., K.F. Lechtreck, T. Sakai, M. Ikebe, G.B. Witman, and W.F. Marshall. 2009a. Total internal reflection fluorescence (TIRF) microscopy of Chlamydomonas flagella. *Methods Cell Biol*. 93:157-177.

Engel, B.D., W.B. Ludington, and W.F. Marshall. 2009b. Intraflagellar transport particle size scales inversely with flagellar length: revisiting the balance-point length control model. *The Journal of cell biology*. 187:81-89.

Enserink, M., and E. Pennisi. 2016. Nobel honors discoveries in how cells eat themselves. *Science*. 354:20.

Erdmann, M., A. Scholz, I.M. Melzer, C. Schmetz, and M. Wiese. 2006. Interacting protein kinases involved in the regulation of flagellar length. *Mol Biol Cell*. 17:2035-2045.

Evans, J.E., J.J. Snow, A.L. Gunnarson, G. Ou, H. Stahlberg, K.L. McDonald, and J.M. Scholey. 2006. Functional modulation of IFT kinesins extends the sensory repertoire of ciliated neurons in Caenorhabditis elegans. *The Journal of cell biology*. 172:663-669.

Falk, N., M. Losl, N. Schroder, and A. Giessl. 2015. Specialized Cilia in Mammalian Sensory Systems. *Cells*. 4:500-519.

Fan, Z.C., R.H. Behal, S. Geimer, Z. Wang, S.M. Williamson, H. Zhang, D.G. Cole, and H. Qin. 2010. Chlamydomonas IFT70/CrDYF-1 is a core component of IFT particle complex B and is required for flagellar assembly. *Mol Biol Cell*. 21:2696-2706.

Fisch, C., and P. Dupuis-Williams. 2011. Ultrastructure of cilia and flagella - back to the future! *Biology of the cell / under the auspices of the European Cell Biology Organization*. 103:249-270.

Frankel, J., E.M. Nelsen, and L.M. Jenkins. 1981. Development of the ciliature of *Tetrahymena thermophila*. II. Spatial subdivision prior to cytokinesis. *Dev. Biol.* 88:39-54.

Gaertig, J., D. Wloga, K.K. Vasudevan, M. Guha, and W. Dentler. 2013. Discovery and functional evaluation of ciliary proteins in Tetrahymena thermophila. *Methods in enzymology*. 525:265-284.

Galati, D.F., S. Bonney, Z. Kronenberg, C. Clarissa, M. Yandell, N.C. Elde, M. Jerka-Dziadosz,

T.H. Giddings, J. Frankel, and C.G. Pearson. 2014. DisAp-dependent striated fiber elongation is required to organize ciliary arrays. *The Journal of cell biology*. 207:705-715.

Goehring, N.W., P.K. Trong, J.S. Bois, D. Chowdhury, E.M. Nicola, A.A. Hyman, and S.W. Grill. 2011. Polarization of PAR proteins by advective triggering of a pattern-forming system. *Science*. 334:1137-1141.

Goetz, S.C., F. Bangs, C.L. Barrington, N. Katsanis, and K.V. Anderson. 2017. The Meckel syndrome- associated protein MKS1 functionally interacts with components of the BBSome and IFT complexes to mediate ciliary trafficking and hedgehog signaling. *PloS one*. 12:e0173399.

Grati, M., I. Chakchouk, Q. Ma, M. Bensaid, A. Desmidt, N. Turki, D. Yan, A. Baanannou, R. Mittal, N. Driss, S. Blanton, A. Farooq, Z. Lu, X.Z. Liu, and S. Masmoudi. 2015. A missense mutation in DCDC2 causes human recessive deafness DFNB66, likely by interfering with sensory hair cell and supporting cell cilia length regulation. *Human molecular genetics*. 24:2482-2491.

Hakim, S., J.M. Dyson, S.J. Feeney, E.M. Davies, A. Sriratana, M.N. Koenig, O.V. Plotnikova, I.M. Smyth, S.D. Ricardo, R.M. Hobbs, and C.A. Mitchell. 2016. Inpp5e suppresses polycystic kidney disease via inhibition of PI3K/Akt-dependent mTORC1 signaling. *Human molecular genetics*. 25:2295-2313.

Hamilton, E.P., A. Kapusta, P.E. Huvos, S.L. Bidwell, N. Zafar, H. Tang, M. Hadjithomas, V. Krishnakumar, J.H. Badger, E.V. Caler, C. Russ, Q. Zeng, L. Fan, J.Z. Levin, T. Shea, S.K. Young, R. Hegarty, R. Daza, S. Gujja, J.R. Wortman, B.W. Birren, C. Nusbaum, J. Thomas, C.M. Carey, E.J. Pritham, C. Feschotte, T. Noto, K. Mochizuki, R. Papazyan, S.D. Taverna, P.H. Dear, D.M. Cassidy-Hanley, J. Xiong, W. Miao, E. Orias, and R.S. Coyne. 2016. Structure of the germline genome of Tetrahymena thermophila and relationship to the massively rearranged somatic genome. *eLife*. 5.

Hilton, L.K., K. Gunawardane, J.W. Kim, M.C. Schwarz, and L.M. Quarmby. 2013. The kinases LF4 and CNK2 control ciliary length by feedback regulation of assembly and disassembly rates. *Current biology : CB*. 23:2208-2214.

Hirokawa, N., Y. Noda, Y. Tanaka, and S. Niwa. 2009. Kinesin superfamily motor proteins and intracellular transport. *Nature reviews. Molecular cell biology*. 10:682-696.

Hu, Z., Y. Liang, W. He, and J. Pan. 2015. Cilia disassembly with two distinct phases of regulation. *Cell reports*. 10:1803-1810.

Huang, B., G. Piperno, and D.J. Luck. 1979. Paralyzed flagella mutants of Chlamydomonas reinhardtii. Defective for axonemal doublet microtubule arms. *The Journal of biological chemistry*. 254:3091-3099.

Husson, H., S. Moreno, L.A. Smith, M.M. Smith, R.J. Russo, R. Pitstick, M. Sergeev, S.R. Ledbetter, N.O. Bukanov, M. Lane, K. Zhang, K. Billot, G. Carlson, J. Shah, L. Meijer, D.R. Beier, and O. Ibraghimov-Beskrovnaya. 2016. Reduction of ciliary length through pharmacologic or genetic inhibition of CDK5 attenuates polycystic kidney disease in a model of nephronophthisis. *Human molecular genetics*. 25:2245-2255.

Izawa, I., H. Goto, K. Kasahara, and M. Inagaki. 2015. Current topics of functional links

between primary cilia and cell cycle. *Cilia*. 4:12.

Jerka-Dziadosz, M. 1981. Cytoskeleton-related structures in tetrahymena thermophila: microfilaments at the apical and division-furrow rings. *J Cell Sci*. 51:241-253.

Jiang, L., B.M. Tam, G. Ying, S. Wu, W.W. Hauswirth, J.M. Frederick, O.L. Moritz, and W. Baehr. 2015. Kinesin family 17 (osmotic avoidance abnormal-3) is dispensable for photoreceptor morphology and function. *FASEB journal : official publication of the Federation of American Societies for Experimental Biology*. 29:4866-4880.

Jin, H., S.R. White, T. Shida, S. Schulz, M. Aguiar, S.P. Gygi, J.F. Bazan, and M.V. Nachury. 2010. The conserved Bardet-Biedl syndrome proteins assemble a coat that traffics membrane proteins to cilia. *Cell*. 141:1208-1219.

Kaczanowska, J., E. Joachimiak, L. Buzanska, W. Krawczynska, D.N. Wheatley, and A. Kaczanowski. 1999. Molecular subdivision of the cortex of dividing Tetrahymena is coupled with the formation of the fission zone. *Dev Biol*. 212:150-164.

Kim, S., K. Lee, J.H. Choi, N. Ringstad, and B.D. Dynlacht. 2015. Nek2 activation of Kif24 ensures cilium disassembly during the cell cycle. *Nature communications*. 6:8087.

Kim, S., N.A. Zaghloul, E. Bubenshchikova, E.C. Oh, S. Rankin, N. Katsanis, T. Obara, and L. Tsiokas. 2011. Nde1-mediated inhibition of ciliogenesis affects cell cycle re-entry. *Nat Cell Biol*. 13:351-360.

Kozminski, K.G. 1995. High-resolution imaging of flagella. *Methods Cell Biol*. 47:263-271.

Kozminski, K.G., P.L. Beech, and J.L. Rosenbaum. 1995. The Chlamydomonas kinesin-like protein FLA10 is involved in motility associated with the flagellar membrane. *The Journal of cell biology*. 131:1517-1527.

Kozminski, K.G., K.A. Johnson, P. Forscher, and J.L. Rosenbaum. 1993. A motility in the eukaryotic flagellum unrelated to flagellar beating. *Proceedings of the National Academy of Sciences of the United States of America*. 90:5519-5523.

Kubo, T., J.M. Brown, K. Bellve, B. Craige, J.M. Craft, K. Fogarty, K.F. Lechtreck, and G.B. Witman. 2016. Together, the IFT81 and IFT74 N-termini form the main module for intraflagellar transport of tubulin. *Journal of cell science*. 129:2106-2119.

Kubo, T., M. Hirono, T. Aikawa, R. Kamiya, and G.B. Witman. 2015. Reduced tubulin polyglutamylation suppresses flagellar shortness in Chlamydomonas. *Mol Biol Cell*. 26:2810-2822.

Kukic, I., F. Rivera-Molina, and D. Toomre. 2016. The IN/OUT assay: a new tool to study ciliogenesis. *Cilia*. 5:23.

Kushida, Y., M. Takaine, K. Nakano, T. Sugai, K.K. Vasudevan, M. Guha, Y.Y. Jiang, J. Gaertig, and O. Numata. 2016. Kinesin-14 is Important for Chromosome Segregation During Mitosis and Meiosis in the Ciliate Tetrahymena thermophila. *The Journal of eukaryotic microbiology*.

Lechtreck, K.F. 2013. In vivo imaging of IFT in Chlamydomonas flagella. *Methods in enzymology*. 524:265-284.

Lechtreck, K.F., P. Delmotte, M.L. Robinson, M.J. Sanderson, and G.B. Witman. 2008.

Mutations in Hydin impair ciliary motility in mice. *The Journal of cell biology*. 180:633-643.

Lechtreck, K.F., and S. Geimer. 2000. Distribution of polyglutamylated tubulin in the flagellar apparatus of green flagellates. *Cell motility and the cytoskeleton*. 47:219-235.

Lechtreck, K.F., E.C. Johnson, T. Sakai, D. Cochran, B.A. Ballif, J. Rush, G.J. Pazour, M. Ikebe, and G.B. Witman. 2009. The Chlamydomonas reinhardtii BBSome is an IFT cargo required for export of specific signaling proteins from flagella. *The Journal of cell biology*. 187:1117-1132.

Lechtreck, K.F., J.C. Van De Weghe, J.A. Harris, and P. Liu. 2017. Protein transport in growing and steady-state cilia. *Traffic*.

LeDizet, M., and G. Piperno. 1995. The light chain p28 associates with a subset of inner dynein arm heavy chains in Chlamydomonas axonemes. *Mol Biol Cell*. 6:697-711.

Lee, K.H., Y. Johmura, L.R. Yu, J.E. Park, Y. Gao, J.K. Bang, M. Zhou, T.D. Veenstra, B. Yeon Kim, and K.S. Lee. 2012. Identification of a novel Wnt5a-CK1varepsilon-Dvl2-Plk1-mediated primary cilia disassembly pathway. *The EMBO journal*. 31:3104-3117.

Lefebvre, P.A., S.A. Nordstrom, J.E. Moulder, and J.L. Rosenbaum. 1978. Flagellar elongation and shortening in Chlamydomonas. IV. Effects of flagellar detachment, regeneration, and resorption on the induction of flagellar protein synthesis. *The Journal of cell biology*. 78:8-27.

Levy, D.L., and R. Heald. 2012. Mechanisms of intracellular scaling. *Annual review of cell and developmental biology*. 28:113-135.

Li, A., M. Saito, J.Z. Chuang, Y.Y. Tseng, C. Dedesma, K. Tomizawa, T. Kaitsuka, and C.H. Sung. 2011. Ciliary transition zone activation of phosphorylated Tctex-1 controls ciliary resorption, S-phase entry and fate of neural progenitors. *Nat Cell Biol*. 13:402-411.

Liang, Y., D. Meng, B. Zhu, and J. Pan. 2016. Mechanism of ciliary disassembly. *Cellular and molecular life sciences : CMLS*. 73:1787-1802.

Liang, Y., and J. Pan. 2013. Regulation of flagellar biogenesis by a calcium dependent protein kinase in Chlamydomonas reinhardtii. *PloS one*. 8:e69902.

Liang, Y., Y. Pang, Q. Wu, Z. Hu, X. Han, Y. Xu, H. Deng, and J. Pan. 2014. FLA8/KIF3B Phosphorylation Regulates Kinesin-II Interaction with IFT-B to Control IFT Entry and Turnaround. *Developmental cell*. 30:585-597.

Lim, Y.S., and B.L. Tang. 2013. Getting into the cilia: nature of the barrier(s). *Mol Membr Biol*. 30:350-354.

Lin, H., Z. Zhang, S. Guo, F. Chen, J.M. Kessler, Y.M. Wang, and S.K. Dutcher. 2015. A NIMA-Related Kinase Suppresses the Flagellar Instability Associated with the Loss of Multiple Axonemal Structures. *PLoS genetics*. 11:e1005508.

Liu, Q., J. Zuo, and E.A. Pierce. 2004. The retinitis pigmentosa 1 protein is a photoreceptor microtubule-associated protein. *The Journal of neuroscience : the official journal of the Society for Neuroscience*. 24:6427-6436.

Liu, S., W. Lu, T. Obara, S. Kuida, J. Lehoczky, K. Dewar, I.A. Drummond, and D.R. Beier.

2002. A defect in a novel Nek-family kinase causes cystic kidney disease in the mouse and in zebrafish. *Development*. 129:5839-5846.

Long, H., and K. Huang. 2013. Analysis of flagellar protein ubiquitination. *Methods in enzymology*. 524:59-73.

Long, H., Q. Wang, and K. Huang. 2015. Ciliary/Flagellar Protein Ubiquitination. *Cells*. 4:474-482.

Lucker, B.F., R.H. Behal, H. Qin, L.C. Siron, W.D. Taggart, J.L. Rosenbaum, and D.G. Cole. 2005. Characterization of the intraflagellar transport complex B core: direct interaction of the IFT81 and IFT74/72 subunits. *The Journal of biological chemistry*. 280:27688-27696.

Ludington, W.B., K.A. Wemmer, K.F. Lechtreck, G.B. Witman, and W.F. Marshall. 2013. Avalanche-like behavior in ciliary import. *Proceedings of the National Academy of Sciences of the United States of America*.

Luo, M., M. Cao, Y. Kan, G. Li, W. Snell, and J. Pan. 2011. The phosphorylation state of an aurora-like kinase marks the length of growing flagella in Chlamydomonas. *Current biology : CB*. 21:586-591.

Marshall, W.F., H. Qin, M. Rodrigo Brenni, and J.L. Rosenbaum. 2005. Flagellar length control system: testing a simple model based on intraflagellar transport and turnover. *Mol Biol Cell*. 16:270-278.

Marshall, W.F., and J.L. Rosenbaum. 2001. Intraflagellar transport balances continuous turnover of outer doublet microtubules: implications for flagellar length control. *The Journal of cell biology*. 155:405-414.

Maskey, D., M.C. Marlin, S. Kim, S. Kim, E.C. Ong, G. Li, and L. Tsiokas. 2015. Cell cycle-dependent ubiquitylation and destruction of NDE1 by CDK5-FBW7 regulates ciliary length. *The EMBO journal*. 34:2424-2440.

Massinen, S., M.E. Hokkanen, H. Matsson, K. Tammimies, I. Tapia-Paez, V. Dahlstrom-Heuser, J. Kuja-Panula, J. Burghoorn, K.E. Jeppsson, P. Swoboda, M. Peyrard-Janvid, R. Toftgard, E. Castren, and J. Kere. 2011. Increased expression of the dyslexia candidate gene DCDC2 affects length and signaling of primary cilia in neurons. *PloS one*. 6:e20580.

Meehl, J.B., B.A. Bayless, T.H. Giddings, Jr., C.G. Pearson, and M. Winey. 2016. Tetrahymena Poc1 ensures proper intertriplet microtubule linkages to maintain basal body integrity. *Mol Biol Cell*. 27:2394-2403.

Meng, D., and J. Pan. 2016. A NIMA-related kinase, CNK4, regulates ciliary stability and length. *Mol Biol Cell*. 27:838-847.

Michelmore, R.W., I. Paran, and R.V. Kesseli. 1991. Identification of markers linked to disease-resistance genes by bulked segregant analysis: a rapid method to detect markers in specific genomic regions by using segregating populations. *Proceedings of the National Academy of Sciences of the United States of America*. 88:9828-9832.

Minevich, G., D.S. Park, D. Blankenberg, R.J. Poole, and O. Hobert. 2012. CloudMap: a cloud-based pipeline for analysis of mutant genome sequences. *Genetics*. 192:1249-1269.

Miyamoto, T., K. Hosoba, H. Ochiai, E. Royba, H. Izumi, T. Sakuma, T. Yamamoto, B.D. Dynlacht, and S. Matsuura. 2015. The Microtubule-Depolymerizing Activity of a Mitotic Kinesin Protein KIF2A Drives Primary Cilia Disassembly Coupled with Cell Proliferation. *Cell reports*.

Mohieldin, A.M., H.S. Zubayer, A.J. Al Omran, H.C. Saternos, A.A. Zarban, S.M. Nauli, and W.A. AbouAlaiwi. 2016. Vascular Endothelial Primary Cilia: Mechanosensation and Hypertension. *Curr Hypertens Rev*. 12:57-67.

Moon, H., J. Song, J.O. Shin, H. Lee, H.K. Kim, J.T. Eggenschwiller, J. Bok, and H.W. Ko. 2014. Intestinal cell kinase, a protein associated with endocrine-cerebro-osteodysplasia syndrome, is a key regulator of cilia length and Hedgehog signaling. *Proceedings of the National Academy of Sciences of the United States of America*. 111:8541-8546.

Motegi, F., S. Zonies, Y. Hao, A.A. Cuenca, E. Griffin, and G. Seydoux. 2011. Microtubules induce self-organization of polarized PAR domains in Caenorhabditis elegans zygotes. *Nat Cell Biol*. 13:1361-1367.

Nachury, M.V., A.V. Loktev, Q. Zhang, C.J. Westlake, J. Peranen, A. Merdes, D.C. Slusarski, R.H. Scheller, J.F. Bazan, V.C. Sheffield, and P.K. Jackson. 2007. A core complex of BBS proteins cooperates with the GTPase Rab8 to promote ciliary membrane biogenesis. *Cell*. 129:1201-1213.

Numata, O., H. Suzuki, H. Ohba, and Y. Watanabe. 1995. The mutant gene product of a Tetrahymena cell-division-arrest mutant cdaA is localized in the accessory structure of specialized basal body close to the division furrow. *Zoolog.Sci.* 12:133-135.

O'Hagan, R., B.P. Piasecki, M. Silva, P. Phirke, K.C. Nguyen, D.H. Hall, P. Swoboda, and M.M. Barr. 2011. The tubulin deglutamylase CCPP-1 regulates the function and stability of sensory cilia in C. elegans. *Current biology : CB*. 21:1685-1694.

Oda, T., H. Yanagisawa, R. Kamiya, and M. Kikkawa. 2014. A molecular ruler determines the repeat length in eukaryotic cilia and flagella. *Science*. 346:857-860.

Omori, Y., T. Chaya, K. Katoh, N. Kajimura, S. Sato, K. Muraoka, S. Ueno, T. Koyasu, M. Kondo, and T. Furukawa. 2010. Negative regulation of ciliary length by ciliary male germ cell-associated kinase (Mak) is required for retinal photoreceptor survival. *Proceedings of the National Academy of Sciences of the United States of America*. 107:22671-22676.

Orias, E. 2012. Tetrahymena thermophila genetics: concepts and applications. *Methods Cell Biol*. 109:301-325.

Ou, G., O.E. Blacque, J.J. Snow, M.R. Leroux, and J.M. Scholey. 2005. Functional coordination of intraflagellar transport motors. *Nature*. 436:583-587.

Oud, M.M., C. Bonnard, D.A. Mans, U. Altunoglu, S. Tohari, A.Y. Ng, A. Eskin, H. Lee, C.A. Rupar, N.P. de Wagenaar, K.M. Wu, P. Lahiry, G.J. Pazour, S.F. Nelson, R.A. Hegele, R. Roepman, H. Kayserili, B. Venkatesh, V.M. Siu, B. Reversade, and H.H. Arts. 2016. A novel ICK mutation causes ciliary disruption and lethal endocrine-cerebro-osteodysplasia syndrome. *Cilia*. 5:8.

Ozgul, R.K., A.M. Siemiatkowska, D. Yucel, C.A. Myers, R.W. Collin, M.N. Zonneveld, A.

Beryozkin, E. Banin, C.B. Hoyng, L.I. van den Born, C. European Retinal Disease, R. Bose, W. Shen, D. Sharon, F.P. Cremers, B.J. Klevering, A.I. den Hollander, and J.C. Corbo. 2011. Exome sequencing and cis-regulatory mapping identify mutations in MAK, a gene encoding a regulator of ciliary length, as a cause of retinitis pigmentosa. *American journal of human genetics*. 89:253-264.

Pan, J., and W.J. Snell. 2005. Chlamydomonas shortens its flagella by activating axonemal disassembly, stimulating IFT particle trafficking, and blocking anterograde cargo loading. *Developmental cell*. 9:431-438.

Pan, J., and W.J. Snell. 2014. Organelle Size: A Cilium Length Signal Regulates IFT Cargo Loading. *Current biology : CB*. 24:R75-78.

Pan, J., Q. Wang, and W.J. Snell. 2004. An aurora kinase is essential for flagellar disassembly in Chlamydomonas. *Developmental cell*. 6:445-451.

Pan, X., G. Ou, G. Civelekoglu-Scholey, O.E. Blacque, N.F. Endres, L. Tao, A. Mogilner, M.R. Leroux, R.D. Vale, and J.M. Scholey. 2006. Mechanism of transport of IFT particles in C. elegans cilia by the concerted action of kinesin-II and OSM-3 motors. *The Journal of cell biology*. 174:1035-1045.

Pathak, N., T. Obara, S. Mangos, Y. Liu, and I.A. Drummond. 2007. The zebrafish fleer gene encodes an essential regulator of cilia tubulin polyglutamylation. *Mol Biol Cell*. 18:4353-4364.

Pazour, G.J., B.L. Dickert, and G.B. Witman. 1999. The DHC1b (DHC2) isoform of cytoplasmic dynein is required for flagellar assembly. *The Journal of cell biology*. 144:473-481.

Pazour, G.J., C.G. Wilkerson, and G.B. Witman. 1998. A dynein light chain is essential for the retrograde particle movement of intraflagellar transport (IFT). *The Journal of cell biology*. 141:979-992.

Pearson, C.G., D.P. Osborn, T.H. Giddings, Jr., P.L. Beales, and M. Winey. 2009. Basal body stability and ciliogenesis requires the conserved component Poc1. *The Journal of cell biology*. 187:905-920.

Pigino, G., A. Maheshwari, K.H. Bui, C. Shingyoji, S. Kamimura, and T. Ishikawa. 2012. Comparative structural analysis of eukaryotic flagella and cilia from Chlamydomonas, Tetrahymena, and sea urchins. *Journal of structural biology*. 178:199-206.

Piperno, G., and K. Mead. 1997. Transport of a novel complex in the cytoplasmic matrix of Chlamydomonas flagella. *Proceedings of the National Academy of Sciences of the United States of America*. 94:4457-4462.

Piperno, G., E. Siuda, S. Henderson, M. Segil, H. Vaananen, and M. Sassaroli. 1998. Distinct mutants of retrograde intraflagellar transport (IFT) share similar morphological and molecular defects. *The Journal of cell biology*. 143:1591-1601.

Porter, M.E., R. Bower, J.A. Knott, P. Byrd, and W. Dentler. 1999. Cytoplasmic dynein heavy chain 1b is required for flagellar assembly in Chlamydomonas. *Mol Biol Cell*. 10:693-712.

Portman, R.W., E.L. LeCluyse, and W.L. Dentler. 1987. Development of microtubule capping structures in ciliated epithelial cells. *Journal of cell science*. 87 (Pt 1):85-94.

Prasad, R.M., X. Jin, and S.M. Nauli. 2014. Sensing a sensor: identifying the mechanosensory function of primary cilia. *Biosensors (Basel)*. 4:47-62.

Pugacheva, E.N., S.A. Jablonski, T.R. Hartman, E.P. Henske, and E.A. Golemis. 2007. HEF1-dependent Aurora A activation induces disassembly of the primary cilium. *Cell*. 129:1351-1363.

Rajagopalan, V., A. Subramanian, D.E. Wilkes, D.G. Pennock, and D.J. Asai. 2009. Dynein-2 affects the regulation of ciliary length but is not required for ciliogenesis in Tetrahymena thermophila. *Mol Biol Cell*. 20:708-720.

Reck, J., A.M. Schauer, K. VanderWaal Mills, R. Bower, D. Tritschler, C.A. Perrone, and M.E. Porter. 2016. The role of the dynein light intermediate chain in retrograde IFT and flagellar function in Chlamydomonas. *Mol Biol Cell*. 27:2404-2422.

Reiner, O., F.M. Coquelle, B. Peter, T. Levy, A. Kaplan, T. Sapir, I. Orr, N. Barkai, G. Eichele, and S. Bergmann. 2006. The evolving doublecortin (DCX) superfamily. *BMC genomics*. 7:188.

Reiter, J.F., O.E. Blacque, and M.R. Leroux. 2012. The base of the cilium: roles for transition fibres and the transition zone in ciliary formation, maintenance and compartmentalization. *EMBO reports*. 13:608-618.

Rohatgi, R., and W.J. Snell. 2010. The ciliary membrane. *Current opinion in cell biology*. 22:541-546.

Rosenbaum, J.L., and K. Carlson. 1969. Cilia regeneration in Tetrahymena and its inhibition by colchicine. *The Journal of cell biology*. 40:415-425.

Rosenbaum, J.L., J.E. Moulder, and D.L. Ringo. 1969a. FLAGELLAR ELONGATION AND SHORTENING IN CHLAMYDOMONAS : The Use of Cycloheximide and Colchicine to Study the Synthesis and Assembly of Flagellar Proteins. *The Journal of cell biology*. 41:600-619.

Rosenbaum, J.L., J.E. Moulder, and D.L. Ringo. 1969b. Flagellar elongation and shortening in Chlamydomonas. The use of cycloheximide and colchicine to study the synthesis and assembly of flagellar proteins. *The Journal of cell biology*. 41:600-619.

Salo, E., and J. Baguna. 1984. Regeneration and pattern formation in planarians. I. The pattern of mitosis in anterior and posterior regeneration in Dugesia (G) tigrina, and a new proposal for blastema formation. *Journal of embryology and experimental morphology*. 83:63-80.

Satir, P. 1980. Structural basis of ciliary movement. *Environ Health Perspect*. 35:77-82.

Satir, P., T. Heuser, and W.S. Sale. 2014. A Structural Basis for How Motile Cilia Beat. *Bioscience*. 64:1073-1083.

Shah, A.S., Y. Ben-Shahar, T.O. Moninger, J.N. Kline, and M.J. Welsh. 2009. Motile cilia of human airway epithelia are chemosensory. *Science*. 325:1131-1134.

Shakir, M.A., T. Fukushige, H. Yasuda, J. Miwa, and S.S. Siddiqui. 1993. C. elegans osm-3 gene mediating osmotic avoidance behaviour encodes a kinesin-like protein. *Neuroreport*. 4:891-894.

Shang, Y., X. Song, J. Bowen, R. Corstanje, Y. Gao, J. Gaertig, and M.A. Gorovsky. 2002. A

robust inducible-repressible promoter greatly facilitates gene knockouts, conditional expression, and overexpression of homologous and heterologous genes in Tetrahymena thermophila. *Proceedings of the National Academy of Sciences of the United States of America*. 99:3734-3739.

Signor, D., K.P. Wedaman, J.T. Orozco, N.D. Dwyer, C.I. Bargmann, L.S. Rose, and J.M. Scholey. 1999. Role of a class DHC1b dynein in retrograde transport of IFT motors and IFT raft particles along cilia, but not dendrites, in chemosensory neurons of living Caenorhabditis elegans. *The Journal of cell biology*. 147:519-530.

Sirajuddin, M., L.M. Rice, and R.D. Vale. 2014. Regulation of microtubule motors by tubulin isotypes and post-translational modifications. *Nat Cell Biol*. 16:335-344.

Slaats, G.G., C.R. Isabella, H.Y. Kroes, J.C. Dempsey, H. Gremmels, G.R. Monroe, I.G. Phelps, K.J. Duran, J. Adkins, S.A. Kumar, D.M. Knutzen, N.V. Knoers, N.J. Mendelsohn, D. Neubauer, S.D. Mastroyianni, J. Vogt, L. Worgan, N. Karp, S. Bowdin, I.A. Glass, M.A. Parisi, E.A. Otto, C.A. Johnson, F. Hildebrandt, G. van Haaften, R.H. Giles, and D. Doherty. 2016. MKS1 regulates ciliary INPP5E levels in Joubert syndrome. *Journal of medical genetics*. 53:62-72.

Snow, J.J., G. Ou, A.L. Gunnarson, M.R. Walker, H.M. Zhou, I. Brust-Mascher, and J.M. Scholey. 2004. Two anterograde intraflagellar transport motors cooperate to build sensory cilia on C. elegans neurons. *Nat Cell Biol*. 6:1109-1113.

Song, L., and W.L. Dentler. 2001. Flagellar protein dynamics in Chlamydomonas. *The Journal of biological chemistry*. 276:29754-29763.

Sorokin, S. 1962. Centrioles and the formation of rudimentary cilia by fibroblasts and smooth muscle cells. *The Journal of cell biology*. 15:363-377.

Sorokin, S.P. 1968a. Centriole formation and ciliogenesis. *Aspen Emphysema Conf*. 11:213-216.

Sorokin, S.P. 1968b. Reconstructions of centriole formation and ciliogenesis in mammalian lungs. *Journal of cell science*. 3:207-230.

Stepanek, L., and G. Pigino. 2016. Microtubule doublets are double-track railways for intraflagellar transport trains. *Science*. 352:721-724.

Stone, E.M., X. Luo, E. Heon, B.L. Lam, R.G. Weleber, J.A. Halder, L.M. Affatigato, J.B. Goldberg, A. Sumaroka, S.B. Schwartz, A.V. Cideciyan, and S.G. Jacobson. 2011. Autosomal recessive retinitis pigmentosa caused by mutations in the MAK gene. *Investigative ophthalmology & visual science*. 52:9665-9673.

Suryavanshi, S., B. Edde, L.A. Fox, S. Guerrero, R. Hard, T. Hennessey, A. Kabi, D. Malison, D. Pennock, W.S. Sale, D. Wloga, and J. Gaertig. 2010. Tubulin glutamylation regulates ciliary motility by altering inner dynein arm activity. *Current biology : CB*. 20:435-440.

Szymanska, K., and C.A. Johnson. 2012. The transition zone: an essential functional compartment of cilia. *Cilia*. 1:10.

Takao, D., and K.J. Verhey. 2016. Gated entry into the ciliary compartment. *Cellular and molecular life sciences : CMLS*. 73:119-127.

Tam, L.W., and P.A. Lefebvre. 1993. Cloning of flagellar genes in Chlamydomonas reinhardtii

by DNA insertional mutagenesis. *Genetics*. 135:375-384.

Tam, L.W., P.T. Ranum, and P.A. Lefebvre. 2013. CDKL5 Regulates Flagellar Length and Localizes to the Base of the Flagella in Chlamydomonas. *Mol Biol Cell*.

Tammachote, R., C.J. Hommerding, R.M. Sinders, C.A. Miller, P.G. Czarnecki, A.C. Leightner, J.L. Salisbury, C.J. Ward, V.E. Torres, V.H. Gattone, 2nd, and P.C. Harris. 2009. Ciliary and centrosomal defects associated with mutation and depletion of the Meckel syndrome genes MKS1 and MKS3. *Human molecular genetics*. 18:3311-3323.

Taschner, M., S. Bhogaraju, and E. Lorentzen. 2012. Architecture and function of IFT complex proteins in ciliogenesis. *Differentiation; research in biological diversity*. 83:S12-22.

Taschner, M., and E. Lorentzen. 2016. The Intraflagellar Transport Machinery. *Cold Spring Harb Perspect Biol*. 8.

Taylor, S.P., T.J. Dantas, I. Duran, S. Wu, R.S. Lachman, C. University of Washington Center for Mendelian Genomics, S.F. Nelson, D.H. Cohn, R.B. Vallee, and D. Krakow. 2015. Mutations in DYNC2LI1 disrupt cilia function and cause short rib polydactyly syndrome. *Nature communications*. 6:7092.

Thiel, C., K. Kessler, A. Giessl, A. Dimmler, S.A. Shalev, S. von der Haar, M. Zenker, D. Zahnleiter, H. Stoss, E. Beinder, R. Abou Jamra, A.B. Ekici, N. Schroder-Kress, T. Aigner, T. Kirchner, A. Reis, J.H. Brandstatter, and A. Rauch. 2011. NEK1 mutations cause short-rib polydactyly syndrome type majewski. *American journal of human genetics*. 88:106-114.

Thorpe, S.D., S. Gambassi, C.L. Thompson, C. Chandrakumar, A. Santucci, and M.M. Knight. 2017. Reduced Primary Cilia Length and Altered Arl13b Expression Are Associated with Deregulated Chondrocyte Hedgehog Signalling in Alkaptonuria. *Journal of cellular physiology*.

Tilley, A.E., M.S. Walters, R. Shaykhiev, and R.G. Crystal. 2015. Cilia dysfunction in lung disease. *Annu Rev Physiol*. 77:379-406.

Tooze, S.A., and I. Dikic. 2016. Autophagy Captures the Nobel Prize. *Cell*. 167:1433-1435.

Upadhya, P., E.H. Birkenmeier, C.S. Birkenmeier, and J.E. Barker. 2000. Mutations in a NIMA-related kinase gene, Nek1, cause pleiotropic effects including a progressive polycystic kidney disease in mice. *Proceedings of the National Academy of Sciences of the United States of America*. 97:217-221.

Urbanska, P., K. Song, E. Joachimiak, L. Krzemien-Ojak, P. Koprowski, T. Hennessey, M. Jerka-Dziadosz, H. Fabczak, J. Gaertig, D. Nicastro, and D. Wloga. 2015. The CSC proteins FAP61 and FAP251 build the basal substructures of radial spoke 3 in cilia. *Mol Biol Cell*. 26:1463-1475.

Vasudevan, K.K., Y.Y. Jiang, K.F. Lechtreck, Y. Kushida, L.M. Alford, W.S. Sale, T. Hennessey, and J. Gaertig. 2015. Kinesin-13 regulates the quantity and quality of tubulin inside cilia. *Mol Biol Cell*. 26:478-494.

Vincensini, L., T. Blisnick, and P. Bastin. 2011. 1001 model organisms to study cilia and flagella. *Biology of the cell / under the auspices of the European Cell Biology Organization*. 103:109-130.

Waclawek, E., E. Joachimiak, M.H. Hall, H. Fabczak, and D. Wloga. 2017. Regulation of katanin activity in the ciliate Tetrahymena thermophila. *Molecular microbiology*. 103:134-150.

Walther, Z., M. Vashishtha, and J.L. Hall. 1994. The Chlamydomonas FLA10 gene encodes a novel kinesin-homologous protein. *The Journal of cell biology*. 126:175-188.

Wickstead, B., and K. Gull. 2007. Dyneins across eukaryotes: a comparative genomic analysis. *Traffic*. 8:1708-1721.

Winyard, P., and D. Jenkins. 2011. Putative roles of cilia in polycystic kidney disease. *Biochimica et biophysica acta*. 1812:1256-1262.

Wloga, D., A. Camba, K. Rogowski, G. Manning, M. Jerka-Dziadosz, and J. Gaertig. 2006. Members of the NIMA-related kinase family promote disassembly of cilia by multiple mechanisms. *Molecular biology of the cell*. 17:2799-2810.

Wloga, D., E. Joachimiak, P. Louka, and J. Gaertig. 2016. Posttranslational Modifications of Tubulin and Cilia. *Cold Spring Harb Perspect Biol*.

Wloga, D., K. Rogowski, N. Sharma, J. Van Dijk, C. Janke, B. Edde, M.H. Bre, N. Levilliers, V. Redeker, J. Duan, M.A. Gorovsky, M. Jerka-Dziadosz, and J. Gaertig. 2008. Glutamylation on alpha-tubulin is not essential but affects the assembly and functions of a subset of microtubules in Tetrahymena thermophila. *Eukaryotic cell*. 7:1362-1372.

Wloga, D., D.M. Webster, K. Rogowski, M.H. Bre, N. Levilliers, M. Jerka-Dziadosz, C. Janke, S.T. Dougan, and J. Gaertig. 2009. TTLL3 Is a tubulin glycine ligase that regulates the assembly of cilia. *Developmental cell*. 16:867-876.

Wren, K.N., J.M. Craft, D. Tritschler, A. Schauer, D.K. Patel, E.F. Smith, M.E. Porter, P. Kner, and K.F. Lechtreck. 2013. A differential cargo-loading model of ciliary length regulation by IFT. *Current biology : CB*. 23:2463-2471.

Yang, Y., N. Roine, and T.P. Makela. 2013. CCRK depletion inhibits glioblastoma cell proliferation in a cilium-dependent manner. *EMBO reports*.

CHAPTER 2

TOTAL INTERNAL REFLECTION FLUORESCENCE MICROSCOPY OF INTRAFLAGELLAR TRANSPORT IN *TETRAHYMENA THERMOPHILA*[1]

[1] Jiang, Y.Y., K. Lechtreck, and J. Gaertig. 2015. *Methods Cell Biol.* 127:445-456. Reprinted here with permission of the publisher.

ABSTRACT

Live imaging has become a powerful tool in studies of ciliary proteins. *Tetrahymena thermophila* is an established ciliated model with well-developed genetic and biochemical approaches, but its large size, complex shape and the large number of short and overlapping cilia, have made live imaging of ciliary proteins challenging. Here we describe a method that combines paralysis of cilia by nickel ions and total internal reflection microscopy for live imaging of fluorescent proteins inside cilia of *Tetrahymena*. Using this method, we quantitatively documented the intraflagellar transport in *Tetrahymena*.

INTRODUCTION

Many features make *Tetrahymena thermophila* an excellent model for studies of cilia, including the large number of cilia per cell, rapid growth in axenic media, and high maximal cell density (1 x 10^6 cells/ml), (reviewed in Gaertig et al. (2013)). Each *Tetrahymena* cell possesses between 500-1000 locomotory and oral cilia that can be excised from the cell body by artificial deciliation, which triggers rapid regeneration of a new set of cilia. The *Tetrahymena* population can be synchronized in the cell cycle either by starvation (Mowat et al., 1974) or by size selection using centrifugation/elutriation (Marsh et al., 2000). Classical genetics (including ability to make whole genome homozygotes) can be combined with gene targeting by homologous DNA recombination (reviewed by Orias (2012)). Conditional gene overexpression based on heavy metal-inducible promoters can be used to produce and purify proteins or to create hypermorphic phenotypes (Shang et al., 2002b). Gene products can be localized with precision by fusion with an epitope tag at the native loci (reviewed in (Gaertig et al., 2013)). While detection of gene products of interest can be done with ease in fixed cells using

fluorescence or electron microscopy, live imaging of fluorescence-tagged proteins has been used only sparingly (reviewed in Winey et al. (2012)).

Imaging ciliary proteins *in vivo* has been technically challenging in *Tetrahymena*. In particular, studies of the intraflagellar transport (IFT) have been limited by the lack of an imaging solution. IFT is a bidirectional motility that occurs inside cilia and is required for assembly and maintenance of cilia. During IFT, motor proteins, kinesin-2 and IFT dynein (DH1B), move protein complexes, IFT trains, along the side of outer doublet microtubules; the IFT trains carry ciliary precursors as cargo (reviewed in (Pedersen and Rosenbaum, 2008; Scholey, 2003)). IFT was discovered in cilia of *Chlamydomonas reinhardtii* by video-enhanced differential interference microscopy (Kozminski et al., 1993).

Not limited to imaging of IFT, TIRFM is highly suitable for detection of non-abundant ciliary proteins, and tracking of ciliary protein dynamics in real time. TIRFM has brought new information about the mechanisms that govern cilia assembly, disassembly, length regulation and cilia-based signaling (Avasthi and Marshall, 2012; Engel et al., 2009; Lechtreck et al., 2009; Ludington et al., 2013; Pan and Snell, 2014; Wren et al., 2013). Here we describe an approach that allows the application of TIRFM to study IFT in *Tetrahymena*. Combined with the existing biochemical, genetic and traditional microscopy capabilities, TIRFM-based live imaging greatly increases the value of the *Tetrahymena* model for studies of cilia.

TIRF MICROSCOPE CONFIGURATION AND DATA ANALYSIS IN APPLICATION TO IFT IN *TETRAHYMENA*

The configuration of the TIRF microscope is the same as recently described for *Chlamydomonas* (Lechtreck, 2013). In brief, we used a TIRF system house-built around a Nikon Eclips Ti-U microscope. The microscope is equipped with a GFP/mCherry TIRF filter cube, a

60x NA 1.49 TIRF objective and an Andor iXON X3 DU897 EMCCD camera (with a C mount and a 2.5 x lens). The GFP is excited using a 488-nm diode laser, 40 mW (Spectraphysics) with two density filter wheels (Newport) to adjust the illumination intensity. The images and videos are digitally recorded with the Nikon Elements emission software module.

The analysis of imaging data is also adopted from Lechtreck (2013). NIH ImageJ (Rasband, 1997-2014) was used to generate kymographs and measure IFT particle velocities. In brief, videos of 30 sec were recorded at a frame rate of 15 fps. Some of the videos are not suitable because the imaged cells are not sufficiently immobilized (see III.B.). A high quality video typically covers a few dozens of cilia with detectable IFT in one cell. Only a handful of these cilia are selected for generating kymographs of IFT particles. The individual cilia that are suitable for the production of kymographs fulfill the following criteria: 1) remain in focus along the entire length, 2) are relatively straight and remain immobile, 3) do not overlap with other cilia and 4) their base to tip orientation can be determined. Using ImageJ, a straight line is manually drawn to highlight the selected cilium, from its base to the tip. Then a kymograph is generated with the "Multiple Kymograph" function of the Kymograph plugin (Rietdorf and Seitz, 2004) of ImageJ. After rotating the kymograph 90 degree counterclockwise, the time lapses from left to right and the bottom of the image indicate the base of the cilium. A diagonal trajectory shown in the kymograph represent an actively moving IFT particle. An anterograde IFT will result in a trajectory from left-bottom to right-top, and a retrograde IFT will produce a trajectory from the left-top to the right-bottom. The velocity is measured as the distance divided by the time period of an IFT movement.

USING A TIRF MICROSCOPE TO IMAGE *TETRAHYMENA* CILIA

Tetrahymena cells are challenging for live imaging of cilia. The cells move rapidly and do not adhere to glass. The *Tetrahymena* cell has a relatively large diameter (20-60 µm) compared to the length of the cilia (about 6 µm), and the locomotory cilia are located inside cortical grooves (reviewed in Wloga and Frankel (2012)). Despite the absence of chloroplasts, there is noticeable autofluorescence in the cell body that interferes with imaging even at a steep TIRF illuminating angle. When the cells are trapped under the coverglass, the cilia overlap and bundle. Consequently, the positions of the ciliary tips and the bases are difficult or impossible to determine, preventing the orientation of IFT tracks. Our approach to reduce the impact of some of these obstacles was to combine trapping of cells in a limited volume of medium with immobilization of cilia using nickel ions (see below).

GFP-Dyf1 is a suitable IFT marker in *Tetrahymena*

Using TIRFM, we tested several GFP-tagged IFT proteins as markers for imaging IFT, including Kin1p, a motor subunit of kinesin-2, the anterograde IFT motor (Brown et al., 1999), and components of the IFT complex B: Ift52p (Brown et al., 2003) and Dyf1p (Dave et al., 2009). In each case, the GFP fusion was expressed in its own gene knockout background and rescued the loss of cilia phenotype, indicating its functionality. The GFP-Kin1p was expressed under its own promoter and in its own locus, while the GFP-Ift52p and the GFP-Dyf1p were expressed under the cadmium-inducible *MTT1* promoter (Shang et al., 2002a) in the non-essential *BTU1* locus (these cells were maintained without cadmium induction as the non-induced *MTT1* promoter has a basal level of expression that is sufficient for rescue of the respective null phenotype). GFP-Dyfp1 was found to be a superior IFT marker that revealed IFT tracks with the highest signal intensity and few stationary particles (supplemental videos 1 and 2).

Immobilization of *Tetrahymena* cilia to observe IFT

Simply pressing the *Tetrahymena* cells with a coverglass does not immobilize most cilia sufficiently well. Occasionally, a cilium is sufficiently immobile for imaging but this is rare. Most cilia continue to beat and at some point, bundle (Fig. 1.1A). Among cilia that do not bundle, most do not lay straight (Fig. 1.1B). Neither bundled nor bent cilia are suitable for quantification of IFT events.

We tried several methods to immobilize *Tetrahymena* cells prior to TIRFM observations. Coating coverglasses with poly-L-lysine did not increase the adhesion and immobilization of cells. Embedding cells in 2-5% low melting temperature point agarose resulted in encapsulation of cells, which maintain vigorously beating cilia (the agar failed to solidify in a narrow zone around beating cilia). We found that the most practical immobilization method is simply placing cells in a small volume of media, which results in a pressure from the coverglass that flattens the cells and presses the cilia against the glass, and allows for a 15-25 min observation, before the cells burst. Under these conditions, however, most cilia continue to twitch and the number of cilia suitable for imaging is very low.

To further reduce the motility of cilia, in one attempt we labeled the surface of cells with NHS-LC-LC-biotin, and mounted onto a coverglass coated with streptavidin. The attachment of biotinylated cilia to the streptavidin-coated coverglass was noticeable, yet too weak to hold the cilia sufficiently stable for a 30 sec recording, as the cilia continued to twitch. We had similar negative experiences with the use of coverglasses coated with lectins, (concanavalin A, peanut agglutinin). We then used Ni^{2+} ions, an established axonemal dynein inhibitor, to inhibit ciliary beating (Larsen and Satir, 1991). We found that in the presence of 2-3 µM $NiCl_2$, the cells stop moving within 3 min and most cilia remain immobile when pressed against the glass. In the Ni^{2+}

observation medium (see section III.C.), the cells burst within 10-15 min post mounting. Most cells treated with Ni^{2+} are suitable for recording. For each microscope slide, we were able to record about ten 30 sec videos, each covering a large number of cilia on one cell (supplemental videos 1 and 2). Under these conditions, the anterograde IFT is slower, more frequent and uniform in size, as compared to the retrograde IFT (Fig. 1.2). We noticed a significant variation in the frequencies of both the anterograde and retrograde IFT events between cilia on one cell and between different cells, which is likely a result of differential pressure against the glass (see section IV).

Experimental Protocol

Preparation of Tetrahymena cells:

Grow cells in SPP medium to 1-3 x 105 cells/ml.

Pellet 0.5-1 ml of cell culture by centrifugation at 1700 x g for 1 min.

Wash the pellet once with 10 mM Tris-HCl, pH 7.5 (Tris buffer).

This step is optional but highly recommended as it reduces the background of fluorescent debris from the medium.

Suspend the cells in 100-300 µl of Tris buffer.

Preparation of a slide specimen for TIRF imaging:

Mix 1 µl of 20 µM NiCl2 and 10 µl of washed cells (final concentration of NiCl2 is 2 µM) at the center of a 22 x 22 mm2 No. 1.5 coverglass (VWR #48366-227). If the cells are imaged in the SPP medium (containing 0.003% w/v EDTA-Fe-Na) a higher concentration of NiCl2 may be needed.

Use a glass slide to gently touch the droplet, and pick the coverglass up, forming an upside down assembled slide.

Mount the assembled slide onto the microscope stage with the coverglass facing down and hanging over the objective. Be cautious as flipping, shaking or resting the assembly will cause the coverglass to glide and this will crush the cells or rip off the cilia.

Recording images and videos of cilia and IFT:

Using bright-field illumination, find the correct focal position.

As the cells slow down within the first few min, the larger cells flatten first and the cilia at the mid-section of their cell bodies become “squeezed” onto the coverglass. Such cilia are optimal for imaging IFT as they are flat, uniformly close to glass and often aligned in one direction.

Perform TIRF imaging at a sufficiently steep angle to avoid autofluorescence of the cell bodies.

Under the above conditions, most slides last for 10-15 min. As the cells round up, IFT events become slower and less frequent and soon the cells burst. We avoid recording videos of IFT after the first 10 min since the slide assembles.

Effect of Ni^{2+} on the velocities of IFT

We were concerned about the potential side effect of Ni^{2+} on the retrograde IFT driven by the cytoplasmic dynein that contains the heavy chain DH1B (Pazour et al., 1999; Signor et al., 1999). However, unlike another dynein inhibitor, vanadate, that decreases the ATPase activity of both the axonemal outer and inner dynein arm (ODA and IDA) (Gibbons et al., 1978; Vale and Toyoshima, 1988) and the cytoplasmic dynein heavy chains (Cande and Wolniak, 1978; Kobayashi et al., 1978), Ni^{2+} abolishes IDA , but has only a minor effect on the ODA ATPase activity (Larsen and Satir, 1991), suggesting a degree of selectivity toward dynein subtypes. The retrograde IFT dynein heavy chain, DH1B, belongs to the cytoplasmic dynein subgroup of the dynein superfamily, that is evolutionarily distant from both IDA and ODA axonemal dyneins

(Wickstead and Gull, 2007; Wilkes et al., 2008). Nevertheless, we could not exclude a possibility that Ni^{2+} has a side effect on the IFT dynein heavy chain and consequently on the retrograde IFT in *Tetrahymena*.

We compared the anterograde and retrograde IFT velocities in the Ni^{2+} treated and untreated cells (while fewer cilia were suitable for imaging without Ni^{2+} immobilization, we were able to gather enough of data by examining a larger number of untreated cells). Using GFP-Dyf1p as a marker, the velocities of IFT particles were measured as is described in section II. To our surprise, the mean velocities of the anterograde and retrograde IFT of Ni^{2+} treated cilia were significantly higher than those from the untreated cilia (Fig. 1.3A, B). Both the anterograde and retrograde IFT velocities were increased by about 25%, suggesting the effect of Ni^{2+} is grounded in the methodology and does not reflect a real stimulatory effect of Ni^{2+} on the IFT motors.

We noticed that the IFT velocities histograms of the Ni^{2+}-treated cilia fit the normal distribution curves, while those of the untreated cilia lean towards the lower values (Fig. 1.3A', B'). Using an approach similar to ours, Brooks and Wallingford (2012) measured the velocities of the anterograde and retrograde IFT in *Xenopus* multiciliated cells, in cilia that were pressed against the coverglass by the gravity of the embryos. Their reported histograms of IFT velocities appear to fit the normal distribution (Figure 2 in Brooks and Wallingford (2012)), which are in agreement with our measurements from the Ni^{2+}-treated cilia. The simplest interpretation of the effect of Ni^{2+} in our experiments is that the slower IFT velocities of untreated cilia are an artifact caused by the inability to distinguish between cilia or their segments that lay flat on the cover glass or slightly bend away from the glass. When using the Kymograph ImageJ plugin to analyze IFT velocity, it is crucial that the straight line is fitted to a straight cilium. If the straight line is fitted to a slightly curved cilium and used to calculate the velocity of an IFT movement, the

measured velocity is the true velocity times the cosine of the curving angle. Curved cilia are clearly more frequent in untreated specimens (Fig. 1.1). Ni^{2+} rapidly impairs cilia motility and reduces cilia curving and bundling. In addition, Ni^{2+}-treated cilia are often aligned in one direction (Fig. 1.1C). This may be caused by a small drift of the cell body after cilia paralysis. In summary, Ni^{2+} does not appear to affect the IFT DH1B dynein and its paralyzing effect on cilia greatly facilitates the scale and quality of IFT imaging

LIMITATIONS

Our method is the first step towards routine employment of live imaging tools such as TIRFM to study of ciliary proteins in *Tetrahymena*. To our knowledge, we are first to report the velocities of IFT for *Tetrahymena*. There are certain limitations of our approach. In particular, there is major variability in the frequency and intensity of IFT particles between different cells on the same slide and even among individual cilia within the same cell. This makes the determination of IFT event frequency and estimation of the IFT particle size distribution challenging. In contrast to the *Chlamydomonas* TIRF approach that relies on the natural adhesion of flagella to glass, in our method, the cilia of *Tetrahymena* are pressed against but do not adhere to glass. The closeness of the imaged cilia to the coverglass varies between different cells depending on the degree of their flattening, which in turn depends on the cell size (cell cycle stage), the side on which the cell lands on glass (ventral, dorsal, lateral), and the local differences in the medium layer height across the coverglass. Within the same cell, different cilia experience a different level of pressure against the glass depending on their position on the antero-posterior and circumferential axes, and whether they are immobilized between or along the cortical grooves. In TIRFM, the energy exciting the fluorescence decreases exponentially with the

distance away from the coverglass. Thus, a slight variation in the closeness of cilia to the coverglass can greatly affect the intensity of the ciliary signals.

Nevertheless, even with the current limitations, our approach can be used to determine the IFT velocities. In the future, dual color imaging should be feasible to simultaneously image cargoes and IFT trains. Multiple selectable markers (Chalker, 2012; Iwamoto et al., 2014) will allow for incorporation of IFT markers into various gene knockout backgrounds, to enable functional studies on the mechanism of IFT.

ACKNOWLEDGEMENT

We acknowledge the support of research in our laboratories by grants from the National Institutes of Health (GM0571173 to JG and GM110413 to KL).

REFERENCES

Avasthi, P., and W.F. Marshall. 2012. Stages of ciliogenesis and regulation of ciliary length. *Differentiation; research in biological diversity*. 83:S30-42.

Brooks, E.R., and J.B. Wallingford. 2012. Control of vertebrate intraflagellar transport by the planar cell polarity effector Fuz. *The Journal of cell biology*. 198:37-45.

Brown, J.M., N.A. Fine, G. Pandiyan, R. Thazhath, and J. Gaertig. 2003. Hypoxia regulates assembly of cilia in suppressors of Tetrahymena lacking an intraflagellar transport subunit gene. *Mol Biol Cell*. 14:3192-3207.

Brown, J.M., C. Marsala, R. Kosoy, and J. Gaertig. 1999. Kinesin-II is preferentially targeted to assembling cilia and is required for ciliogenesis and normal cytokinesis in Tetrahymena. *Mol Biol Cell*. 10:3081-3096.

Cande, W.Z., and S.M. Wolniak. 1978. Chromosome movement in lysed mitotic cells is inhibited by vanadate. *The Journal of cell biology*. 79:573-580.

Chalker, D.L. 2012. Transformation and strain engineering of Tetrahymena. *Methods Cell Biol*. 109:327-345.

Dave, D., D. Wloga, N. Sharma, and J. Gaertig. 2009. DYF-1 Is required for assembly of the axoneme in Tetrahymena thermophila. *Eukaryotic cell*. 8:1397-1406.

Engel, B.D., W.B. Ludington, and W.F. Marshall. 2009. Intraflagellar transport particle size scales inversely with flagellar length: revisiting the balance-point length control model. *The Journal of cell biology*. 187:81-89.

Gaertig, J., D. Wloga, K.K. Vasudevan, M. Guha, and W. Dentler. 2013. Discovery and functional evaluation of ciliary proteins in Tetrahymena thermophila. *Methods in*

enzymology. 525:265-284.

Gibbons, I.R., M.P. Cosson, J.A. Evans, B.H. Gibbons, B. Houck, K.H. Martinson, W.S. Sale, and W.J. Tang. 1978. Potent inhibition of dynein adenosinetriphosphatase and of the motility of cilia and sperm flagella by vanadate. *Proceedings of the National Academy of Sciences of the United States of America*. 75:2220-2224.

Iwamoto, M., C. Mori, Y. Hiraoka, and T. Haraguchi. 2014. Puromycin resistance gene as an effective selection marker for ciliate Tetrahymena. *Gene*. 534:249-255.

Kobayashi, T., T. Martensen, J. Nath, and M. Flavin. 1978. Inhibition of dynein ATPase by vanadate, and its possible use as a probe for the role of dynein in cytoplasmic motility. *Biochemical and biophysical research communications*. 81:1313-1318.

Kozminski, K.G., K.A. Johnson, P. Forscher, and J.L. Rosenbaum. 1993. A motility in the eukaryotic flagellum unrelated to flagellar beating. *Proceedings of the National Academy of Sciences of the United States of America*. 90:5519-5523.

Larsen, J., and P. Satir. 1991. Analysis of Ni(2+)-induced arrest of Paramecium axonemes. *Journal of cell science*. 99 (Pt 1):33-40.

Lechtreck, K.F. 2013. In vivo imaging of IFT in Chlamydomonas flagella. *Methods in enzymology*. 524:265-284.

Lechtreck, K.F., E.C. Johnson, T. Sakai, D. Cochran, B.A. Ballif, J. Rush, G.J. Pazour, M. Ikebe, and G.B. Witman. 2009. The Chlamydomonas reinhardtii BBSome is an IFT cargo required for export of specific signaling proteins from flagella. *The Journal of cell biology*. 187:1117-1132.

Ludington, W.B., K.A. Wemmer, K.F. Lechtreck, G.B. Witman, and W.F. Marshall. 2013. Avalanche-like behavior in ciliary import. *Proceedings of the National Academy of Sciences of the United States of America*.

Marsh, T.C., E.S. Cole, K.R. Stuart, C. Campbell, and D.P. Romero. 2000. RAD51 is required for propagation of the germinal nucleus in Tetrahymena thermophila. *Genetics*. 154:1587-1596.

Mowat, D., R.E. Pearlman, and J. Engberg. 1974. DNA synthesis following refeeding of starved Tetrahymena pyriformis GL: starved cells are arrested in G 1. *Experimental cell research*. 84:282-286.

Orias, E. 2012. Tetrahymena thermophila genetics: concepts and applications. *Methods Cell Biol*. 109:301-325.

Pan, J., and W.J. Snell. 2014. Organelle Size: A Cilium Length Signal Regulates IFT Cargo Loading. *Current biology : CB*. 24:R75-78.

Pazour, G.J., B.L. Dickert, and G.B. Witman. 1999. The DHC1b (DHC2) isoform of cytoplasmic dynein is required for flagellar assembly. *The Journal of cell biology*. 144:473-481.

Pedersen, L.B., and J.L. Rosenbaum. 2008. Intraflagellar transport (IFT) role in ciliary assembly, resorption and signalling. *Current topics in developmental biology*. 85:23-61.

Rasband, W.S. 1997-2014. ImageJ, U.S. National Institutes of Health, Bethesda, Maryland, USA, http://imagej.nih.gov/ij/.

Rietdorf, J., and A. Seitz. 2004. ImageJ Kymograph http://www.embl.de/eamnet/html/body_kymograph.html.

Scholey, J.M. 2003. Intraflagellar transport. *Annual review of cell and developmental biology*. 19:423-443.

Shang, Y., B. Li, and M.A. Gorovsky. 2002a. Tetrahymena thermophila contains a conventional gamma-tubulin that is differentially required for the maintenance of different microtubule-organizing centers. *The Journal of cell biology*. 158:1195-1206.

Shang, Y., X. Song, J. Bowen, R. Corstanje, Y. Gao, J. Gaertig, and M.A. Gorovsky. 2002b. A robust inducible-repressible promoter greatly facilitates gene knockouts, conditional expression, and overexpression of homologous and heterologous genes in Tetrahymena thermophila. *Proceedings of the National Academy of Sciences of the United States of America*. 99:3734-3739.

Signor, D., K.P. Wedaman, J.T. Orozco, N.D. Dwyer, C.I. Bargmann, L.S. Rose, and J.M. Scholey. 1999. Role of a class DHC1b dynein in retrograde transport of IFT motors and IFT raft particles along cilia, but not dendrites, in chemosensory neurons of living Caenorhabditis elegans. *The Journal of cell biology*. 147:519-530.

Vale, R.D., and Y.Y. Toyoshima. 1988. Rotation and translocation of microtubules in vitro induced by dyneins from Tetrahymena cilia. *Cell*. 52:459-469.

Wickstead, B., and K. Gull. 2007. Dyneins across eukaryotes: a comparative genomic analysis. *Traffic*. 8:1708-1721.

Wilkes, D.E., H.E. Watson, D.R. Mitchell, and D.J. Asai. 2008. Twenty-five dyneins in Tetrahymena: A re-examination of the multidynein hypothesis. *Cell motility and the cytoskeleton*. 65:342-351.

Winey, M., A.J. Stemm-Wolf, T.H. Giddings, Jr., and C.G. Pearson. 2012. Cytological analysis of Tetrahymena thermophila. *Methods Cell Biol*. 109:357-378.

Wloga, D., and J. Frankel. 2012. From molecules to morphology: cellular organization of Tetrahymena thermophila. *Methods Cell Biol*. 109:83-140.

Wren, K.N., J.M. Craft, D. Tritschler, A. Schauer, D.K. Patel, E.F. Smith, M.E. Porter, P. Kner, and K.F. Lechtreck. 2013. A differential cargo-loading model of ciliary length regulation by IFT. *Current biology : CB*. 23:2463-2471.

FIGURES AND FIGURE LEGENDS

Figure 1.1. **Inhibition of axonemal dynein with nickel ions improves the quality of live imaging of IFT in cilia of *Tetrahymena thermophila*.** TIRF Images of *Tetrahymena* cells expressing GFP-Dyf1p. (A) A dividing cell that was not treated with Ni^{2+}. Note tangles of multiple cilia (arrows) that are not usable for measuring IFT. The old and new oral apparatuses are marked (o.a.). (B) A non-dividing cell that was not treated with Ni^{2+}. Many cilia are bent (arrows) and not suitable for measuring IFT. Note the (shorter) assembling cilia (arrowheads) have a higher GFP-Dyf1p signal intensity. (C) A cell that was treated with Ni^{2+}. Note that the cilia are relatively straight, and most cilia are not bundled. In addition, many cilia are aligned in

the same direction facilitating the orientation of IFT events in the relation to the position of the basal bodies. Scale bar = 10 µm

Fig. 1.1

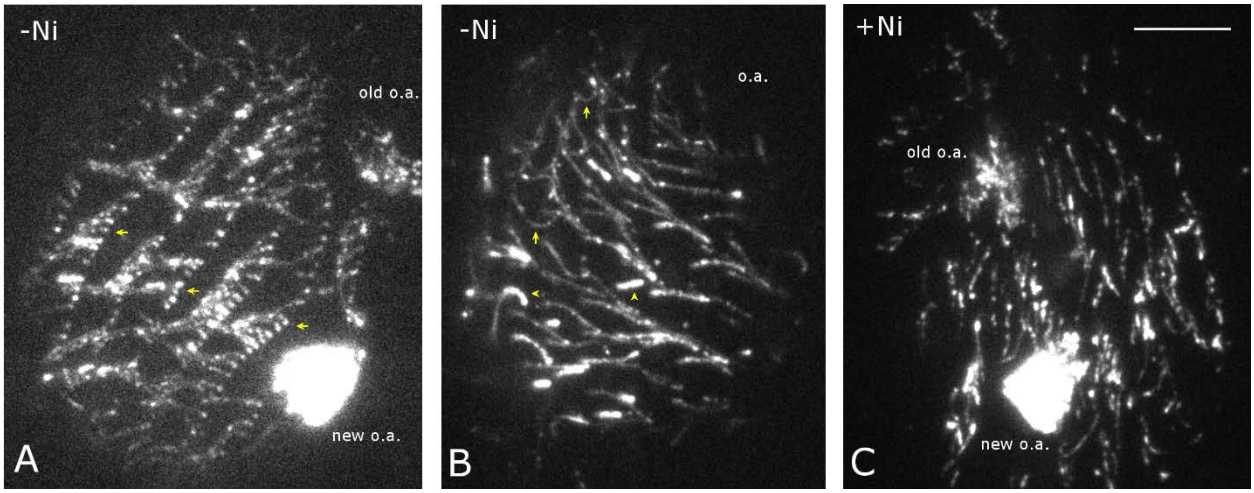

Figure 1.2. **Bent or detached cilia can lead to artifacts when measuring the IFT velocity. Paralyzing cilia with Ni^{2+} reduces these artifacts.** (A) A kymograph obtained for an untreated cilium that is likely to be partially detached from the coverglass surface at its mid-section. The arrowheads point at the segments of the tracks that appear fuzzier and where the apparent velocity rate is reduced. Such segments most likely represent a regions of the cilium that is detached from the coverglass surface. (B) A kymograph obtained for a Ni^{2+}-treated cilium. The IFT tracks (arrows) are sharp and consistent in the angle (velocity), indicating that the cilium is uniformly attached to the coverglass. Notice that the retrograde IFT particles are more varied in size as compared to the anterograde IFT particles. Time: left to right. The proximal end of the cilium is at the bottom. Scale bars = 1 second and 1 μm.

Fig. 1.2

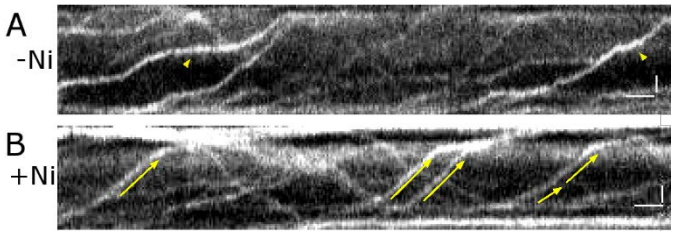

Figure 1.3. **Inhibition of axonemal dynein with nickel ions does not have a side effect on IFT**. The velocities of the anterograde (A) and retrograde (B) IFT, without (blue) or with Ni^{2+} treatment (red) are shown as data points along with their box and whisker plots. Crosses indicate the means. The measured untreated anterograde IFT velocity is 0.98 ± 0.01 μm/sec, n = 207. The measured Ni^{2+}-treated anterograde IFT velocity is 1.22 ± 0.02 μm/sec, n = 132. The difference is significant, $p < 1 \times 10^{-6}$. The measured untreated retrograde IFT velocity is 1.81 ± 0.02 μm/sec, n= 71. The measured Ni^{2+}-treated retrograde IFT velocity is 1.43 ± 0.02 μm/sec, n = 100. The difference is significant, $p < 1 \times 10^{-7}$. (A', B'). The histograms of the same data sets as in A and B are compared with their normal distribution curves. The Ni^{2+}-treated anterograde and retrograde IFT velocities fit the normal distribution curves closely. The measured untreated anterograde and retrograde IFT velocities lean toward the lower values. In the absence of Ni^{2+} the measured velocities are likely to be underestimated due to curving and detachment of cilia (see Fig. 1.2).

Fig. 1.3

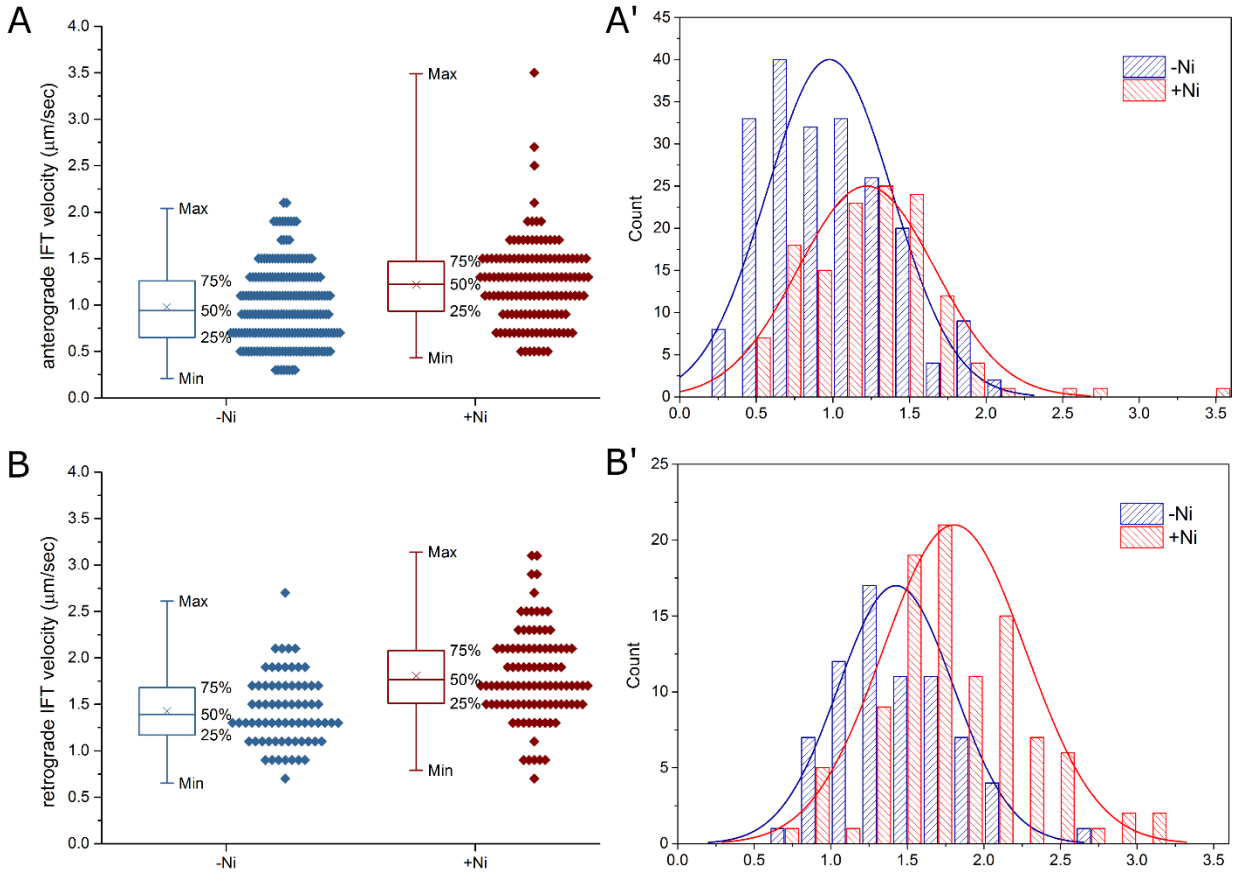
A
anterograde IFT velocity (µm/sec)
Max
75%
50%
25%
Min
-Ni
+Ni
A'
Count
-Ni
+Ni
B
retrograde IFT velocity (µm/sec)
B'

Supplemental videos 1 and 2. **Two Ni^{2+}-treated cells expressing GFP-Dyf1p as IFT marker.** Frame rate is 3 times of the real time. Scale bar = 10 μm

CHAPTER 3

LF2 RELATED DYF18 DETERMINES THE DOSAGE OF LF4 WITHIN THE CONSERVED KINASE NETWORK THAT REGULATES CILIA LENGTH IN *TETRAHYMENA*[2]

[2] Yu-Yang Jiang, Wolfgang Maier, Ralf Baumeister, Gregory Minevich, Dorota Wloga, Zheng Ruan, Natarajan Kannan, Anoosh Bahraini,Stephen Bocarro,Krishna Kumar Vasudevan, Karl Lechtreck, Eduardo Orias, and Jacek Gaertig. To be submitted to Journal of Cell Biology

ABSTRACT

Cilium length is actively maintained and important. Conserved LF4/MOK kinases inhibit cilium elongation through an unknown mechanism. In *Tetrahymena*, the loss of an LF4 ortholog LF4A, lengthened the locomotory cilia, increased the rate of cilia assembly and IFT velocity. LF4A was uniformly distributed along the cilium, mostly immobile but occasionally moved as an IFT cargo. Overproduced LF4A shortened cilia, causing cell paralysis in a kinase activity-dependent manner. LF4A phosphorylated a kinesin-2 motor *in vitro*, but this was not required for the cilia-shortening activity *in vivo*. A mutation in DYF18, a DYF-18/CCRK/LF2-related protein, was isolated as an extragenic suppressor of LF4A overexpression. A knockout of DYF18 produced longer locomotory cilia and oral cilia. A loss of DYF18 reduced the level of overexpressed LF4A, and a mildly elevated LF4A rescued the longer cilia caused by the loss of DYF18. Thus, the main if not only function of DYF18 is to regulate the abundance of LF4.

INTRODUCTION

Cilia are conserved microtubule-based organelles that are present in most eukaryotic species where they support important motile and sensory functions. The length is a functionally important attribute of cilia. The classical “long-short” cilia experiments in the flagellate *Chlamydomonas* showed that the length of cilia is actively monitored and regulated; when one of the two cilia of *Chlamydomonas* is amputated, the remaining cilium shortens until it reaches the length of the regenerating cilium, and both cilia continue to grow with the same rate to achieve an equal steady-state length (Rosenbaum et al., 1969). A number of ciliopathies (Joubert syndrome (Bielas et al., 2009; Slaats et al., 2016), Meckel syndrome, (Slaats et al., 2016; Tammachote et al., 2009), encodrine-

cerebro-osteodysplasia synchrome (Moon et al., 2014; Oud et al., 2016), short rib polydactyly syndrome (Taylor et al., 2015; Thiel et al., 2011), retinitis pigmentosa (Ozgul et al., 2011; Stone et al., 2011) , non-syndromic recessive deafness (Grati et al., 2015), polycystic kidney disease (Hakim et al., 2016; Liu et al., 2002; Upadhya et al., 2000) and juvenile epilepsy (Castren et al., 2011)) are caused by mutations in proteins implicated in cilium length regulation.

The homeostasis of cilium length relies on a balance of assembly and disassembly of cilia. The assembly requires a supply of precursors from the cell body as well as a motility mechanism that distributes components inside the cilium known as the intraflagellar transport (IFT). IFT complexes that carry cargo proteins that are building blocks of cilia, including tubulin (Kubo et al., 2016; Marshall and Rosenbaum, 2001), are driven by motor proteins along the axonemal microtubules. Kinesin-2 operates in the anterograde direction from the cilium base to the tip, where IFT cargoes are incorporated into the axoneme, while IFT dynein returns recycled components to the ciliary base and the cell body. Both motors move on different subfibers of the outer microtubule doublets of the axoneme (Stepanek and Pigino, 2016). Cilia assembly fails when IFT is compromised, for example due to a loss of kinesin-2 (Cole et al., 1998; Kozminski et al., 1995). The mechanism of cilium disassembly is less understood but is known to involve protein modifications such as ubiquitination and phosphorylation and several signaling pathways (reviewed in (Liang et al., 2016)). The rates of assembly (IFT) and disassembly determine the steady-state cilium length. On the assembly side, IFT activity (measured by the IFT train size and entry rate) (Engel et al., 2009; Ludington et al., 2013) and cargo loading rate (measured by the frequency of IFT carrying a cargo tubulin protein) (Craft et

al., 2015) increase during cilia regeneration or in short cilia and decrease as the cilia approach full length. Furthermore, IFT complexes carry little or no cargo when the cilium disassembles (Pan and Snell, 2005). Despite that the composition and principles of operation of IFT are well characterized, it is not clear whether and how IFT is adjusted to regulate cilium length. This could involve cilium length-dependent feedback-based influences on the multiple aspects of IFT, including cargo loading and unloading, motor velocity and processivity, turnover of IFT trains at the tip, and IFT particles recycling versus exchange from the cell body (Craft et al., 2015; Dentler, 2005; Engel et al., 2009; Liang et al., 2014; Ludington et al., 2013; Marshall et al., 2005; Marshall and Rosenbaum, 2001).

While the mechanisms that sense and adjust the cilium length are poorly understood, it is firmly established that protein phosphorylation is of critical importance. Several conserved kinases negatively regulate cilium length including LF4/MOK (Berman et al., 2003; Broekhuis et al., 2014; Hilton et al., 2013), DYF-5/ICK/MAK (Broekhuis et al., 2014; Burghoorn et al., 2007; Chaya et al., 2014; Erdmann et al., 2006; Yang et al., 2013), LF2/CCRK (Tam et al., 2007; Yang et al., 2013), CALK (Cao et al., 2013; Luo et al., 2011; Pan et al., 2004), NIMA-related kinases NRK/NEK (Bradley and Quarmby, 2005; Hilton et al., 2013; Lin et al., 2015; Meng and Pan, 2016; Wloga et al., 2006), LF5/CDKL5 (Tam et al., 2013)). Consistently, inhibition of protein phosphatases including PP1, shortens cilia (Abdul-Majeed et al., 2012; Lefebvre et al., 1978; Pan et al., 2004). On the other side, there are also kinases that promote ciliary elongation (Husson et al., 2016). In some cases, the activities of cilium-associated kinases have been linked to specific ciliary substrates. CDK5 phosphorylates NDE1, a negative regulator of cilium

length, and causes its proteolysis by SCF^{FBW7} (Maskey et al., 2015). CDPK1 in *Chlamydomonas* phosphorylates kinesin-2 motor FLA8. This phosphorylation inactivates FLA8 and impairs its interaction with the IFT complex proteins IFT172 and IFT81, causing the shortening of cilia. CCRK, an LF2-related kinase phosphorylates and activates ICK kinase which inhibits ciliogenesis and shortens cilia. However, the substrate specificity of many other kinases involved in cilia length regulation remains to be uncovered. Furthermore, the nature of the sensor that reports on the length of cilia remains unknown.

Among the many kinases involved in cilia length regulation, LF4 (long flagella 4) was among the first cilium length regulators discovered in a seminal genetic screen for cilium length mutants in *Chlamydomonas* (Asleson and Lefebvre, 1998). In *Chlamydomonas*, a loss of LF4 makes cilia twice as long as the wild-type (Berman et al., 2003). Its mammalian homolog MOK (MAPK/MAK/MRK-overlapping kinase) also negatively regulates cilium length. Mutation or knockdown of LF4/MOK in *Chlamydomonas* and mammalian cells lead to increased cilia length, cilia assembly rate, and the entry rate of kinesin-2 motors (Broekhuis et al., 2014; Hilton et al., 2013; Ludington et al., 2013). Yet the exact mechanism of how LF4/MOK shortens cilia is still unknown, largely due to the lack of knowledge about its phosphorylation substrates. Furthermore, we do not know whether and how LF4 is integrated into the unknown signaling mechanism that senses the cilium length.

LF4/MOK and closely-related MAK/ICK kinases are members of the RCK (*ros* cross-hybridizing kinases) kinase family, within the CMGC group. The RCK members share a TXY motif in the activation loop (TDY for MAK/ICK, TEY for LF4/MOK) that is

phosphorylated at two amino acids through autophosphorylation and, at least in the case of mammalian ICK by CCRK, an LF2-type kinase (Fu et al., 2006). The RCK kinases have been extensively documented to negatively regulate cilium length (Bengs et al., 2005; Berman et al., 2003; Burghoorn et al., 2007; Hilton et al., 2013; Moon et al., 2014; Omori et al., 2010; Yang et al., 2013) (except that some studies revealed a cilia lengthening or assembly-promoting effects of ICK (Chaya et al., 2014)). Most ciliated species have homologs of both LF4/MOK and MAK/ICK, indicating that the two subgroups of RCK have evolved by gene duplication from a common ancestral kinase during eukaryotic evolution. However, in some organisms, LF4/MOK function is dispensable, most likely because its function is fulfilled by ICK/MAK. It is possible that all RCK family members have the same substrate specificity and that the evolutionarily conserved sequence differences between LF4/MOK and ICK/MAK reflect other properties such as differences in their regulation by upstream components. Alternatively, LF4/MOK and ICK/MAK could phosphorylate different protein substrates toward the same functional output (e.g. different components of IFT) or different phosphosites on the same substrate to accomplish the same functional outcome.

The substrate phosphorylation motif of ICK was determined using a peptide library screen (Fu et al., 2006) and has been consistently shown to be utilized by both ICK and MAK in pathways not directly related to cilia (Wang and Kung, 2012; Wu et al., 2012). In addition, Chaya et al. (2014) also showed based on both in vitro and in vivo experiments that ICK phosphorylates one of the murine kinesin-2 motors, KIF3A, at a conserved R-P-R-T674-S-K-G motif within the C-terminal tail. A KIF3A T674A mutant restores ciliogenesis more than a wild-type KIF3A when endogenous KIF3A is knocked

down in NIH3T3 cells, which fits an inhibitory role of T674 phosphorylation. This is consistent with two reports that knockdowns of ICK in NIH3T3 and IMCD-3 cells cause elongation of cilia (Broekhuis et al., 2014; Yang et al., 2013). More work is needed to understand whether LF4/MOK also phosphorylates kinesin-2 motor proteins and how this phosphorylation affects cilia assembly.

The *Tetrahymena* model also offers a unique perspective on the cilium length regulation. *Tetrahymena* has two kinds of cilia: oral cilia, which form several short rows below the anterior apex that propel food particles prior to phagocytosis, and locomotory cilia that are distributed in longitudinal rows along the entire cell. Importantly, the length of *Tetrahymena* cilia is dependent on their type and position in the cell. The oral cilia are shorter than the average locomotory cilia. The length of the locomotory cilia depends on their position within the cell, with the anterior end cilia being the shortest and the posterior end cilia being the longest. At the early stage of cell division, the new oral cilia assemble in the forming posterior daughter cell. At about the same time, the old oral cilia partially disassemble and reassemble in phase with the growing new oral cilia. The majority of new locomotory cilia assemble near the cell's equator during the mid-stage of cell division from the basal bodies that were formed much earlier (Frankel et al., 1981). *Tetrahymena* offers an interesting entry point to examine the mechanisms where multiple types of cilia are regulated differently in a single cell. One key question is how *Tetrahymena* can maintain cilia of different length in the same cytoplasm. This is an important question as in other organisms, most notably *Chlamydomonas*, there is a mechanism that equalizes the length of the two cilia in the same cell (reviewed in (Wemmer and Marshall, 2007)). The understanding of how *Tetrahymena* manages the

cilia length differentially may also be applicable to multicellular organisms with multiciliated epithelial cells.

Genetic interactor screens are a powerful tool for the discovery of pathway components including substrates of post-translational modifications such as phosphorylation (Nurse and Thuriaux, 1980). While several cilium length kinases were discovered in genetic screens, to our knowledge, forward genetics has not been utilized to discover genetic interactors. One limitation is that the cilium length kinases uncovered by genetic screens thus far, LF2, LF4, and LF5, all negatively regulate cilia length. The mutant carrying loss of function alleles of such kinases do make cilia (albeit longer) and remain motile. Consequently, isolating a suppressor would require a sophisticated and likely time-consuming screen based on a subtle change toward the normalization of the swim pattern. On the other side, a gain-of-function of a cilium length kinase could shorten or completely disassemble cilia causing cell paralysis, a phenotype more amenable for isolation of motile suppressors. Here we explore this idea in *Tetrahymena*. We constructed a gain-of-function allele of LF4 based on its overexpression that causes extensive cilia shortening and cell paralysis. In a screen for suppressors of LF4overexpression, we isolated several intragenic suppressions caused by mutations in the LF4 kinase domain and one extragenic suppression in a mutation in DYF18, a kinase related to the known cilium length regulators LF2/CCRK. DYF18 appears to primarily act as an upstream regulator of LF4 abundance. Our LF4 overexpression suppressor screen is not saturated and should be suitable for isolation of additional cilium length regulation components including the substrates of phosphorylation of several kinases.

RESULTS

LF4A is a negative regulator of cilium length and positive regulator of the number of cilia in *Tetrahymena*

To determine the number of potential homologs of various cilia length kinases in *Tetrahymena*, we performed a phylogenetic analysis of related kinases (based on reciprocal BLASTP searches) in several ciliated species including *Tetrahymena*. In the analysis, we included potential LF4/MOK, MAK/ICK, LF2/CCRK, and LF5 type kinases as they all belong to a single family of kinases, CGMC, and all are important for cilium length regulation. *Tetrahymena* has two LF4 orthologs: LF4A (TTHERM_00058800) and LF4B (TTHERM_00822360). *Tetrahymena* also has several kinases most closely related to MAK/ICK, as well as single homologs of LF5 and LF2 kinases. The LF4/MOK and MAK homologs of various species are clearly related, but they consistently fall into separate clades and most ciliated species have both an LF4/MOK and a MAK/ICK homolog (Fig. 2.1A). Likely, the MAK/ICK and LF4/MOK kinases originated from a common RCK ancestor and had split before the emergence of opisthokonts. Thus, LF4/MOK and MAK kinases are likely to have related but non-identical activities. On the other hand, some species, including zebrafish and *C. elegans*, lack an LF4/MOK but have a MAK/ICK. Thus, the function of LF4 in the cilia length regulation can be fulfilled by a MAK/ICK type kinase in some species. This is not the case of *Chlamydomonas* (Asleson and Lefebvre, 1998), and *Tetrahymena* (see below) where LF4 null mutants have excessively long cilia despite these species having multiple MAK kinases.

We disrupted one of the two *Tetrahymena* homologs of LF4/MOK gene. *LF4A* (TTHERM_00058800) in the germline micronucleus and used crosses to construct

macronuclear homozygotes that express a null phenotype (LF4A-KO). The disruption of LF4A resulted in locomotory cilia that were 32% longer than the wild type (Fig.1B and C). However, the anterior-posterior gradient of increasing cilium length that is present in wild-type cells is still preserved in the LF4A-KO, indicating that LF4A is not responsible for the position-dependent individualization of cilium length. In addition, the LF4A-KO cells carry fewer cilia, especially in the posterior/dorsal region. Oral cilia length seemed unaffected. In *Chlamydomonas*, LF4 is believed to act by decreasing the rate of assembly of cilia while it may not affect the rate of disassembly (Hilton et al., 2013; Ludington et al., 2013). To determine the rate of cilia assembly, we amputated *Tetrahymena* cilia by a pH shock, and measured the elongation of cilia during regeneration. The LF4A-KO locomotory cilia regenerated at a faster rate than the wild type, while the regeneration of oral cilia seemed unaffected (Fig. 2.2A and B). Overall, our results are consistent with previous observations (Berman et al., 2003; Broekhuis et al., 2014; Hilton et al., 2013), and indicate that LF4A negatively regulates the length of the locomotory cilia by decreasing the rate of cilia assembly.

LF4A localization

We added a GFP to the C-terminus of LF4A by engineering the native locus using homologous DNA recombination. LF4A-GFP was present at a relatively low level; using confocal microscopy, it could only be detected above the background by immunostaining with anti-GFP antibodies. LF4A-GFP was present in the basal bodies of locomotory cilia and at a lower level within the shafts of locomotory cilia (Fig. 2.3A and B). Within the cilia, LF4A-GFP appeared as dots spread uniformly along the length. The ciliary but not the basal body LF4A-GFP was sensitive to Triton X-100 (Fig. 2.3C), suggesting that in

cilia LF4A is in the soluble matrix-membrane fraction or is weakly bound to the axoneme.

Total internal reflection fluorescence (TIRF) microscopy provided sufficient sensitivity for live imaging of the ciliary LF4A-GFP and confirmed its enrichment at the base of the locomotory cilia and the weaker presence along the entire cilium length (Fig. 2.3D). Most of the LF4A-GFP particles were immobile, and the patterns consistent with diffusion (Lechtreck, 2015) were rare. However, occasionally LF4A-GFP moved either in the anterograde or retrograde direction (Fig. 2.3E) with velocities comparable to the speeds of IFT (Fig. 2.4B). Thus, the majority of LF4A-GFP could be weakly anchored to the axoneme or reside on non-mobile IFT particles and a small fraction moves as IFT cargo.

LF4A kinase activity shortens cilia.

To test further whether LF4A shortens cilia, we overproduced a GFP-tagged LF4A (ovGFP-LF4A) using a Cd^{2+}-inducible promoter *MTT1p* (Shang et al., 2002). In cells that were not exposed to exogenous Cd^{2+}, GFP-LF4A was uniformly distributed along the length of cilia, similar to the natively-expressed LF4A-GFP described above (TIRFM data not shown). The signal was significantly more intense than that of LF4A-GFP under its own promoter, suggesting a mild overproduction of GFP-LF4A occurs even without added Cd^{2+} ions.

With the addition of Cd^{2+} for an hour, GFP-LF4A strongly accumulated at the bases of cilia (including oral cilia) and simultaneously the cilia shortened (Fig. S2.1A and Fig. 2.4A). GFP-LF4 also decorated two microtubule-based structures specific to *Tetrahymena*: longitudinal microtubules and contractile vacuole pores (Sharma et al.,

2007). This observation suggests that GFP-LF4 has a microtubule-binding activity. After 6-8 hours of GFP-LF4A overproduction, cilia, including oral cilia, continued to shorten to become stubs and the cells became nearly paralyzed. However, the GFP-LF4A-overproducing cells continued to grow in size and progress through the cell cycle, except that they frequently failed to complete cytokinesis and became compound cells with multiple cortical "subcells" and nuclei, indicating repeated failures at cytokinesis (Fig. S2.1B). The cytokinesis defects are an expected outcome of the loss of locomotory cilia, which in *Tetrahymena* are required for rotokinesis, a ciliary-force dependent separation of daughter cells (Brown et al., 1999).

LF4 of *Chlamydomonas* phosphorylates a generic substrate of serine/threonine kinases, myelin basic protein (MBP) and autophosphorylates (Berman et al., 2003). Similarly, GFP-LF4A pulled down from overproducing *Tetrahymena* phosphorylated both MBP and itself *in vitro* (Fig. 2.4B). To test if the kinase activity is necessary for LF4's cilia shortening activity, we mutated F82, a key residue at the active site, with either an alanine or glycine. GFP-LF4A--F82A was produced at a higher level compared to GFP-LF4A while GFP-LF4A--F82G was less abundant (Fig. S2.1C). Both mutated GFP-LF4A proteins showed a greatly reduced kinase activity *in vitro* (Fig. 2.4B). The variation in production might be related to the copy number of the transgene in the macronuclei (see Material and Methods) or protein structure instability caused by the point mutation.

Neither GFP-LF4A--F82A nor GFP-LF4A--F82G overexpression caused cilia shortening even though one of these variants was present at the level comparable to the non-mutated GFP-LF4A (Fig. 2.4A and C). The cilia length of cells expressing either of

the two kinase-weak variants were indistinguishable from cells overproducing GFP alone as a negative control. During the same time (3-6 hours with Cd^{2+}), cilia in the GFP-LF4A overproducing cells shortened to 75% of wild-type. Furthermore, both kinase-weak variants accumulated near the tips of cilia (in both locomotory and oral cilia), contrasting with the strong GFP-LF4A accumulation at the base of cilia (Fig. 2.4A and Fig. S2.1A). In addition, GFP-LF4A--F82A and GFP-LF4A--F82G were seen moving along the cilia at a velocity similarly to LF4A-GFP and IFT (Fig. S2.1D). We conclude that the kinase activity of LF4A is required for its cilia shortening activity but not required for its transport by IFT.

LF4A affects IFT velocities

The tip accumulation of the mutated GFP-LF4A is similar to the consequences of overproduction of other ciliary proteins including GFP-TTLL9, and GFP-FAP206 (Vasudevan et al., 2015; Wloga et al., 2008). Therefore, we hypothesized that the tip accumulation is mainly the result of overproduction and the rate of entry of mutated GFP-LF4A, presumably driven by IFT, exceeded the rate of its removal of GFP-LF4A in cilia. One simple possibility for why the active, overproduced GFP-LF4 accumulates at the ciliary base is that an excessive activity of LF4A kinase inhibits IFT and therefore prevents its own entry into the cilium. To explore this hypothesis further, we examined whether IFT is affected by the levels of LF4.

DYF-1/IFT70 is an IFT complex B protein that is essential for cilia assembly in multiple models including *Tetrahymena* (Dave et al., 2009b). GFP-DYF1 is a suitable marker for imaging IFT in *Tetrahymena* using TIRF microscopy (Jiang et al., 2015c). The anterograde and retrograde GFP-DYF1 velocities were measured in the ovGFP-

LF4A (4-5 hours in Cd^{2+}) or LF4–KO cells, respectively. Overexpression of GFP-LF4A decelerated both the anterograde and retrograde movements (Fig. 2.5A). Conversely, both IFT directions gained speed in the LF4A-KO cilia (Fig. 2.5B and C). Thus, LF4A negatively regulates the IFT velocities and this could be the main if not only route through which LF4 shortens cilia.

LF4A phosphorylates KIN1, a kinesin-2 motor subunit *in vitro*, but *in vivo* shortens cilia via other unknown substrates.

The above data and those by others establish firmly that the cilia-shortening activity of LF4A is mediated through phosphorylation of an unknown substrate that may act by decreasing IFT activity and subsequently inhibiting cilia assembly. Therefore, we reasoned that IFT components are the most likely candidates for LF4A phosphorylation substrate(s). The murine ICK (a relative of LF4A in RCK family) phosphorylates KIF3A kinesin-2 motor subunit at a conserved C-terminal motif, R-P-R-T674-S-K-G. We followed up on this observation to explore whether LF4A of *Tetrahymena* can phosphorylate a heterotrimeric kinesin-2 subunit KIN1 within the corresponding C-terminal motif R-P-T-S695-K-P-G.

We engineered a strain that overproduces GFP-KIN1, and two additional IFT proteins GFP-DYF1 and GFP-IFT52. We developed a novel *in vitro* "substrate proximity" thiophosphorylation assay where a GFP-tagged target and GFP-LF4A are overexpressed in separate *Tetrahymena* strains and brought to proximity by capture on the same GFP-trap beads from a mixture of lysates (see Material and Methods). LF4A phosphorylated KIN1 but not two other IFT proteins (Fig. 2.6A).

The corresponding thiol-phosphorylated KIN1 gel bands were subjected to in-gel trypsin digestion and tandem mass spectrometry analysis. No thiol-phosphorylated tryptic peptide of GFP-KIN1 was detected likely due to a low peptide coverage (Fig. S2.2A). Interestingly, a few tryptic peptides of LF4A were phosphorylated (Fig. S2.2B and C), including S-N-N-S347-N-M-Y that was thiol-phosphorylated. This autophosphorylation site is of unclear significance as it is different from the previously reported autophosphorylation sites of ICK and MAK within the TXY motif (Fu et al., 2006; Fu et al., 2005; Wang and Kung, 2012) and the amino acid motif is not conserved among RCK members. We also identified (non-phosphorylated) tryptic peptides of KIN3 (TTHERM_00297200). This strongly suggest that KIN3 is a partner of KIN1 (and its redundant paralog KIN2) within the heterotrimeric kinesin-2 complex.

With the lack of success in the identification of *in vitro* (thio)phosphorylation site on KIN1, we focused on the C-terminal R-P-T-S695-K-P-G homologous in sequence and position to the motif used on KIF3A kinesin-2 motor subunit by ICK (Chaya et al., 2014) and an adjacent similar motif R-P-Q-S708-G-V-K. Both motifs fit the previously reported substrate consensus for ICK, R-P-X-S/T-P/A/T/S, except for the +1 position but RCK kinase are known to have relaxed requirements for this position (Howard et al., 2014). We tested a series of GFP-tagged KIN1 proteins with a part or the entire C-terminal tail truncated, or carrying substitutions at the phosphorylatable amino acids. Using these variations of GFP-KIN1 as substrates for the kinase activity assay, we concluded that the S695 of KIN1 is responsible for more than 70% of the phosphorylation of GFP-LF4A *in vitro* (Fig. 2.6B). This, or a similar motif, is not present in the paralog KIN2 or KIN3. The adjacent S708 of KIN1 was responsible for less than 20% of the *in vitro*

phosphorylation. This motif is also present near the C-terminus of the likely partner of KIN1 in the kinesin-2 complex, KIN3 (R-P-Q-S-G-L-K).

KIN2 (TTHERM_00263330) is paralog of KIN1 (Wickstead et al., 2010) (and likely alternative partner of KIN3) and is sufficient for assembling cilia in cells lacking KIN1(Brown et al., 1999). KIN2 is genetically redundant to KIN1 (see discussion). Yet it does not have a phosphosite that would fit the R-P-X-S/T-P/A/T/S consensus that emerged from this and previous studies for various LF4/MOK or MAK/ICK homologs. To test whether phosphorylation of KIN1 by LF4A is necessary for shortening of cilia, we overproduced GFP-LF4A in the KIN1-KO cells where the anterograde IFT is thought to be driven by a kinesin heterotrimeric motor consisting of KIN2 and KIN3. As expected, cells carrying ovGFP-LF4A with or without KIN1 formed cilia normally in Cd^{2+} free medium. With Cd^{2+} added, cilia were shortened by overproduction of GFP-LF4A with similar kinetics, regardless of the presence or absence of KIN1 (Fig. 2.6C). This suggests that either the remaining R-P-X-(S/T)-X site on KIN3 is sufficient to confer cilia shortening or that in fact LF4A acts through another substrate different from subunits of kinesin-2. At the least these studies confirm the motif that LF4A phosphorylates in vitro on kinesin-2 of *Tetrahymena* is consistent with the ICK motif uncovered in earlier studies. However, our observations also expose the weaknesses of the reverse genetic approach in linking the modifying enzyme to the modification sites, complicated by the potential multiplicity of the sites on one protein as well as the potential use of partially redundant sites or differences between the site utilization *in vitro* and *in vivo*. A similar level of complexity was earlier encountered in the murine ICK study (Chaya et al., 2014).

Development of a genetic screen for LF4 interactors based on suppression of GFP-LF4A overexpression

We sought to develop a forward genetic approach with the goal of identifying genetic interactors of LF4A including its potential phosphorylation substrates. An overexpression of LF4A causes a phenotype that is exactly opposite to the loss-of-function of LF4A. It therefore appears that the overexpression phenotype is a hypermorph, and the cilia-shortening is due to excessive phosphorylation of the physiological substrate of LF4A. Theoretically, a loss of the phosphorylation residue or a null of the LF4A substrate is expected to result in cilia being insensitive to shortening caused by LF4A overproduction. With the long-term goal of identifying the phosphorylation substrate(s) of LF4A, we developed a genetic screen for suppressors of GFP-LF4A overexpression, taking advantage of the cell paralysis, an easily selectable phenotype.

We introduced GFP-LF4A overexpressing transgene (ovGFP-LF4A) along with neo5 (paromomycin resistance) selective marker into the (germline) micronucleus by replacing the endogenous LF4A locus (Fig. 2.7 a). A heterokaryon strain (mic: ovGFP-LF4A/ovGFP-LF4, mac: wild-type) was mutagenized with nitrosoguanidine (Fig. 2.7 b). The mutated cells were subjected to a uniparental cytogamy (UPC) self-cross (Cole and Bruns, 1992) (Fig. 2.7 c). This technique yields progeny that are mostly homozygous homokaryons (Fig. 2.7 d) and express the post-mutagenesis phenotypes. Overexpression of GFP-LF4A was induced in the mutagenized progeny cells, and suppressors were isolated as cells capable of swimming to the top of the vertically positioned test tubes (Fig. 2.7 e and f). Importantly, a negative control revealed no suppressors among the 3 x 10^7 non-mutagenized cells derived from the ovGFP-LF4A heterokaryon self-cross that

was subjected to the same manipulations as the mutagenized set. Suppressors appeared in the mutagenized set, multiple suppressors were isolated from independently selected batches and were analyzed further.

The suppressor F0 clones were outcrossed and the F1 heterozygotes were analyzed for linkage to the transgene ovGFP-LF4A, which would indicate an intragenic suppression. F2s were produced by a second self-cross and progeny that contained the ovGFP-LF4A transgene (that were resistant to paromomycin owing to the presence of *neo5* closely linked with the ovGFP-LF4A transgene) were isolated and tested for suppression by overexpression of GFP-LF4A. A suppressor clone giving exclusively paromomycin-resistant F2s clones that are all suppressed (remain mobile upon induction with Cd^{2+}), is likely to carry an intragenic mutation, presumably within the GFP-LF4A ORF. For an extragenic unlinked suppression, paromomycin-resistant F2 clones were expected to segregate the suppressed and unsuppressed phenotypes (1:1 for a suppression caused by a single unlinked mutation). Among the 5 suppressors analyzed, 4 were judged to be intragenic as their F2s were exclusively suppressed and one suppressor (sup1) was judged to be extragenic, with the suppressed versus unsuppressed phenotypes segregating 1:2 (29: 60).

The overproduction of GFP-LF4A was also examined in the suppressor F2 clones upon induction with Cd^{2+}. Among the four intragenic suppressors, sup6 lacked a GFP signal (not shown). The other three intragenic suppressors: sup3, sup4, and sup5, had a strong signal of GFP-LF4A signal at the tips of cilia (Fig. 2.8A) that was exactly the pattern seen in cells overproducing GFP-LF4A with mutations lowering the kinase activity (Fig. 2.4A). The single extragenic suppressor, sup1, showed GFP-LF4A at the

cilia bases, along the length of some cilia and occasionally was slightly enriched at the ciliary tips (suppressed F2 in Fig. 2.8B right with insert). The subset of cilia that showed uniform GFP-LF4A in sup1 were all very short, likely assembling cilia.

Sanger DNA sequencing of the ovGFP-LF4A transgene ORFs revealed that sup6 had several point mutations including two in the *MTT1p* promoter, two in the GFP portion and a G to A mutation at the 5' end of the predicted intron 1 in LF4A (splicing donor site), consistent with the loss of GFP signal. The intragenic sup3, sup4 and sup5 carried single point mutations, producing E132K, G13S and E160K substitutions, respectively, in the LF4A protein. Specifically, all three mutations are at conserved residues in the kinase domain of LF4. To estimate the impact of these mutations on the kinase activity, we produced a homology-based model of the *Tetrahymena* LF4A kinase domain using Cyclin-dependent kinase of *Cryptosporidium* (Chain A of PDB 3NIZ) as template (Artz et al., 2011; Fiser et al., 2000). All three amino acids are in the areas adjacent to the kinase active site (Fig. 2.8C, zoom). While it is not clear how exactly these mutations affect the LF4A kinase activity, G13 and E132 mutations are frequently disease-associated (Torkamani et al., 2008). It is likely that all mutations interfere with catalytic activity or impair the binding to the substrate peptide.

We used the recently established methodology for comparative whole genome sequencing (Jiang et al., 2017) based on a bulked segregant approach, to identify the causal mutation(s) for the extragenic suppressor sup1. The self-cross F2 progeny clones derived from a single sup1/sup1+ heterozygote were grouped into suppressed and non-suppressed pools. The homogeneity of the phenotypes of the two pools was verified by immunofluorescence, based on the length of cilia and GFP patterns (Fig. 2.8B). Genomic

DNAs of both pools were sequenced; the sequence reads were aligned to the macronuclear reference genome and the detected variants were subjected to multiple steps of subtraction and filtering (Fig. 2.9A) (Chapter 4) to generate a list of strong candidate variants that were unique to the suppressed F2 pool and in which most of the sequence reads contained a variant base(s). This yielded three variants that met all the criteria, all of which are predicted to have an affected gene product (Table 1).

The three candidate variants are each located on different macronuclear chromosomes. To determine which of the 3 variants is more likely to be the causal mutation for the suppression, we examined the frequency of variant cosegregation with the suppression phenotype as a function of the position along all 5 micronuclear chromosomes. This revealed a peak of variant co-segregation on the micronuclear chromosome 3 between 9 to 10 Mb (Fig. 2.9B). This region intersected with one of three candidates identified by subtraction and filtration, scf_8254401:105680 T to C. This variant also showed the most extreme bias in the ratio of the alt and ref sequences. In the suppressed (mutated) pool all sequence reads contained an alt base, while in the unsuppressed (wild-type) pool 8% (3 in 37 reads) contained an alt base (Fig. 2.9C and table 2.1).

The top candidate for causal mutation is within the gene TTHERM_01080590, which encodes a protein kinase related to LF2/CCRC (see below). The mutation changes the predicted stop codon 5'-TG<u>A</u>-3' (reverse strand: 5'-<u>T</u>CA-3') into 5'-TG<u>G</u>-3' (tryptophan, reverse strand: 5'-<u>C</u>CA-3'). This would add a few extra amino acids in the form of a sequence WIRNLLILNG to the C-terminus of the TTHERM_01080590 gene product (Fig. 2.9D).

DYF18 is a negative regulator of cilia length and regulator of LF4A abundance

BLASTP searches revealed that the closest homologs of TTHERM_01080590 are LF2/CCRK kinases and the sequence homology is limited to the kinase domain of TTHERM_01080590. The most closely related sequence in other species is that of DYF-18 (H01G02.2) an LF2-related kinase that is already implicated in the cilium length regulation in *C. elegans* (Phirke et al., 2011). Thus, we named TTHERM_01080590 *DYF18*.

DYF18 does not have an R-P-X-(S/T)-X motif, and therefore is unlikely to be the phosphorylation substrate of LF4. To learn about the function of DYF18, we knocked its gene out in the germline and produced homozygous homokaryons. The locomotory cilia of DYF18-KO cells were significantly longer than the wild-type cilia and the average length of the locomotory cilia was similar to that of LF4A-KO. There was also a reduction in the density of locomotory cilia in the posterior-dorsal region as seen in LF4A-KO. Thus, in regard to the locomotory cilia, the phenotype of DYF18-KO is remarkably similar to that of LF4A-KO (Fig. 2.10A and B). Strikingly, while the oral cilia that seemed unaffected in LF4A-KO, they were exceptionally long in the DYF18-KO cells. Unlike wild-type and LF4A-KO cells, DYF-18 KO cells could only be grown on the specialized medium MEPP (that support proliferation of phagocytosis-minus mutants) but not on the standard SPP, an indication that these cells were defective in phagocytosis, a function that requires motile oral cilia (Brown et al., 1999; Orias and Rasmussen, 1976). Overall the phenotype of DYF18-KO cells was more severe as compared to the LF4A-KO cells specifically in the lengthening of the oral cilia. The double knockout DYF18-KO+LF4A-KO cells had the phenotype closely resembling that

of the single knockout DYF18-KO (Fig. 2.10A). Previous studies indicate that LF2/CCRK acts upstream of LF4/MOK and ICK/MAK (Asleson and Lefebvre, 1998; Fu et al., 2006; Wang and Kung, 2012; Yang et al., 2013). Our observations are consistent with the locomotory cilia length being regulated by LF4A and DYF18 in the same linear pathway, while the oral cilia length are affected by DYF18 but not by LF4A.

The sup1 mutation adds 10 residues at the C-terminus and its effect on the DYF18 protein functionality is unknown. Recently a similar stop codon shift that caused addition of a few amino acids at the C-terminus of an unrelated protein led to a loss of function (Sellami et al., 2016). We hypothesized that the sup1 mutation is a loss-of-function mutation. To test whether a loss-of-function of DYF18 suppresses overexpression of GFP-LF4A, we constructed a DYF18 null strain that also carries the GFP-LF4 overexpression transgene: DYF18-KO+ovGFP-LF4A, and evaluated whether DYF18 knockout rescues cilia shortening caused by overexpression of GFP-LF4A. The locomotory cilia length were measured at 0 hours, 6 hours, and overnight after adding Cd^{2+} to cells carrying LF4A transgene with or without DYF18, and compared the results to the two sup1 F2 pools (Fig. 2.10C). Unexpectedly, the locomotory cilia lengths of all four strains at 0 hour were similar (see below) and then shortened to nearly the same extent after 6 hours' overproduction of GFP-LF4A. The overnight overproduction of GFP-LF4A shortened cilia further in the presence of the wild-type allele of DYF18, but not in cells with the sup1 allele or DYF18-KO allele. This is consistent with the sup1 mutant allele being a loss-of-function mutation of DYF18.

After 6 hours of overexpression in the DYF18 null background, instead of the exclusive basal body pattern, GFP-LF4A was visible in short (presumably growing) cilia

(Fig. S2.3A). This is similar to the pattern seen in sup1 cells (Fig. 2.8B). However, the specific kinase activity of GFP-LF4A purified from cells without DYF18 was not lower when normalized for the GFP-LF4A input (Fig. S2.3B). After overnight exposure to Cd^{2+} cells with DYF18 had GFP-LF4A-positive granules in the cell body, and had consistently short cilia. The cells that were DYF18 null had more variable patterns of GFP-LF4A accumulation in the cell body, and their cilia length appeared inversely correlated to the amount of GFP-LF4A. A western blot (Fig. 2.10D) showed that the loss of DYF18 led to the reduction of total abundance of overexpressed GFP-LF4A. Thus, most cilia shortening caused by overproduction of GFP-LF4A was suppressed by a reduction in the GFP-LF4A abundance.

Importantly, without Cd^{2+} induction, the ovGFP-LF4A transgene rescued the DYF18-KO phenotype. The double mutant cells that are DYF18 null and have the ovGFP-LF4A transgene had shorter locomotory and oral cilia than the DYF18-KO cells and grew well in SPP (while the DYF18-KO cells did not) (Fig. 2.10 B). Most likely the slightly elevated GFP-LF4A expression (due to leaky *MTT1p* promoter in Cd^{2+}-free media) was able to compensate the loss of DYF18. This suggests that an elevated level of LF4A rescues the loss of DYF18. These data are consistent with DYF18 acting solely to regulate the abundance of LF4.

DISCUSSION

MOK and MAK/ICK

The RCK family members LF4/MOK, MAK/ICK share significant amino acid sequence similarity within the kinase domain (Chen et al., 2013; Fu et al., 2006). Our phylogenetic analysis point to the MAK/ICK and LF4/MOK kinases as separate

subfamilies within the RCK family. There is certainly more of diversity in the MAK/ICK group. In the mouse, ICK is expressed uniformly while MAK shows tissue-specific expression patterns (Chen et al., 2013).

We also note that some non-ciliated species have RCK kinases including the slime mold *Dictyostelium discoideum* (Fig. 2.1A) and yeast (Smith and Mitchell, 1989). The ancestor RCK kinases likely have evolved with cilia and perhaps MAK/ICK and MOK have evolved to use non-ciliary targets in lineages that have lost cilia. Overall the phylogenetic studies and functional studies cited above indicate that MAK/ICK and MOK represent distinct subgroups of RCKs that may have non-identical substrates or non-identical sites on the same protein target. While MAK and ICK knockout studies have identified functions of these kinases in diverse (but invariably ciliated) cell types, a MOK mutant to our knowledge has not been analyzed. However, expression knockdown studies support non-identical roles for MAK/ICK and MOK. Broekhuis et al. (2014) showed that ICK and MOK are both localized to the primary cilium of IMCD-3 (murine inner medullary collecting duct) cells. Knockdowns of either ICK or MOK lengthen the primary cilium. While a knockdown of ICK increases the anterograde IFT velocity and overproduction of ICK causes the cilium to shorten, such effects were not observed for similar manipulations applied to MOK. Clearly however, a MAK kinase can be the sole RCK to support ciliary functions in *C. elegans* and zebrafish.

In *Tetrahymena,* LF4 regulates the cilia length and number

Cilium length is determined by an equilibrium of the assembly and disassembly rates. The work by others and this study have shown that the loss of LF4 causes cilia to regenerate faster (Asleson and Lefebvre, 1998; Ludington et al., 2013). At similar length,

the disassembly rate of LF4 mutant cilia is not any greater than that of the wild-type (Hilton et al., 2013). Therefore, LF4 is likely to act solely by decreasing the rate of cilia assembly (Hilton et al., 2013).

In *Tetrahymena*, the locomotory cilia are longer in steady state and regenerate faster upon the loss of LF4. It is important to emphasize that in the wild-type, not all the locomotory cilia are of the same length. The cilia at the anterior end are shorter than the posterior ones. The anterior-posterior gradient in cilium length is not compromised in LF4A-KO cells (both in steady state and during cilia regeneration). We also do not see obvious changes in the abundance of LF4A-GFP allocated to each basal body/cilium unit (Fig. 2.4C). Thus, LF4A is not involved in the position-dependent regulation of the cilium length. The antero-posterior axis differential in cilia length must be executed by other factors than LF4A. One candidate is the NRK/NEK/CNK kinase group that have been linked to the disassembly pathway. This group has significantly expanded in the number of paralogs in *Tetrahymena* and specific paralogs are targeted to a subset of cilia along the cell's anteroposterior and circumferential axes (Wloga et al., 2006). It is also possible that several MAK paralogs have position-dependent functions. While it appears that LF4A is a generic non-cell position dependent factor, an exception is that LF4A appears not to act on oral cilia. It is most likely that the paralog LF4B is targeted to the oral cilia where it acts in the same manner as LF4A in the locomotory cilia. There already are cases where *Tetrahymena* paralogs have diverged to serve specifically oral cilia (Wloga et al., 2009).

It is not clear why a loss of LF4A reduces the density of ciliation in the posterior-dorsal area. The unciliated area is variable in size in affected cells and the cilia

regeneration at this region is similarly reduced in wild-type and LF4-KO. This argues that the basal bodies in the posterior-dorsal region are not competent for ciliation.

Intriguingly, the phenotype of LF4A null cells is reminiscent of the phenotype of the loss of function of subunits of IFT dynein (dynein-2): shorter but fewer cilia and more variable in length (Rajagopalan et al., 2009). Based on both cases, a loss of a cilium length regulator correlates with reduced ciliogenesis. We therefore can speculate that in *Tetrahymena* there is a link between cilium length regulation and initiation of ciliation. A similar complication is observed in the case of another cilium length kinase, LF2/CCRK which is also involved in cilia length regulation and ciliogenesis. Several LF2-null mutant alleles in *Chlamydomonas* assemble cilia of variable length within the cell cycle, but have a defect in regenerating cilia after deciliation by pH shock. Further, a weak LF2 mutant (*lf2-2*, two amino acids lost) displays longer cilia and delayed cilia regeneration (Asleson and Lefebvre, 1998; Barsel et al., 1988; Tam et al., 2007). A CCRK knockdown in NIH3T3 cells consistently lengthens cilia, but encourages earlier ciliogenesis after serum starvation (Yang et al., 2013). How the LF2/CCRK-LF4/MOK pathway is involved in the coordination between cilia length regulation and cilia assembly or ciliogenesis is largely not explored.

LF4 regulates IFT

LF4A-GFP localizes uniformly along the length of the axoneme. Others and this study have shown that LF4/MOK is a ciliary protein and moves in a velocity similar to IFT, indicating that LF4 is a cargo of IFT (Berman et al., 2003; Broekhuis et al., 2014). In *Chlamydomonas*, when normalized in length, LF4 loss-of-function mutant cilia have a higher amount of the IFT entering cilia per unit time than wild-type cilia (Ludington et

al., 2013). We show that the speed of IFT (interestingly in both directions) is negatively regulated by LF4. While in IMCD-3 cells, knockdown of MOK results in longer cilium while overproduction of MOK does not shorten cilium. The IFT velocity is not significantly affected in either knockdown or overproduction of MOK (Broekhuis et al., 2014). It's possible a threshold for detecting an IFT change was not achieved in the knockdown experiments, or that the effect on IFT is subtle but sufficient to lengthen the cilium over longer time. We further suggest that cargo transport by IFT is also inhibited by LF4. The kinase-weak variants of GFP-LF4A can be transported as IFT cargo and accumulate at the distal region due to overproduction. Similar observations were made for overexpressed kinase dead mutant of ICK in NIH 3T3 cells (Moon et al., 2014) and IMCD-3 cells (Broekhuis et al., 2014). The wild-type GFP-LF4A instead accumulates at the basal region of the cilia, despite its overproduction and capacity to be transported by IFT. This basal accumulation is clearly not due to clogging but inhibition of IFT cargo transport at this region due to excessive LF4 kinase activity. Whether IFT transport of other cargoes are also affected by excessive LF4 is yet to be tested.

IFT carries many cilia proteins as cargo, including tubulins and axoneme binding components into cilia (Craft et al., 2015; Wren et al., 2013). Loss of anterograde IFT kinesin-2 motor results in loss of all IFT proteins in the cilia, an immediate arrest of cilia assembly and gradual shortening of cilia in 3-6 hours (Kozminski et al., 1995). A strong knockdown as well as a temperature-sensitive mutation in dynein heavy chain 1b, an IFT dynein motor subunit required for retrograde IFT, results in greatly reduced velocity and frequency of retrograde IFT, reduced frequency but not velocity of anterograde IFT and accumulation of IFT proteins in cilia. The cilia remained the same length for 36 hours

before starting to slowly shorten, but fail to regenerate after deciliation by pH shock (Engel et al., 2012; Reck et al., 2016). Although the anterograde IFT is the immediate deliverer of ciliary proteins, the retrograde IFT might affect cilia assembly indirectly. They are two aspects of the same transportation mechanism, and it is understandable that their impact, direct or indirect, on cilia assembly and disassembly is synergistic instead of opposite. The rapid shortening of cilia caused by the overproduction of GFP-LF4A strongly suggests that LF4 inhibits the anterograde IFT while the effect on the retrograde IFT could be indirect through the modulation of the anterograde IFT. Alternatively, LF4 could also inhibit IFT dynein, for these effects on the motor could be direct or indirect by the regulation of the cargo load (Engel et al., 2012). Taken together, the results suggest that LF4 is intimately linked to IFT, by being a cargo as well as being an important regulator of IFT.

Whether LF4/MOK and MAK/ICK shorten cilia by phosphorylating the tail of kinesin-2 remains unresolved.

As LF4 kinase activity is necessary for its function as a negative regulator of IFT and cilia length, the identity of the relevant substrate(s) of phosphorylation is without a doubt the most significant piece of knowledge that is missing. Several studies have looked into the substrate specificity of another RCK family member ICK/MRK. Fu et al. (2006) first reported that ICK recognizes a phosphorylation consensus motif R-P-X-S/T-P/A/T/S based on a peptide library screen. Functional studies point at IFT components as strong candidates for the relevant substrates of RCKs. The murine KIF3A kinesin-2 motor subunit is phosphorylated by ICK in vitro and in vivo at a conserved R-P-R-T674-S-K-G motif. After a knockdown of endogenous KIF3A NIH3T3 cells, reintroduction of KIF3A

T674A substitution produces longer cilia than wild-type KIF3A. This is consistent with longer primary cilia in ICK knockdown NIH3T3 and IMCD-3 cells (Broekhuis et al., 2014; Yang et al., 2013), but contradicts the loss of cilia in ICK-KO MEF cells in an independent study (Chaya et al., 2014). Two independent ICK knockout mice generated around the same time also indicate that ICK has multiple effects on cilia length and ciliogenesis. The limb bud from an ICK knockout mouse has 2.5 fold longer primary cilia (Moon et al., 2014) while the other ICK knockout mouse has short cilia at the neural tube (Chaya et al., 2014). Although a reintroduction of KIF3A mutant with all adjacent serine and threonine substituted with alanine shows a ciliogenesis defect, it is not clear whether this defect is related to KIF3A inactivation by loss of ICK phosphorylation or more profound loss-of-function KIF3A. In the end, the functional connection between T674 phosphorylation of kinesin-2 and cilium length control have not been firmly established.

Tetrahymena has six motor subunits of kinesin-2. Three of them: KIN1, KIN2 and KIN3 are orthologs of the well-studied FLA10/FLA8 kinesin-2 subunits and the remaining three KIN5, KIN6 and KIN7 that are homologous to the OSM-3/KIF17 subtype of kinesin-2 (Wickstead et al., 2010). In *C. elegans,* Osm3 plays a specialized role in the assembly of the distal segment of cilia (Pan et al., 2006), while in mammals and *Tetrahymena* where distal segment is relatively short, losses of OSM-3/KIF17 or knockdown of KIN5 do not affect cilia assembly (Awan et al., 2009; Jenkins et al., 2006; Jiang et al., 2015a). On the other side, KIN1-GFP was detected moving with IFT speeds inside *Tetrahymena* cilia (data not shown). KIN1 and KIN2 are paralogs that are partially redundant and one of them is required for cilia assembly. A loss of both KIN1 and KIN2 causes the loss of cilia, cell paralysis and cytokinesis defect, similarly to the loss of Fla10

in *Chlamydomonas* (Brown et al., 1999) and is identical to the phenotype of overproduction of GFP-LF4A. It is therefore most likely that KIN1/KIN3 or KIN2/KIN3 motors provide the principal kinesin-2 activity in IFT in *Tetrahymena* and is the logical substrate of cilia length kinases, especially LF4.

We show that KIN1 is phosphorylated by LF4A *in vitro* at the high efficiency phosphorylation site, S695, conserved with KIF3A phosphorylation site by ICK above. Among the 3 subunits that likely form the principal kinesin-2 motor, KIN1, KIN2 and KIN3, only KIN1 has this motif (R-P-T-S695-K-P-G) for phosphorylation established for the RCK members. There is a similar motif that includes S708 that is far more weakly phosphorylated by LF4A *in vitro* (less than the autophosphorylation on GFP-LF4). A deletion of KIN1 does not visibly change or delay the kinetics of loss of cilia upon overexpression suggesting that the stronger phosphorylated site unique to KIN1 is not used by LF4A at all to shorten cilia. The weakly phosphorylated motif found in KIN1 is also present on KIN3 C-terminus. It is therefore possible that the weak site on KIN3 or another unidentified site on KIN2 or KIN3 is used by LF4A to mediate shortening of cilia. Overall, we cannot exclude a possibility that KIN1/KIN2/KIN3 provide the sought phosphorylation site(s) for LF4, though we feel that it is more likely that LF4A uses a different substrate to inhibit IFT and shorten cilia.

Model

Our results show that LF4 is an IFT cargo, inhibits IFT activity, and inhibits cilia assembly. Further, we show that LF4A-GFP is weakly bound to the axoneme and further GFP-LF4A accumulation in the cell body binds to some cytoskeletal structures with bundled microtubules. Both results are consistent with a weak interaction between LF4

and axonemal microtubules. We suggest that the axoneme affinity allows LF4 to stably and evenly distribute along the length of cilia (instead of free diffusion), an expected feature of a sensory and feedback role that tightly regulates cilia length. Therefore, we hypothesize a "time-of-flight" model: the LF4 is transported by IFT in to cilia and weakly binds to the axoneme. The axoneme-bound LF4 stochastically inhibits IFT activity, likely by phosphorylating an IFT protein. The longer the cilium, the more inhibited the IFT activity is. The "time-of flight" model projects that the steady-state cilium length is determined by the allocated amount of LF4 per basal body/cilium unit.

LF4A is not related to the anterior-posterior gradient in cilia length. Similarly, this autonomous model also has difficulty explaining how the cilia length responds to an external signal from the cell body. In a *Chlamydomonas* "long-short" assay, the wild-type length cilium shortens when the other cilium is amputated. It is unlikely that the IFT pool is depleted due to the loss of the IFT proteins within one cilium (Rosenbaum et al., 1969). It has been suggested that another regulator exclusively located at the basal region, such as CDKL5 in *Chlamydomonas*, regulates entry of proteins into the cilia, including ciliary regulatory proteins such as LF4 (Tam et al., 2013). In addition, IFT activity (including train size, speed and cargo loading) is also shown to be regulated at the base and/or distal region (cargo release and IFT turnaround) (Liang et al., 2014; Ludington et al., 2013). How both regulation at various ciliary compartments converge into a mechanism that regulates IFT activity and cilia length is still unclear. We can't exclude that LF4 is unrelated to IFT and cilia length regulation responding to external signal, though we think LF4A might still be regulated by cytoplasmic factors.

DYF18 regulates the abundance of LF4

We identified a mutation in *DYF18,* a DYF-18/LF2/CCRK related protein as a genetic suppressor of LF4A gain-of-function in *Tetrahymena*. Loss of its closest homolog, DYF-18 in *C. elegans*, leads to accumulation of some IFT proteins in ciliated chemosensory neurons (Phirke et al., 2011). In *Chlamydomonas*, several LF2 mutant alleles show on average longer (but also more variable in length) cilia than wild-type and is epistatic to LF4 mutant (Barsel et al., 1988).

RCK family member ICK is phosphorylated at the TDY activation motif and activated by the mammalian ortholog of LF2, CCRK *in vitro*, but not by the closely-related kinase, CDK7 that has not been reported in association with cilia (Fu et al., 2006; Fu et al., 2005). LF2/CCRK phosphorylates MAK affecting cell cycle in LNCaP prostate cancer cells which does not have a cilium (Wang and Kung, 2012) and ICK in HEK293 cells (Wu et al., 2012). Though not directly tested, LF4/MOK is also thought to autophosphorylate and be activated by LF2/CCRK as the mutation at the TEY motif impairs its kinase activity (Miyata et al., 1999). Related to cilia, a knockdown of CCRK (cyclin-dependent kinase 20) elongates cilia and promotes early ciliogenesis post starvation and a delayed cilium disassembly when mammalian cells return to the cell cycle upon addition of serum (Yang et al., 2013). The increase in cilium length and upregulation of ciliogenesis are reversed when overexpressing ICK that is perpetually activated by mutation at the activation loop (EDY instead of TDY), supporting that CCRK acts through ICK as an activator**.**

Our data in *Tetrahymena* show that DYF18 is a negative regulator of cilia length. Cells without DYF18 have locomotory cilia that are longer than wild type yet similar to

LF4A-KO. Additionally, DYF18-KO has longer oral cilia which is not observed in LF4A-KO. Double knockout of DYF18 and LF4A has the same phenotype as DYF18-KO. One explanation is that DYF18 activates LF4A and regulates locomotory cilia length. DYF18 also negatively regulates oral cilia length while LF4A does not. Old oral cilia partially disassemble and reassemble during cell division, while the old locomotory cilia remain the same, also indicating that the length of these two types of cilia are regulated differently. We propose that a pathway separate from LF4A, is also activated by DYF18 and regulates oral cilia length. Assuming that DYF18 is the upstream activator of LF4 and the other pathway possibly by direct phosphorylation, one simple candidate is LF4B (TTHERM_00822360) -the paralog of LF4A- which also has the same TEY activation loop phosphorylated by CCRK in MOK (TDY for ICK and MAK).

Interestingly, the LF2/CCRK is largely limited to the cell body and is not found inside cilia (Ko et al., 2010; Tam et al., 2007; Yang et al., 2013). We failed to detect any DYF18-GFP signal above the background, using anti-GFP antibodies and confocal microscopy or in cilia by TIRF microscopy (not shown). On the other hand, *Chlamydomonas* LF4, mammalian MOK and *Tetrahymena* LF4 are consistently found primarily in the cilia and at the basal body (Berman et al., 2003; Broekhuis et al., 2014). How does DYF18 activate LF4? GFP-LF4A purified from cells with DYF18 does not show higher kinase activity than from DYF18 null cells. It is possible that the sensitivity of this in vitro assay testing for a small increase of LF4 kinase activity is undermined by the excessive amount of GFP-LF4A. However, GFP-LF4A, without DYF18 activation, shorten cilia with either mildly elevated or high level of expression *in vivo*.

In the previously mentioned example where (overexpressed) perpetual ICK activation (EDY) shortens cilia and rescue increased ciliogenesis in CCRK knockdown, replacing ICK with ADY (cannot be phosphorylated by CCRK but can autophosphorylate) at the activation loop also partially rescues the increased ciliogenesis (Yang et al., 2013). Our data provides strong evidence that a complete loss of DYF18 activation is compensated by increased abundance of GFP-LF4A. We are reminded that ICK also weakly activates by autophosphorylation (Fu et al., 2005). The activity from an increased amount of kinase with this weak self-activation can be comparable to or surpass the activity from an endogenous amount of fully activated kinase. This self-activation may even be physiologically relevant when the downstream target such as LF4/MOK is autonomously activated due to restricted compartmentalization and is unable to access the external activator such as LF2/CCRK/DYF18. The abundance is the most direct mechanism of regulating the activity of an enzyme and a good indicator of its activity in the cell.

Alternatively, the phosphorylation by DYF18 may not only activate LF4 kinase activity but also regulate its abundance. The accumulation of GFP-LF4A due to overexpression by a *MTT1p* (heavy metal inducible promotor for metallothionein (Shang et al., 2002), unrelated to cilia) is greatly reduced by the loss of DYF18. Thus, DYF18 may be acting by preventing degradation of LF4. There is no direct evidence that LF4/MOK is regulated by protein degradation. However, ubiquitination has been implicated in the cilia length regulation. There is an increase in the levels of ubiquitinated ciliary proteins during cilia disassembly in *Chlamydomonas* (Huang et al., 2009). APC/C^{Cdc20} E3 ubiquitin ligase regulates cilium length and disassembly, as well as axonemal microtubule stability by degrading Nek1 kinase (Wang et al., 2014). Kim and

colleagues recently described a CDK5-Scf^{Fbw7}-Nde1 pathway through which the cell cycle progression governs the abundance of Nde1, a negative regulator of cilia length and ciliogenesis, by ubiquitination (Kim et al., 2011; 2015).

More interestingly, Wang and Kung (2012) showed that wild-type MAK interacts with the WD40 domain of CDH1 but not CDC20, two substrate recognition subunits of APC/C E3 ligase. The WD40 domain of CDH1 is involved in substrate binding and subsequent ubiquitination by APC/C^{CDH1}. An inactive MAK, either with K33R kinase activity mutation or an ADF activation loop mutation, show reduced interaction with CDH1. Overexpression of MAK can inhibit CDH1 interaction with CDC27 in the APC/C complex, and impair ubiquitination of Aurora A, suggesting MAK as both a substrate and a competitive inhibitor of APC/C^{CDH1}. This shows how the activity of an RCK kinase may affect its binding to the ubiquitination machinery and that its increased expression may lead to inhibition of ubiquitination on another target. This collaborating ubiquitination mechanism and phosphorylation activation by CCRK may direct RCK members into temporal and spatial regulation of multiple functions such as cell growth, ciliogenesis and cilia length regulation, allowing utilizing one activation pathway fulfilling related or even seemingly opposite functions such as the old oral cilia disassembly, maintaining locomotory cilia and ciliogenesis of new oral cilia and locomotory cilia around cell division in sync-step.

MATERIALS AND METHODS

Strains and cultures

SPP medium (Gorovsky and Woodard, 1969) was used to grow *Tetrahymena* strains with the exception that strains with severe cilia defects and resulting poor phagocytosis

were maintained in MEPP medium (Orias and Rasmussen, 1976) with added 2 µg/ml dextrose (MEPPD) (Gaertig et al., 2013). 2.5ug/ml $CdCl_2$ was added to SPP to induce *MTT1* promoter-driven overproduction of proteins.

Somatic and Germline transformation.

Plasmid and respective transformed strains are outlined below:

pMTT1-GFP	@	CU522,
pMTT1-GFP-LF4A	@	CU522
pMTT1-GFP-LF4A F82A	@	CU522
pMTT1-GFP-LF4A F82G	@	CU522
pNeo3 LF4A NLE	@	CU428
pNeo4 LF4A-KO	@	CU428+B2086 germline
pNeo5 DYF18 KO	@	CU428+B2086 germline
pMTT1-GFP-KINI	@	CU522
pMTT1-GFP-KINI 1-599	@	CU522
pMTT1-GFP-KINI 1-694	@	CU522
pMTT1-GFP-KINI S695A	@	CU522
pMTT1-GFP-KINI S708A	@	CU522
pMTT1-GFP-KINI S688G	@	CU522
pMTT1-GFP-KINI S688G S695A	@	CU522
pNeo5		
pNeo5 MTT1-GFP-LF4A (LF4)	@	CU428+B2086 germline and Dyf1GFP rescue
pNeo5 LF4A-KO	@	DYF1-GFP rescue

Confocal and TIRF microscopy

For immunofluorescence, cells were stained as described (Dave et al., 2009b) using simultaneous fixation (with 2% paraformaldehyde) and permeabilization (0.5% Triton X-100). To test for association with the cytoskeleton, cells were permeabilized with Triton X-100 prior to fixation with paraformaldehyde. Primary antibodies were: anti-GFP (1:50, rabbit, Rockland 600-401-215), anti-centrin 20H5 (1:200, mouse, Millipore 04-1624), anti-polyglycine serum 2302 (1:200, rabbit, gift of Martin Gorovsky, University of Rochester). Secondary antibodies were from Jackson Immuno Research. Images were taken using a Zeiss LSM 710 confocal microscope (63x oil immersion, 1x or 1.5x digital zoom) and analyzed with Fiji-ImageJ software (Schindelin et al., 2012).

Total internal reflection fluorescence microscopy of *Tetrahymena* was as described in (Jiang et al., 2015b). In experiments that required recording of IFT in cilia, only cells pressed under the coverslip for less than 25 minutes were recorded. Alternatively, a thin coat of petroleum jelly was used on the brim of the coverglasses to minimize the pressure due to rapid evaporation. Images and video recordings were processed in Fiji-ImageJ (Schindelin et al., 2012).

Western blots

Protein samples were separated on a 10% SDS-PAGE. The gels were either stained with blue silver (Candiano et al., 2004), or proteins were transferred onto PVDF membrane for western blotting. Primary antibodies used with western blots were: anti-GFP (1:5000, rabbit, Abcam ab6556 or 1:500, rabbit, Rockland 600-401-215), anti-thiophosphate ester 51-8 (1:2000-5000, rabbit, Abcam ab92570). Colorimetric images of

stained gels and immunoluminescent images of western blots were collected using ChemiDoc MP System and processed with Image Lab (Biorad).

Immunoprecipitations and on-beads *in vitro* kinase assay

Cultures of cells (30 ml for ovGFP-LF4A and/or ovGFP-LF4A F82A, F82G or 50-100 ml for GFP-KINI Full length, 1-599, 1-694, S688G, S695A, S708A) were used at $2x10^5$ /ml. Cells were exposed to 2.5 μg/ml $CdCl_2$ for 3-5 hr, then collected at 2700 rcf for 3 min and washed once with 10 mM Tris-HCl (pH 7.5) buffer. Lysis buffer (5 ml per 30 ml of Cd^{2+} induced cells) was added that contained 0.5% NP-40, phosphatase inhibitor cocktail (20 mM beta-glycerophosphoate, 1 mM sodium orthovanadate, 1 mM Na4P2O7, 20 mM NaF) and 70 mM E64, in TBS (20 mM Tris-HCl pH 7.5, 150 mM NaCl). PMSF was added to 1 mM immediately before suspending the cell pellets. The mixtures were kept on ice and were pipetted vigorously every 10 minutes for 3 times. Then, the mixtures were spun at 20,000 rcf for 15 minutes. Supernatants were collected, diluted with 2 volumes of TBS so that the NP-40 concentration is below 0.2% for immunoprecipitation with GFP-Trap beads (agarose, ACC0CM-GFA0050, Allele). Desired substrate candidates were GFP-tagged, such as GFP-KINI, GFP-IFT52 or GFP-DYF1, lysates were mixed with the GFP-LF4A lysate. When myelin basic protein was used as generic substrate, it was added after immunoprecipitation along with the kinase buffer (see below).

GFP-Trap beads (10-15 μl) were added to the diluted lysate (per 30 ml of the starting culture). The mixtures were then incubated at 4 °C for 2 hr. The beads were pelleted at 2700 rcf for 2 min, washed with TBS, washed with TBS with 500 mM NaCl, and washed with the kinase buffer (50 mM Tris-HCl pH 7.2, 100 mM NaCl, 10mM MgCl2).

The kinase buffer with phosphatase inhibitors (30 µl, 1 mM DTT and 100 µM ATP-gamma-S (Biolog 88453-52-5)) were added to no more than 25 µl of the beads slurry. If needed, 20 µg MBP (Active Motif 31314) was added. The kinase assay mixtures were incubated for 30-60 minutes at 30°C followed by addition of 2.5 mM PNBM (Abcam ab138910) and incubation for 2 hr at room temperature. The samples were then separated by SDS-PAGE. Alternatively, the kinase assay mixtures were incubated for 2 hr at 30 °C (omitting incubation with PNBM), the mixtures were separated on SDS-PAGE so that the corresponding bands (thio-phosphorylated KIN1) could be cut out for in-gel digestion and mass spectrometry.

In-gel digestion and mass spectrometry were performed at the Proteomics and Mass Spectrometry Core Facility at the University of Georgia.

Cilia regeneration

Deciliation and cilia regeneration were done as described in (Gaertig et al., 2013). Samples at the appropriate time points were retrieved for immunofluorescence.

Genetic screen for suppressors of GFP-LF4A overexpression

Mutagenesis and uniparental cytogamy

The neo5-MTT1_GFP-LF4A fragment was targeted to the LF4A locus in the micronucleus by biolistic transformation as described (Dave et al., 2009a). The heterokaryon strain ovGFP-LF4A-HE-3B (mic: neo5-ovGFP-LF4A mac: wild type, VII) were grown to $1x10^5$ /ml (40ml total). The growing culture was exposed to 10 µg/ml of nitrosoguanidine (Sigma-Aldrich) for 3 hr. The mutagenized culture was subjected to starvation by pelleting cells and suspending in Dryl's buffer (Dryl, 1959) (1.7 mM NaCitrate, 1 mM NaH_2P0_4 , 1 mM Na_2HPO_4 and 1.5 mM $CaCl_2$), overnight at 30°C. The

mutagenized cells were mixed with an equal volume and number of starved B*VI and subjected to uniparental cytogamy (Cole and Bruns, 1992). Briefly, 5-6 hours after mixing, the conjugating cells were treated with 1.4% glucose for 45 minutes and diluted with 7-10 volumes of sterile water. The cells were spun down, suspended in 30 ml of SPP and split into 5 ml samples, each kept inside a 500 ml capped bottle (six total) at room temperature overnight to complete self-fertilization.

Suppressor screen

SPP (45 ml) was added to each bottle, followed by incubation at 30 ℃ for 3 hr. Paromomycin (pm) was added to the final concentration of 200 μg/ml to select the conjugation progeny. After 24-36 hr of pm selection at 30 ℃, the progeny cells were collected by centrifugation and suspended in fresh 40 ml SPP with 2.0 μg/ml $CdCl_2$ (SPP + Cd) and incubated in standard polypropylene 50 ml conical centrifuge tubes in vertical positions overnight at room temperature. Due to GFP-LF4A overproduction and the resulting loss of cilia, unsuppressed cells become paralyzed and sink to the bottom of the tubes. Cells carrying suppressor mutations remain motile. Supernatant (4-5 ml) was collected from the top of each vertically positioned tube and cells were transferred into 5 ml fresh Cd^{2+}-free SPP in 15 ml conical tubes, incubated horizontally for 6 hr to overnight, then washed and resuspended in 10 ml SPP + Cd and the tubes were kept vertically oriented overnight. Single cell clones were isolated from the top 1 ml of culture from each tube. Individual clones were established, grown and retested for suppression in small scale cultures on 96-well plates. Best two suppressed closes from each tube were kept as F0 suppressor clones. For this study, 6 clones were isolated, each from a different selected batch.

Outcross and verification of the germ-line presence of the suppression.

The F0s were mated to the cycloheximide resistance (cy-r) heterokaryon CU427 (mic: *chx1-1*/*chx1-1*, mac: + VI) or CU427.7 (mic: *chx1-1*/*chx1-1*, mac: + VII) and the F1 progeny was recovered as pm-r and cy-r cells.

The F1 clones were matured and allowed to assort to paromomycin sensitivity (pm-s). The assorted pm-s F1 were used for the uniparental cytogamy (UPC cross) as follows.

Generation of F2 progeny

An F1 culture (~$2x10^5$ cells/ml, 40 ml) was mated to same volume of either B*VI or B*VII and subjected to UPC a described above. After the dilution of the osmotically-shocked culture, the cells were suspended in 25 ml of SPP. Twenty ml of cells were plated onto four 96-well plates at 50 µl per well. SPP + pm (400 µg/ml) were added to each well (50 µl) on the next day to select for F2 UPC progeny (for 36-48 hr).

Four 96-well plates of F2s were cloned by picking pm-r cells from different wells grown in SPP and tested on SPP + Cd by replica plating to test for segregation patterns for the cell paralysis as a proxy of cilia shortening. For the intragenic suppressors, 100% of pm-r clones became paralyzed with addition of Cd^{2+}. A single extragenic clone sup1 showed segregation of cell paralysis and resistance to paralysis among the pm-r F2 progeny.

Identification of the causal mutations for suppressors.

For the intragenic suppressors, total genomic DNA was extracted from a pool of F2s and the neo5-MTT1p-ovGFP-LF4A gene was amplified and sequenced using Sanger method.

For the single extragenic suppressor sup1, pools were prepared for the wild-type F2s that underwent paralysis in Cd^{2+} (12 clones) and suppressed F2s that resisted paralysis in Cd^{2+} (14 clones). The pools were grown as mixed cultures in 25 ml volumes starved overnight in 60 mM Tris-HCl and total genomic DNAs were extracted, using the urea method as described (Gaertig et al., 1994). The genomic DNAs were subjected to whole genome sequencing as described (Jiang et al., 2017). Variants were aligned to the macronuclear reference genome (June 2014 version, GenBank assembly accession GCA_000189635.1) (Eisen et al., 2006) and variants were detected filtered and subtracted as described (Jiang et al., 2017). In parallel, the suppressor and non-suppressor reads where aligned to the micronuclear reference genome (Hamilton et al., 2016) and the allelic contrast analysis was performed as described (Jiang et al., 2017) to detect a micronuclear chromosome location with increased frequency of variant cosegregation with the mutant (suppressed) phenotype using a *Tetrahymena*-customized MiModD (https://sourceforge.net/projects/mimodd/).

Structural Modeling of LF4A kinase

Th cyclin-dependent kinase from Cryptosporidium (Chain A of PDB 3NIZ) with highest similarity (37% sequence identity) was chosen as the template. Modeller program (version 9.12) was used to generate the homology model for LF4A from 3NIZ using the automodel module (Fiser et al., 2000). ADP and magnesium ions present in the template are also included in the modeled structure of LF4A. Visualization of the modeled structure was performed using PyMOL (Schrodinger, 2015).

REREFENCES

Abdul-Majeed, S., B.C. Moloney, and S.M. Nauli. 2012. Mechanisms regulating cilia growth and cilia function in endothelial cells. *Cellular and molecular life*

sciences : CMLS. 69:165-173.

Artz, J.D., A.K. Wernimont, A. Allali-Hassani, Y. Zhao, M. Amani, Y.H. Lin, G. Senisterra, G.A. Wasney, O. Fedorov, O. King, A. Roos, V.V. Lunin, W. Qiu, P. Finerty, Jr., A. Hutchinson, I. Chau, F. von Delft, F. MacKenzie, J. Lew, I. Kozieradzki, M. Vedadi, M. Schapira, C. Zhang, K. Shokat, T. Heightman, and R. Hui. 2011. The Cryptosporidium parvum kinome. *BMC genomics*. 12:478.

Asleson, C.M., and P.A. Lefebvre. 1998. Genetic analysis of flagellar length control in Chlamydomonas reinhardtii: a new long-flagella locus and extragenic suppressor mutations. *Genetics*. 148:693-702.

Awan, A., A.J. Bell, and P. Satir. 2009. Kin5 knockdown in Tetrahymena thermophila using RNAi blocks cargo transport of Gef1. *PloS one*. 4:e4873.

Barsel, S.E., D.E. Wexler, and P.A. Lefebvre. 1988. Genetic analysis of long-flagella mutants of Chlamydomonas reinhardtii. *Genetics*. 118:637-648.

Bengs, F., A. Scholz, D. Kuhn, and M. Wiese. 2005. LmxMPK9, a mitogen-activated protein kinase homologue affects flagellar length in Leishmania mexicana. *Molecular microbiology*. 55:1606-1615.

Berman, S.A., N.F. Wilson, N.A. Haas, and P.A. Lefebvre. 2003. A novel MAP kinase regulates flagellar length in Chlamydomonas. *Current biology : CB*. 13:1145-1149.

Bielas, S.L., J.L. Silhavy, F. Brancati, M.V. Kisseleva, L. Al-Gazali, L. Sztriha, R.A. Bayoumi, M.S. Zaki, A. Abdel-Aleem, O. Rosti, H. Kayserili, D. Swistun, L.C. Scott, E. Bertini, E. Boltshauser, E. Fazzi, L. Travaglini, S.J. Field, S. Gayral, M. Jacoby, S. Schurmans, B. Dallapiccola, P.W. Majerus, E.M. Valente, and J.G. Gleeson. 2009. Mutations in the inositol polyphosphate-5-phosphatase E gene link phosphatidyl inositol signaling to the ciliopathies. *Nature genetics*. 41:1032-1036.

Bradley, B.A., and L.M. Quarmby. 2005. A NIMA-related kinase, Cnk2p, regulates both flagellar length and cell size in Chlamydomonas. *Journal of cell science*. 118:3317-3326.

Broekhuis, J.R., K.J. Verhey, and G. Jansen. 2014. Regulation of Cilium Length and Intraflagellar Transport by the RCK-Kinases ICK and MOK in Renal Epithelial Cells. *PloS one*. 9:e108470.

Brown, J.M., C. Marsala, R. Kosoy, and J. Gaertig. 1999. Kinesin-II is preferentially targeted to assembling cilia and is required for ciliogenesis and normal cytokinesis in Tetrahymena. *Mol Biol Cell*. 10:3081-3096.

Burghoorn, J., M.P. Dekkers, S. Rademakers, T. de Jong, R. Willemsen, and G. Jansen. 2007. Mutation of the MAP kinase DYF-5 affects docking and undocking of kinesin-2 motors and reduces their speed in the cilia of Caenorhabditis elegans. *Proceedings of the National Academy of Sciences of the United States of America*. 104:7157-7162.

Candiano, G., M. Bruschi, L. Musante, L. Santucci, G.M. Ghiggeri, B. Carnemolla, P.

Orecchia, L. Zardi, and P.G. Righetti. 2004. Blue silver: a very sensitive colloidal Coomassie G-250 staining for proteome analysis. *Electrophoresis*. 25:1327-1333.

Cao, M., D. Meng, L. Wang, S. Bei, W.J. Snell, and J. Pan. 2013. Activation loop phosphorylation of a protein kinase is a molecular marker of organelle size that dynamically reports flagellar length. *Proceedings of the National Academy of Sciences of the United States of America*.

Castren, M., E. Gaily, C. Tengstrom, J. Lahdetie, H. Archer, and S. Ala-Mello. 2011. Epilepsy caused by CDKL5 mutations. *Eur J Paediatr Neurol*. 15:65-69.

Chaya, T., Y. Omori, R. Kuwahara, and T. Furukawa. 2014. ICK is essential for cell type-specific ciliogenesis and the regulation of ciliary transport. *The EMBO journal*.

Chen, T., D. Wu, C.A. Moskaluk, and Z. Fu. 2013. Distinct expression patterns of ICK/MAK/MOK protein kinases in the intestine implicate functional diversity. *PloS one*. 8:e79359.

Cole, D.G., D.R. Diener, A.L. Himelblau, P.L. Beech, J.C. Fuster, and J.L. Rosenbaum. 1998. Chlamydomonas Kinesin-II–dependent Intraflagellar Transport (IFT): IFT Particles Contain Proteins Required for Ciliary Assembly in Caenorhabditis elegans Sensory Neurons. *The Journal of cell biology*. 141:993-1008.

Cole, E.S., and P.J. Bruns. 1992. Uniparental cytogamy: a novel method for bringing micronuclear mutations of Tetrahymena into homozygous macronuclear expression with precocious sexual maturity. *Genetics*. 132:1017-1031.

Craft, J.M., J.A. Harris, S. Hyman, P. Kner, and K.F. Lechtreck. 2015. Tubulin transport by IFT is upregulated during ciliary growth by a cilium-autonomous mechanism. *The Journal of cell biology*. 208:223-237.

Dave, D., D. Wloga, and J. Gaertig. 2009a. Manipulating ciliary protein-encoding genes in Tetrahymena thermophila. *Methods Cell Biol*. 93:1-20.

Dave, D., D. Wloga, N. Sharma, and J. Gaertig. 2009b. DYF-1 Is required for assembly of the axoneme in Tetrahymena thermophila. *Eukaryotic cell*. 8:1397-1406.

Dentler, W. 2005. Intraflagellar transport (IFT) during assembly and disassembly of Chlamydomonas flagella. *The Journal of cell biology*. 170:649-659.

Dryl, S. 1959. Antigenic transformation in Paramecium aurelia after homologous antiserum treatment during autogamy and conjugation. *The Journal of protozoology*. 6:25.

Eisen, J.A., R.S. Coyne, M. Wu, D. Wu, M. Thiagarajan, J.R. Wortman, J.H. Badger, Q. Ren, P. Amedeo, K.M. Jones, L.J. Tallon, A.L. Delcher, S.L. Salzberg, J.C. Silva, B.J. Haas, W.H. Majoros, M. Farzad, J.M. Carlton, R.K. Smith, Jr., J. Garg, R.E. Pearlman, K.M. Karrer, L. Sun, G. Manning, N.C. Elde, A.P. Turkewitz, D.J. Asai, D.E. Wilkes, Y. Wang, H. Cai, K. Collins, B.A. Stewart, S.R. Lee, K. Wilamowska, Z. Weinberg, W.L. Ruzzo, D. Wloga, J. Gaertig, J. Frankel, C.C. Tsao, M.A. Gorovsky, P.J. Keeling, R.F. Waller, N.J. Patron, J.M. Cherry, N.A. Stover, C.J. Krieger, C. del Toro, H.F. Ryder, S.C. Williamson, R.A. Barbeau, E.P. Hamilton, and E. Orias. 2006. Macronuclear genome sequence of the ciliate

Tetrahymena thermophila, a model eukaryote. *PLoS biology*. 4:e286.

Engel, B.D., H. Ishikawa, K.A. Wemmer, S. Geimer, K. Wakabayashi, M. Hirono, B. Craige, G.J. Pazour, G.B. Witman, R. Kamiya, and W.F. Marshall. 2012. The role of retrograde intraflagellar transport in flagellar assembly, maintenance, and function. *The Journal of cell biology*. 199:151-167.

Engel, B.D., W.B. Ludington, and W.F. Marshall. 2009. Intraflagellar transport particle size scales inversely with flagellar length: revisiting the balance-point length control model. *The Journal of cell biology*. 187:81-89.

Erdmann, M., A. Scholz, I.M. Melzer, C. Schmetz, and M. Wiese. 2006. Interacting protein kinases involved in the regulation of flagellar length. *Mol Biol Cell*. 17:2035-2045.

Fiser, A., R.K. Do, and A. Sali. 2000. Modeling of loops in protein structures. *Protein science : a publication of the Protein Society*. 9:1753-1773.

Frankel, J., E.M. Nelsen, and E. Martel. 1981. Development of the ciliature of Tetrahymena thermophila. II. Spatial subdivision prior to cytokinesis. *Developmental biology*. 88:39-54.

Fu, Z., K.A. Larson, R.K. Chitta, S.A. Parker, B.E. Turk, M.W. Lawrence, P. Kaldis, K. Galaktionov, S.M. Cohn, J. Shabanowitz, D.F. Hunt, and T.W. Sturgill. 2006. Identification of yin-yang regulators and a phosphorylation consensus for male germ cell-associated kinase (MAK)-related kinase. *Molecular and cellular biology*. 26:8639-8654.

Fu, Z., M.J. Schroeder, J. Shabanowitz, P. Kaldis, K. Togawa, A.K. Rustgi, D.F. Hunt, and T.W. Sturgill. 2005. Activation of a nuclear Cdc2-related kinase within a mitogen-activated protein kinase-like TDY motif by autophosphorylation and cyclin-dependent protein kinase-activating kinase. *Molecular and cellular biology*. 25:6047-6064.

Gaertig, J., T.H. Thatcher, L. Gu, and M.A. Gorovsky. 1994. Electroporation-mediated replacement of a positively and negatively selectable beta-tubulin gene in Tetrahymena thermophila. *Proceedings of the National Academy of Sciences of the United States of America*. 91:4549-4553.

Gaertig, J., D. Wloga, K.K. Vasudevan, M. Guha, and W. Dentler. 2013. Discovery and functional evaluation of ciliary proteins in Tetrahymena thermophila. *Methods in enzymology*. 525:265-284.

Gorovsky, M.A., and J. Woodard. 1969. STUDIES ON NUCLEAR STRUCTURE AND FUNCTION IN TETRAHYMENA PYRIFORMIS: I. RNA Synthesis in Macro- and Micronuclei. *The Journal of cell biology*. 42:673-682.

Grati, M., I. Chakchouk, Q. Ma, M. Bensaid, A. Desmidt, N. Turki, D. Yan, A. Baanannou, R. Mittal, N. Driss, S. Blanton, A. Farooq, Z. Lu, X.Z. Liu, and S. Masmoudi. 2015. A missense mutation in DCDC2 causes human recessive deafness DFNB66, likely by interfering with sensory hair cell and supporting cell cilia length regulation. *Human molecular genetics*. 24:2482-2491.

Hakim, S., J.M. Dyson, S.J. Feeney, E.M. Davies, A. Sriratana, M.N. Koenig, O.V. Plotnikova, I.M. Smyth, S.D. Ricardo, R.M. Hobbs, and C.A. Mitchell. 2016. Inpp5e suppresses polycystic kidney disease via inhibition of PI3K/Akt-dependent mTORC1 signaling. *Human molecular genetics*. 25:2295-2313.

Hamilton, E.P., A. Kapusta, P.E. Huvos, S.L. Bidwell, N. Zafar, H. Tang, M. Hadjithomas, V. Krishnakumar, J.H. Badger, E.V. Caler, C. Russ, Q. Zeng, L. Fan, J.Z. Levin, T. Shea, S.K. Young, R. Hegarty, R. Daza, S. Gujja, J.R. Wortman, B.W. Birren, C. Nusbaum, J. Thomas, C.M. Carey, E.J. Pritham, C. Feschotte, T. Noto, K. Mochizuki, R. Papazyan, S.D. Taverna, P.H. Dear, D.M. Cassidy-Hanley, J. Xiong, W. Miao, E. Orias, and R.S. Coyne. 2016. Structure of the germline genome of Tetrahymena thermophila and relationship to the massively rearranged somatic genome. *eLife*. 5.

Hilton, L.K., K. Gunawardane, J.W. Kim, M.C. Schwarz, and L.M. Quarmby. 2013. The kinases LF4 and CNK2 control ciliary length by feedback regulation of assembly and disassembly rates. *Current biology : CB*. 23:2208-2214.

Howard, C.J., V. Hanson-Smith, K.J. Kennedy, C.J. Miller, H.J. Lou, A.D. Johnson, B.E. Turk, and L.J. Holt. 2014. Ancestral resurrection reveals evolutionary mechanisms of kinase plasticity. *eLife*. 3.

Huang, K., D.R. Diener, and J.L. Rosenbaum. 2009. The ubiquitin conjugation system is involved in the disassembly of cilia and flagella. *The Journal of cell biology*. 186:601-613.

Husson, H., S. Moreno, L.A. Smith, M.M. Smith, R.J. Russo, R. Pitstick, M. Sergeev, S.R. Ledbetter, N.O. Bukanov, M. Lane, K. Zhang, K. Billot, G. Carlson, J. Shah, L. Meijer, D.R. Beier, and O. Ibraghimov-Beskrovnaya. 2016. Reduction of ciliary length through pharmacologic or genetic inhibition of CDK5 attenuates polycystic kidney disease in a model of nephronophthisis. *Human molecular genetics*. 25:2245-2255.

Jenkins, P.M., T.W. Hurd, L. Zhang, D.P. McEwen, R.L. Brown, B. Margolis, K.J. Verhey, and J.R. Martens. 2006. Ciliary targeting of olfactory CNG channels requires the CNGB1b subunit and the kinesin-2 motor protein, KIF17. *Current biology : CB*. 16:1211-1216.

Jiang, L., B.M. Tam, G. Ying, S. Wu, W.W. Hauswirth, J.M. Frederick, O.L. Moritz, and W. Baehr. 2015a. Kinesin family 17 (osmotic avoidance abnormal-3) is dispensable for photoreceptor morphology and function. *FASEB journal : official publication of the Federation of American Societies for Experimental Biology*. 29:4866-4880.

Jiang, Y.-Y., K. Lechtreck, and J. Gaertig. 2015b. Total internal reflection fluorescence microscopy of intraflagellar transport in Tetrahymena thermophila. *In* Methods in Cell Biology. Academic Press.

Jiang, Y.-Y., W. Maier, R. Baumeister, G. Minevich, E. Joachimiak, Z. Ruan, N. Kannan, D. Clarke, J. Frankel, and J. Gaertig. 2017. The Hippo Pathway Maintains the Equatorial Division Plane in the Ciliate Tetrahymena. *Genetics*.

Jiang, Y.Y., K. Lechtreck, and J. Gaertig. 2015c. Total internal reflection fluorescence microscopy of intraflagellar transport in Tetrahymena thermophila. *Methods Cell Biol*. 127:445-456.

Kim, S., N.A. Zaghloul, E. Bubenshchikova, E.C. Oh, S. Rankin, N. Katsanis, T. Obara, and L. Tsiokas. 2011. Nde1-mediated inhibition of ciliogenesis affects cell cycle re-entry. *Nat Cell Biol*. 13:351-360.

Ko, H.W., R.X. Norman, J. Tran, K.P. Fuller, M. Fukuda, and J.T. Eggenschwiler. 2010. Broad-minded links cell cycle-related kinase to cilia assembly and hedgehog signal transduction. *Developmental cell*. 18:237-247.

Kozminski, K.G., P.L. Beech, and J.L. Rosenbaum. 1995. The Chlamydomonas kinesin-like protein FLA10 is involved in motility associated with the flagellar membrane. *The Journal of cell biology*. 131:1517-1527.

Kubo, T., J.M. Brown, K. Bellve, B. Craige, J.M. Craft, K. Fogarty, K.F. Lechtreck, and G.B. Witman. 2016. Together, the IFT81 and IFT74 N-termini form the main module for intraflagellar transport of tubulin. *Journal of cell science*. 129:2106-2119.

Lechtreck, K.F. 2015. IFT-Cargo Interactions and Protein Transport in Cilia. *Trends in biochemical sciences*. 40:765-778.

Lefebvre, P.A., S.A. Nordstrom, J.E. Moulder, and J.L. Rosenbaum. 1978. Flagellar elongation and shortening in Chlamydomonas. IV. Effects of flagellar detachment, regeneration, and resorption on the induction of flagellar protein synthesis. *The Journal of cell biology*. 78:8-27.

Liang, Y., D. Meng, B. Zhu, and J. Pan. 2016. Mechanism of ciliary disassembly. *Cellular and molecular life sciences : CMLS*. 73:1787-1802.

Liang, Y., Y. Pang, Q. Wu, Z. Hu, X. Han, Y. Xu, H. Deng, and J. Pan. 2014. FLA8/KIF3B Phosphorylation Regulates Kinesin-II Interaction with IFT-B to Control IFT Entry and Turnaround. *Developmental cell*. 30:585-597.

Lin, H., Z. Zhang, S. Guo, F. Chen, J.M. Kessler, Y.M. Wang, and S.K. Dutcher. 2015. A NIMA-Related Kinase Suppresses the Flagellar Instability Associated with the Loss of Multiple Axonemal Structures. *PLoS genetics*. 11:e1005508.

Liu, S., W. Lu, T. Obara, S. Kuida, J. Lehoczky, K. Dewar, I.A. Drummond, and D.R. Beier. 2002. A defect in a novel Nek-family kinase causes cystic kidney disease in the mouse and in zebrafish. *Development*. 129:5839-5846.

Ludington, W.B., K.A. Wemmer, K.F. Lechtreck, G.B. Witman, and W.F. Marshall. 2013. Avalanche-like behavior in ciliary import. *Proceedings of the National Academy of Sciences of the United States of America*.

Luo, M., M. Cao, Y. Kan, G. Li, W. Snell, and J. Pan. 2011. The phosphorylation state of an aurora-like kinase marks the length of growing flagella in Chlamydomonas. *Current biology : CB*. 21:586-591.

Marshall, W.F., H. Qin, M. Rodrigo Brenni, and J.L. Rosenbaum. 2005. Flagellar length control system: testing a simple model based on intraflagellar transport and

turnover. *Mol Biol Cell*. 16:270-278.

Marshall, W.F., and J.L. Rosenbaum. 2001. Intraflagellar transport balances continuous turnover of outer doublet microtubules: implications for flagellar length control. *The Journal of cell biology*. 155:405-414.

Maskey, D., M.C. Marlin, S. Kim, S. Kim, E.C. Ong, G. Li, and L. Tsiokas. 2015. Cell cycle-dependent ubiquitylation and destruction of NDE1 by CDK5-FBW7 regulates ciliary length. *The EMBO journal*. 34:2424-2440.

Meng, D., and J. Pan. 2016. A NIMA-related kinase, CNK4, regulates ciliary stability and length. *Mol Biol Cell*. 27:838-847.

Miyata, Y., M. Akashi, and E. Nishida. 1999. Molecular cloning and characterization of a novel member of the MAP kinase superfamily. *Genes to cells : devoted to molecular & cellular mechanisms*. 4:299-309.

Moon, H., J. Song, J.O. Shin, H. Lee, H.K. Kim, J.T. Eggenschwiller, J. Bok, and H.W. Ko. 2014. Intestinal cell kinase, a protein associated with endocrine-cerebro-osteodysplasia syndrome, is a key regulator of cilia length and Hedgehog signaling. *Proceedings of the National Academy of Sciences of the United States of America*. 111:8541-8546.

Nurse, P., and P. Thuriaux. 1980. Regulatory genes controlling mitosis in the fission yeast Schizosaccharomyces pombe. *Genetics*. 96:627-637.

Omori, Y., T. Chaya, K. Katoh, N. Kajimura, S. Sato, K. Muraoka, S. Ueno, T. Koyasu, M. Kondo, and T. Furukawa. 2010. Negative regulation of ciliary length by ciliary male germ cell-associated kinase (Mak) is required for retinal photoreceptor survival. *Proceedings of the National Academy of Sciences of the United States of America*. 107:22671-22676.

Orias, E., and L. Rasmussen. 1976. Dual capacity for nutrient uptake in Tetrahymena. IV. Growth without food vacuoles and its implications. *Experimental cell research*. 102:127-137.

Oud, M.M., C. Bonnard, D.A. Mans, U. Altunoglu, S. Tohari, A.Y. Ng, A. Eskin, H. Lee, C.A. Rupar, N.P. de Wagenaar, K.M. Wu, P. Lahiry, G.J. Pazour, S.F. Nelson, R.A. Hegele, R. Roepman, H. Kayserili, B. Venkatesh, V.M. Siu, B. Reversade, and H.H. Arts. 2016. A novel ICK mutation causes ciliary disruption and lethal endocrine-cerebro-osteodysplasia syndrome. *Cilia*. 5:8.

Ozgul, R.K., A.M. Siemiatkowska, D. Yucel, C.A. Myers, R.W. Collin, M.N. Zonneveld, A. Beryozkin, E. Banin, C.B. Hoyng, L.I. van den Born, C. European Retinal Disease, R. Bose, W. Shen, D. Sharon, F.P. Cremers, B.J. Klevering, A.I. den Hollander, and J.C. Corbo. 2011. Exome sequencing and cis-regulatory mapping identify mutations in MAK, a gene encoding a regulator of ciliary length, as a cause of retinitis pigmentosa. *American journal of human genetics*. 89:253-264.

Pan, J., and W.J. Snell. 2005. Chlamydomonas shortens its flagella by activating axonemal disassembly, stimulating IFT particle trafficking, and blocking anterograde cargo loading. *Developmental cell*. 9:431-438.

Pan, J., Q. Wang, and W.J. Snell. 2004. An aurora kinase is essential for flagellar disassembly in Chlamydomonas. *Developmental cell*. 6:445-451.

Pan, X., G. Ou, G. Civelekoglu-Scholey, O.E. Blacque, N.F. Endres, L. Tao, A. Mogilner, M.R. Leroux, R.D. Vale, and J.M. Scholey. 2006. Mechanism of transport of IFT particles in C. elegans cilia by the concerted action of kinesin-II and OSM-3 motors. *The Journal of cell biology*. 174:1035-1045.

Phirke, P., E. Efimenko, S. Mohan, J. Burghoorn, F. Crona, M.W. Bakhoum, M. Trieb, K. Schuske, E.M. Jorgensen, B.P. Piasecki, M.R. Leroux, and P. Swoboda. 2011. Transcriptional profiling of C. elegans DAF-19 uncovers a ciliary base-associated protein and a CDK/CCRK/LF2p-related kinase required for intraflagellar transport. *Developmental biology*. 357:235-247.

Rajagopalan, V., A. Subramanian, D.E. Wilkes, D.G. Pennock, and D.J. Asai. 2009. Dynein-2 affects the regulation of ciliary length but is not required for ciliogenesis in Tetrahymena thermophila. *Mol Biol Cell*. 20:708-720.

Reck, J., A.M. Schauer, K. VanderWaal Mills, R. Bower, D. Tritschler, C.A. Perrone, and M.E. Porter. 2016. The role of the dynein light intermediate chain in retrograde IFT and flagellar function in Chlamydomonas. *Mol Biol Cell*. 27:2404-2422.

Rosenbaum, J.L., J.E. Moulder, and D.L. Ringo. 1969. FLAGELLAR ELONGATION AND SHORTENING IN CHLAMYDOMONAS : The Use of Cycloheximide and Colchicine to Study the Synthesis and Assembly of Flagellar Proteins. *The Journal of cell biology*. 41:600-619.

Schindelin, J., I. Arganda-Carreras, E. Frise, V. Kaynig, M. Longair, T. Pietzsch, S. Preibisch, C. Rueden, S. Saalfeld, B. Schmid, J.-Y. Tinevez, D.J. White, V. Hartenstein, K. Eliceiri, P. Tomancak, and A. Cardona. 2012. Fiji: an open-source platform for biological-image analysis. *Nat Meth*. 9:676-682.

Schrodinger, LLC. 2015. The PyMOL Molecular Graphics System, Version 1.8.

Sellami, S., M. Cherif, and K. Jamoussi. 2016. Effect of adding amino acids residues in N- and C-terminus of Vip3Aa16 (L121I) toxin. *J Basic Microbiol*. 56:654-661.

Shang, Y., X. Song, J. Bowen, R. Corstanje, Y. Gao, J. Gaertig, and M.A. Gorovsky. 2002. A robust inducible-repressible promoter greatly facilitates gene knockouts, conditional expression, and overexpression of homologous and heterologous genes in Tetrahymena thermophila. *Proceedings of the National Academy of Sciences of the United States of America*. 99:3734-3739.

Sharma, N., J. Bryant, D. Wloga, R. Donaldson, R.C. Davis, M. Jerka-Dziadosz, and J. Gaertig. 2007. Katanin regulates dynamics of microtubules and biogenesis of motile cilia. *The Journal of cell biology*. 178:1065-1079.

Slaats, G.G., C.R. Isabella, H.Y. Kroes, J.C. Dempsey, H. Gremmels, G.R. Monroe, I.G. Phelps, K.J. Duran, J. Adkins, S.A. Kumar, D.M. Knutzen, N.V. Knoers, N.J. Mendelsohn, D. Neubauer, S.D. Mastroyianni, J. Vogt, L. Worgan, N. Karp, S. Bowdin, I.A. Glass, M.A. Parisi, E.A. Otto, C.A. Johnson, F. Hildebrandt, G. van Haaften, R.H. Giles, and D. Doherty. 2016. MKS1 regulates ciliary INPP5E levels in Joubert syndrome. *Journal of medical genetics*. 53:62-72.

Smith, H.E., and A.P. Mitchell. 1989. A transcriptional cascade governs entry into meiosis in Saccharomyces cerevisiae. *Molecular and cellular biology*. 9:2142-2152.

Stepanek, L., and G. Pigino. 2016. Microtubule doublets are double-track railways for intraflagellar transport trains. *Science*. 352:721-724.

Stone, E.M., X. Luo, E. Heon, B.L. Lam, R.G. Weleber, J.A. Halder, L.M. Affatigato, J.B. Goldberg, A. Sumaroka, S.B. Schwartz, A.V. Cideciyan, and S.G. Jacobson. 2011. Autosomal recessive retinitis pigmentosa caused by mutations in the MAK gene. *Investigative ophthalmology & visual science*. 52:9665-9673.

Tam, L.W., P.T. Ranum, and P.A. Lefebvre. 2013. CDKL5 Regulates Flagellar Length and Localizes to the Base of the Flagella in Chlamydomonas. *Mol Biol Cell*.

Tam, L.W., N.F. Wilson, and P.A. Lefebvre. 2007. A CDK-related kinase regulates the length and assembly of flagella in Chlamydomonas. *The Journal of cell biology*. 176:819-829.

Tammachote, R., C.J. Hommerding, R.M. Sinders, C.A. Miller, P.G. Czarnecki, A.C. Leightner, J.L. Salisbury, C.J. Ward, V.E. Torres, V.H. Gattone, 2nd, and P.C. Harris. 2009. Ciliary and centrosomal defects associated with mutation and depletion of the Meckel syndrome genes MKS1 and MKS3. *Human molecular genetics*. 18:3311-3323.

Taylor, S.P., T.J. Dantas, I. Duran, S. Wu, R.S. Lachman, C. University of Washington Center for Mendelian Genomics, S.F. Nelson, D.H. Cohn, R.B. Vallee, and D. Krakow. 2015. Mutations in DYNC2LI1 disrupt cilia function and cause short rib polydactyly syndrome. *Nature communications*. 6:7092.

Thiel, C., K. Kessler, A. Giessl, A. Dimmler, S.A. Shalev, S. von der Haar, M. Zenker, D. Zahnleiter, H. Stoss, E. Beinder, R. Abou Jamra, A.B. Ekici, N. Schroder-Kress, T. Aigner, T. Kirchner, A. Reis, J.H. Brandstatter, and A. Rauch. 2011. NEK1 mutations cause short-rib polydactyly syndrome type majewski. *American journal of human genetics*. 88:106-114.

Torkamani, A., N. Kannan, S.S. Taylor, and N.J. Schork. 2008. Congenital disease SNPs target lineage specific structural elements in protein kinases. *Proceedings of the National Academy of Sciences of the United States of America*. 105:9011-9016.

Upadhya, P., E.H. Birkenmeier, C.S. Birkenmeier, and J.E. Barker. 2000. Mutations in a NIMA-related kinase gene, Nek1, cause pleiotropic effects including a progressive polycystic kidney disease in mice. *Proceedings of the National Academy of Sciences of the United States of America*. 97:217-221.

Vasudevan, K.K., K. Song, L.M. Alford, W.S. Sale, E.E. Dymek, E.F. Smith, T. Hennessey, E. Joachimiak, P. Urbanska, D. Wloga, W. Dentler, D. Nicastro, and J. Gaertig. 2015. FAP206 is a microtubule-docking adapter for ciliary radial spoke 2 and dynein c. *Mol Biol Cell*. 26:696-710.

Wang, L.Y., and H.J. Kung. 2012. Male germ cell-associated kinase is overexpressed in prostate cancer cells and causes mitotic defects via deregulation of APC/CCDH1. *Oncogene*. 31:2907-2918.

Wang, W., T. Wu, and M.W. Kirschner. 2014. The master cell cycle regulator APC-Cdc20 regulates ciliary length and disassembly of the primary cilium. *eLife*. 3:e03083.

Wemmer, K.A., and W.F. Marshall. 2007. Flagellar length control in chlamydomonas--paradigm for organelle size regulation. *International review of cytology*. 260:175-212.

Wickstead, B., K. Gull, and T.A. Richards. 2010. Patterns of kinesin evolution reveal a complex ancestral eukaryote with a multifunctional cytoskeleton. *BMC evolutionary biology*. 10:110.

Wloga, D., A. Camba, K. Rogowski, G. Manning, M. Jerka-Dziadosz, and J. Gaertig. 2006. Members of the NIMA-related kinase family promote disassembly of cilia by multiple mechanisms. *Molecular biology of the cell*. 17:2799-2810.

Wloga, D., K. Rogowski, N. Sharma, J. Van Dijk, C. Janke, B. Edde, M.H. Bre, N. Levilliers, V. Redeker, J. Duan, M.A. Gorovsky, M. Jerka-Dziadosz, and J. Gaertig. 2008. Glutamylation on alpha-tubulin is not essential but affects the assembly and functions of a subset of microtubules in Tetrahymena thermophila. *Eukaryotic cell*. 7:1362-1372.

Wloga, D., D.M. Webster, K. Rogowski, M.H. Bre, N. Levilliers, M. Jerka-Dziadosz, C. Janke, S.T. Dougan, and J. Gaertig. 2009. TTLL3 Is a tubulin glycine ligase that regulates the assembly of cilia. *Developmental cell*. 16:867-876.

Wren, K.N., J.M. Craft, D. Tritschler, A. Schauer, D.K. Patel, E.F. Smith, M.E. Porter, P. Kner, and K.F. Lechtreck. 2013. A differential cargo-loading model of ciliary length regulation by IFT. *Current biology : CB*. 23:2463-2471.

Wu, D., J.R. Chapman, L. Wang, T.E. Harris, J. Shabanowitz, D.F. Hunt, and Z. Fu. 2012. Intestinal cell kinase (ICK) promotes activation of mTOR complex 1 (mTORC1) through phosphorylation of Raptor Thr-908. *The Journal of biological chemistry*. 287:12510-12519.

Yang, Y., N. Roine, and T.P. Makela. 2013. CCRK depletion inhibits glioblastoma cell proliferation in a cilium-dependent manner. *EMBO reports*.

FIGURES AND FIGURE LEGENDS

Figure 2.1. **LF4/MOK is a RCK family member, negatively regulates cilium length in *Tetrahymena*.** (A) A maximum likelihood phylogenetic tree obtained using PhyML for subset of CMGC kinases group including homologs of LF2/CCRK/DYF-18, LF4/MOK, ICK/MAK, and CDK. The human ERK1 kinase was used as an outgroup. The numbers on branches represent a LRT SH-like support values. The numbers in parenthesis represent branch support values obtained by bootstrapping. Only values above 0.5 are shown. (B) A knockout of LF4A lengthens the locomotory cilia. Wild-type and LF4A-KO cells were stained with anti-polyG (serum 2302) antibodies to visualize cilia (green), anti-centrin 20H5 antibody to mark the basal bodies (red) and DAPI to detect the nuclei (blue). Arrowheads indicate posterior-dorsal region of the cell. Abbreviation: oral apparatus (oa). (C) A histogram of locomotory cilia length for wild-type and LF4A-KO

cells. Cilia from no less than ten (10) of wildtype and LF4A-KO cells were measured. The average cilium length for the wild type (n = 216) is 5.88 µm, SD: 0.38 µm; the average cilia length from LF4A-KO (n = 367) is 7.74 µm, SD: 1.82 µm. $p < 0.1\%$.

Figure 2.1

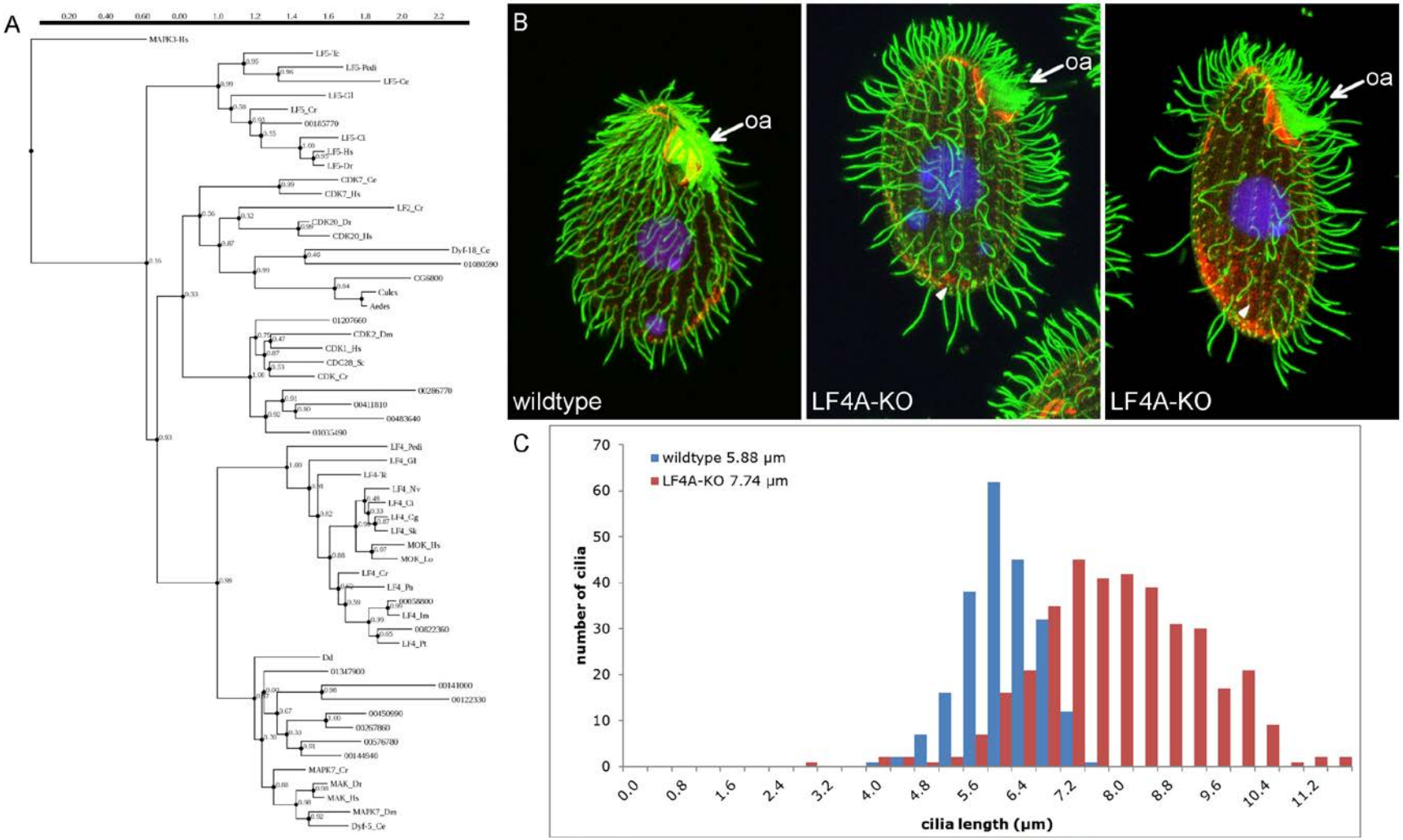
A
0.20 0.40 0.60 0.80 1.0 1.2 1.4 1.6 1.8 2.0 2.2
MAPK3-Hs
LF5-Tc
LF5-Pedi
LF5-Ce
LF5-Cl1
LF5_Cr
00165770
LF5-Cl
LF5-Hs
LF5-Dr
CDK7_Ce
CDK7_Hs
LF2_Cr
CDK20_Dr
CDK20_Hs
Dyf-18_Ce
01080590
CG6800
Culex
Aedes
01207660
CDK2_Dm
CDK1_Hs
CDC28_Sc
CDK_Cr
00286770
00411810
00483640
01035490
LF4_Pedi
LF4_Gl
LF4-Tc
LF4_Nv
LF4_Cl
LF4_Cg
LF4_Sk
MOK_Hs
MOK_Lo
LF4_Cr
LF4_Pa
00058600
LF4_Im
00822360
LF4_Pt
Dd
01347900
00141000
00122330
00450690
03267860
00576780
00144940
MAPK7_Cr
MAK_Dr
MAK_Hs
MAPK7_Dm
Dyf-5_Ce
B
oa
wildtype
oa
LF4A-KO
oa
LF4A-KO
C
wildtype 5.88 µm
LF4A-KO 7.74 µm
number of cilia
0
10
20
30
40
50
60
70
0.0 0.8 1.6 2.4 3.2 4.0 4.8 5.6 6.4 7.2 8.0 8.8 9.6 10.4 11.2
cilia length (µm)

Figure 2.2. **LF4A-KO cilia regenerate faster than the wild type.** (A) The length of the wild-type and LF4A-KO cilia at several times after deciliation by pH shock. Four to six cells, 50 - 150 cilia were used per each time point. Error bars indicate standard deviations. Asterisks (*) indicate significant difference between the mutant and wild-type averages at the time point ($p < 0.1\%$ for each pair). (B) Wildtype and LF4A-KO cells at 60 min or 180 min post deciliation labeled with anti-polyG (green), anti-centrin (red) and DAPI (blue). Note that the oral cilia in the LF4A-KO appeared to regenerate, slower than surrounding locomotory cilia and more in line with the wild-type.

Figure 2.2

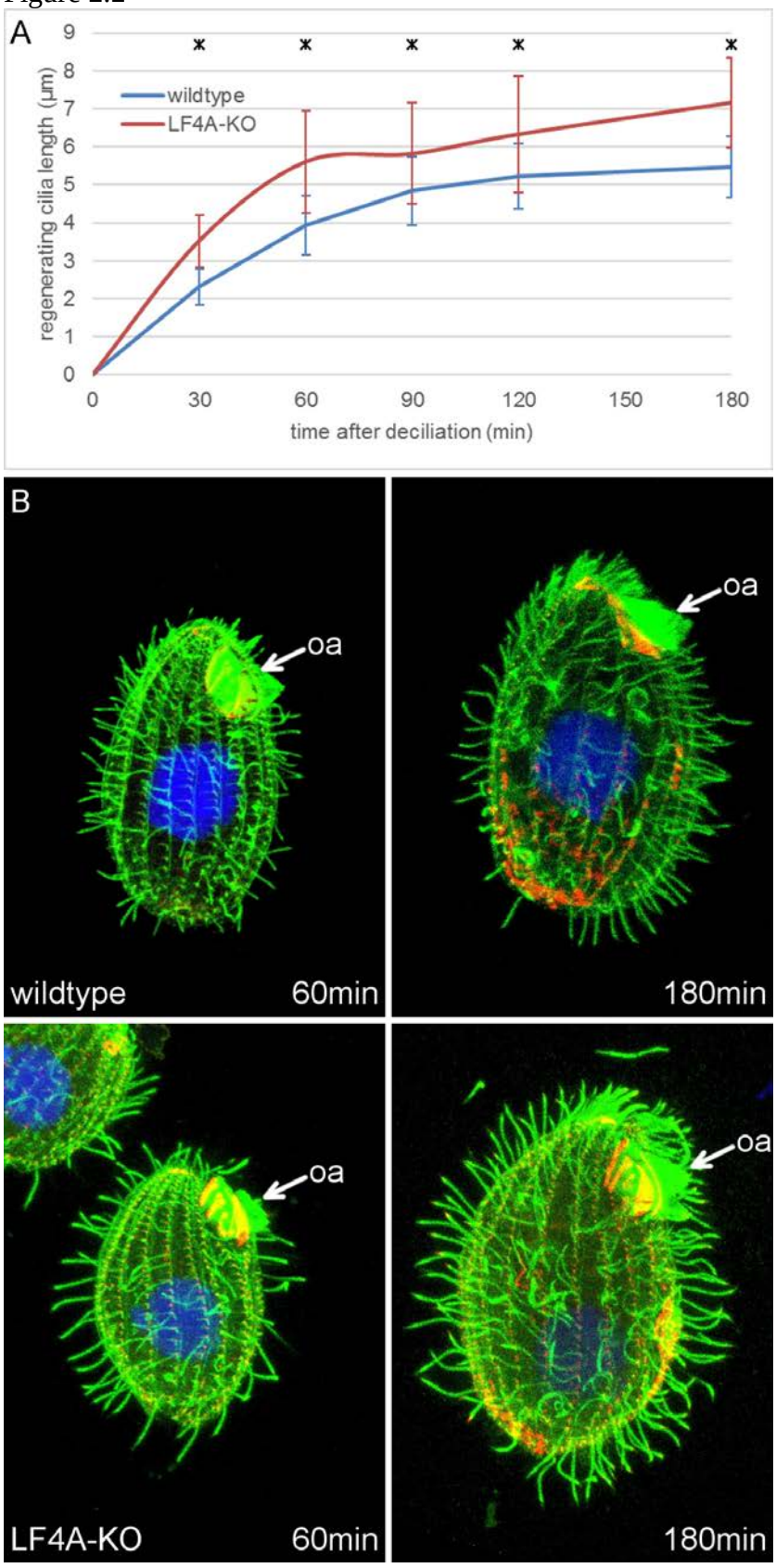
A
regenerating cilia length (µm)
time after deciliation (min)
wildtype
LF4A-KO
0
30
60
90
120
150
180
B
oa
wildtype
60min
180min
LF4A-KO

Figure 2.3. **LF4A-GFP localizes to the basal bodies and along the cilia, and is transported by IFT.** (A–B) A Negative control (wild-type) cell (A) and a cell expressing LF4A-GFP under the native promoter (B) subjected to immunofluorescence that included a simultaneous fixation/permeabilization with paraformaldehyde and Triton X-100 prior to staining with ant-GFP (red) antibodies and DAPI (blue). Note that background staining in the cell body and occasionally at the tips of cilia (A inset). The specific signal (B) is detected in the basal body and more weakly present along the locomotory cilia length (B inset). (C) An LF4A-GFP cell that was first permeabilized (by Triton X-100) then fixed by paraformaldehyde prior to immunofluorescence. Compare to B. GFP signal remained near the basal bodies but disappeared along the axonemes Thus LF4A-GFP near the basal bodies is mostly detergent-resistant and likely bound to the cytoskeleton and the ciliary pool is labile. (D) A TIRF microscopy image of a live LF4A-GFP cell. Arrowheads indicate the basal bodies within the locomotory row, arrows point to ciliary shafts. (E) Three kymographs obtained from videos of LF4A-GFP cells. Ciliary LF4A-GFP protein were mostly stationary but infrequently moved along the cilia at velocities similar to those recorded for an IFT particle marker GFP-DYF1 (Fig. 2.5B) (anterograde: 0.84 μm / sec, average of three events; retrograde: 1.53 μm / sec average of two events). Scale bar: 1 μm x 1 s.

Figure 2.3

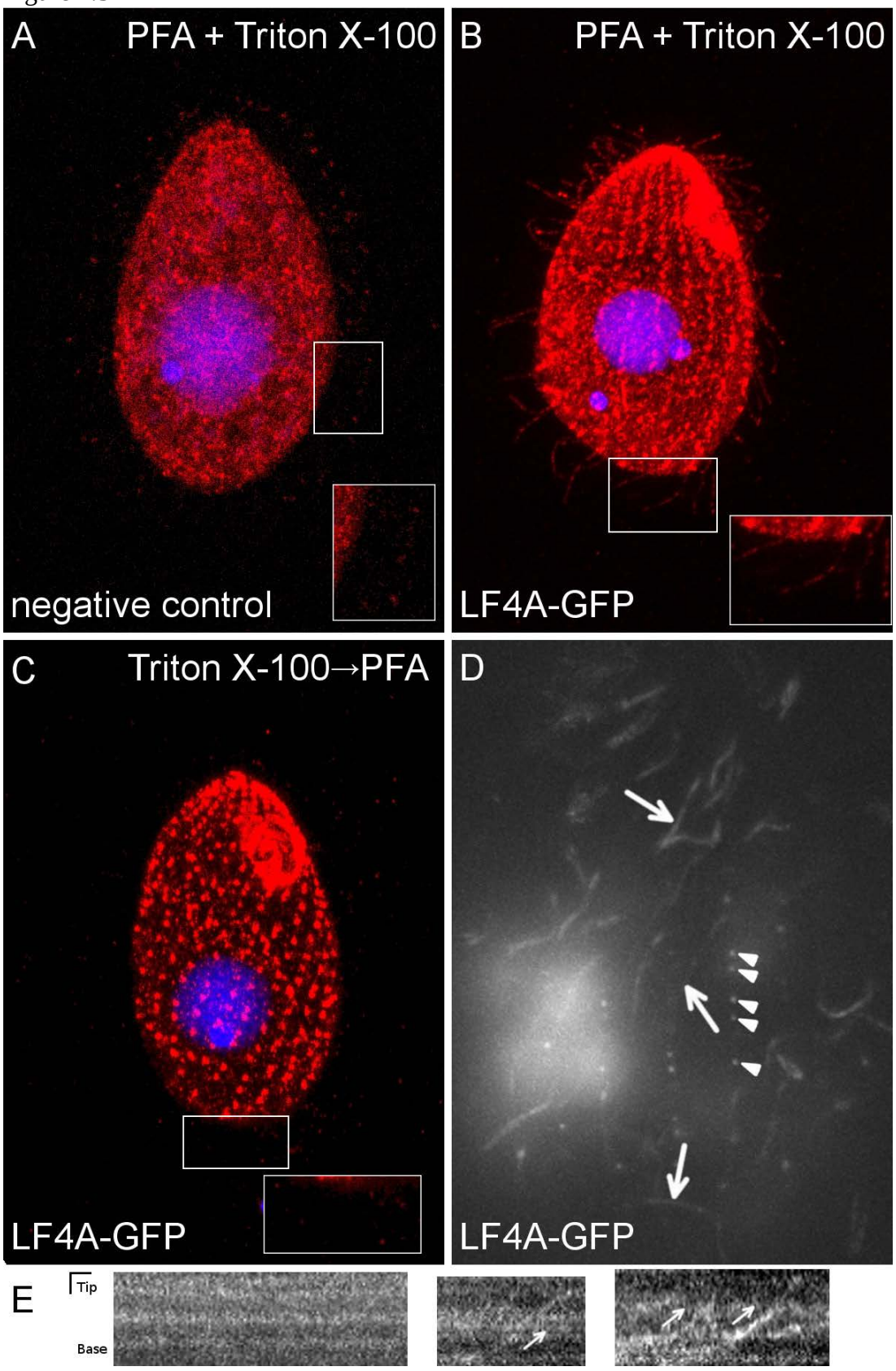
A
PFA + Triton X-100
negative control
B
PFA + Triton X-100
LF4A-GFP
C
Triton X-100→PFA
LF4A-GFP
D
LF4A-GFP
E
Tip
Base

Figure 2.4. **Excessive LF4A kinase activity shortens cilia.** (A) Cells overexpressing (under *MTT1p* and induced by Cd^{2+} for 3 hours) either GFP, GFP-LF4A or two mutated GFP-LF4A variants (F82A and F82G) showing GFP signal and labeled by anti-polyG antibodies (red) and DAPI (blue). Note the shortening of cilia is evident only in the cell expressing GFP-LF4A without kinase domain mutations and GFP-LF4A is enriched at the basal bodies. The mutant GFP-LF4A accumulates at the tips of cilia while the basal body signal is not apparent. (B) The results of an *in vitro* kinase assay using wild-type GFP-LF4A and its two mutated variants, F82A and F82G. Each protein was overexpressed and immunoprecipitated on GFP-beads (IP input). The beads were then incubated with myelin basic protein (MBP) and ATP-γ-S. The reactions products were separated by SDS-PAGE and detected using western blotting and anti-thiophosphorylation 51-8 antibody (top). The relative amounts of each GFP-LF4A were estimated on a western blot using anti-GFP antibodies (bottom). (C) A chart documenting the lengths of locomotory cilia of cells overexpressing that overproduce either GFP, GFP-LF4A or two mutated GFP-LF4A variants F82A and F82G. The cilia lengths of GFP, GFP-LF4A--F82A and GFP-LF4A--F82G are not significantly different ($p > 1\%$), while GFP-LF4A cilia length was significantly shorter (75% of GFP, Asterisk (*) indicates significant difference, $p < 0.1\%$).

Figure 2.4

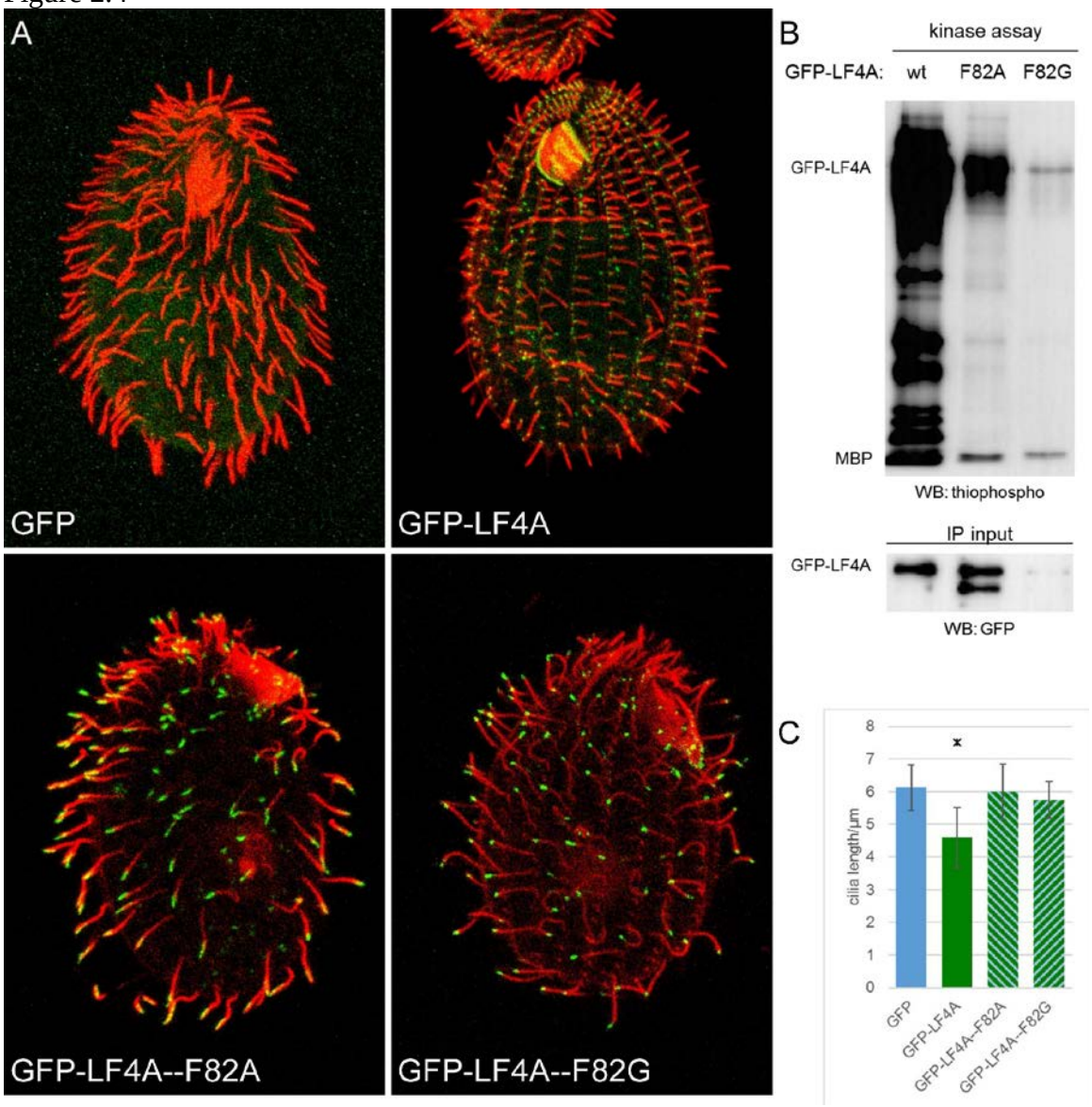
A
GFP
GFP-LF4A
GFP-LF4A--F82A
GFP-LF4A--F82G
B
kinase assay
GFP-LF4A: wt F82A F82G
GFP-LF4A
MBP
WB: thiophospho
IP input
GFP-LF4A
WB: GFP
C
cilia length/μm
0
1
2
3
4
5
6
7
8
GFP
GFP-LF4A
GFP-LF4A--F82A
GFP-LF4A--F82G

Figure 2.5. **LF4A negatively regulate IFT velocities.** (A) A chart showing IFT velocities in cells that express DYF1-GFP as an IFT marker that are either otherwise wildtype or GFP-LF4A-overexpressing. Both strains were exposed to Cd2+ for 3 hours. Both the anterograde (left) and retrograde IFT (right) velocities were significantly decreased due to overexpression of GFP-LF4A (paIFT < 0.1%, prIFT <0.1%). (B) A chart showing the IFT velocities (based on DYF1-GFP) in the wild-type and LF4A-KO cilia. Both the anterograde and retrograde IFT velocities significantly increased due to the loss of LF4A (paIFT < 0.1%, prIFT < 0.1%). (C) A chart of the cilia lengths of DYF1-GFP cells and DYF1-GFP+LF4A-KO cells. (p < 0.1%). Error bars indicate SDs. Asterisks (*) indicate significant difference from the respective control.

Figure 2.5

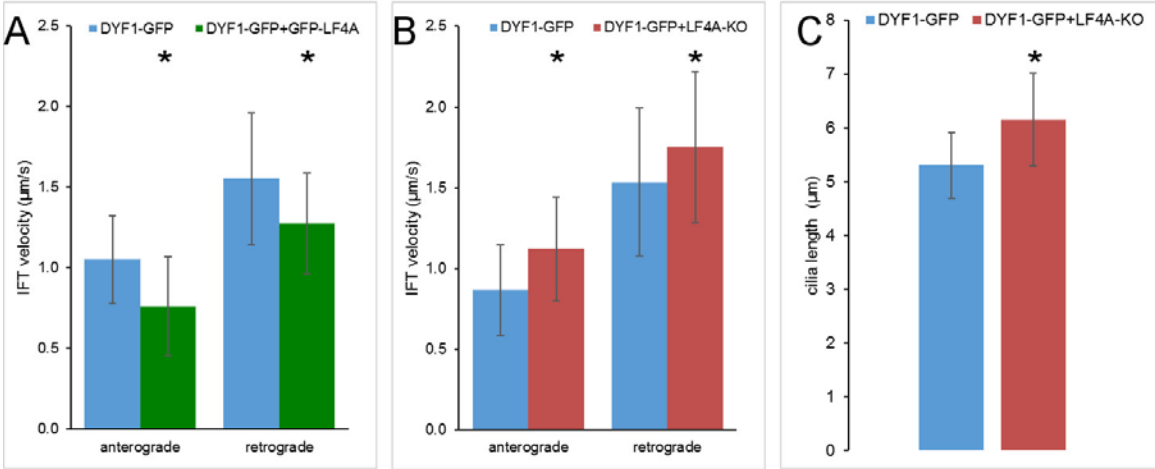
A
DYF1-GFP
DYF1-GFP+GFP-LF4A
IFT velocity (μm/s)
2.5
2.0
1.5
1.0
0.5
0.0
*
*
anterograde
retrograde
B
DYF1-GFP
DYF1-GFP+LF4A-KO
IFT velocity (μm/s)
2.5
2.0
1.5
1.0
0.5
0.0
*
*
anterograde
retrograde
C
DYF1-GFP
DYF1-GFP+LF4A-KO
cilia length (μm)
8
7
6
5
4
3
2
1
0
*

Figure 2.6. **KIN1 motor subunit of kinesin-2 is phosphorylated by LF4A *in vitro*, but is not required for the cilia shortening activity of LF4A *in vivo*.** (A) Western blots that document *in vitro* kinase assays using GFP-LF4A and three substrates that are GFP-tagged IFT proteins. GFP-LF4A and a substrate protein were simultaneously immunoprecipitated on anti-GFP-beads incubated with ATP-γ-S and the reaction products were analyzed by SDS-PAGE and western blotting using an anti-thiophosphate antibody (top panel) or anti-GFP antibodies (bottom panel). The blots show that GFP-LF4A phosphorylated GFP-KIN1 (red boxes) but not GFP-IFT52 or GFP-DYF1 (black boxes). (B) Western blots on the products of *in vitro* kinase assays of GFP-LF4A (as enzyme) and several GFP-tagged KIN1 variants of different length or carrying substitutions within the C-terminal tail domain (as substrates). The outcome of phosphorylation is documented using a western blot with an anti-thio-phosphate antibody (top panel) and the relative amounts of the enzyme and substrate are documented using a western blot with anti-GFP antibodies (bottom). The conclusion is that GFP-LF4A primarily (>70% of total activity) phosphorylates S695. Red boxes indicate strong phosphorylation. (C) Cells that have the ovGFP-LF4 overproducing transgene and are either wild-type or null for KIN1 (KIN1-KO), without or with overproduction (homokaryons, Cd^{2+} induced) for 3 or 6 hours. The cells show GFP–LF4A (green) and polyG tubulin (red).

Figure 2.6

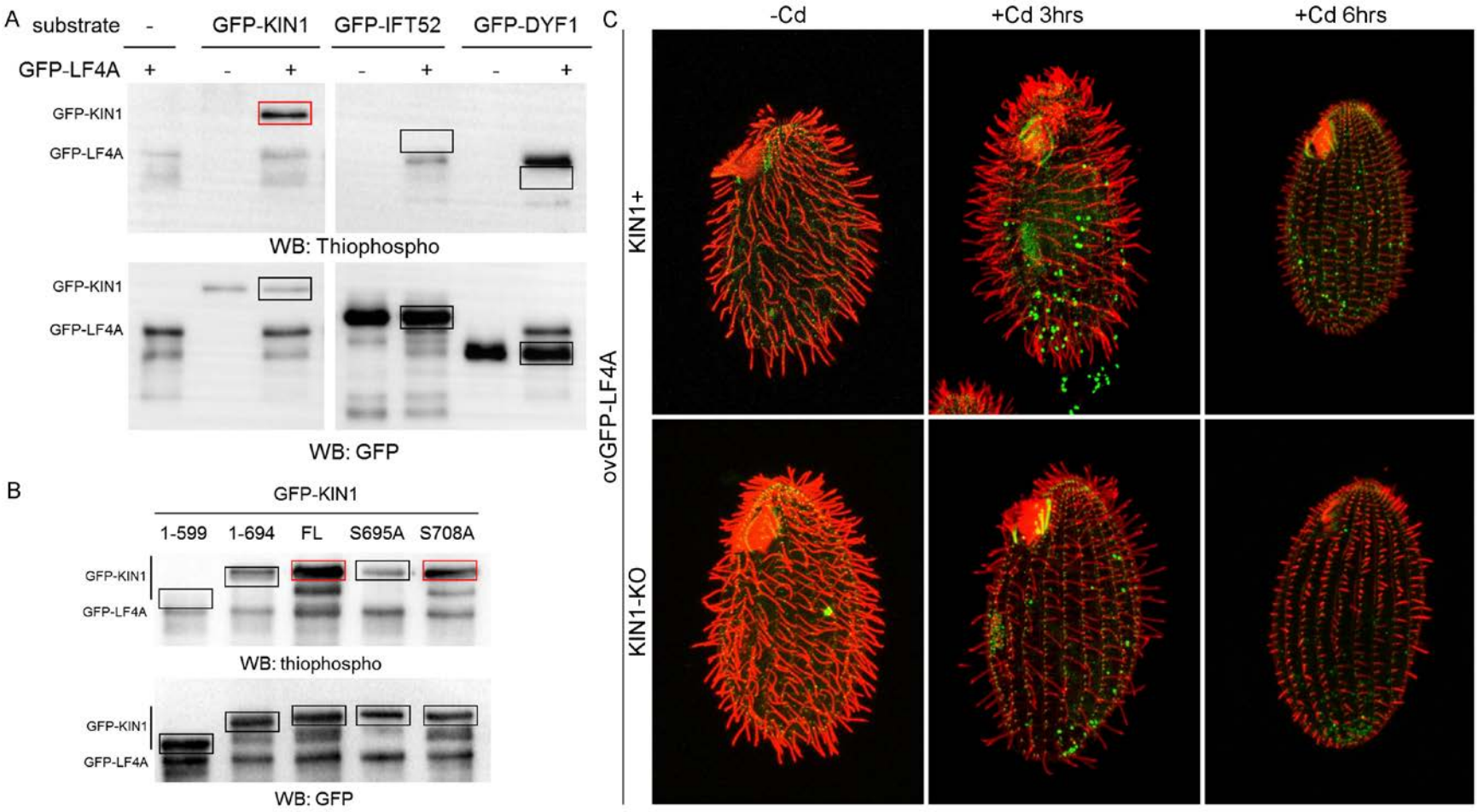
A
substrate
-
GFP-KIN1
GFP-IFT52
GFP-DYF1
GFP-LF4A
+
-
+
-
+
-
+
GFP-KIN1
GFP-LF4A
WB: Thiophospho
GFP-KIN1
GFP-LF4A
WB: GFP
B
GFP-KIN1
1-599
1-694
FL
S695A
S708A
GFP-KIN1
GFP-LF4A
WB: thiophospho
GFP-KIN1
GFP-LF4A
WB: GFP
C
-Cd
+Cd 3hrs
+Cd 6hrs
KIN1+
KIN1-KO
ovGFP-LF4A

Figure 2.7. **A Schematic drawing of the workflow used for the isolation of suppressors of overexpression of GFP-LF4A.** (a) The genomic location and structure of the transgene that was place in the micronucleus. The transgene uses MTT1p to overproduce GFP-LF4. A *neo5* is in the proximity of the ovGFP-LF4 transgene. The transgene replaces the endogenous LF4A. (b-d) Steps involved in mutagenesis and crosses to generate cells for selection of suppressors. (b) A heterokaryon with the ovGFP-LF4A transgene in the micronucleus is subjected to mutagenesis with nitrosoguanidine. (c-d) The mutagenized heterokaryon is subjected to a self-cross (uniparental cytogamy) that involves a mating to a star strain that lacks a functional micronucleus. (d) the progeny of the self-cross is selected based on paromomycin resistance. The progeny clones either carry a suppressor mutation (green crosses) or not the background or unrelated (non-suppressing) mutations that are either preexisting or induced in this experiment are shown as black cross. (e-f) The mutagenize progeny population is transferred to tubes, and cells are treated with Cd2+ while tubes are kept in a vertical position. The progeny that lacks a suppressing mutation shortens cilia and sinks to the tube bottom. The suppressors remain motile and accumulate near the top of the tube due to negative gravitaxis that is depend on ciliary motility(f).

Figure 2.7

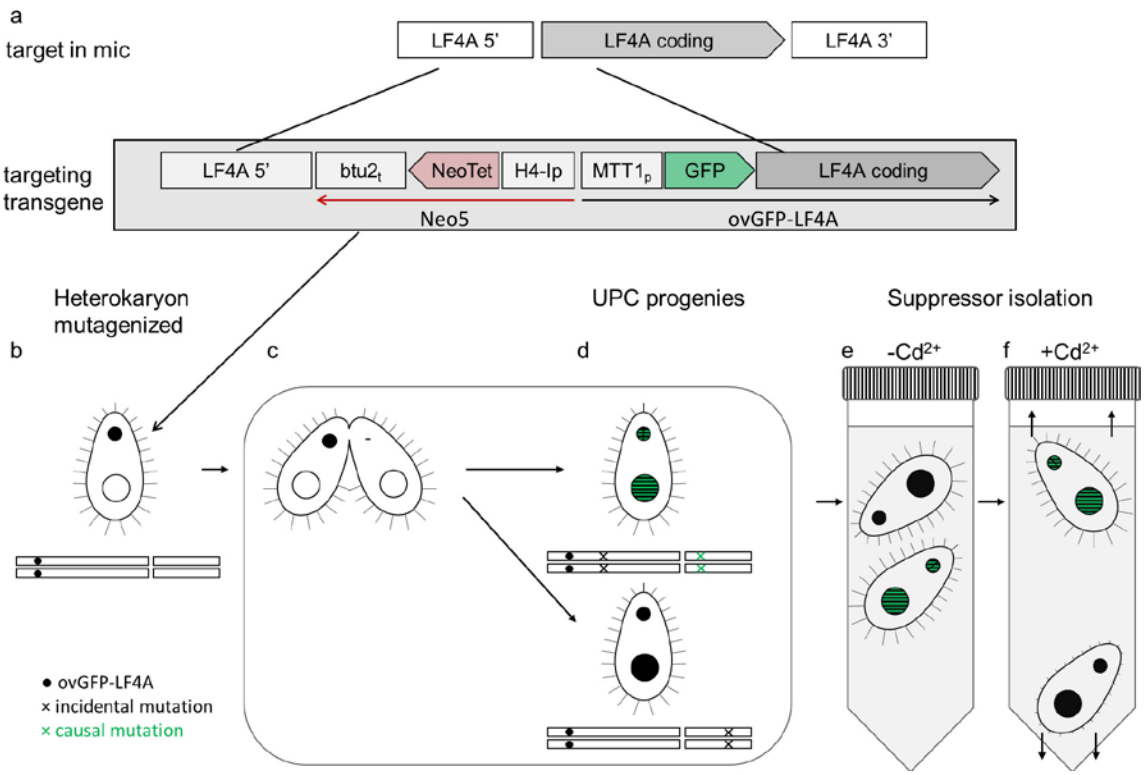
a
target in mic
LF4A 5'
LF4A coding
LF4A 3'
targeting transgene
LF4A 5'
btu2t
NeoTet
H4-Ip
MTT1p
GFP
LF4A coding
Neo5
ovGFP-LF4A
Heterokaryon mutagenized
UPC progenies
Suppressor isolation
b
c
d
e -Cd2+
f +Cd2+
● ovGFP-LF4A
× incidental mutation
× causal mutation

Figure 2.8. **Phenotypes of intragenic and extragenic suppressors of GFP-LF4A overexpression, identification of intragenic suppressors.** (A) F2 progeny of a self-cross of intragenic and extragenic suppressors of GFP-LF4A overexpression. All strains contain the overproducing GFP-LF4A transgene and have suppressor mutations. The left to right representative cells of the following strains are shown after 6 hr of exposure to Cd^{2+}: non-mutated control (ovGFP-LF4A), extragenic suppressor sup1 (suppressed pool) and three intragenic suppressors: sup3, sup4 and sup5. All cells were subjected to immunofluorescence and show the direct GFP signal (green) and polyG tubulin (red). Note that the extragenic suppressor has longer cilia and some short presumably assembling cilia show a uniform pattern of GFP-LF4A. The extragenic suppressors maintain long cilia that have tips enriched in GFp-LF4A. (B) Images of pools of F2 progeny derived by a self-cross of a sup1/SUP1 heterozygote that are either non-suppressed (left panel) or suppressed (right panel) and exposed to Cd^{2+} for overnight. The insets show magnified cortical areas to document the patterns of GFP-LF4A inside cilia. (C) Three-dimensional protein structure of the kinase domain of LF4A based on homology-directed modeling using Cyclin-dependent kinase from *Cryptosporidium* (Chain A of PDB 3NIZ) as a template. Three locations of substitutions found in the intragenic suppressors are shown as sticks: Sup3 (E132K), sup4 (G13S) and sup5 (E160K).

Figure 2.8

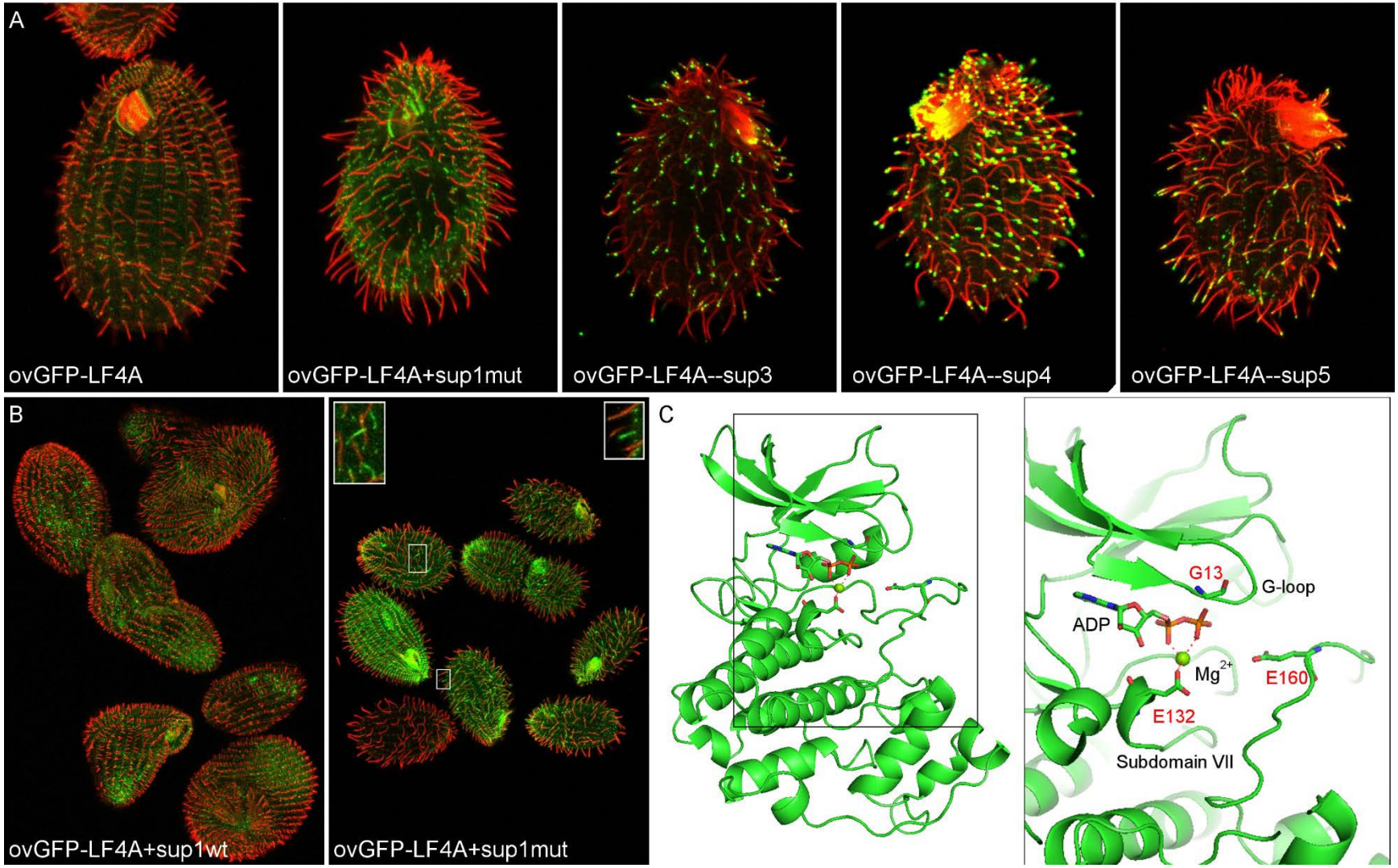
A
ovGFP-LF4A
ovGFP-LF4A+sup1mut
ovGFP-LF4A--sup3
ovGFP-LF4A--sup4
ovGFP-LF4A--sup5
B
ovGFP-LF4A+sup1wt
ovGFP-LF4A+sup1mut
C
G13
G-loop
ADP
Mg2+
E160
E132
Subdomain VII

Figure 2.9. **Extragenic suppressor sup1 is identified as a point mutation in DYF18.** (A) Results of variant subtraction and filtering based on the alignment of whole genome sequencing reads for the suppressed and nonsuppressed pool to the macronuclear reference genome. The final three candidate variants are described in detail in Table 1. (B) Variant density mapping based on the micronuclear genome. Normalized linkage scores are shown that reflect the frequency of variant co-segregation with the suppressed phenotype along the length of each of the 5 micronuclear chromosomes. This analysis reveals a cluster of co-segregating variants at 9-10 Mb on the micronuclear chromosome 3. (C) AN IGV browser view of the scf_8254401:105680 T to C variant on the micronuclear chromosome 3. (D) The scf_8254401:105680 T to C variant results in a point mutation in the coding region of the *DYF18* gene that shifts the stop codon introduces a short peptide to the C-terminus of the predicted DYF18 protein.

Figure 2.9

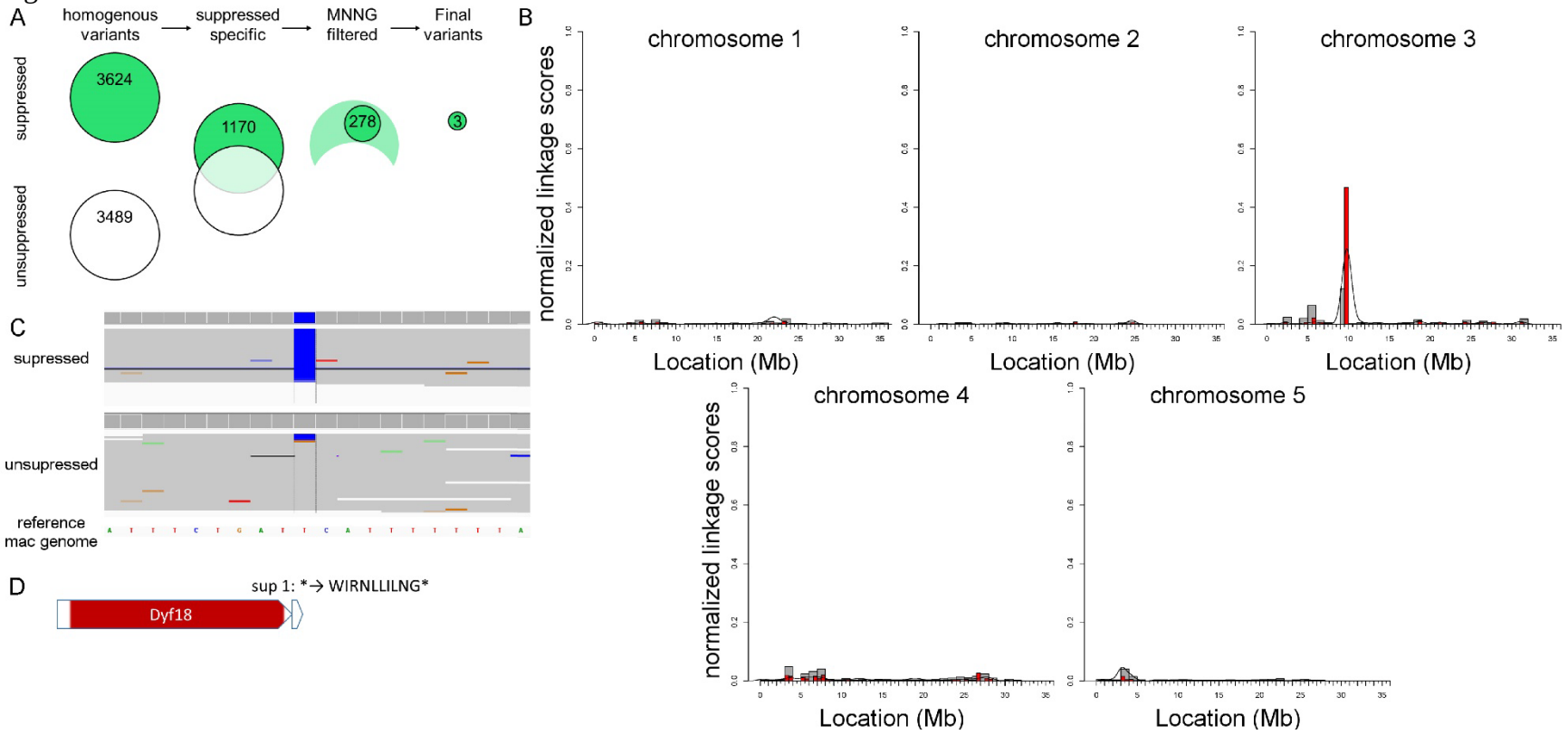
A
homogenous variants
suppressed specific
MNNG filtered
Final variants
suppressed
unsuppressed
3624
3489
1170
278
3
B
normalized linkage scores
chromosome 1
chromosome 2
chromosome 3
chromosome 4
chromosome 5
Location (Mb)
C
supressed
unsupressed
reference mac genome
D
sup 1: *→ WIRNLLILNG*
Dyf18

Figure 2.10. **A loss of DYF18 lengthens the locomotory and oral cilia and partially rescues GFP-LF4A overexpression by reducing the abundance of GFP-LF4A.** An uninduced GFP-lF4 transgene rescues the loss of DYF18. (A) Wildtype, and mutant cells with the genotypes indicated above the panel that are either in interphase (top row) or dividing (bottom row). The cells were stained with anti-polyG antibodies (green) antibodies and anti-centrin (red). Note a similar pattern of long locomotory cilia between the LF4A-KO and DYF18-KO cells, but the latter also have extraordinarily long oral cilia. The presence of the uninduced ovGFp-LF4A transgene rescues the DYF18-KO phenotype. (B) A chart showing the lengths of locomotory cilia in different genetic backgrounds. The cilia length in LF4A-KO, DYF18-KO and the double knockout strain are similar ($p > 5\%$) but all are significantly longer than the wild-type cilia ($p < 0.1\%$). Cilia length of ovGFP-LF4A+DYF18-KO without Cd^{2+} was significantly shorter than DYF18-KO alone ($p < 0.1\%$) as well as wildtype ($P < 0.1\%$). Error bars indicate standard deviations. (C) The chart documents the effect of various genotypes on the kinetics of cilia shortening mediated by the ovGFP-LF4 transgene at multiple times of exposure to Cd2+.

Figure 2.10

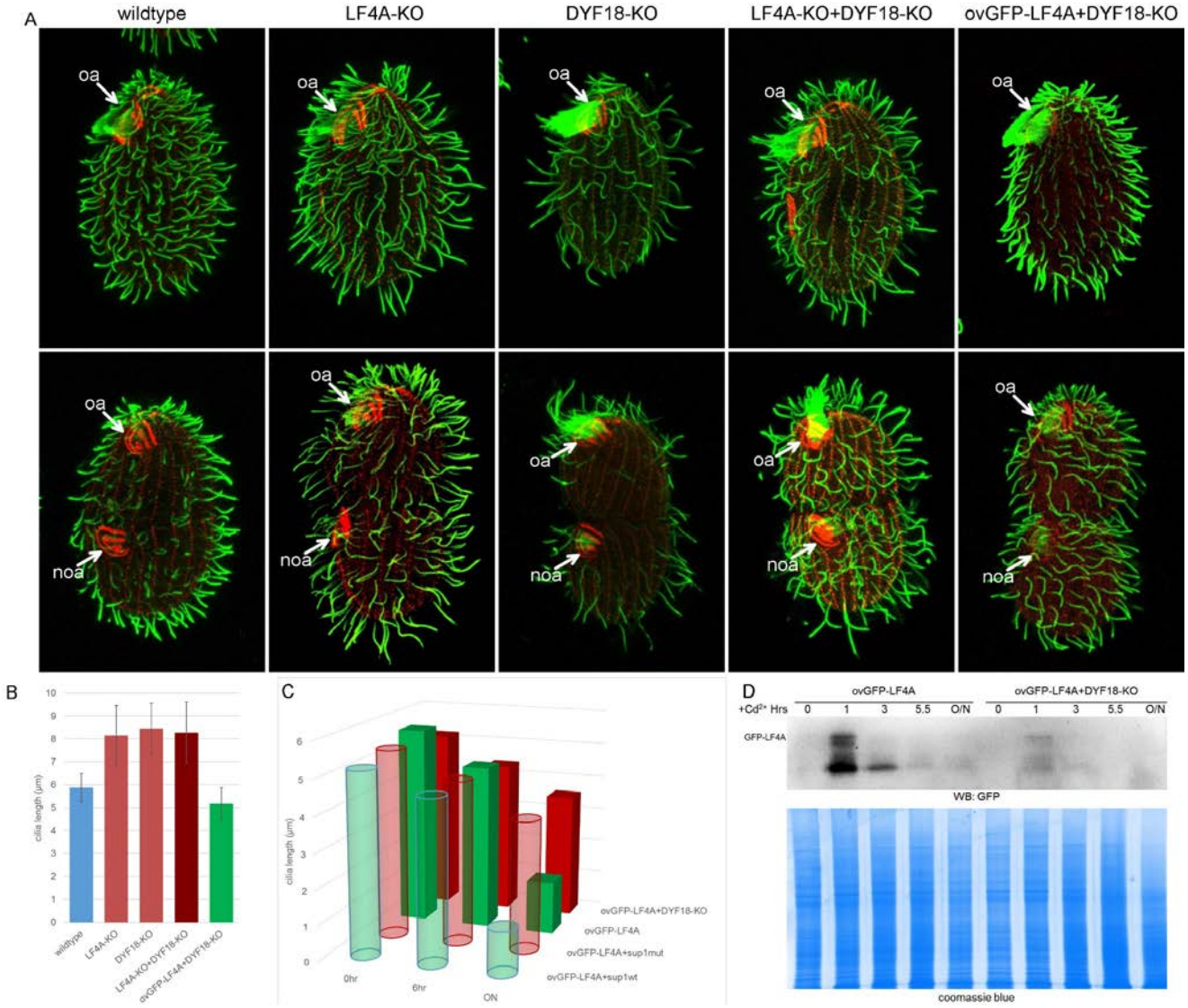
A
wildtype
LF4A-KO
DYF18-KO
LF4A-KO+DYF18-KO
ovGFP-LF4A+DYF18-KO
oa
noa
B
cilia length (μm)
wildtype
LF4A-KO
DYF18-KO
LF4A-KO+DYF18-KO
ovGFP-LF4A+DYF18-KO
C
cilia length (μm)
0hr
6hr
ON
ovGFP-LF4A+DYF18-KO
ovGFP-LF4A
ovGFP-LF4A+sup1mut
ovGFP-LF4A+sup1wt
D
ovGFP-LF4A
ovGFP-LF4A+DYF18-KO
+Cd2+ Hrs
0
1
3
5.5
O/N
GFP-LF4A
WB: GFP
coomassie blue

Figure S2.1. **Overexpressed wildtype and kinase-dead GFP-LF4A differently related to their kinase activity.** (A) TIRF microscopy images of cells overexpressing wildtype GFP-LF4A and two mutated variants F82A and F82 (Cd^{2+} exposure for 1-2 hours). (B) A cell with GFP-LF4A overproduction after overnight induction, showing GFP-LF4A accumulation, shortened cilia (and cell paralysis) and cytokinesis defect. (C) Overproduction of GFP, GFP-LF4A and two mutated GFP-LF4A variants F82A and F82G. Western blot with anti-GFP antibody and coomassie blue staining of the whole cell lysate after 3 hours of Cd^{2+} induction. (D) Kymographs extracted from GFP-LF4A--F82A and GFP-LF4A--F82G cilia.

Figure S2.1

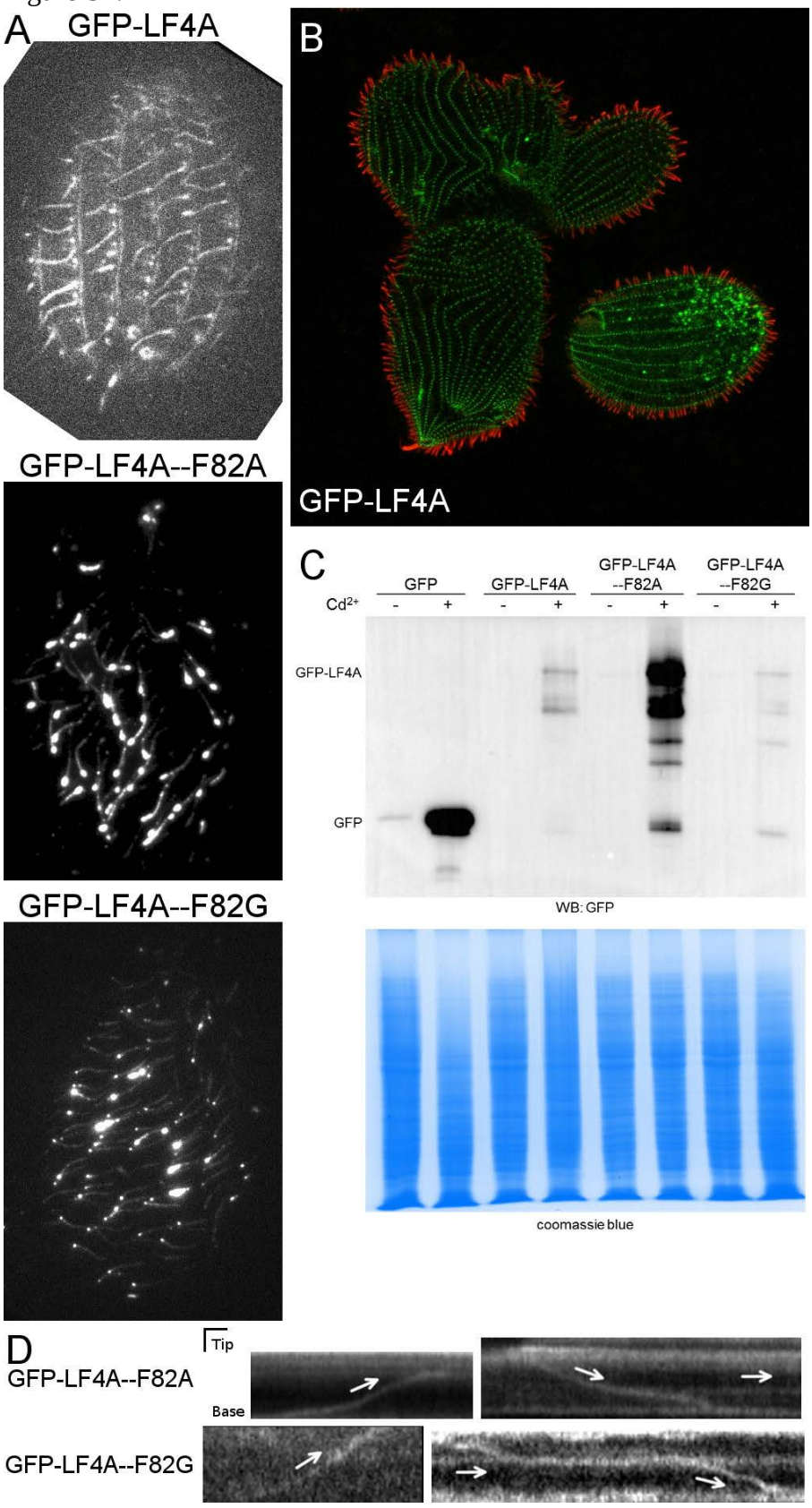
A
GFP-LF4A
GFP-LF4A--F82A
GFP-LF4A--F82G
B
GFP-LF4A
C
GFP
GFP-LF4A
GFP-LF4A --F82A
GFP-LF4A --F82G
Cd2+
- + - + - + - +
GFP-LF4A
GFP
WB: GFP
coomassie blue
D
Tip
Base
GFP-LF4A--F82A
GFP-LF4A--F82G

Figure S2.2. **MS analysis fails to identify LF4A phosphosite but LF4A autophosphorylation.** (A) KIN1 coverage map. Confidence is color coded as indicated in the right bottom corner. Possible phosphorylation of the tryptic peptides at the C-terminal was of low confident and represents regular phosphorylation but not thiophosphorylation by LF4A in the *in vitro* assay. (B) and (C) MS analysis of the thiophosphorylated GFP-LF4A may indicate autophosphorylation. Tryptic peptides of LF4A were detected within the gel piece corresponding to GFP-Kin1 with fair confidence. One of the tryptic peptide was detected as thiophosphorylated. Chromatogram (B) and list of detected b (red) and y (blue) fragments (C) indicated a thio-phosphorylated S347 in LF4A.

Figure S2.2

A

B

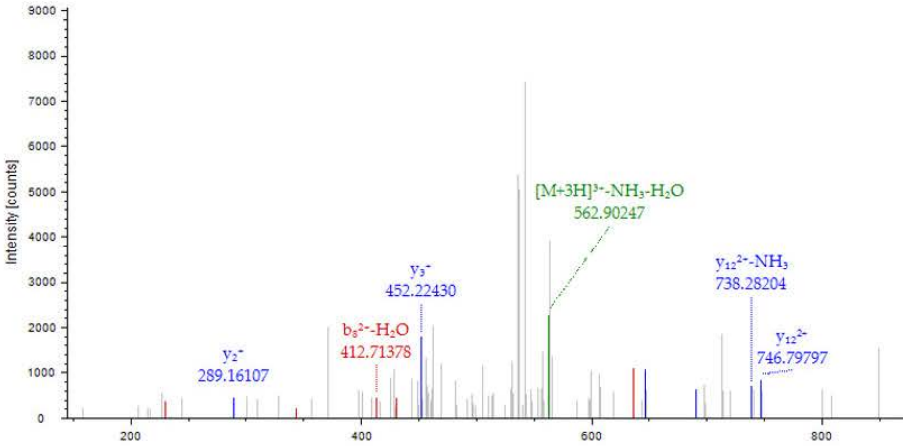

C

#1	b+	b2+	b-H2O2+	Seq.	y+	y2+	y-NH32+	#2
1	102.05496	51.53112	42.52583	T				14
2	230.14993	115.57860	106.57332	K	1620.66589	810.83658	802.32331	13
3	343.23400	172.12064	163.11535	L	1492.57092	746.78910	738.27582	12
4	430.26603	215.63665	206.63137	S	1379.48685	690.24706	681.73379	11
5	527.31880	264.16304	255.15775	P	1292.45482	646.73105	638.21777	10
6	614.35083	307.67905	298.67377	S	1195.40205	598.20466	589.69139	9
7	728.39376	364.70052	355.69523	N	1108.37002	554.68865	546.17537	8
8	842.43669	421.72198	412.71670	N	994.32709	497.66718	489.15391	7
9	1025.41220	513.20974	504.20446	S-Thiophospho	880.28416	440.64572	432.13244	6
10	1139.45513	570.23121	561.22592	N	697.30864	349.15796	340.64468	5
11	1270.49563	635.75146	626.74617	M	583.26571	292.13649	283.62322	4
12	1433.55895	717.28312	708.27783	Y	452.22521	226.61624	218.10297	3
13	1547.60188	774.30458	765.29930	N	289.16189	145.08458	136.57131	2
14				R	175.11896	88.06312	79.54984	1

Figure S2.3. **Loss of DYF18 causes GFP-LF4A relocating into cilia, does not reduce GFP-LF4A kinase activity but reduces its accumulation in the cell.** (A) Cells overexpressing GFP-LF4A with or without DYF18 showing GFP signal and anti-glycylation 2302 (red) staining. In addition to the basal body region localization, GFP-LF4A was also observed along the cilia (insert) in cells without DYF18. (B) GFP-LF4A purified from cells with or without DYF18 had similar kinase activity. Left: western blots of GFP-LF4A and its autophosphorylation and kinase activity. Right: quantification of relative kinase activity of GFP-LF4A in the kinase assay, percentage normalized to MBP phosphorylation per amount of GFP-LF4A. (C) Cells overexpressing GFP-LF4A, with or without DYF18, exposed to Cd^{2+} for overnight. Left: cells showing GFP signal and anti-glycylation 2302 (red) staining. Right: percentage of total cell counts with and without vacuole accumulation of GFP-LF4A in these two strain.

Figure S2.3

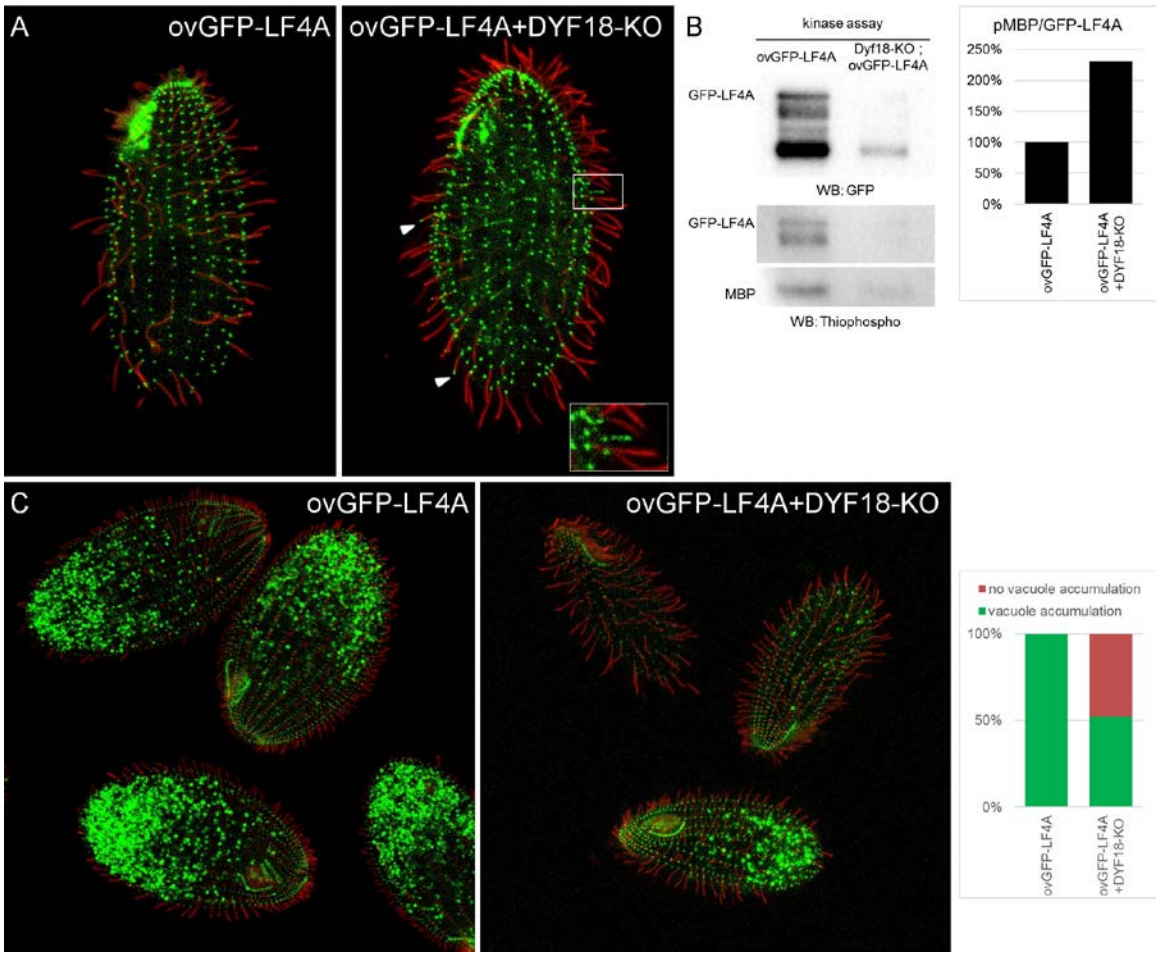
A
ovGFP-LF4A
ovGFP-LF4A+DYF18-KO
B
kinase assay
ovGFP-LF4A
Dyf18-KO ; ovGFP-LF4A
GFP-LF4A
WB: GFP
GFP-LF4A
MBP
WB: Thiophospho
pMBP/GFP-LF4A
250%
200%
150%
100%
50%
0%
ovGFP-LF4A
ovGFP-LF4A +DYF18-KO
C
ovGFP-LF4A
ovGFP-LF4A+DYF18-KO
no vacuole accumulation
vacuole accumulation
100%
50%
0%
ovGFP-LF4A
ovGFP-LF4A +DYF18-KO

Tables

Table 2.1. **Macronuclear genome alignment based subtraction and filtering results in a list of strong candidate variants that were unique to the suppressed F2 pool (high ALT% in suppressed genome).**

Mac Chromosome	Position	Ref	Alt	Alt% in suppressed	Alt% in unsuppressed	Affected Gene	mRNA	Mic Chromosome (JCVI)	Position of the gene
scf_8254401	105680	T	C	100% 26/26	8% 3/37	TTHERM_01080590	133.m000819	chr3	9838679 to 9839991
scf_8254385	317769	G	A	100% 24/24	56% 18/32	TTHERM_00532630	705.m003592	chr4	22762047 to 22764484
scf_8254763	129784	G	A	95% 20/21	55% 17/31	TTHERM_00560020	302.m002700	chr2	4855627 to 4859161

CHAPTER 4

THE HIPPO PATHWAY MAINTAINS THE EQUATORIAL DIVISION PLANE IN THE CILIATE *TETRAHYMENA*[3]

[3] Yu-Yang Jiang, Wolfgang Maier, Ralf Baumeister, Gregory Minevich, Ewa Joachimiak, Zheng Ruan, Natarajan Kannan, Diamond Clarke, Joseph Frankel, and Jacek Gaertig. 2017 *Genetics*.
Reprinted here with permission of the publisher

ABSTRACT

The mechanisms that govern pattern formation within the cell are poorly understood. Ciliates carry on their surface an elaborate pattern of cortical organelles that are arranged along the anteroposterior and circumferential axes by largely unknown mechanisms. Ciliates divide by tandem duplication: the cortex of the pre-division cell is remodeled into two similarly-sized and complete daughters. In the conditional *cdaI-1* mutant of *Tetrahymena thermophila*, the division plane migrates from its initially correct equatorial position toward the cell's anterior, resulting in unequal cell division, and defects in nuclear divisions and cytokinesis. We used comparative whole genome sequencing, to identify the cause of *cdaI-1* as a mutation in a Hippo/Mst kinase. CdaI is a cortical protein with a cell cycle-dependent, highly polarized localization. Early in cell division, CdaI marks the anterior half of the cell, and later concentrates at the posterior end of the emerging anterior daughter. Despite the strong association of CdaI with the new posterior cell end, *the cdaI-1* mutation does not affect the patterning of the new posterior cortical organelles. We conclude that in *Tetrahymena*, the Hippo pathway maintains an equatorial position of the fission zone and by this activity specifies the relative dimensions of the anterior and posterior daughter cell.

SUMMARY

We investigate the mechanism of the intracellular pattern formation using the ciliate *Tetrahymena thermophila* as a model. We address how the cell duplicates its cortical pattern during cell division. We used whole genome sequencing to identify the causal mutation in the *cdaI-1* mutant that divides asymmetrically with a consistent anterior shift of the division plane. The CdaI protein is a Hippo/Mst kinase that marks the cortex of the emerging anterior daughter.

CdaI is not needed for the initial positioning of the division plane, but is needed for keeping the division plane at the cell's equator.

INTRODUCTION

Ciliates are among the most structurally complex cell types known, due to their nuclear dualism and the intricate organization of their surface. Ciliates have two structurally and functionally distinct nuclei that operate in one cytoplasm: the germline micronucleus that undergoes mitosis (or meiosis), and the somatic macronucleus that divides by amitosis, a unique mode of nuclear division that does not involve chromatin condensation or a bipolar spindle formation (reviewed in (Ruehle et al., 2016)). During the vegetative cell cycle, these two nuclei divide at different times, with the mitosis of the micronucleus preceding the amitosis of the macronucleus (Fig. 3.1). In addition, during cell division, ciliates duplicate the cortex, to produce a tandem of daughter cells (reviewed in (Wloga and Frankel, 2012)).

The tandem duplication of the cortical pattern has to be precisely coordinated with cytokinesis in time and space. The cortical regions immediately anterior and posterior to the fission zone undergo vastly different morphogenetic routines, to develop new cortical ends (see Fig. 3.1). The division plane establishes an asymmetry in the cell cortex that is manifested by different organelles that appear on each side of the cleavage furrow: the new cytoproct and contractile vacuole pores form above, and the new cell apex emerges below the cleavage furrow, respectively (Fig. 3.1). The first sign of cell division is the formation of the oral primordium (a developing new oral apparatus) within the confines of the posterior subcell[4] (Fig. 3.1). Next, in the region directly anterior to the oral primordium, the ciliary rows become interrupted by a gap, the "cortical subdivision", which demarcates the emerging daughters (Fig. 3.1). At about the

[4] The term "subcell" is used to describe a half of the dividing cell that will give rise to either the anterior or the posterior daughter.

same time, the new cortical ends start to differentiate, and this is manifested by the appearance of the new contractile vacuole pores and the new cytoproct at the posterior end of the anterior daughter (Fig. 3.1). How the cortical events of tandem duplication are accomplished, and specifically, how they are coordinated with cytokinesis is not known.

A set of potentially informative conditional *Tetrahymena* mutants that are affected in cell division, have been generated by random chemical mutagenesis, but most of the responsible genes remain unknown (Frankel, 2008; Frankel et al., 1976; Frankel et al., 1977). Recently, comparative whole genome sequencing has been used for identification of causative mutations in *Tetrahymena*, and in another ciliate, *Paramecium* (Galati et al., 2014; Kontur et al., 2016; Marker et al., 2014). An important breakthrough was the identification of the first mutation that alters the cortical pattern in *Tetrahymena*, *disA-1* (Galati et al., 2014). Here we use whole genome sequencing to identify the causative mutation for *cdaI-1*, a temperature-sensitive mutation that results in unequal cell division (Frankel, 2008), in a homolog of Hippo/Mst kinases, a conserved upstream component of Hippo signaling (reviewed in (Yu et al., 2015)). *cdaI-1* phenocopies a loss-of-function of the conserved key substrate of Hippo/Mst kinases, Mob1 (Tavares et al., 2012). We conclude that ciliates utilize the conserved Hippo pathway for achieving equatorial division. Our observations also indicate that ciliates must have additional yet unknown mechanisms, independent of CdaI, for setting up the anteroposterior and circumferential axes.

MATERIALS AND METHODS

Tetrahymena strains

To identify the causal mutation for *cdaI-1*, *we used* the strain, IA237 *cdaI-1*/*cdaI-1* (*cdaI-1*, II). For the outcross, we used the heterokaryon strain CU427 *chx1-1*/*chx1-1* (*CHX1*, cy-s, mt VI).

The CU428 strain *mpr1-1*/*mpr1-1*, (*MPR1*, mp-s, mt VII) was used as a wild type for comparisons of phenotypes. The B*VII strain was used for the self-cross. The expression of CdaI-GFP transgene was performed in CU428 as well as in the background of *elo1-1,* a mutation that shifts the division plane posteriorly, using strain IA388 *elo1-1*/*elo1-1* (*elo1-1*; I). All strains were obtained from the *Tetrahymena* Stock Center, Cornell University (Ithaca, NY). Cells were grown in SPP medium (Gorovsky, 1973) with antibiotics (SPPA, (Gaertig et al., 2013)) at 28-30°C (standard temperature that is permissive for *cdaI-1*) or 39-40°C (restrictive temperature for *cdaI-1*).

Crosses and preparation of pools for next generation sequencing

Standard methods for crosses and analyses of progeny (Orias et al., 2000) were used unless mentioned otherwise. To identify the causative mutation for *cdaI-1,* we used a modified "bulked segregant" approach (Birkeland et al., 2010; Michelmore et al., 1991) that includes a self-cross. The IA237 *cdaI-1* mutant strain was crossed to the heterokaryon CU427, and F1 heterozygotes were recovered based on cycloheximide resistance (cy-r, 15 μg/ml). Several cy-r F1 heterozygotes were cloned and grown for > 60 generations for sexual maturation and macronuclear assortment to cycloheximide sensitivity. A single fertile cy-s F1 was used for a self-cross to B*VII to produce the progeny type known as "short circuit genomic exclusion, (SCGE)" (Bruns et al., 1976) as follows. The *CDAI/cdaI-1* cy-s F1 and B*VII cells were grown to ~2-3 x 10^5 cell/ml in 5 ml of SPPA at 30°C. The cells were washed, suspended in 5 ml of 10 mM Tris-HCl pH 7.5 and starved for 18 hr at 30°C. The starved F1 and B*VII cells (400 μl each) were mixed in a single well of a 24-well microtiter plate and allowed to mate at 30°C for 6.5 hr. The mating cells were diluted to 10 ml with SPPA and plated on a 96-well microtiter plate at 50 μl/well. The plates were incubated for 18 hr at 30 °C and 50 μl of SPPA with 30 μg/ml of cy

were added to each well. After 2 days of selection, 192 single cy-r F2 cells (each from a different well to ensure that they come from independent meioses) were isolated into drops of SPPA on Petri dishes. The F2 cy-r clones were replicated onto 96-well microtiter plates with 100 μl/well of SPPA, incubated overnight at 39 °C and scored for either a wild-type or *cdaI-1* phenotype. Thirty-six wildtype and separately 36 *cdaI-1* F2 clones were pooled. The clonal pools were grown overnight in 25 ml of SPPA, washed and suspended in 60 mM Tris-HCl pH 7.5 (this unusual concentration of Tris-HCl is used to block pairing (Bruns and Brussard, 1974)), and starved for 2 days at the room temperature. Total genomic DNAs were extracted from the two F2 pools with the urea method as described (Dave et al., 2009).

Whole genome sequencing and causative variant identification using the macronuclear reference genome

The pool DNAs were used to prepare libraries using Illumina Truseq adapters and sequenced by the Illumina MiSeq instrument to generate paired-end reads of 300 bp with 30x coverage. The following sequence analyses were performed using the Galaxy web-based platform (Afgan et al., 2016) (https://usegalaxy.org). The sequence reads were aligned to the macronuclear reference genome (June 2014 version, GenBank assembly accession GCA_000189635.1) (Eisen et al., 2006). FASTQ Quality Trimmer was used to remove ends of reads with aggregate quality score <20 (Blankenberg et al., 2010). The reads were aligned to the macronuclear reference genome using BWA-MEM (Li and Durbin, 2009) and realigned around indels using GATK (DePristo et al., 2011; McKenna et al., 2010). PCR duplicates were removed using Picard (http://broadinstitute.github.io/picard). Homozygous variants were called using GATK Unified Genotyper. Next we used the GATK Select Variants tool to remove variants from the mutant pool that were also present in: 1) the sister F2 wild-type pool and 2) six pools that originated

from independent projects using non-*cdaI-1* backgrounds and the same genetic scheme (our unpublished data). The remaining variants were filtered for the types of mutations that are commonly induced by nitrosoguanidine (Ohnishi et al., 2008) using SnpSift (Cingolani et al., 2012) with the expression: ((REF = 'G') & (ALT = 'A')) | ((REF = 'C') & (ALT = 'T')) | ((REF = 'T') & (ALT = 'C')) | ((REF = 'A') & (ALT = 'G')). Following variant subtraction, the remaining candidate variants were annotated using SnpEff (Cingolani et al., 2012). Sequence reads containing candidate variants were inspected manually in the IGV genome browser (Robinson et al., 2011; Thorvaldsdottir et al., 2013).

Identification of the causative micronuclear chromosomal region by allelic composition contrast analysis

To map the location of the causative variant on the micronuclear genome, we used a customized version of MiModD (https://sourceforge.net/projects/mimodd/) as follows. We aligned the mutant and wild-type pool reads to the micronuclear genome assembly of *T. thermophila*, strain SB210 (GenBank assembly accession GCA_000261185.1) (Hamilton et al., 2016) and performed joint variant calling of both pools against the reference, keeping all variants that appeared at least heterozygous in one of the two samples. A linkage score quantifying the difference in the allelic composition between the mutant and the wild-type pool was then computed at each variant site. When plotted against genomic coordinates, this score is expected to peak near the location of the causative variant.

Rescue

To rescue the *cdaI-1* mutant (IA237 strain), a fragment of *TTHERM_00971920* was amplified from the wild-type genomic DNA (CU428 strain) using primers: 5'-tgttactgcaacaccaga-3' and 5'- ggtcaaggctcatatggaa-3' and introduced by biolistic bombardment (Bruns and Cassidy-Hanley,

2000) into starved *cdaI-1* IA237 cells that were subsequently grown on the 96-well plates at the restrictive temperature and periodically inspected for the appearance of wild-type cells. Mock-transformed cells were used as a negative control.

Imaging of CdaI-GFP and analyses of CdaI mutants

To determine the localization of the *CDAI* gene product, CdaI, a GFP sequence was added to the 3' end of the ORF predicted for *TTHERM_00971920*, using a linked *neo5* gene marker (Busch et al., 2010). The macronuclear assortment of the tagged allele was promoted by growing cells in increasing concentrations of paromomycin starting at 120 μg/ml. The GFP tagging of CdaI was done in the wild-type background (CU428), and in the *elo1-1* mutant (IA388). To evaluate the morphological phenotypes, cells were labeled by immunofluorescence with simultaneous fixation and permeabilization (Gaertig et al., 2013), using 20H5 monoclonal anti-centrin antibody (Millipore), or 6-11 B-1 anti-acetyl-K40 α-tubulin antibody (Piperno and Fuller, 1985) or polyclonal anti-GFP (Rockland) antibodies, followed by secondary antibodies coupled to either CY3 or fluorescein (Rockland). DNA was stained using DAPI. The imaging was done on a Zeiss LSM 710 confocal fluorescence microscope.

RESULTS

Cortical and nuclear defects in *cdaI-1 Tetrahymena* mutants

The *cdaI-1 Tetrahymena* clone was isolated in a screen for cell division mutants, which involved exposure to nitrosoguanidine (Frankel et al., 1976) followed by cytogamy to bring mutations to expression (Orias et al., 1979). *cdaI-1* is a temperature-sensitive, recessive mutation. The *cdaI-1* cells appear morphologically normal when grown at 28-30ºC and undergo a severe anterior displacement of the division furrow at 39-40ºC (Frankel, 2008). We used anti-centrin antibodies (Sanders and Salisbury, 1994) to evaluate the cortical organization in the wild

type and *cdaI-1* mutants. The anti-centrin antibodies label the basal bodies of both the locomotory ciliary rows that span the entire cell length, and the four sets of short ciliary rows that are parts of the oral apparatus. In the wild-type cells or in the *cdaI-1* cells grown at the permissive temperature, the first sign of cell division is the appearance of the new oral apparatus (oral primordium), as a cluster of basal bodies that form adjacent to the right postoral ciliary row at a sub-medial location (Fig. 3.1 stage 2; Fig. 3.2A). Next, the basal bodies of the oral primordium organize into subsets that give rise to the oral rows (Fig. 3.1 stage 3; Fig. 3.2B). Coincident with the completed differentiation of these structures, the longitudinal ciliary rows develop the "cortical subdivision", a gap that circumscribes the cell at a medial location (Fig. 3.1 stage 4, Fig 3.2C). The subsequent cytokinesis occurs within the cortical subdivision (Fig. 3.1 stage 5; Fig. 3.2D). The micronucleus undergoes closed mitosis around the time of the initiation of cortical subdivision (Fig. 3.1 stages 3-4; Fig. 3.2C), while the macronucleus divides by amitosis at the time of constriction of the contractile ring (Fig. 3.1 stage 4, Fig. 3.2D).

At the restrictive temperature, the *cdaI* mutants initially develop an oral primordium at a correct medial and circumferential position (Fig. 3.3A, B). However, at the later stage of development, the new oral apparatus was seen immediately posterior to the old oral apparatus (Fig. 3.3C), most likely due to its anterior translocation. The basal bodies of the two postoral rows that in wild type are positioned between the new and the old oral apparatus, in the mutants shorten or completely disappear (Fig. 3.3C and data not shown). Consistently with the anterior shift of the new OA, the cortical subdivision forms at an excessively anterior position but still in the space between the two OAs (Fig. 3.3C). Based on the staging of nuclear divisions, the cortical subdivision and the subsequent cytokinesis are delayed but eventually subcells differentiate except that they are unequal in size (Fig. 3.3D, F; Fig. 3.1). Often, the smaller

anterior subcell tilts resulting in a “hammerhead” shape of the dividing cell (Fig. 3.3D, F). The tilting could be a consequence of an incomplete or asymmetrically delayed cortical subdivision; often in the same hammerhead, some of the ciliary rows are subdivided, while other rows maintain continuity between the anterior and posterior subcell, which could produce an asymmetry in the growth of the cortex (Fig. 3.3D, F). The progression of the mutant phenotype outlined above is supported by the quantification of the morphological phenotypes at 3 and 6 hr at the restrictive temperature (Fig. 3.3H). In some *cdaI-1* cells, cytokinesis, while delayed, runs to completion, generating an excessively large posterior daughter (Fig. 3.3D, E) and an excessively small anterior daughter (Fig. 3.3E). In other mutant cells cytokinesis fails, and the posterior cell enters a new cell cycle, producing a second generation anterior subcell (Fig. 3.3G). The mitotic division of the micronucleus takes place in the majority of mutant cells, but often the anterior subcell does not receive a progeny micronucleus (Fig. 3.3G, I). In contrast, in most mutants, the macronucleus fails to divide and remains in the posterior subcell (Fig. 3.3D, E, G, I). Consequently, when the abscission is successful, often the anterior daughter lacks a macronucleus or lacks the nuclei altogether (Fig. 3.3E, G, I, 3.9G).

Identification of the causal mutation of *cdaI-1* by whole genome sequencing

We aimed at identifying the causative mutation for *cdaI-1* using comparative whole genome sequencing. We used a modified “bulked segregant” approach (Birkeland et al., 2010; Michelmore et al., 1991) that includes a self-cross, similar to what was used with *Paramecium tetraurelia* (Marker et al., 2014). The principle is to subject an F1 heterozygote to a number of independent meioses, and to identify a mutation that among the F2 progeny strictly co-segregates with the mutant phenotype. We performed an SCGE self-cross by mating an F1 to B*VII (a strain that lacks a functional micronucleus), with the intention of producing progeny that are

homozygous post-meiotic derivatives of the F1 genome, as reported (Bruns et al., 1976). The SCGE F2s were expected to display a 1:1 segregation of the mutant versus wild-type phenotypes. Among a total of 100 F2 clones picked, at the restrictive temperature, 63 were wild-type and 37 were *cdaI-1* (1.7:1 ratio). The apparent deviation of the segregation pattern from the expected 1:1 ratio is explained by our subsequent observation that the SCGE cross, in addition to expected homozygotes apparently also produced some F2 heterozygotes (see below). We prepared pools of 36 F2 clones that were phenotypically either wild type or *cdaI-1*. Both pools were subjected to whole genome sequencing and variant identification.

We aligned the mutant and wild-type pool sequence reads to the macronuclear reference genome (Eisen et al., 2006). Following variant calling we narrowed down the list of candidate mutations through stepwise variant filtering and subtraction as follows (Fig. 3.4A). We detected 3444 and 3566 variants that were prominent enough in the *cdaI-1* and the wild-type pool, respectively, and 1009 of these were unique to *cdaI-1* and were analyzed further (Fig. 3.4A). We subtracted those mutant pool variants that were also detected in 6 DNA pools obtained by the same genetic scheme in non-*cdaI-1* backgrounds (our unpublished data), which led to 341 remaining variants. Sixty-nine of these variants were base transitions compatible with the mutagen used, nitrosoguanidine (G/C to A/T and A/T to G/C)(Ohnishi et al., 2008). A manual inspection of the individual sequence reads across the positions of these 69 variants revealed only a single variant, scf_8254051:142648 C to T, in the coding region of the gene *TTHERM_00971920*, where 100% of sequence reads contained an alternate base (Fig. 3.4B). In the *cdaI-1* pool genome, 100% of sequence reads (28) had an alternate base and among them 96% (27) contained a C to T substitution (one sequence had an A but this position was near the end of the read and thus is more likely to be a sequencing error (Mandoiu and Zelikovsky,

2016)). Within the wild-type pool DNA, 91% (21) of reads encoded the reference base C, and ~9% (2) had the alternate base T (Fig. 3.4B). Since the pools of F2 clones were assembled based on their phenotypes, most likely SCGE, in addition to the expected homozygotes (Bruns et al., 1976) also produced some heterozygotes; given the recessive character of *cdaI-1* such heterozygotes cannot be distinguished from the wild-type homozygotes, which explains the skewing of the phenotypic segregation ratio toward the wild-type (as mentioned above).

In parallel to the variant subtractions and filtering approach based on the macronuclear genome, we took advantage of the recently sequenced micronuclear (germ-line) genome (Hamilton et al., 2016), to map the chromosome interval of the candidate causative mutation region. We performed this mapping using the whole-genome sequencing data of the mutant and the wild-type F2 pools in a manner similar to the approach used in other organisms including *C. elegans* (Minevich et al., 2012). We aligned the mutant and wild-type sequence reads to the micronuclear chromosome assembly, and determined the density of variant co-segregation with the mutant phenotype by comparing the allelic composition at variant sites between the mutant and the wild-type pool. Normalized variant co-segregation density plots revealed a single peak on the micronuclear chromosome 4, around 24 MB (Fig. 3.4D). In the macronucleus, *TTHERM_00971920* is a part of the chromosome scaffold scf_8254051 that maps to the region between 23.7 to 23.9 Mb on the micronuclear chromosome 4. The close match between the micronucleus-based chromosome interval mapping and the macronucleus-based variant identification achieved by subtractions and filtering, gave us confidence that we had indeed identified the causative variant.

The *cdaI-1* mutation is recessive (Frankel, 2008). A fragment of the wild-type TTHERM_00971920 (spanning the base that we found mutated in *cdaI-1*), when introduced by

biolistic transformation into vegetative *cdaI-1* cells, produced rescue clones that divided normally at the restrictive temperature (Fig. 3.5A, B), while no rescues were seen in the negative control that was mock-transformed (n=10^7 cells). Sanger DNA sequencing of two rescue clone DNAs detected the mutant base (T) and the wild-type base (C) at the same position (Fig. 3.5C and data not shown), indicating that both alleles are present in the same cells, consistent with a partial replacement of the mutant alleles by a wild-type allele in the polycopy macronucleus (reviewed in (Chalker, 2012)). Thus, we conclude that the scf_8254051:142648 C to T mutation in *TTHERM_00971920* causes *cdaI-1*.

The *TTHERM_00971920* gene that we now rename *CDAI*, encodes a protein, CdaI, with a single N-terminally located kinase domain (Fig. 3.4C). Based on reciprocal BLASTP searches, the closest homologs of the predicted CdaI protein are kinases belonging to the Hippo/Mst group, including Hippo in *Drosophila melanogaster*, MST2 in humans and Kic1 in the budding yeast. For example, the kinase domain of CdaI is 47% identical (65% similar) to that of human MST2. The scf_8254051:142648 C to T mutation translates into a P216S substitution in CdaI, which is located within the kinase domain (Fig. 3.4C). We used homology modeling to predict the 3D structure of the CdaI kinase domain based on the structure of human MST2 (PDB: 4LGD) (Ni et al., 2013) (Fig. 3.5D). P216 maps to the αF-αG loop a region involved in substrate binding and protein recognition (Kannan and Neuwald, 2004; Kannan and Neuwald, 2005; Lodowski et al., 2006; Sours et al., 2008). P216S is predicted to impact substrate binding by altering the conformation of the αF-αG loop (Fig. 3.5D). It is also possible that the mutant S216 serves as a gained phosphorylation site (Radivojac et al., 2008) that alters the activity or substrate specificity of CdaI.

CdaI is expressed in a highly polarized pattern during cell division

To localize CdaI protein within the cell, we tagged the ORF of *CDAI* by adding a GFP-encoding sequence at the 3' end, so that the gene product is expressed under its own promoter. We could not detect CdaI-GFP in non-dividing cells (Fig. 3.6A). In cells approaching cell division that started to develop an oral primordium, CdaI-GFP was present as lines of dots or dashes that corresponded to the ciliary rows, but the signal was much stronger in the anterior half of the cell that gives rise to the future anterior daughter (Fig. 3.6B-D). At this stage, most cells had a uniform circumferential pattern of CdaI-GFP (Fig. 3.6D), while in some the signal was stronger on the ventral side, above the oral primordium (Fig. 3.6B, C). When the cortical subdivision appeared (staged by the completed micronuclear mitosis), the signal of CdaI-GFP was enhanced as a circumferential band of short ribbons above the division plane (Fig. 3.6E). The oral apparatuses, both old and new, also appeared positive for CdaI-GFP (Fig. 3.6E), but the background fluorescence tends to be higher in these locations (Fig. 3.6I, J). During early cytokinesis/macronuclear division, CdaI-GFP remained strong on the anterior side of the fission zone (Fig. 3.6F). At this stage, CdaI-GFP also marked the new contractile vacuole pores (CVPs) that assemble on the right side of the cell near the posterior end of the emerging anterior daughter (Fig. 3.6G arrows). When the constriction zone became narrow, the CdaI-GFP signal was present near the posterior end of the emerging anterior daughter cell (Fig. 3.6H).

The appearance of the CdaI-GFP signal coincides with the onset of cortical subdivision and the subsequent cytokinesis. To examine in detail the relationship between CdaI and cortical morphogenesis, we labeled the CdaI-GFP-expressing cells with anti-centrin to detect the basal bodies (Fig. 3.7 green) and anti-GFP antibodies (red) to detect the cortical CdaI. Cortical CdaI-GFP first appeared in the anterior half of the dividing cell in the early stage of the oral

primordium development (Fig. 3.7A-A'). CdaI-GFP became prominent and uniform along all ciliary rows of the anterior subcell when the oral primordium was advanced to the stage of individualization of the oral rows, but before the first signs of cortical subdivision (Fig. 3.7B-B'). Thus, it appears that the establishment of the posterior edge of the CdaI-GFP lines does not require a cortical subdivision. The CdaI-GFP lines were composed of dots that roughly corresponded to the basal bodies, as well as dashes that were located between or on the side of the basal bodies (Fig. 3.7B-B' inset). When the cortical subdivision appeared, CdaI-GFP lines polarized by increasing in intensity near the anterior side the cortical subdivision, but a weaker signal was still present across and below the cortical subdivision (Fig. 3.7C-C'). When the division plane started to constrict, the CdaI-GFP signal was limited to the anterior side of the cortical subdivision. CdaI-GFP was also present between the neighboring ciliary rows along the constriction plane (Fig. 3.7D-D', also see Fig. 3.6F). During more advanced cytokinesis, CdaI-GFP was concentrated along the portions of the ciliary rows near the posterior end of the anterior subcell (Fig. 3.7E-E').

***elo1-1* shifts both the division plane and the posterior boundary of CdaI**

To explore how the CdaI localization is influenced by the cell division events, we analyzed the pattern of CdaI-GFP in another cell division mutant, *elo1-1*, in which the division plane is dramatically shifted to the posterior cell pole (Frankel, 2008). In *elo1-1*, the division plane is shifted already at the stage of the early oral primordium, the first sign of cell division (Fig. 3.8A-B'). Despite the posterior shift, the course of cell division in *elo1-1* cell appeared normal except for twisting of ciliary rows that was apparent at cytokinesis (Fig. 3.8). In the *elo1-1* background, the pattern of CdaI-GFP lines conformed to the new position of the division plane but was otherwise normal. On the ventral side, the posterior edge of the CdaI-GFP lines reached the top

of the oral primordium. Strikingly, the ends of CdaI-GFP lines on the dorsal side were at a wild-type equatorial position and the ends of lines on the cell's sides were intermediate in their anteroposterior position (Fig. 3.8B-D). This creates a remarkable slant in the position of the posterior boundary of the CdaI lines (Fig. 3.8B-D) as compared to an equatorial position of the CdaI edge in the wild type (Fig. 3.7B-D). This indicates that Elo1 acts primarily within the oral circumferential sector. Thus, the CdaI pattern is influenced by earlier cell division events that position the division plane and the *ELO1* gene product is probably upstream of CdaI. We also note that in addition to the signal of CdaI-GFP within the anterior subcell, there was a consistent signal near the posterior (old) cell's end, especially in *elo1-1* cells with a cortical subdivision (Fig. 3.8C-E' arrowheads). Wild-type cells also had weaker but consistently present foci of CdaI-GFP near the posterior cell's end (Fig. 3.6D-H, 3.7B, D arrowheads) that appeared specific as they were not seen in the negative controls (Fig. 3.6I, J). The extreme posterior CdaI-GFP may represent a pool of CdaI that interacts with its likely substrate, Mob1, that was deposited in the previous cell cycle (see the Discussion).

***cdaI-1* does not abolish the correct placement of the posterior end cortical organelles**

Since CdaI eventually becomes focused on the posterior end of the anterior subcell, we explored whether its deficiency affects the assembly and placement of the new CVPs that form near the new posterior end (see Fig. 3.1). CVPs contain microtubules that are enriched in the acetyl-K40 α-tubulin (Gaertig et al., 1995), which can be detected with the 6-11 B-1 antibody (Piperno and Fuller, 1985). In the *cdaI-1* cells grown at the permissive temperature, we detected the CVPs at a proper posterior location in 97% of interphase cells (n=73) (Fig. 3.9A, B). Furthermore, new CVPs were readily seen above the fission zone whenever the cortical subdivision was also present (Fig. 3.9C, D). To determine whether the *cdaI-1* cells assemble new

CVPs at the restrictive temperature, we examined cells that were the anterior products of a complete cell division but with clear signs of CdaI deficiency, based on their small size and an absence of a macronucleus. Surprisingly, in 75% (n=33) of those anterior daughters, CVPs were present at proper posterior positions (Fig. 3.9G-K). The true frequency of CVPs in the anterior offspring is probably higher because some of them have disorganized ciliary rows that likely result from an incomplete cortical subdivision, making the identification of CVPs more difficult. In the hammerhead cells, (many of which appear to have failed cytokinesis), CVPs were present in 61% of anterior subcells (n=55). However, in the CVP-positive hammerheads, the positions of CVPs within the anterior subcells were often incorrect (38%, n=34), with CVPs located either at the same anteroposterior level as the old oral apparatus (Fig. 3.9E-E'), or strikingly, above the old oral apparatus (Fig. 3.9F-F'). At the least, the assembly of the CVPs is less dependent on CdaI as compared to other cell cycle events such as the equatorial cortical subdivision, cytokinesis and macronuclear division. Likely, CdaI is not required for the assembly of the CVPs; it is difficult to determine whether the abnormal placement of the new CVPs in the hammerheads is a result of the CdaI deficiency or is secondary to the variable cortical defects. In summary, CdaI does not seem to play a major patterning role in the assembly of at least one posterior cortical organelle, the CVP, but may have some role in limiting the placement of these organelles near the posterior cell end.

DISCUSSION

The core of Hippo signaling is conserved in ciliates

The elements of the Hippo pathway that are highly conserved and essential for Hippo signaling (the Hippo core) are: 1) upstream kinase Hippo/Mst, 2) downstream kinase Warts/Lats, and 3) Warts/Lats activator, Mats/Mob1, (reviewed in (Hilman and Gat, 2011; Meng et al., 2016;

Sebe-Pedros et al., 2012; Thompson and Sahai, 2015)). We show that a mutation in a Hippo/Mst kinase of *Tetrahymena*, CdaI, causes an anterior migration of the division plane, and defects in cytokinesis and nuclear divisions. The Hippo/Mst kinases phosphorylate themselves, the Warts/Lats kinase and its activator Mats/Mob1 (reviewed in (Meng et al., 2016)). All three phosphorylations are needed to produce an active tertiary complex of Hippo/Mst-Warts/Lats-Mats/Mob1 (Gogl et al., 2015). Importantly, a knockdown of Mob1 in *Tetrahymena* generates a cell division phenotype that closely resembles that of *cdaI-1* (Tavares et al., 2012), indicating that CdaI and Mob1 are in the same pathway and that *cdaI-1* is likely a loss-of-function mutation. Furthermore, an RNAi knockdown of Mob1 affects cytokinesis and cell shape in *Stentor* (Slabodnick et al., 2014). Thus, ciliates use a canonical Hippo core during cell division. The respective localizations of CdaI and Mob1 show a striking overlap, but also some informative differences. CdaI appears earlier in the cell cycle and marks the anterior half of the cell, shortly before the cortical subdivision (Fig. 3.1, stage 3). Mob1 appears later near the posterior boundary of CdaI (Fig. 3.1, stage 4), (Tavares et al., 2012). CdaI is in the right place and time to phosphorylate Mob1 and this event could stabilize Mob1 and enable its accumulation in the fission zone. This is based on the observations in budding yeast, where the proper localization of Mob1 requires activity of a Hippo/Mst kinase, Cdc15 (Luca et al., 2001) that phosphorylates a scaffolding protein, Nud1, to create a binding site for Mob1 on the spindle pole body (SPB) (Rock et al., 2013). Interestingly, in *Tetrahymena*, the signal of CdaI around the fission zone also increases at about the time when Mob1 appears (Fig. 3.1 stage 4). There could be a positive feedback where the active CdaI-Mob1-Warts/Lats complex amplifies CdaI. Such a feedback loop operates in the fission yeast (Feoktistova et al., 2012) .

Tetrahymena pyriformis cells treated with a serine-threonine kinase inhibitor, 6-dimethylaminopurine, arrest in cytokinesis, with an anteriorly displaced division plane (Kaczanowska et al., 1999), which is a partial phenocopy of *cdaI-1*. Thus, 6-dimethylaminopurine could inhibit CdaI or another kinase in the same pathway. The anterior cell contraction and the hammerhead shape could be useful for high throughput screens for additional inhibitors of the Hippo pathway, which are of therapeutic interest in the context of cancer and organ regeneration (Anand et al., 2009; Ehmer and Sage, 2016; Fan et al., 2016).

In other species, the Hippo components associate with the cytoskeleton, namely microtubules and microfilaments. In fungi, the Hippo pathway proteins associate with the SPBs, the contractile ring and septum (Frenz et al., 2000; Luca et al., 2001; Menssen et al., 2001). In *Tetrahymena*, both CdaI and Mob1 strongly accumulate along the ciliary rows, and on the microtubule-based CVPs (this study and (Tavares et al., 2012)). It should be noted however, that cell division is almost normal in the *disA-1 Tetrahymena* mutant, in which the ciliary rows are disorganized (Galati et al., 2014; Jerka-Dziadosz et al., 1995). Thus, in *Tetrahymena*, the Hippo pathway may not require a correct pattern of cortical organelles, but it remains to be determined whether some microtubule-binding activity is important, as is the case in budding yeast (Menssen et al., 2001).

Another conserved property of the Hippo signaling is the asymmetry of its components. In budding yeast, during mitosis, Cdc15 initially associates with the mother (new) SPB and later becomes enriched at the daughter (old) SPB (Menssen et al., 2001). In fission yeast, the Hippo/Mst kinase Cdc7 first localizes to both SPBs but later becomes enriched at the old SPB (Guertin et al., 2000; Sohrmann et al., 1998). In *Tetrahymena*, CdaI undergoes a step-wise polarization: first it marks the anterior half of the cell, and later focuses at the posterior end of the anterior subcell. In fission yeast, time-dependent post-translational modifications have been

proposed to distinguish between the old and new SPB to confer polarization of the Hippo components (Johnson et al., 2012). In ciliates, the new oral apparatus, appears shortly before the cortical CdaI. Thus, the difference in age between the new and old oral apparatus could contribute to the subsequent asymmetry of the Hippo components: CdaI and Mob1. Curiously, in budding yeast, when the daughter SPB is ablated, the Hippo components become enriched on the "wrong" (mother) SPB and this reverse asymmetry is sufficient for cytokinesis (Magidson et al., 2006). In the light of the directional flexibility of the Hippo core observed in fungi, it perhaps is not surprising that ciliates utilize this pathway in the unique context of tandem duplication (Fig. 3.1).

Hippo signaling and cytokinesis in ciliates

The Hippo pathway is important for cytokinesis in diverse eukaryotes including fungi, protists, plants and mammals (Bui et al., 2016; Citterio et al., 2005; Gromley et al., 2003; Hammarton et al., 2005; Hergovich and Hemmings, 2012; Ma et al., 2010; Meitinger et al., 2013; Rohlfs et al., 2007; Slabodnick et al., 2014; Tavares et al., 2012; Yabuta et al., 2007; Yang et al., 2004). The *cdaI-1* mutants either delay or abort cytokinesis. A stronger allele, *cdaI-3*, causes an almost complete block in cytokinesis (JF unpublished data). In fungi and animals, the Hippo signaling renders phosphorylations of the components of the contractile ring to drive its assembly and constriction (Meitinger et al., 2013; Yang et al., 2004). However, in ciliates the molecular mechanism of cytokinesis is divergent; ciliates do not use septins in cell division (Wloga et al., 2008), and the contractile ring operates without myosin-2 and possibly even without conventional actin (Shimizu et al., 2013; Sugita et al., 2011; Sugita et al., 2009). In fission yeast, overexpression of a MEN Hippo/Mst kinase, Cdc7, induces ectopic contractile rings (Fankhauser and Simanis, 1994). However, in *Tetrahymena*, depletion of CdaI causes

multiple defects that occur before cytokinesis (see below) or about the time of cytokinesis (and amitosis). Thus, either CdaI controls multiple subroutines in cell division including cytokinesis, or it acts at an earlier step and affects cytokinesis as a downstream consequence.

CdaI may not play a major role in cortical patterning of the emerging daughters

In all three of the *Tetrahymena cdaI* mutants: *cdaI-1*, *cdaI-2* and *cdaI-3* ((Frankel, 2008), this study and JF unpublished observations), the anterior subcell collapses after its initially correct demarcation, which is manifested by a close juxtaposition of the old oral apparatus and oral primordium. Thus, Hippo signaling may play a role in the morphogenesis of the emerging daughters. In this scenario, even the first sign of depletion of CdaI, the migration of the oral primordium, could be a consequence of failure in specifying the anterior compartment. Such a morphogenetic function would be analogous to what has been documented in budding yeast, where Hippo signaling activates transcription specifically in the daughter cell nucleus (Colman-Lerner et al., 2001). The main if not only output of CdaI activity is likely the generation of a pool of active tertiary complex with Mob1 at the new posterior end. However, we find here that the posterior end cortical markers, CVPs, assemble correctly in the *cdaI-1* anterior cells that have managed to separate, despite their severe defects in nuclear division and segregation. It remains to be determined whether CdaI plays a role in other activities that take place at the new ends of emerging cortices, on either side of the cortical subdivision including the remodeling of the submembranous cytoskeleton, and control of ciliation of basal bodies (Cole et al., 2008; Frankel et al., 1981; Gonda et al., 1999; Jerka-Dziadosz, 1981; Kaczanowska et al., 1999; Numata et al., 1995; Ohba et al., 1986). To conclude, there is no evidence that CdaI plays a role in the organelle patterning at the posterior end of the anterior daughter, besides its role in sizing the anterior compartment by maintaining the fission zone at a proper equatorial position.

How is CdaI activated and patterned

It is unclear how the cortical CdaI is spatially regulated and why its pattern changes so dramatically as the cell division progresses. The cortical lines of CdaI appear first when cell division is already under way, after the oral primordium starts to develop. Based on the pattern of CdaI-GFP in the *elo1-1* mutant, it appears that the new oral apparatus influences the posterior boundary of CdaI cortical lines and that this effect weakens further away from the oral sector. The posterior boundary of CdaI-GFP lines is established before the cortical subdivision appears (Fig. 3.7B, 3.8B). Clearly, in addition to the *ELO1* gene product, other unknown factors pattern CdaI along the anteroposterior axis. In yeast, the Hippo/MEN pathway activity is a consequence of activation of a G protein, Tem1/Spg1, that is asymmetrically enriched on the daughter SPB (Bardin et al., 2000). It is unlikely however that in ciliates the factors that pattern CdaI originate from the mitotic spindle or more broadly from the nuclei. The macronucleus divides by amitosis relatively late, at the time of cytokinesis (Williams and Williams, 1976), using microtubules that lack a bipolar spindle organization (Fujiu and Numata, 2000). The micronucleus divides by mitosis at about the time of initiation of cortical subdivision (Joachimiak et al., 2004; Kaczanowska et al., 1993), but this is a closed mitosis that occurs without centriolar centrosomes or a structure similar to the SPB of fungi (LaFountain and Davidson, 1979; LaFountain and Davidson, 1980). Also, there is a viable strain of *T. thermophila* that lacks a micronucleus (Kaney and Speare, 1983), and other *Tetrahymena* species have lost the micronucleus during evolution (Doerder, 2014). Thus, the signal that activates and spatially restricts Hippo in ciliates is unlikely to come from the nuclei. To the contrary, there is evidence of a reverse “outside to inside” signaling in which the cortex affects the nuclei (Cohen and Beisson, 1980; de Terra,

1973; de Terra, 1975; Gaertig and Cole, 2000). Thus, the signal that activates CdaI in ciliates is likely to be intrinsic to the cortex.

In interphase, Mob1 may act without CdaI

In interphase, Mob1 remains associated with the posterior end of the cell (Tavares et al., 2012), while CdaI is not detectable (Fig. 3.1, stages 1-3). The persistence of Mob1 at the posterior end of interphase cells was also documented in *Stentor*, using anti-Mob1 antibodies (Slabodnick et al., 2014). The old Mob1 pool is likely present during cell division based on the presence of foci of CdaI-GFP at the posterior end of the dividing cells (Fig. 3.7 and 3.8 arrowheads). Since the expression of CdaI appears to be limited to cell division, during interphase Mob1 may be activated by one of the three additional Hippo/Mst kinase paralogs (TTHERM_00933100, TTHERM_01246760 and TTHERM_00580440). A function of Mob1 in interphase is supported by the observation that a depletion of Mob1 in *Stentor* affects the ability of this large ciliate to regenerate its body shape after surgical dissection (Slabodnick et al., 2014). To explore the potential interphase and early cell division functions of Mob1, it will be useful to generate a fast-acting conditional allele of Mob1; such mutations have been isolated in budding yeast (Luca et al., 2001; Luca and Winey, 1998).

SUMMARY

We show that *Tetrahymena* uses the conserved Hippo core to maintain equatorial cell division. Despite the unique mode of cell division by tandem duplication, in ciliates the Hippo signaling shows many conserved properties, including polarization of the signaling components across the axis of cell division. More work is needed to determine the exact mechanism of how Hippo signaling maintains the equatorial division plane in ciliates. Finally, it is compelling that under CdaI deficiency the plane of cell division is initially set correctly on both the

anteroposterior and circumferential axes. Thus, unknown polarity factors must act upstream of CdaI to control the positional information. Among them, the *ELO1* gene product may play a critical role in specifying the anteroposterior position of the oral apparatus.

ACKNOWLEDGEMENTS

We are grateful to Eileen Hamilton and Eduardo Orias (University of California Santa Barbara) and Robert Coyne and Vivek Krishnakumar (Craig J. Venter Institute) for giving us access to the assembled micronuclear genome of *T. thermophila* prior to publication. This work was supported by a bridge funding from the Office of the Vice-President for Research and the Department of Cellular Biology at the University of Georgia to JG. Funding for NK from the National Science Foundation (MCB-1149106) is acknowledged. The work in the RB laboratory was funded by grants from Deutsche Forschungsgemeinschaft (CRC746 and CRC850). EJ was supported by a Polish Ministry of Science and Higher Education Grant (N N303 817840). GM was supported by a pre-doctoral fellowship from the National Institutes of Health (1F31NS074841-01).

LITERATURE CITED

Afgan, E., D. Baker, M. van den Beek, D. Blankenberg, D. Bouvier, M. Cech, J. Chilton, D. Clements, N. Coraor, C. Eberhard, B. Gruning, A. Guerler, J. Hillman-Jackson, G. Von Kuster, E. Rasche, N. Soranzo, N. Turaga, J. Taylor, A. Nekrutenko, and J. Goecks. 2016. The Galaxy platform for accessible, reproducible and collaborative biomedical analyses: 2016 update. *Nucleic Acids Res.* 44:W3-W10.

Anand, R., J. Maksimoska, N. Pagano, E.Y. Wong, P.A. Gimotty, S.L. Diamond, E. Meggers, and R. Marmorstein. 2009. Toward the development of a potent and selective organoruthenium mammalian sterile 20 kinase inhibitor. *Journal of medicinal chemistry*. 52:1602-1611.

Bardin, A.J., R. Visintin, and A. Amon. 2000. A mechanism for coupling exit from mitosis to partitioning of the nucleus. *Cell*. 102:21-31.

Birkeland, S.R., N. Jin, A.C. Ozdemir, R.H. Lyons, Jr., L.S. Weisman, and T.E. Wilson. 2010. Discovery of mutations in Saccharomyces cerevisiae by pooled linkage analysis and whole-genome sequencing. *Genetics*. 186:1127-1137.

Blankenberg, D., A. Gordon, G. Von Kuster, N. Coraor, J. Taylor, A. Nekrutenko, and T. Galaxy. 2010. Manipulation of FASTQ data with Galaxy. *Bioinformatics*. 26:1783-1785.

Bruns, P.J., and T.B. Brussard. 1974. Pair formation in *Tetrahymena pyriformis*, an inducible developmental system. *J.Exp.Zool.* 188:337-344.

Bruns, P.J., T.B. Brussard, and A.B. Kavka. 1976. Isolation of homozygous mutants after induced self-fertilization in Tetrahymena. *Proc Natl Acad Sci U S A*. 73:3243-3247.

Bruns, P.J., and D. Cassidy-Hanley. 2000. Biolistic transformation of macro- and micronuclei. *Methods Cell Biol*. 62:501-512.

Bui, D.A., W. Lee, A.E. White, J.W. Harper, R.C. Schackmann, M. Overholtzer, L.M. Selfors, and J.S. Brugge. 2016. Cytokinesis involves a nontranscriptional function of the Hippo pathway effector YAP. *Sci Signal*. 9:ra23.

Busch, C.J., A. Vogt, and K. Mochizuki. 2010. Establishment of a Cre/loxP recombination system for N-terminal epitope tagging of genes in Tetrahymena. *BMC microbiology*. 10:191.

Chalker, D.L. 2012. Transformation and strain engineering of Tetrahymena. *Methods Cell Biol*. 109:327-345.

Cingolani, P., V.M. Patel, M. Coon, T. Nguyen, S.J. Land, D.M. Ruden, and X. Lu. 2012. Using Drosophila melanogaster as a Model for Genotoxic Chemical Mutational Studies with a New Program, SnpSift. *Front Genet*. 3:35.

Citterio, S., E. Albertini, S. Varotto, E. Feltrin, M. Soattin, G. Marconi, S. Sgorbati, M. Lucchin, and G. Barcaccia. 2005. Alfalfa Mob 1-like genes are expressed in reproductive organs during meiosis and gametogenesis. *Plant Mol Biol*. 58:789-807.

Cohen, J., and J. Beisson. 1980. Genetic analysis of the relationships between the cell surface and the nuclei in Paramecium tetraurella. *Genetics*. 95:797-818.

Cole, E.S., P.C. Anderson, R.B. Fulton, M.E. Majerus, M.G. Rooney, J.M. Savage, D. Chalker, J. Honts, M.E. Welch, A.L. Wentland, E. Zweifel, and D.J. Beussman. 2008. A proteomics approach to cloning fenestrin from the nuclear exchange junction of tetrahymena. *J Eukaryot Microbiol*. 55:245-256.

Colman-Lerner, A., T.E. Chin, and R. Brent. 2001. Yeast Cbk1 and Mob2 activate daughter-specific genetic programs to induce asymmetric cell fates. *Cell*. 107:739-750.

Dave, D., D. Wloga, and J. Gaertig. 2009. Manipulating ciliary protein-encoding genes in Tetrahymena thermophila. *Methods Cell Biol*. 93:1-20.

de Terra, N. 1973. Further evidence for cortical control over replication of the macronucleus and basal bodies of Stentor. *Dev.Biol.* 32:313-316.

de Terra, N. 1975. Evidence for cell surface control of macronuclear DNA synthesis in Stentor. *Nature*. 258:300-303.

DePristo, M.A., E. Banks, R. Poplin, K.V. Garimella, J.R. Maguire, C. Hartl, A.A. Philippakis, G. del Angel, M.A. Rivas, M. Hanna, A. McKenna, T.J. Fennell, A.M. Kernytsky, A.Y. Sivachenko, K. Cibulskis, S.B. Gabriel, D. Altshuler, and M.J. Daly. 2011. A framework for variation discovery and genotyping using next-generation DNA sequencing data. *Nat*

Genet. 43:491-498.

Doerder, F.P. 2014. Abandoning sex: multiple origins of asexuality in the ciliate Tetrahymena. *BMC Evol Biol*. 14:112.

Ehmer, U., and J. Sage. 2016. Control of Proliferation and Cancer Growth by the Hippo Signaling Pathway. *Mol Cancer Res*. 14:127-140.

Eisen, J.A., R.S. Coyne, M. Wu, D. Wu, M. Thiagarajan, J.R. Wortman, J.H. Badger, Q. Ren, P. Amedeo, K.M. Jones, L.J. Tallon, A.L. Delcher, S.L. Salzberg, J.C. Silva, B.J. Haas, W.H. Majoros, M. Farzad, J.M. Carlton, R.K. Smith, Jr., J. Garg, R.E. Pearlman, K.M. Karrer, L. Sun, G. Manning, N.C. Elde, A.P. Turkewitz, D.J. Asai, D.E. Wilkes, Y. Wang, H. Cai, K. Collins, B.A. Stewart, S.R. Lee, K. Wilamowska, Z. Weinberg, W.L. Ruzzo, D. Wloga, J. Gaertig, J. Frankel, C.C. Tsao, M.A. Gorovsky, P.J. Keeling, R.F. Waller, N.J. Patron, J.M. Cherry, N.A. Stover, C.J. Krieger, C. del Toro, H.F. Ryder, S.C. Williamson, R.A. Barbeau, E.P. Hamilton, and E. Orias. 2006. Macronuclear genome sequence of the ciliate Tetrahymena thermophila, a model eukaryote. *PLoS biology*. 4:e286.

Fan, F., Z. He, L.L. Kong, Q. Chen, Q. Yuan, S. Zhang, J. Ye, H. Liu, X. Sun, J. Geng, L. Yuan, L. Hong, C. Xiao, W. Zhang, X. Sun, Y. Li, P. Wang, L. Huang, X. Wu, Z. Ji, Q. Wu, N.S. Xia, N.S. Gray, L. Chen, C.H. Yun, X. Deng, and D. Zhou. 2016. Pharmacological targeting of kinases MST1 and MST2 augments tissue repair and regeneration. *Sci Transl Med*. 8:352ra108.

Fankhauser, C., and V. Simanis. 1994. The cdc7 protein kinase is a dosage dependent regulator of septum formation in fission yeast. *EMBO J*. 13:3011-3019.

Feoktistova, A., J. Morrell-Falvey, J.S. Chen, N.S. Singh, M.K. Balasubramanian, and K.L. Gould. 2012. The fission yeast septation initiation network (SIN) kinase, Sid2, is required for SIN asymmetry and regulates the SIN scaffold, Cdc11. *Mol Biol Cell*. 23:1636-1645.

Frankel, J. 2008. What do genic mutations tell us about the structural patterning of a complex single-celled organism? *Eukaryot Cell*. 7:1617-1639.

Frankel, J., L.M. Jenkins, F.P. Doerder, and E.M. Nelsen. 1976. Mutations affecting cell division in Tetrahymena pyriformis. I. Selection and genetic analysis. *Genetics*. 83:489-506.

Frankel, J., E.M. Nelsen, and L.M. Jenkins. 1977. Mutations affecting cell division in Tetrahymena pyriformis, syngen 1. II. Phenotypes of single and double homozygotes. *Dev Biol*. 58:255-275.

Frankel, J., E.M. Nelsen, and L.M. Jenkins. 1981. Development of the ciliature of *Tetrahymena thermophila*. II. Spatial subdivision prior to cytokinesis. *Dev. Biol*. 88:39-54.

Frenz, L.M., S.E. Lee, D. Fesquet, and L.H. Johnston. 2000. The budding yeast Dbf2 protein kinase localises to the centrosome and moves to the bud neck in late mitosis. *J Cell Sci*. 113 Pt 19:3399-3408.

Fujiu, K., and O. Numata. 2000. Reorganization of microtubules in the amitotically dividing macronucleus of Tetrahymena. *Cell Motil Cytoskeleton*. 46:17-27.

Gaertig, J., and E.S. Cole. 2000. The role of cortical geometry in the nuclear development of Tetrahymena thermophila. *J Eukaryot Microbiol*. 47:590-596.

Gaertig, J., M.A. Cruz, J. Bowen, L. Gu, D.G. Pennock, and M.A. Gorovsky. 1995. Acetylation of lysine 40 in alpha-tubulin is not essential in Tetrahymena thermophila. *J Cell Biol*. 129:1301-1310.

Gaertig, J., D. Wloga, K.K. Vasudevan, M. Guha, and W.L. Dentler. 2013. Discovery and functional evaluation of ciliary proteins in Tetrahymena thermophila. *In* Cilia, part B. Vol. 255. W.F. Marshall, editor.

Galati, D.F., S. Bonney, Z. Kronenberg, C. Clarissa, M. Yandell, N.C. Elde, M. Jerka-Dziadosz, T.H. Giddings, J. Frankel, and C.G. Pearson. 2014. DisAp-dependent striated fiber elongation is required to organize ciliary arrays. *The Journal of cell biology*. 207:705-715.

Gogl, G., K.D. Schneider, B.J. Yeh, N. Alam, A.N. Nguyen Ba, A.M. Moses, C. Hetenyi, A. Remenyi, and E.L. Weiss. 2015. The Structure of an NDR/LATS Kinase-Mob Complex Reveals a Novel Kinase-Coactivator System and Substrate Docking Mechanism. *PLoS Biol*. 13:e1002146.

Gonda, K., K. Nishibori, H. Ohba, A. Watanabe, and O. Numata. 1999. Molecular cloning of the gene for p85 that regulates the initiation of cytokinesis in Tetrahymena. *Biochemical and biophysical research communications*. 264:112-118.

Gorovsky, M.A. 1973. Macro- and micronuclei of *Tetrahymena pyriformis*: a model system for studying the structure and function of eukaryotic nuclei. *J.Protozool.* 20:19-25.

Gromley, A., A. Jurczyk, J. Sillibourne, E. Halilovic, M. Mogensen, I. Groisman, M. Blomberg, and S. Doxsey. 2003. A novel human protein of the maternal centriole is required for the final stages of cytokinesis and entry into S phase. *J Cell Biol*. 161:535-545.

Guertin, D.A., L. Chang, F. Irshad, K.L. Gould, and D. McCollum. 2000. The role of the sid1p kinase and cdc14p in regulating the onset of cytokinesis in fission yeast. *EMBO J.* 19:1803-1815.

Hamilton, E.P., A. Kapusta, P.E. Huvos, S.L. Bidwell, N. Zafar, H. Tang, M. Hadjithomas, V. Krishnakumar, J.H. Badger, E.V. Caler, C. Russ, Q. Zeng, L. Fan, J.Z. Levin, T. Shea, S.K. Young, R. Hegarty, R. Daza, S. Gujja, J.R. Wortman, B.W. Birren, C. Nusbaum, J. Thomas, C.M. Carey, E.J. Pritham, C. Feschotte, T. Noto, K. Mochizuki, R. Papazyan, S.D. Taverna, P.H. Dear, D.M. Cassidy-Hanley, J. Xiong, W. Miao, E. Orias, and R.S. Coyne. 2016. Structure of the germline genome of Tetrahymenathermophila and relationship to the massively rearranged somatic genome. *Elife*. 5.

Hammarton, T.C., S.G. Lillico, S.C. Welburn, and J.C. Mottram. 2005. Trypanosoma brucei MOB1 is required for accurate and efficient cytokinesis but not for exit from mitosis. *Mol Microbiol*. 56:104-116.

Hergovich, A., and B.A. Hemmings. 2012. Hippo signalling in the G2/M cell cycle phase: lessons learned from the yeast MEN and SIN pathways. *Seminars in cell & developmental biology*. 23:794-802.

Hilman, D., and U. Gat. 2011. The evolutionary history of YAP and the hippo/YAP pathway. *Molecular biology and evolution*. 28:2403-2417.

Jerka-Dziadosz, M. 1981. Cytoskeleton-related structures in tetrahymena thermophila:

microfilaments at the apical and division-furrow rings. *J Cell Sci*. 51:241-253.

Jerka-Dziadosz, M., L.M. Jenkins, E.M. Nelsen, N.E. Williams, R. Jaeckel-Williams, and J. Frankel. 1995. Cellular polarity in ciliates: persistence of global polarity in a disorganized mutant of Tetrahymena thermophila that disrupts cytoskeletal organization. *Dev. Biol.* 169:644-661.

Joachimiak, E., J. Kaczanowska, M. Kiersnowska, and A. Kaczanowski. 2004. Syndrome of the failure to turn off mitotic activity in Tetrahymena thermophila: in cdaA1 phenotypes. *Acta Protozoologica*. 43:291-301.

Johnson, A.E., D. McCollum, and K.L. Gould. 2012. Polar opposites: Fine-tuning cytokinesis through SIN asymmetry. *Cytoskeleton (Hoboken)*. 69:686-699.

Kaczanowska, J., L. Buzanska, and M. Ostrowski. 1993. Relationship between spatial pattern of basal bodies and membrane skeleton (epiplasm) during the cell cycle of Tetrahymena: cdaA mutant and anti-membrane skeleton immunostaining. *J Eukaryot Microbiol*. 40:747-754.

Kaczanowska, J., E. Joachimiak, L. Buzanska, W. Krawczynska, D.N. Wheatley, and A. Kaczanowski. 1999. Molecular subdivision of the cortex of dividing Tetrahymena is coupled with the formation of the fission zone. *Dev Biol*. 212:150-164.

Kaney, A.R., and V.J. Speare. 1983. An amicronucleate mutant of *Tetrahymena thermophila*. *Exp.Cell Res.* 143:461-467.

Kannan, N., and A.F. Neuwald. 2004. Evolutionary constraints associated with functional specificity of the CMGC protein kinases MAPK, CDK, GSK, SRPK, DYRK, and CK2alpha. *Protein Sci*. 13:2059-2077.

Kannan, N., and A.F. Neuwald. 2005. Did protein kinase regulatory mechanisms evolve through elaboration of a simple structural component? *J Mol Biol*. 351:956-972.

Kontur, C., S. Kumar, X. Lan, J.K. Pritchard, and A.P. Turkewitz. 2016. Whole Genome Sequencing Identifies a Novel Factor Required for Secretory Granule Maturation in Tetrahymena thermophila. *G3 (Bethesda)*. 6:2505-2516.

LaFountain, J.R., Jr., and L.A. Davidson. 1979. An analysis of spindle ultrastructure during prometaphase and metaphase of micronuclear division in Tetrahymena. *Chromosoma*. 75:293-308.

LaFountain, J.R., Jr., and L.A. Davidson. 1980. An analysis of spindle ultrastructure during anaphase of micronuclear division in Tetrahymena. *Cell motility*. 1:41-61.

Li, H., and R. Durbin. 2009. Fast and accurate short read alignment with Burrows-Wheeler transform. *Bioinformatics*. 25:1754-1760.

Lodowski, D.T., V.M. Tesmer, J.L. Benovic, and J.J. Tesmer. 2006. The structure of G protein-coupled receptor kinase (GRK)-6 defines a second lineage of GRKs. *J Biol Chem*. 281:16785-16793.

Luca, F.C., M. Mody, C. Kurischko, D.M. Roof, T.H. Giddings, and M. Winey. 2001. Saccharomyces cerevisiae Mob1p is required for cytokinesis and mitotic exit. *Molecular and cellular biology*. 21:6972-6983.

Luca, F.C., and M. Winey. 1998. MOB1, an essential yeast gene required for completion of mitosis and maintenance of ploidy. *Mol Biol Cell*. 9:29-46.

Ma, J., C. Benz, R. Grimaldi, C. Stockdale, P. Wyatt, J. Frearson, and T.C. Hammarton. 2010. Nuclear DBF-2-related kinases are essential regulators of cytokinesis in bloodstream stage Trypanosoma brucei. *J Biol Chem*. 285:15356-15368.

Magidson, V., F. Chang, and A. Khodjakov. 2006. Regulation of cytokinesis by spindle-pole bodies. *Nat Cell Biol*. 8:891-893.

Mandoiu, I., and A. Zelikovsky. 2016. Computational methods for next generation data analysis. John Wiley & Sons, Hoboken, New Jersey.

Marker, S., Q. Carradec, V. Tanty, O. Arnaiz, and E. Meyer. 2014. A forward genetic screen reveals essential and non-essential RNAi factors in Paramecium tetraurelia. *Nucleic Acids Res*. 42:7268-7280.

McKenna, A., M. Hanna, E. Banks, A. Sivachenko, K. Cibulskis, A. Kernytsky, K. Garimella, D. Altshuler, S. Gabriel, M. Daly, and M.A. DePristo. 2010. The Genome Analysis Toolkit: a MapReduce framework for analyzing next-generation DNA sequencing data. *Genome research*. 20:1297-1303.

Meitinger, F., S. Palani, B. Hub, and G. Pereira. 2013. Dual function of the NDR-kinase Dbf2 in the regulation of the F-BAR protein Hof1 during cytokinesis. *Mol Biol Cell*. 24:1290-1304.

Meng, Z., T. Moroishi, and K.L. Guan. 2016. Mechanisms of Hippo pathway regulation. *Genes Dev*. 30:1-17.

Menssen, R., A. Neutzner, and W. Seufert. 2001. Asymmetric spindle pole localization of yeast Cdc15 kinase links mitotic exit and cytokinesis. *Current biology : CB*. 11:345-350.

Michelmore, R.W., I. Paran, and R.V. Kesseli. 1991. Identification of markers linked to disease-resistance genes by bulked segregant analysis: a rapid method to detect markers in specific genomic regions by using segregating populations. *Proceedings of the National Academy of Sciences of the United States of America*. 88:9828-9832.

Minevich, G., D.S. Park, D. Blankenberg, R.J. Poole, and O. Hobert. 2012. CloudMap: a cloud-based pipeline for analysis of mutant genome sequences. *Genetics*. 192:1249-1269.

Nelsen, E.M., J. Frankel, and E. Martel. 1981. Development of the ciliature of Tetrahymena thermophila. I. Temporal coordination with oral development. *Dev. Biol*. 88:27-38.

Ni, L., S. Li, J. Yu, J. Min, C.A. Brautigam, D.R. Tomchick, D. Pan, and X. Luo. 2013. Structural basis for autoactivation of human Mst2 kinase and its regulation by RASSF5. *Structure*. 21:1757-1768.

Numata, O., H. Suzuki, H. Ohba, and Y. Watanabe. 1995. The mutant gene product of a Tetrahymena cell-division-arrest mutant cdaA is localized in the accessory structure of specialized basal body close to the division furrow. *Zoolog.Sci.* 12:133-135.

Ohba, H., I. Ohmori, O. Numata, and Y. Watanabe. 1986. Purification and immunofluorescence localization of the mutant gene product of a Tetrahymena cdaA1 mutant affecting cell division. *J Biochem*. 100:797-808.

Ohnishi, J., H. Mizoguchi, S. Takeno, and M. Ikeda. 2008. Characterization of mutations induced by N-methyl-N'-nitro-N-nitrosoguanidine in an industrial Corynebacterium glutamicum strain. *Mutat Res*. 649:239-244.

Orias, E., E.P. Hamilton, and M. Flacks. 1979. Osmotic shock prevents nuclear exchange and produces whole-genome homozygotes in conjugating Tetrahymena. *Science*. 203:660-663.

Orias, E., E.P. Hamilton, and J.D. Orias. 2000. Tetrahymena as a laboratory organism: useful strains, cell culture, and cell line maintenance. *Methods Cell Biol*. 62:189-211.

Piperno, G., and M.T. Fuller. 1985. Monoclonal antibodies specific for an acetylated form of a-tubulin recognize the antigen in cilia and flagella from a variety of organisms. *J.Cell Biol*. 101:2085-2094.

Radivojac, P., P.H. Baenziger, M.G. Kann, M.E. Mort, M.W. Hahn, and S.D. Mooney. 2008. Gain and loss of phosphorylation sites in human cancer. *Bioinformatics*. 24:i241-247.

Robinson, J.T., H. Thorvaldsdottir, W. Winckler, M. Guttman, E.S. Lander, G. Getz, and J.P. Mesirov. 2011. Integrative genomics viewer. *Nat Biotechnol*. 29:24-26.

Rock, J.M., D. Lim, L. Stach, R.W. Ogrodowicz, J.M. Keck, M.H. Jones, C.C. Wong, J.R. Yates, 3rd, M. Winey, S.J. Smerdon, M.B. Yaffe, and A. Amon. 2013. Activation of the yeast Hippo pathway by phosphorylation-dependent assembly of signaling complexes. *Science*. 340:871-875.

Rohlfs, M., R. Arasada, P. Batsios, J. Janzen, and M. Schleicher. 2007. The Ste20-like kinase SvkA of Dictyostelium discoideum is essential for late stages of cytokinesis. *J Cell Sci*. 120:4345-4354.

Ruehle, M.D., E. Orias, and C.G. Pearson. 2016. Tetrahymena as a Unicellular Model Eukaryote: Genetic and Genomic Tools. *Genetics*. 203:649-665.

Sanders, M.A., and J.L. Salisbury. 1994. Centrin plays an essential role in microtubule severing during flagellar excision in *Chlamydomonas reinhardtii*. *J.Cell Biol*. 124:795-805.

Sebe-Pedros, A., Y. Zheng, I. Ruiz-Trillo, and D. Pan. 2012. Premetazoan origin of the hippo signaling pathway. *Cell reports*. 1:13-20.

Shimizu, Y., Y. Kushida, S. Kiriyama, K. Nakano, and O. Numata. 2013. Formation and ingression of division furrow can progress under the inhibitory condition of actin polymerization in ciliate Tetrahymena pyriformis. *Zoolog Sci*. 30:1044-1049.

Slabodnick, M.M., J.G. Ruby, J.G. Dunn, J.L. Feldman, J.L. DeRisi, and W.F. Marshall. 2014. The kinase regulator mob1 acts as a patterning protein for stentor morphogenesis. *PLoS biology*. 12:e1001861.

Sohrmann, M., S. Schmidt, I. Hagan, and V. Simanis. 1998. Asymmetric segregation on spindle poles of the Schizosaccharomyces pombe septum-inducing protein kinase Cdc7p. *Genes Dev*. 12:84-94.

Sours, K.M., S.C. Kwok, T. Rachidi, T. Lee, A. Ring, A.N. Hoofnagle, K.A. Resing, and N.G. Ahn. 2008. Hydrogen-exchange mass spectrometry reveals activation-induced changes in the conformational mobility of p38alpha MAP kinase. *J Mol Biol*. 379:1075-1093.

Sugita, M., Y. Iwataki, K. Nakano, and O. Numata. 2011. Unique sequences and predicted functions of myosins in Tetrahymena thermophila. *Gene*. 480:10-20.

Sugita, M., K. Nakano, M. Sato, K. Toyooka, and O. Numata. 2009. The roles of actin cytoskeleton and microtubules for membrane recycling of a food vacuole in Tetrahymena thermophila. *Cell Motil Cytoskeleton*. 66:371-377.

Tavares, A., J. Goncalves, C. Florindo, A.A. Tavares, and H. Soares. 2012. Mob1: defining cell polarity for proper cell division. *Journal of cell science*. 125:516-527.

Thompson, B.J., and E. Sahai. 2015. MST kinases in development and disease. *J Cell Biol*. 210:871-882.

Thorvaldsdottir, H., J.T. Robinson, and J.P. Mesirov. 2013. Integrative Genomics Viewer (IGV): high-performance genomics data visualization and exploration. *Brief Bioinform*. 14:178-192.

Williams, N.E., and R.J. Williams. 1976. Macronuclear division with and without microtubules in

Tetrahymena. *J. Cell Sci*. 20:61-67.

Wloga, D., and J. Frankel. 2012. From molecules to morphology: cellular organization of Tetrahymena thermophila. *Methods Cell Biol*. 109:83-140.

Wloga, D., I. Strzyzewska-Jowko, J. Gaertig, and M. Jerka-Dziadosz. 2008. Septins stabilize mitochondria in Tetrahymena thermophila. *Eukaryot Cell*. 7:1373-1386.

Yabuta, N., N. Okada, A. Ito, T. Hosomi, S. Nishihara, Y. Sasayama, A. Fujimori, D. Okuzaki, H. Zhao, M. Ikawa, M. Okabe, and H. Nojima. 2007. Lats2 is an essential mitotic regulator required for the coordination of cell division. *J Biol Chem*. 282:19259-19271.

Yang, X., K. Yu, Y. Hao, D.M. Li, R. Stewart, K.L. Insogna, and T. Xu. 2004. LATS1 tumour suppressor affects cytokinesis by inhibiting LIMK1. *Nat Cell Biol*. 6:609-617.

Yu, F.X., B. Zhao, and K.L. Guan. 2015. Hippo Pathway in Organ Size Control, Tissue Homeostasis, and Cancer. *Cell*. 163:811-828.

FIGURES AND FIGURE LEGENDS

Figure 3.1 A diagram that presents the cortical and nuclear stages of cell division by tandem duplication in *Tetrahymena*. The green and red lines indicate the patterns of Hippo signaling components CdaI (red, this study) and Mob1 (green, based on (Tavares et al., 2012). Abbreviations: mi, micronucleus; ma, macronucleus; oa, oral apparatus; noa, new oral apparatus (primordium); cvp, contractile vacuole pore; ncvp, new contractile vacuole pore; cyp, cytoproct; ncyp, new cytoproct. The stage designations are novel to this paper and the numbers do not correspond to the earlier named stages of oral development (Nelsen et al., 1981).

Fig. 3.1

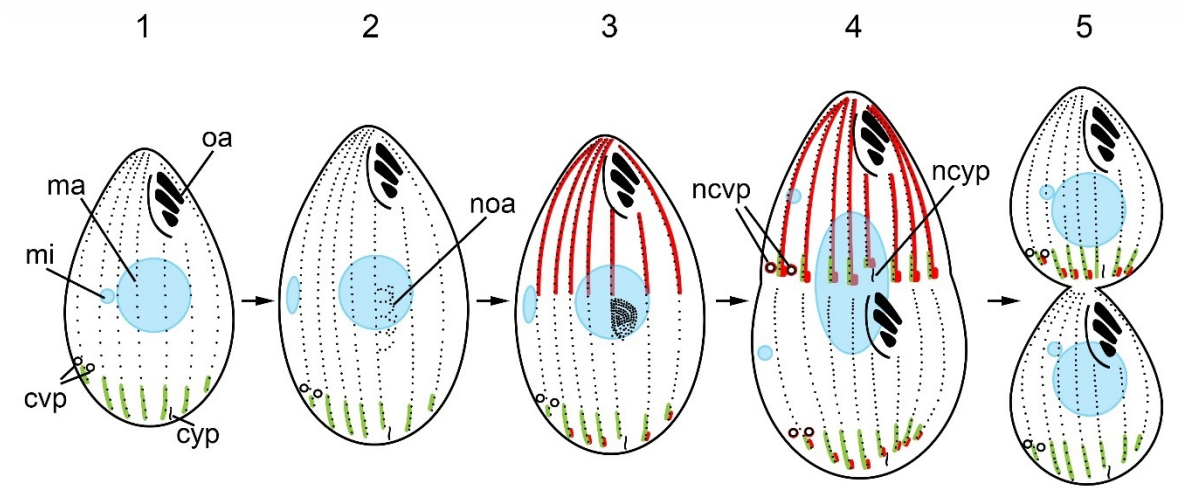

Figure 3.2 Cortical pattern and nuclei during cell division in wild-type *Tetrahymena* grown at 39ºC. The cells were labeled with anti-centrin 20H5 antibodies (green) and DAPI (blue). (A-B) Early stages of cell division. A new oral primordium develops (more advanced in B) but there is no sign of cortical subdivision yet. (C) A cell with a well-developed cortical subdivision but before cytokinesis. The micronucleus has already completed its mitosis and the two progeny micronuclei are present. The macronucleus is elongated, in an early stage of amitosis. (D) A cell in a late stage of cytokinesis, the macronucleus has divided by amitosis. Abbreviations: oa, oral apparatus; noa, new oral apparatus; mi, micronucleus, ma, macronucleus; cs, cortical subdivision.

Fig. 3.2

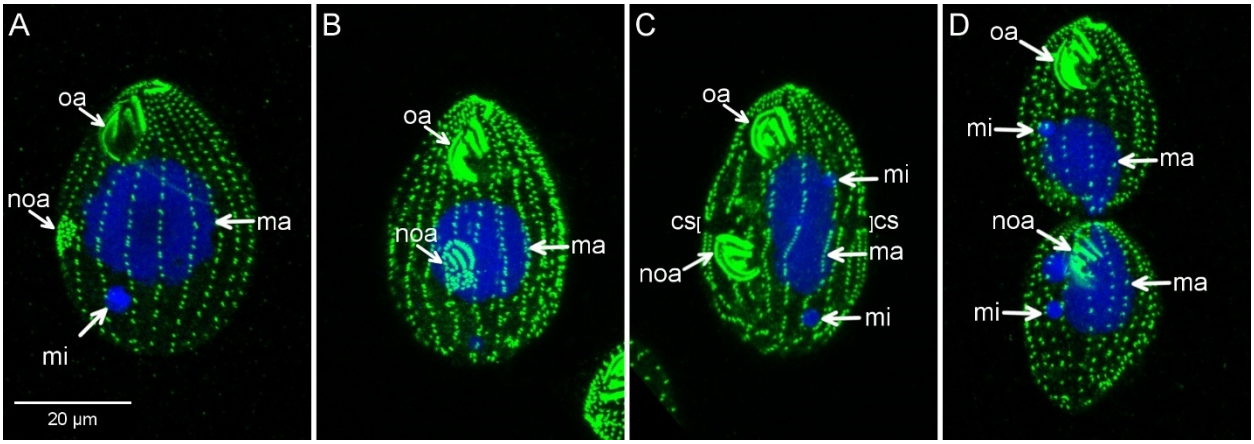
A
oa
noa
ma
mi
20 µm
B
oa
noa
ma
C
oa
mi
cs
ma
noa
mi
D
oa
mi
ma
noa
ma
mi

Figure 3.3 The course of cortical and nuclear division in the *cdaI-1 Tetrahymena* at the restrictive temperature. The cells were labeled with anti-centrin 20H5 antibodies (green) and DAPI (blue). The *cdaI-1* cells were grown for 3 or 6 hr at the restrictive temperature, 39ºC. (A-B) Mutants in an early stage of cell division, with an oral primordium (noa) present at the proper submedial position. (C) The mutant cell after the micronuclear division, with a well-developed new oral apparatus (comparable to the stage 4 in the wild-type in Fig. 3.1C). Note the anterior displacement of the new oral apparatus. The cortical subdivision is present at a proper location in relation to the new oral apparatus, and thus the entire division plane is shifted. (D) A mutant cell with a nearly completed cytokinesis. Note the failure in the division of the macronucleus resulting in the absence of a macronucleus in the anterior daughter. (E) A cell that is an anterior product of a complete *cdaI-1* division, lacking a macronucleus. (F) A hammerhead cell where the anterior compartment is relatively mildly affected. Note an incomplete cortical subdivision; an asymmetry in the breakage of ciliary rows could be behind an unbalanced cortical growth that could produce the tilting of the anterior daughter. (G) A mutant cell that has produced two anterior subcells, and failed cytokinesis in two subsequent generations. (H) A diagram showing the frequencies of the different morphologies observed in the *cdaI-1* cells at 3 and 6 hr after the temperature shift or after 6 hr of incubation at the permissive temperature. (I) A diagram showing the frequency of nuclear end-points of cells with the hammerhead shape. Abbreviations: oa, oral apparatus; noa, new oral apparatus; mi, micronucleus, ma, macronucleus; cs, cortical subdivision.

Fig. 3.3

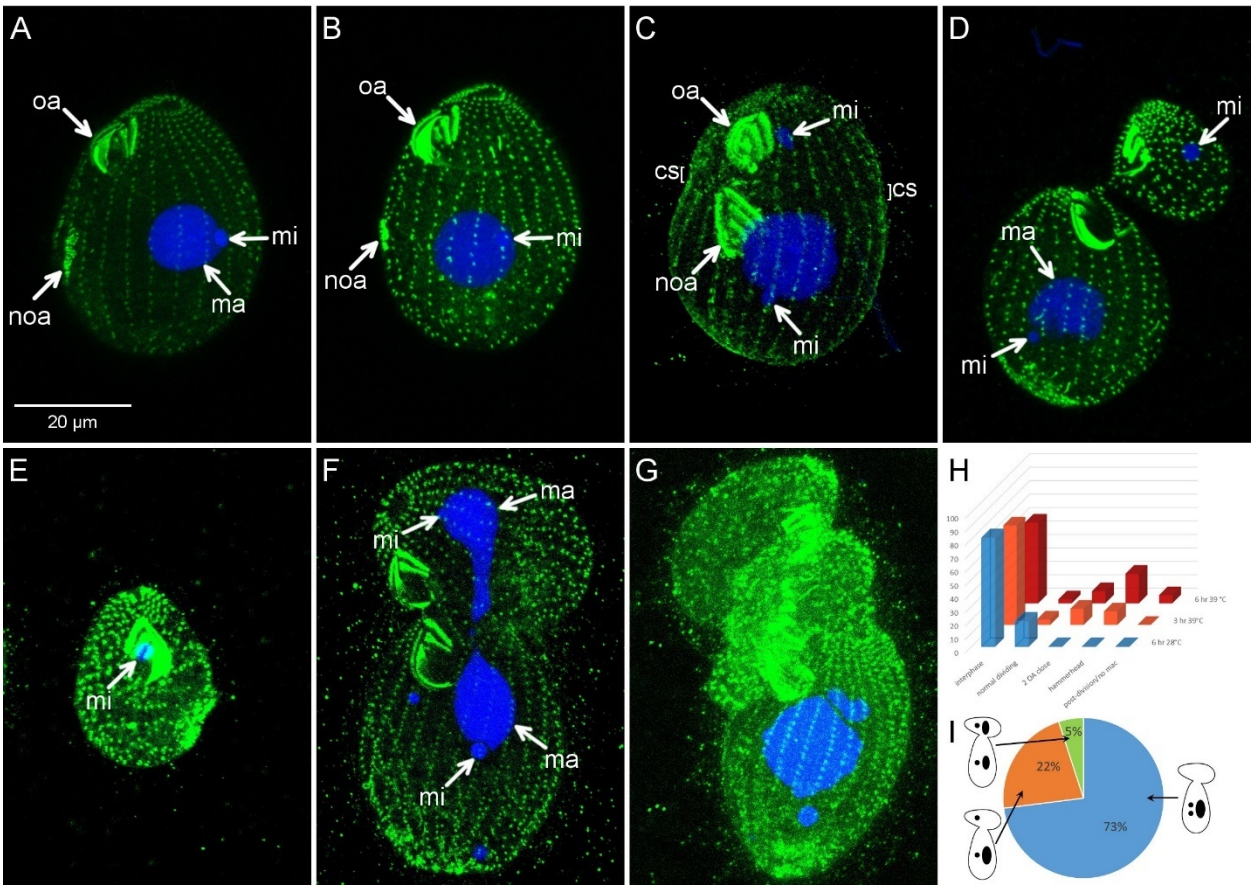
A
oa
mi
noa
ma
20 µm
B
oa
mi
noa
C
oa
mi
noa
mi
D
mi
ma
mi
E
mi
F
ma
mi
ma
mi
G
H
6 hr 39 °C
3 hr 39°C
6 hr 28°C
interphase
normal dividing
2 OA close
hammerhead
post-division no mac
I
5%
22%
73%

Figure 3.4 Identification of the causative mutation of *cdaI-1* in TTHERM_00971920 by comparative whole genome sequencing. (A) The results of variant subtraction and filtering steps using macronuclear reference genome. MNNG is an abbreviation of nitrosoguanidine (B) Whole genome sequencing reads aligned to the region of interest in *TTHERM_00971920* around the causative variant scf_8254051:142648 (C to T) in the *cdaI-1* (top) and wild-type clonal pool (bottom). In this view generated with the IGV browser, the sequences reads are stacked underneath the reference genome sequence to which they were aligned. Reference bases in the reads are shown in grey while non-reference bases are highlighted using the same color code as in the reference genome. (C) The predicted domain organization of TTHERM_00971920 protein. The arrow shows the location of the substitution that results from the scf_8254051:142648 C to T mutation, in the predicted kinase domain of TTHERM_00971920 protein. (D) Variant density mapping on the micronuclear chromosomes. Normalized linkage scores are shown along the length of each of the 5 micronuclear chromosomes.

Fig. 3.4

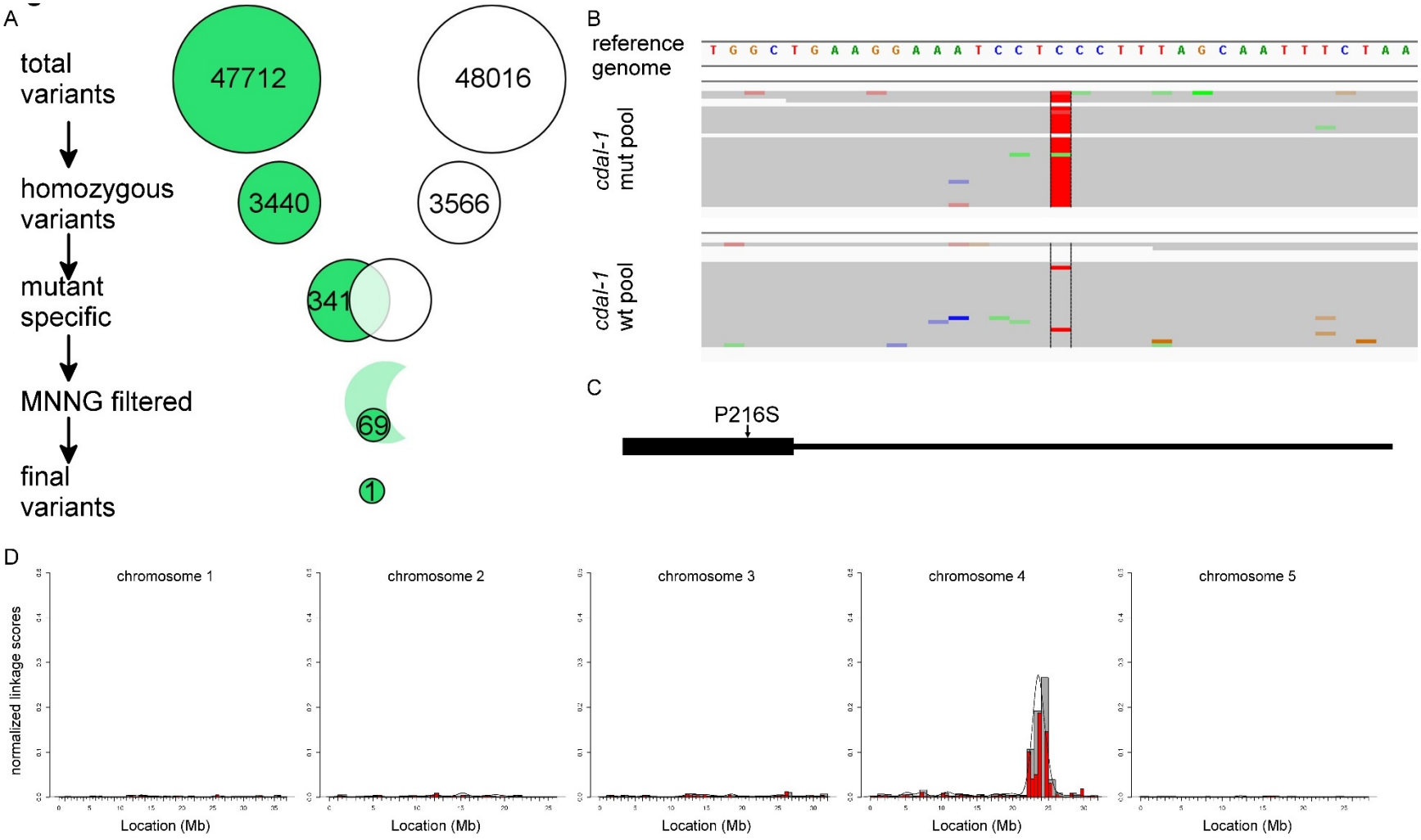
A
total variants
47712
48016
homozygous variants
3440
3566
mutant specific
341
MNNG filtered
69
final variants
1
B
reference genome
T G G C T G A A G G A A A T C C T C C C T T T A G C A A T T T C T A A
cdal-1 mut pool
cdal-1 wt pool
C
P216S
D
normalized linkage scores
chromosome 1
chromosome 2
chromosome 3
chromosome 4
chromosome 5
Location (Mb)

Figure 3.5 A wild-type *TTHERM_00971920* fragment carrying a wild-type codon 216 complements *cdaI-1*. The P216S mutation affects the kinase domain. (A-B) *cdaI-1* cells (A) and *cdaI-1* cells rescued by biolistic transformation with a wild-type TTHERM-00971920 fragment (B), were grown overnight at the restrictive temperature and stained with anti-centrin (green) and DAPI (blue). (C) DNA sequencing chromatograms showing the region of interest within *TTHERM_00971920* ORF (with the mutation site shown in a red box) in the original mutant and a rescue clone. Note the presence of the reference C along with the alternate T base at the position of scf_8254051:142648 in the rescue cells. The presence of both the wild-type and mutant bases is consistent with the anticipated presence of both wild-type and mutant alleles in the rescued cells as is typically the case for a macronuclear transformation. (D-D') Modeled 3D structure of the kinase domain of CdaI in its wild-type (D) and *cdaI-1* (P216S) mutant version (D').

Fig. 3.5

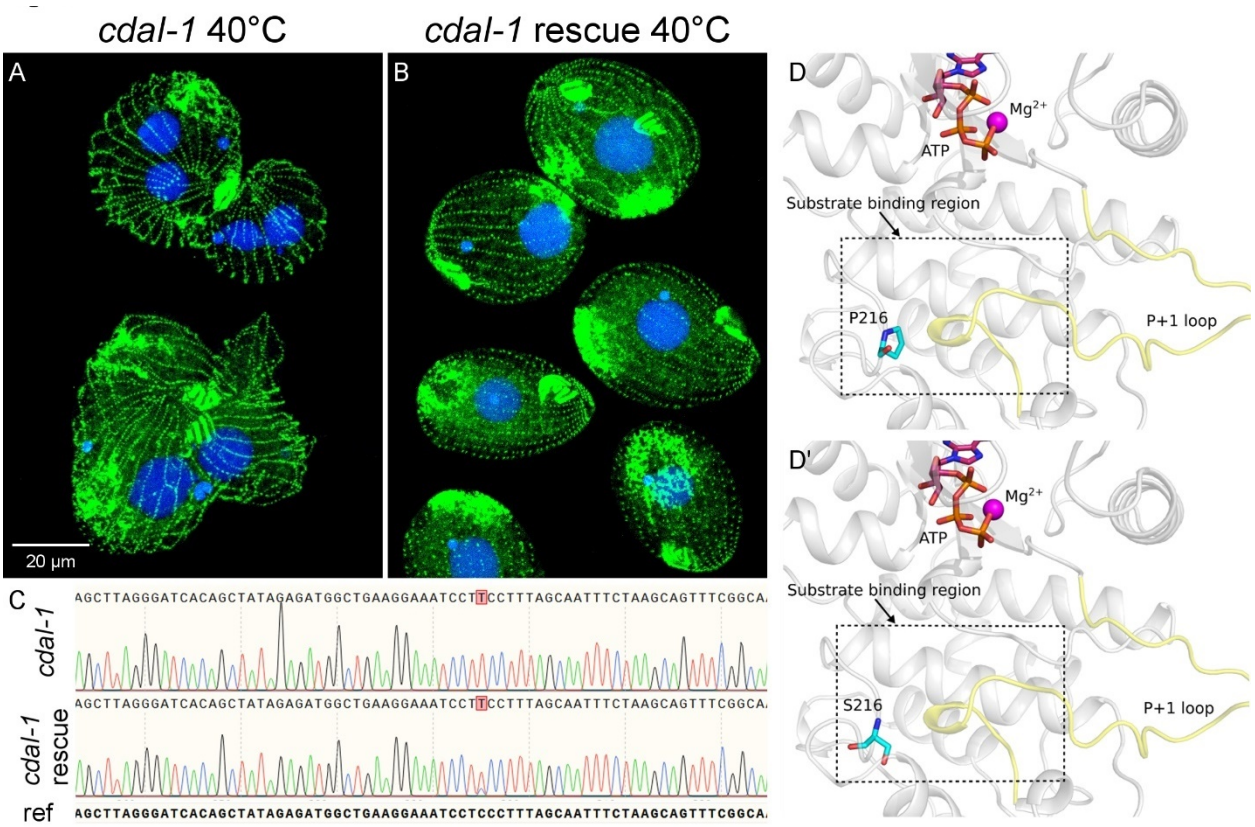
cdal-1 40°C
cdal-1 rescue 40°C
A
B
20 µm
C
cdal-1
cdal-1 rescue
ref
AGCTTAGGGATCACAGCTATAGAGATGGCTGAAGGAAATCCTTCCTTTAGCAATTTCTAAGCAGTTTCGGCA
D
Mg2+
ATP
Substrate binding region
P216
P+1 loop
D'
Mg2+
ATP
Substrate binding region
S216
P+1 loop

Figure 3.6 CdaI is a cortical protein with a polarized and cell cycle-dependent localization and strong association with the division plane. (A-H) Cells that express CdaI-GFP but are otherwise wild-type, were labeled by immunofluorescence with anti-GFP antibodies (red) and co-stained with DAPI (blue). (A) An interphase cell; note the absence of a CdaI-GFP signal above the background (compare to the negative controls in I-J). (B-C) Cells in early cell division with a relatively young oral primordium still lacking well differentiated oral rows (the primordium can be seen based on the background staining). In addition to the anterior subcell bias, CdaI appears stronger along a few ventral rows above the oral primordium especially in the cell shown in B. (D) A cell in an early stage of cortical subdivision (judging by the well-developed oral primordium and the micronucleus in anaphase). CdaI-GFP is strong and uniform along all the ciliary rows of the anterior subcell. (E) A cell with a more advanced cortical subdivision based on the completed mitosis of the micronucleus (this cell has two micronuclei, both have divided, this and other nuclear abnormalities are not uncommon in transgenic strains that are selected with paromomycin). Note the enhancement of CdaI-GFP immediately anterior to the cortical subdivision in the form of short ribbons. (F-G) The same cell in early cytokinesis and early amitosis shown on two sides. Note focusing of CdaI-GFP signal at the posterior border of the anterior subcell. In (G) new CVPs are positive for CdaI-GFP (arrows). (H) A cell in late cytokinesis and late amitosis. The CdaI signal is present mainly at the posterior end of the anterior daughter. (I-J) Negative control wild-type cells lacking the CdaI-GFP transgene and labeled in the same way as the CdaI-GFP expressing cells. Abbreviations: mi, micronucleus; cs, cortical subdivision; ncvp, new CVPs; oa, oral apparatus; noa, new oral apparatus. In D-H the arrowheads point at the speckles of CdaI-GFP at the extreme posterior end of the cell that likely correspond to the preexisting Mob1 (see Fig. 3.1 and Discussion).

Fig. 3.6

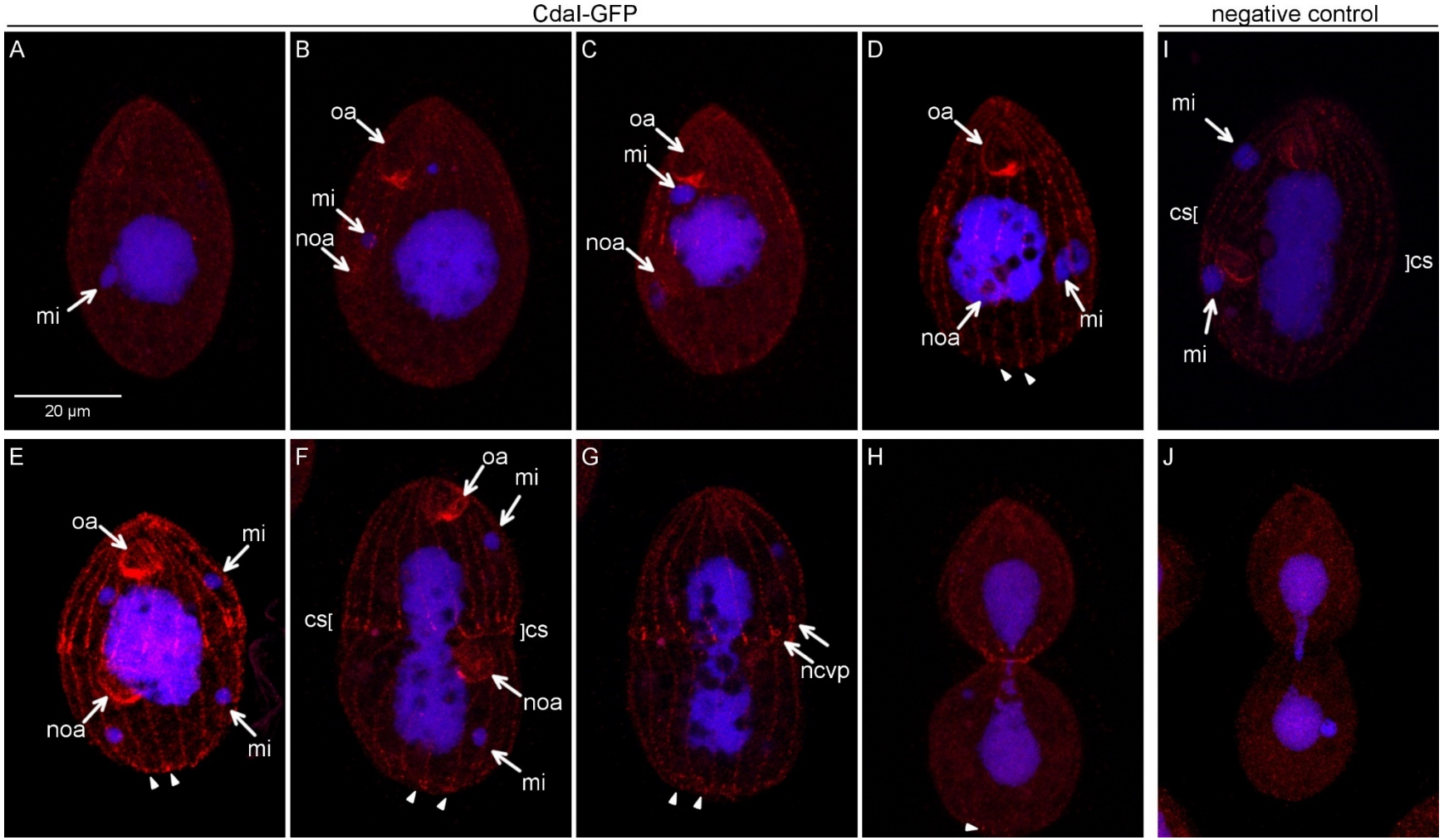
CdaI-GFP
negative control
A
B
C
D
I
E
F
G
H
J
mi
oa
noa
cs[
]cs
ncvp
20 µm

Figure 3.7 The CdaI pattern changes during cortical subdivision and cytokinesis. Cells expressing CdaI-GFP were labeled with anti-GFP antibodies (red, A-E), and anti-centrin (green, A'-E'). Insets show magnified fragments of merged images. (A-B') Cells in an early stage of cell division with a young oral primordium, with the cell in A-A' in an earlier stage as compared to the cell in B-B'. In A-A' a weak cortical CdaI-GFP is present in the anterior cell's half. Arrowheads show the posterior ends of the lines of CdaI-GFP. (C-C') A cell in an early stage of cortical subdivision. Note the presence of the CdaI-GFP mostly on the anterior side of the cortical subdivision (insets). (D-D') A cell in early cytokinesis. CdaI-GFP marks strongly the posterior ends of the ciliary rows (of the anterior subcell) and interconnects the rows above the cortical subdivision. (E-E') A cell in advanced cytokinesis. CdaI-GFP marks the posterior ends of ciliary rows of the anterior subcell. In B and D, the arrowheads mark the speckles of CdaI-GFP at the extreme posterior end. Abbreviations: oa, old oral apparatus; noa, new oral apparatus.

Fig. 3.7

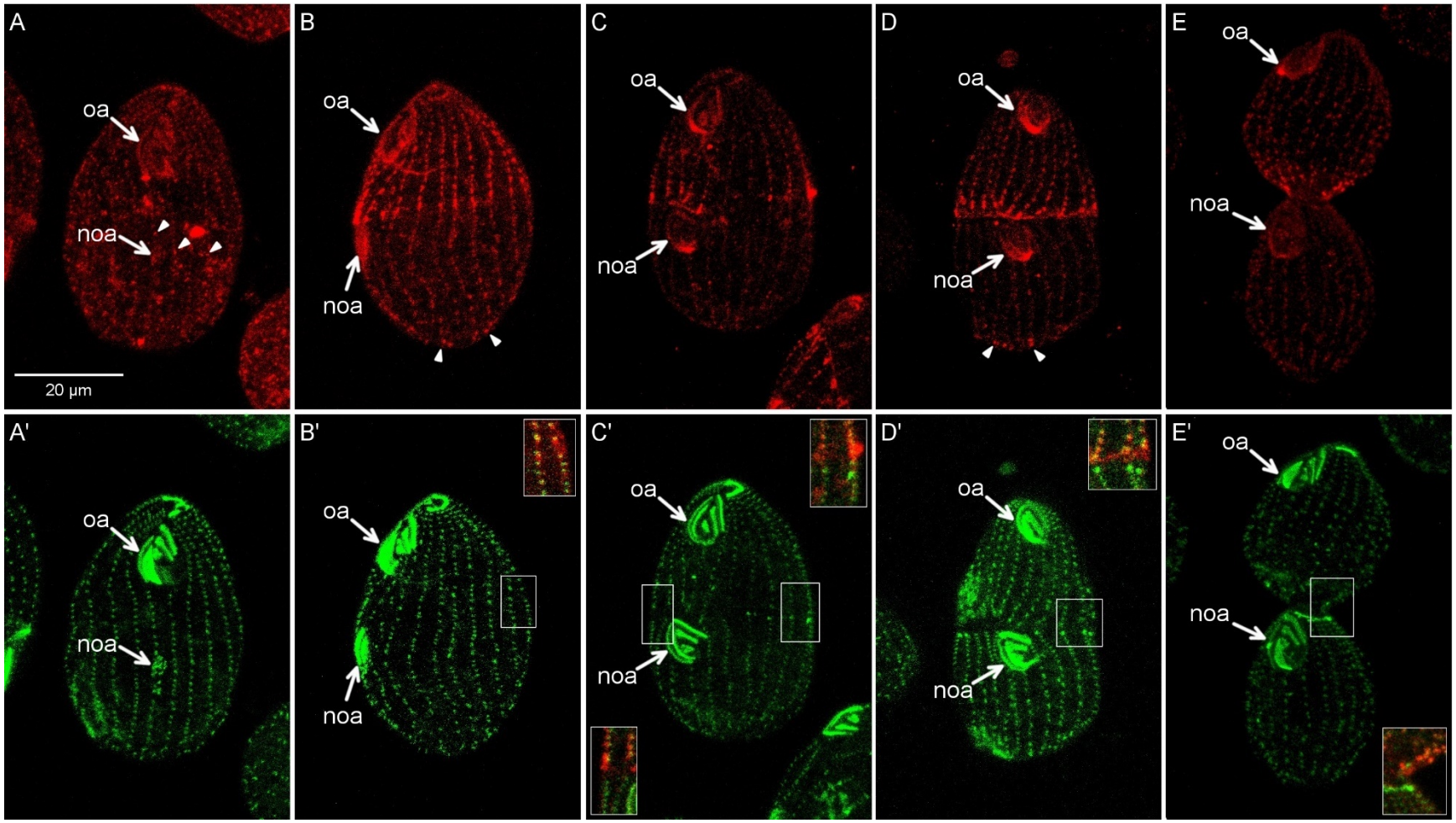

Figure 3.8 The posterior boundary of CdaI is influenced by *ELO1*. CdaI was tagged with a C-terminal GFP and expressed under the native promoter in the cell division mutant *elo1-1* grown at the standard temperature 30^{o}C. Cells were labeled to detect CdaI-GFP (red shown in A-E), centrin (green in A'-E') and DNA with DAPI (blue in A'-E'). (A-A') A cell in an early stage of cell division. Note that the very young primordium assembles at an excessively posterior position. A weak signal of CdaI-GFP is present, stronger in the area immediately above the new oral apparatus. Arrowheads mark the ends of the weak CdaI-GFP lines. (B-B') A cell with a more advanced oral primordium but before the cortical subdivision. The pattern of CdaI-GFP is essentially the same as in the wild type at the similar stage (see Fig. 3.7B-B') except that the posterior boundary of CdaI-GFP is shifted in compliance with the more posterior position of the oral primordium. (C-D') *elo1-1* cells with a cortical subdivision. Note that the posterior shift of the edge of CdaI-GFP is prominent in the oral sector but progressively less apparent in the rows positioned away from the oral sector, and the positions of the ends of CdaI-GFP lines appear normal (equatorial) at the extreme dorsal side. This gives a slant to the edge of the CdaI-GFP lines (compare to Fig. 3.7C, D). (E-E') *elo1-1* mutant in cytokinesis. Note an excessively small size of the posterior daughter. In C-E the arrowheads point to the speckles of CdaI-GFP at the extreme posterior end that may represent CdaI-GFP bound to the old Mob1 (see the Discussion). Abbreviations: cs, cortical subdivision; oa, oral apparatus; noa, new oral apparatus; mi, micronucleus.

Fig. 3.8

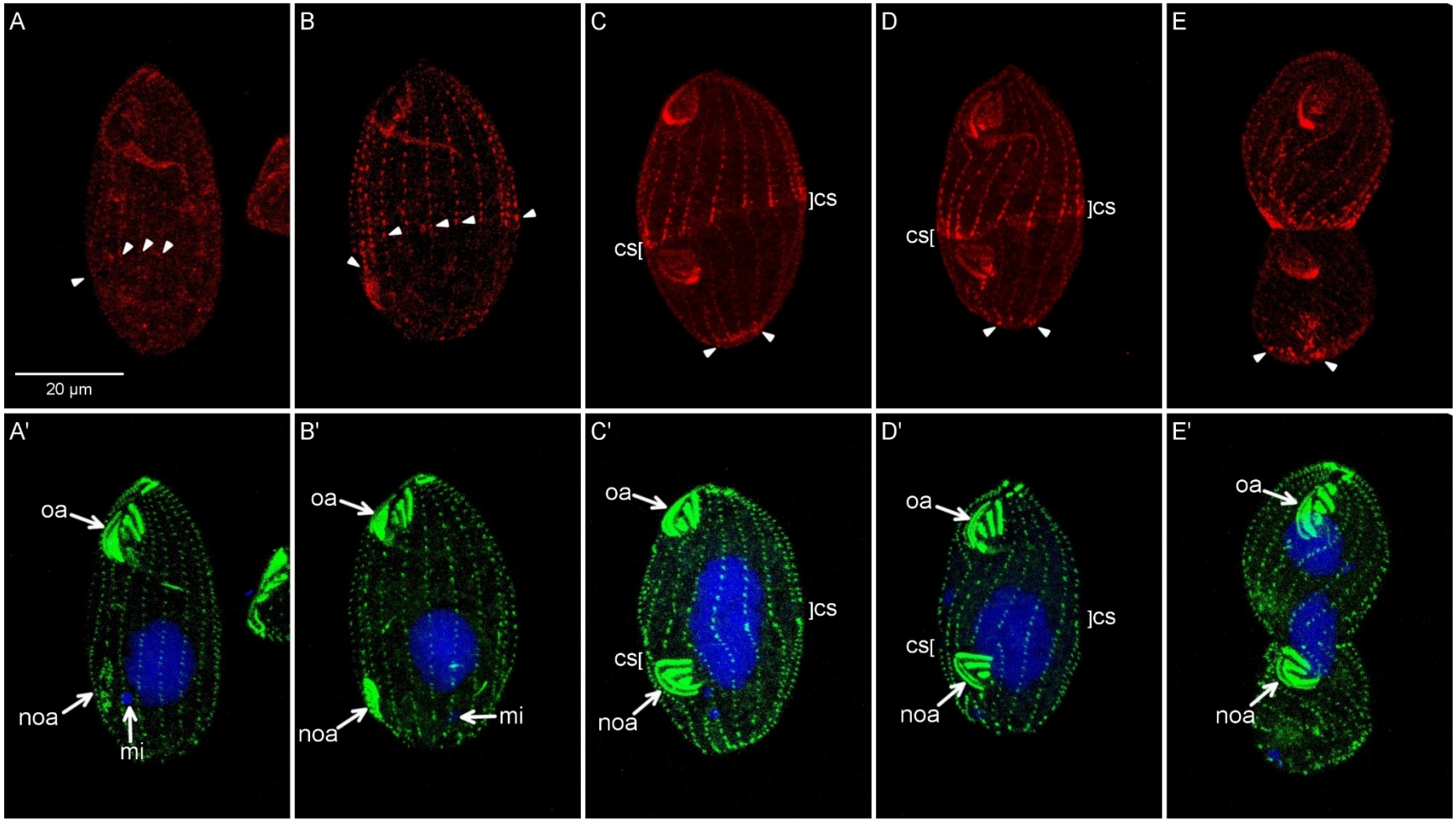
A
B
C
D
E
20 µm
]cs
cs[
]cs
cs[
A'
B'
C'
D'
E'
oa
noa
mi
oa
noa
mi
oa
]cs
cs[
noa
oa
]cs
cs[
noa
oa
noa

Figure 3.9 New CVPs form in the anterior daughter but their locations are disturbed when cytokinesis fails due to CdaI deficiency. (A-K) *cdaI-1* cells grown at the permissive 30^{o}C (A-D) or restrictive (39^{o}C) temperature (E-K) for 5 hr, and labeled with 6-11 B-1 anti-acetyl-K40 α-tubulin (green) and DAPI (blue). Arrowheads show old CVPs and arrowheads/asterisks show new (assembling) CVPs. (A) An interphase cell. (B) A cell shortly before the cortical subdivision. Note that the old CVPs are present but the new ones that will appear along the same meridians are not visible yet. (C) A cell in early cytokinesis. The old and new CVPs are present. (D) A cell in late cytokinesis. The old and new CVPs are present. (E-E') The same hammerhead cell (seen on two sides) in which the posterior subcell has entered the second cell cycle (since the temperature shift) based on the presence of two micronuclei in anaphase. The anterior subcell has failed to separate and receive progeny nuclei. In the anterior subcell, a pair of new CVPs are present on the side of the old oral apparatus. (F-F') The same hammerhead cell (seen on two sides) in which the anterior subcell has failed to separate and receive a nucleus. Note a new CVP present in the anterior subcell above the old oral apparatus. (G-K) Cells that are derived from the anterior subcells of mutants that have managed to separate, despite severe defects in the nuclear divisions (lacking macronuclei). Note the presence of new CVPs at the roughly correct posterior positions.

Fig. 3.9

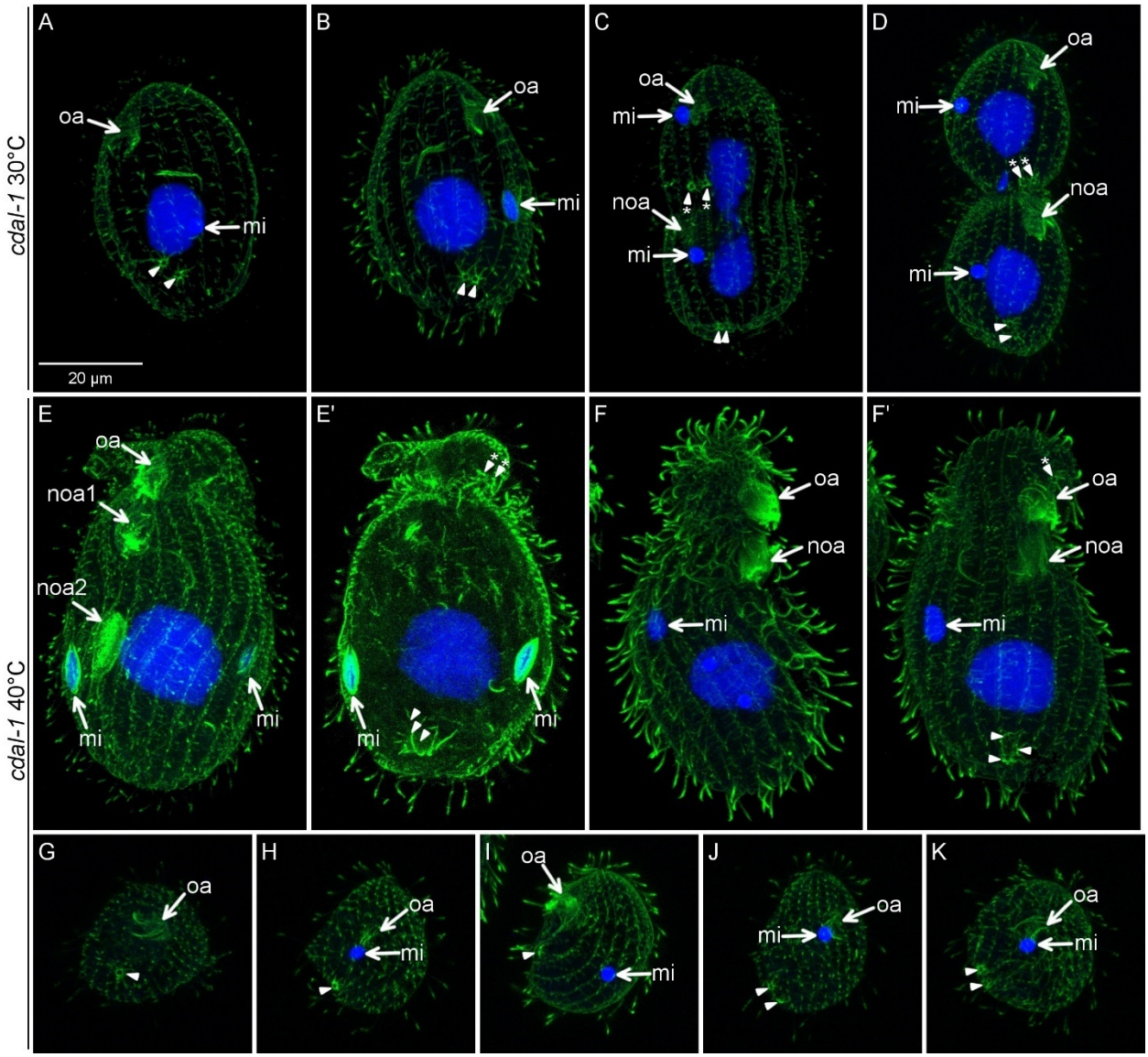

CHAPTER 5

CONCLUSIONS

This dissertation explores the principles of scaling inside the cell at two levels of organization: organelle size (length) and scaling of the entire cell when it divides. *Tetrahymena thermophila* is used as this model provides a wealth of general advantages such as a simple culture and availability of both forward and reverse genetic approaches. The cilia length regulation in *Tetrahymena* represents a case of an unusual scaling mechanism that was not investigated in other models. While in *Chlamydomonas* a mechanism operates to equalize the length of cilia across the cell, in *Tetrahymena* the length of cilia is organelle-type and position-dependent (Wloga et al., 2006). Specifically, the oral cilia are shorter than the locomotory cilia and among the locomotory cilia those near the anterior end are shorter than those in the posterior end. In the context of studies on intracellular scaling, *Tetrahymena* provides a unique opportunity for exploration of the intracellular geometries at an unusually high level of resolution. *Tetrahymena* maintains a sophisticated cortical pattern formed by hundreds of microtubule-rich organelles that are anchored to the cell surface. The cell has easily identifiable anteroposterior and circumferential polarities. The oral apparatus is the marker of the anterior and ventral region while the contractile vacuole pores and the cytoproct are located near the posterior end (Frankel et al., 1981).

In the course of this thesis I improved the tools for both live imaging and genetic analyses of *Tetrahymena*. While I have taken steps toward understanding of the mechanisms of intracellular scaling at two levels of organization (cilia length and scaling during cell division), my

contributions to the methodology could have even more lasting impacts. The TIRF-based live imaging capacity that I helped to develop in collaboration with Karl Lechtreck has already facilitated research in *Tetrahymena* and contributed to improved understanding of cilia biology (Vasudevan et al., 2015a; Vasudevan et al., 2015b). One of the major successes of this thesis is an identification of the first genetic interactor in *Tetrahymena*. While genetic interactor screens have been used extensively in more established genetic models such as *S. cerevisiae, Drosophila* and *C. elegans*, *Tetrahymena* is a newcomer to the elite club of model organisms that offer forward genetics tools. In fact only recently, in 2014, Galati and colleagues published the first successful identification of a causal mutation in *Tetrahymena* using a forward genetics approach based on the new generation sequencing (Galati et al., 2014). The forward genetics pipeline developed here (see Chapter 3 and 4) offers a powerful unbiased strategy for investigations of mechanisms that are difficult to explore in other genetic models including aspects of intracellular scaling. Taken together, the two techniques newly developed here have improved and will continue to improve the utility of *Tetrahymena* as a model organism.

Regarding the cilia length project, I focused on the LF4 kinase, an established negative regulator of cilium length (Berman et al., 2003). Using the novel utility of live imaging of IFT motility based on TIRF microscopy, I found that LF4 inhibits IFT by decreasing the velocities of IFT trains. For the first time in any model, I performed imaging of LF4 in live cells under conditions of expression as close to native as possible (with LF4 expressed under its own promoter). This imaging revealed that LF4 is present inside cilia and that it is distributed evenly along the entire cilium length. Moreover, I found that LF4 is mostly immobile and that an overproduced LF4 showed a microtubule-binding activity. These observations suggest that LF4 is mostly bound to the axoneme and a small pool of LF4 travels with IFT trains. It is therefore

possible that the LF4-axoneme association is important for LF4 activity. A longer cilium would have more LF4 loaded onto its axoneme, hence more inhibition of IFT. This led me to propose a "time-of-flight" model in which LF4 that is distributed along the axoneme stochastically inhibits IFT, therefore autonomously adjusts the rate of assembly of cilia according to the current axoneme length.

One prediction of this model is that longer cilia should have a less active IFT. While I observed that IFT trains are slower in shorter cilia that overproduce LF4 (and faster in longer cilia that lack LF4), in mammalian cells, knockdown of MOK results in elongated cilia but IFT velocity does not significantly change in either knockdown or overexpression of MOK (Broekhuis et al., 2014), suggesting that the change in cilia length is not necessarily directly associated with change of IFT velocity. Furthermore, this prediction is opposed by an observation in *Chlamydomonas* the longer (fully assembled) cilia have faster IFT trains as compared to shorter (assembling) cilia (Engel et al., 2009a; Engel et al., 2009b). The increased assembly rate due to lack of LF4 in *Chlamydomonas* and *Tetrahymena* argues against the possibility that LF4 activity is only prevalent after cilia reach full length (Hilton et al., 2013; Ludington et al., 2013). Therefore, we cannot rule out that the change of IFT velocity may be an indirect consequence of LF4 activity that changes cilia length. It is also unlikely that LF4 acts to encourage premature release of IFT cargo, as no evidence supports that such premature cargo drops occur with increased frequency in longer cilia. What is well established is that in *Chlamydomonas* the IFT trains carry less cargo in longer cilia (Craft et al., 2015; Engel et al., 2009b; Wren et al., 2013) and the size of IFT trains is increased in *lf4* mutant (Ludington et al., 2013). Our data also points to an alternative possibility that LF4 acts at the cargo loading step. Though this activity occurs at the ciliary base, it makes sense to assume that the ciliary presence

of LF4 is important for its activity. One possibility is that the axoneme-distributed LF4 acts to log the travel time of IFT, and affects (perhaps less directly) the ability of IFT components to load the cargo when the trains return from the cilium to the base. Namely, perhaps LF4 phosphorylates an IFT component during its anterograde and/or retrograde run inside the cilium but this phosphorylation is inconsequential until the IFT train returns to the ciliary base, where such a phosphorylated component of IFT would have reduced ability to support cargo loading. Recent study of IFT proteins in *Chlamydomonas* suggests a semi-open system where IFT proteins, in particular IFT-B proteins, exiting cilia (by retrograde IFT) are at least partially recycled into the IFT protein pool at the basal body (unpublished data from Karl Lechtreck). One interesting speculation is that the phosphorylation by cilia length kinases such as LF4 on some IFT-B proteins are the readout of cilia length that when returned to the basal body, communicates the length information within the ciliary unit, causing change in anterograde IFT cargo loading, as well as to the cytoplasm as reporter so that the length of multiple ciliary units in the cell can be coordinated, such as in the "long-short" experiment in *Chlamydomonas* or in different subtypes of cilia in *Tetrahymena*. Ultimately, further exploration of the underlying mechanisms of LF4 regulating IFT activity and cilia length requires the identification of its cilia shortening substrate, which will inform which aspect of the cilia biology (i.e. IFT activity, axoneme stability, microtubule PTMs or else) is affected.

Seeking to uncover the LF4 kinase substrate specificity, I developed a novel hypermorphic allele-based genetic interactor screen, reasoning that a mutation or a loss of the key phosphorylation substrate (that shortens the cilium in response to its phosphorylation by LF4) may reverse the inhibitory effect of overproduced LF4 on IFT and cilia length. In the screen (Chapter 3) I uncovered a number of intragenic suppressors that all carried mutations in the

kinase domain of LF4. In the future, isolation of additional intragenic suppressors could shed light on the function of the non-kinase parts of LF4. In particular, it would be of interest to address whether any non-kinase domain mutations affect the microtubule-binding activity of LF4 and whether microtubule binding is important for LF4 function as a length regulator. I also identified a single extragenic suppression of LF4 gain of function as a mutation in DYF18, a kinase orthologous to the known and conserved cilia length kinases LF2/CCRK/DYF-18. My data suggests that DYF18 increases the LF4 abundance in cilia. The data complement the existing evidence that LF2/CCRK/DYF-18 is an upstream activator of the LF4/MOK kinase activity. All these data taken together suggest that LF4/MOK is both activated and stabilized against degradation by LF2/CCRK/DYF-18. It is intriguing that the screen yielded an apparent upstream regulator of LF4 even though theoretically downstream components in relation to LF4 were anticipated. This brings hope that in the future, among the suppressions there could be mutations that affect additional steps upstream of LF4 including parts of the hypothetical sensor of cilium length. The screen is not saturated and additional extragenic suppressor clones may carry mutations in the components that are downstream of LF4 including its phosphorylation substrates. Finding the key substrate of LF4 kinase remains the highest priority as this could provide a conceptual bridge that explains how LF4 modulates the ciliary assembly pathway to shorten the cilium. As discussed in Chapter 3, others have explored kinesin-2 motor chains and more precisely phosphosites near the C-terminal end of the motor. Kinesin-2 is a logical candidate for being the main target of LF4. A recent study showed that a kinase related to LF4, ICK, phosphorylates a site on the tail of kinesin-2. However, this phosphosite alone is not important and mutating multiple phosphosites on the same kinesin-2 motor subunit (KIF3A) blocks ciliary assembly, a result opposite to the expected cilium shortening activity of this

phosphorylation (Chaya et al., 2014). Another study showed in *Chlamydomonas* another kinase, CDPK1, phosphorylates a similar motif on kinesin-2 motor tail (Liang et al., 2014). However, the loss of CDPK1 results in shorter cilia. In the same study a mutation of the phosphosite serine to alanine (S663A) on the kinesin-2 motor made cilia shorter phenocopying the loss of the kinase CDPK1. On the other side, a phospho-mimicking mutation (S663D) led to a complete loss of flagella, a result that is consistent with phosphorylation acting as an inhibitor of kinesin-2 and indirectly an inhibitor of the anterograde IFT. Additional data in the same paper led to a model that phosphorylation of kinesin-2 by CDPK1 occurs at the ciliary tip and is needed for the dissociation of kinesin-2 from the IFT particles that allows for their return to the cell body via retrograde IFT. It is fair to say that the question of whether the cilium length kinases such as LF4 or more broadly the RCK members shorten cilia by phosphorylating kinesin-2 and downregulating some aspect of IFT remains unanswered. We have fully validated our LF4 gain-of-function suppressor screen by isolating both intragenic suppressors (in LF4 itself) and an extragenic suppressor and likely upstream regulator of LF4, LF2/CCRK/DYF-18. The screen can be easily scaled up and additional extragenic suppressors could identify new components of the LF2-LF4 pathway including the long sought phosphorylation substrates of LF4.

This dissertation initiated the investigation on the activation mechanism of LF2/CCRK/DYF-18-LF4/MOK pathway. This pathway may be the important hub of the long sought-after cilia length feedback network that communicates throughout the cell for (relatively) equal and constant cilia length while also allowing autonomous regulation of cilia length of different cilia types. This is an important issue as cilia length has been implicated as a regulatory factor of cell cycle progress that has relevance to cancer (Dutta and Avasthi, 2017; Izawa et al., 2015; Keeling et al., 2016; Kim et al., 2015; Maskey et al., 2015; Wang et al., 2014; Zhang and Mitchell, 2015).

Understanding the cilia length regulation in multicellular organisms with multiple types of cilia has been challenging as the phenotypic outcome may subject to various limitations such as experimental difficulties, tissue-specific expression and development. As demonstrated in this dissertation, unicellular ciliates including *Tetrahymena* have conserved and comparable cilia length regulation mechanisms and are more advantageous for studying cilia biology. Furthermore, studying the sizing of cilia might further reveal how the organelle size can be controlled at a global level while their functionality may still be programmed to diverge at certain temporal and spatial conditions.

This dissertation also explored the mechanism of whole cell scaling during cell division. Ciliates such as *Tetrahymena* offers a unique perspective on the connection between scaling during cell division and cell polarity, owned to the intricate cortical pattern and the anteroposterior and circumferential axes. Mutational studies in *Tetrahymena* have identified intracellular pattern mutants in which either the overall organization of the cell cortex is altered and/or the division plane is misplaced resulting in unequal cell division (Cole and Frankel, 1991; Cole et al., 1988; Frankel et al., 1993; Frankel and Nelsen, 1986; Frankel et al., 1984). Identification of the responsible mutations will provide more insight regarding the intracellular pattern formation as well as scaling.

In Chapter 4 I studied a cell division mutant of *Tetrahymena*, *cdaI-1*. This mutant was isolated by Joseph Frankel (University of Iowa) in a screen for conditional mutants that fail to divide properly at higher temperature (Frankel et al., 1976). I identified the causal mutation for *cdaI-1* in an ortholog of the Hippo/Mst kinase. CdaI is a cell division-specific protein that shows a highly polarized localization pattern. First, CdaI localizes to the anterior half of the dividing cell and later it condenses along the anterior side of the division plane, marking the posterior end of

the anterior daughter. We propose that CdaI phosphorylates Mob1, based on how the Hippo pathway works in other species (reviewed in (Meng et al., 2016)) as well as based on the remarkable similarity of the phenotype of *cdaI-1* and a knockdown of Mob1, in both cases the affected cells arrest with an anterior displacement of the division plane (Chapter 4 and (Tavares et al., 2012)). Based on the extensive studies of the Hippo pathway, primarily in budding and fission yeast, the only function of Hippo/Mst is likely to activate Mob1 so that its partner kinase, Lats, can be activated (Gogl et al., 2015).

Mob1 knockdown phenotypes were described for *Tetrahymena*, as well as another ciliate, Stentor (Slabodnick et al., 2014; Tavares et al., 2012). Based on the analysis of Mob1, Tavares et al proposed that Mob1 is "a key factor for the establishment of intrinsic cell polarity" (Tavares et al., 2012). Furthermore, Slabodnick et al concluded that in Stentor Mob1 "acts as a patterning protein" (Slabodnick et al., 2014). These statements implicate the Hippo pathway in the establishment of cell polarity and pattern formation in ciliates. Our own analysis of the localization and function of CdaI, the Hippo/Mst kinase, leads to a different view of the role of the Hippo pathway in ciliates. Our data indicate that the Hippo pathway may act mainly in scaling the daughter cells by keeping the division plane at the mother cell's equator. This conclusion is based on careful observations of the timing of when the first defects appear in the cell cycle of the *cdaI-1* mutant. The first sign of the incoming cell division is the formation of the new oral apparatus at the sub-medial-ventral position and this step is unaffected in *cdaI-1*. Furthermore, despite the strong presence of CdaI at the posterior end of the emerging anterior daughter cell at late cell division, in cells lacking CdaI, the posterior end-specific organelles, contractile vacuole pores, assemble at normal positions. Our finding shows that a loss of CdaI (likely causing the inactivation of Hippo pathway) does not disrupt at least some aspects of the

cortical pattern formation. We suggest that the other cortical defects observed in both *cdaI-1* mutants as well as in *Tetrahymena* and *Stentor* Mob1 depleted cells, could to large extent be secondary consequences of delayed, incomplete or arrested events of nuclear divisions and cytokinesis (Chapter 4 and (Slabodnick et al., 2014; Tavares et al., 2012)). These results indicate that without CdaI *Tetrahymena* cells have an ability to properly position new organelles along both the anteroposterior and circumferential axes, and the polarity features of both the anterior (small) and likely also posterior daughter (big) are to large extent preserved. Thus, it is unlikely that CdaI is required for the establishment of cell polarity, rather, CdaI must act downstream of unknown mechanisms that establish the anteroposterior and circumferential axes. We further show evidence that ELO1 could be an important upstream component in relation to CdaI. We conclude therefore that CdaI is important for cell scaling by affecting the division plane but it is not a polarity factor itself.

While there is no evidence that CdaI is a patterning or polarity factor besides its role in keeping the division plane at the equator, we are open to a possibility that the entire Hippo pathway has other roles in addition to those controlled by CdaI. This is based on two observations. First, the *Tetrahymena* genome contains three additional Hippo/Mst kinase sequences that are paralogs of CdaI. Second, Tavares et al showed that unlike CdaI that disappears shortly after cell division and is not detectable in interphase, its likely substrate Mob1 persists at the posterior end of interphase cells (see Fig.1 in Chapter 4 and (Tavares et al., 2012)). Thus, Mob1 could be activated by one or more paralogs of CdaI in interphase, and be active in interphase or early cell division without CdaI. At some point in the cell cycle, Mob1 (possibly in a complex with a paralog of CdaI) is present at the posterior end and the cell enters cell division and assembles a new oral apparatus, which is followed by the appearance of the CdaI zone in the

anterior half of the cell. Eventually the activity of CdaI generates a band of new active Mob1 at the new posterior end of the emerging anterior daughter. One could therefore imagine that the old Mob1 controls some aspects of early cell division, even the placement of the new oral apparatus or more broadly the initial position of the division plane. Thus, the old pool of Mob1 in the mother could affect the generation of the new pool of Mob1 in the daughter. This kind of a trans-generational interaction could have broad effects that go beyond scaling of the daughters. A fast-acting conditional mutation of Mob1 could reveal additional functions of Mob1, for example during early cell division, before the appearance of the first marker of cell division, the new oral apparatus. Fast-acting conditional alleles of Mob1 have been isolated in yeast and could inspire reverse genetic manipulations in *Tetrahymena* (Luca et al., 2001; Luca and Winey, 1998).

In the future, in addition to further dissection of the Hippo pathway components based on reverse genetics, it will be important to address further the mechanism of cell polarity and pattern formation in ciliates in an unbiased way. The genetic pipeline established can be applied to identification of causal mutations in mutant clones that are affected in cell polarity or pattern formation. One promising candidate already mentioned is the *elo1-1* mutant in which the cell division plane is shifted to the posterior end starting at an earliest stage of the oral primordium. The *elo1-1* mutant may have a defect in the functionality of the anteroposterior polarity axis. There also are additional mutants that are defective in the circumferential positioning, including hypoangular *hpo1* mutants (Frankel et al., 1993; Frankel and Nelsen, 1986). Work is already under way toward identification of the causal mutations responsible for the defects in *elo1-1* and *hpo1* mutants. It is important to mention that ciliates lack most homologs of polarity proteins that have been studied in other organisms including Par kinases and components of the Wnt pathway (Eisen et al., 2006). Furthermore, in ciliates the polarity cues are primarily cortical and likely do

not originate from the nuclei or the mitotic spindle as to a large extent is the case of animal cells.

Thus, studies in ciliates could lead to discovery of new pathways that generate cell polarity.

Those pathways may be conserved but unrecognized in other species.

REFERENCES

Berman, S.A., N.F. Wilson, N.A. Haas, and P.A. Lefebvre. 2003. A novel MAP kinase regulates flagellar length in Chlamydomonas. *Current biology : CB*. 13:1145-1149.

Broekhuis, J.R., K.J. Verhey, and G. Jansen. 2014. Regulation of Cilium Length and Intraflagellar Transport by the RCK-Kinases ICK and MOK in Renal Epithelial Cells. *PloS one*. 9:e108470.

Chaya, T., Y. Omori, R. Kuwahara, and T. Furukawa. 2014. ICK is essential for cell type-specific ciliogenesis and the regulation of ciliary transport. *The EMBO journal*.

Cole, E.S., and J. Frankel. 1991. Conjugal blocks in Tetrahymena pattern mutants and their cytoplasmic rescue. II. janus A. *Developmental biology*. 148:420-428.

Cole, E.S., J. Frankel, and L.M. Jenkins. 1988. Interactions between janus and bcd cortical pattern mutants in Tetrahymena thermophila : An investigation of intracellular patterning mechanisms using double-mutant analysis. *Roux Arch Dev Biol*. 197:476-489.

Craft, J.M., J.A. Harris, S. Hyman, P. Kner, and K.F. Lechtreck. 2015. Tubulin transport by IFT is upregulated during ciliary growth by a cilium-autonomous mechanism. *The Journal of cell biology*. 208:223-237.

Dutta, S., and P. Avasthi. 2017. Flagellar Synchronization Is a Simple Alternative to Cell Cycle Synchronization for Ciliary and Flagellar Studies. *mSphere*. 2.

Eisen, J.A., R.S. Coyne, M. Wu, D. Wu, M. Thiagarajan, J.R. Wortman, J.H. Badger, Q. Ren, P. Amedeo, K.M. Jones, L.J. Tallon, A.L. Delcher, S.L. Salzberg, J.C. Silva, B.J. Haas, W.H. Majoros, M. Farzad, J.M. Carlton, R.K. Smith, Jr., J. Garg, R.E. Pearlman, K.M. Karrer, L. Sun, G. Manning, N.C. Elde, A.P. Turkewitz, D.J. Asai, D.E. Wilkes, Y. Wang, H. Cai, K. Collins, B.A. Stewart, S.R. Lee, K. Wilamowska, Z. Weinberg, W.L. Ruzzo, D. Wloga, J. Gaertig, J. Frankel, C.C. Tsao, M.A. Gorovsky, P.J. Keeling, R.F. Waller, N.J. Patron, J.M. Cherry, N.A. Stover, C.J. Krieger, C. del Toro, H.F. Ryder, S.C. Williamson, R.A. Barbeau, E.P. Hamilton, and E. Orias. 2006. Macronuclear genome sequence of the ciliate Tetrahymena thermophila, a model eukaryote. *PLoS biology*. 4:e286.

Engel, B.D., K.F. Lechtreck, T. Sakai, M. Ikebe, G.B. Witman, and W.F. Marshall. 2009a. Total internal reflection fluorescence (TIRF) microscopy of Chlamydomonas flagella. *Methods Cell Biol*. 93:157-177.

Engel, B.D., W.B. Ludington, and W.F. Marshall. 2009b. Intraflagellar transport particle size scales inversely with flagellar length: revisiting the balance-point length control model. *The Journal of cell biology*. 187:81-89.

Frankel, J., L.M. Jenkins, F.P. Doerder, and E.M. Nelsen. 1976. Mutations affecting cell division in Tetrahymena pyriformis. I. Selection and genetic analysis. *Genetics*. 83:489-506.

Frankel, J., L.M. Jenkins, E.M. Nelsen, and C.A. Stoltzman. 1993. Hypoangular: a gene potentially involved in specifying positional information in a ciliate, Tetrahymena thermophila. *Developmental biology*. 160:333-354.

Frankel, J., and E.M. Nelsen. 1986. Intracellular pattern reversal in Tetrahymena thermophila. II. Transient expression of a janus phenocopy in balanced doublets. *Developmental biology*. 114:72-86.

Frankel, J., E.M. Nelsen, J. Bakowska, and L.M. Jenkins. 1984. Mutational analysis of patterning of oral structures in Tetrahymena. II. A graded basis for the individuality of intracellular structural arrays. *Journal of embryology and experimental morphology*. 82:67-95.

Frankel, J., E.M. Nelsen, and E. Martel. 1981. Development of the ciliature of Tetrahymena thermophila. II. Spatial subdivision prior to cytokinesis. *Developmental biology*. 88:39-54.

Galati, D.F., S. Bonney, Z. Kronenberg, C. Clarissa, M. Yandell, N.C. Elde, M. Jerka-Dziadosz, T.H. Giddings, J. Frankel, and C.G. Pearson. 2014. DisAp-dependent striated fiber elongation is required to organize ciliary arrays. *The Journal of cell biology*. 207:705-715.

Gogl, G., K.D. Schneider, B.J. Yeh, N. Alam, A.N. Nguyen Ba, A.M. Moses, C. Hetenyi, A. Remenyi, and E.L. Weiss. 2015. The Structure of an NDR/LATS Kinase-Mob Complex Reveals a Novel Kinase-Coactivator System and Substrate Docking Mechanism. *PLoS biology*. 13:e1002146.

Hilton, L.K., K. Gunawardane, J.W. Kim, M.C. Schwarz, and L.M. Quarmby. 2013. The kinases LF4 and CNK2 control ciliary length by feedback regulation of assembly and disassembly rates. *Current biology : CB*. 23:2208-2214.

Izawa, I., H. Goto, K. Kasahara, and M. Inagaki. 2015. Current topics of functional links between primary cilia and cell cycle. *Cilia*. 4:12.

Keeling, J., L. Tsiokas, and D. Maskey. 2016. Cellular Mechanisms of Ciliary Length Control. *Cells*. 5.

Kim, S., K. Lee, J.H. Choi, N. Ringstad, and B.D. Dynlacht. 2015. Nek2 activation of Kif24 ensures cilium disassembly during the cell cycle. *Nature communications*. 6:8087.

Liang, Y., Y. Pang, Q. Wu, Z. Hu, X. Han, Y. Xu, H. Deng, and J. Pan. 2014. FLA8/KIF3B Phosphorylation Regulates Kinesin-II Interaction with IFT-B to Control IFT Entry and Turnaround. *Developmental cell*. 30:585-597.

Luca, F.C., M. Mody, C. Kurischko, D.M. Roof, T.H. Giddings, and M. Winey. 2001. Saccharomyces cerevisiae Mob1p is required for cytokinesis and mitotic exit. *Molecular and cellular biology*. 21:6972-6983.

Luca, F.C., and M. Winey. 1998. MOB1, an essential yeast gene required for completion of mitosis and maintenance of ploidy. *Mol Biol Cell*. 9:29-46.

Ludington, W.B., K.A. Wemmer, K.F. Lechtreck, G.B. Witman, and W.F. Marshall. 2013. Avalanche-like behavior in ciliary import. *Proceedings of the National Academy of Sciences of the United States of America*.

Maskey, D., M.C. Marlin, S. Kim, S. Kim, E.C. Ong, G. Li, and L. Tsiokas. 2015. Cell cycle-dependent ubiquitylation and destruction of NDE1 by CDK5-FBW7 regulates ciliary length. *The EMBO journal*. 34:2424-2440.

Meng, Z., T. Moroishi, and K.L. Guan. 2016. Mechanisms of Hippo pathway regulation. *Genes & development*. 30:1-17.

Slabodnick, M.M., J.G. Ruby, J.G. Dunn, J.L. Feldman, J.L. DeRisi, and W.F. Marshall. 2014. The kinase regulator mob1 acts as a patterning protein for stentor morphogenesis. *PLoS biology*. 12:e1001861.

Tavares, A., J. Goncalves, C. Florindo, A.A. Tavares, and H. Soares. 2012. Mob1: defining cell polarity for proper cell division. *Journal of cell science*. 125:516-527.

Vasudevan, K.K., Y.Y. Jiang, K.F. Lechtreck, Y. Kushida, L.M. Alford, W.S. Sale, T. Hennessey, and J. Gaertig. 2015a. Kinesin-13 regulates the quantity and quality of tubulin inside cilia. *Mol Biol Cell*. 26:478-494.

Vasudevan, K.K., K. Song, L.M. Alford, W.S. Sale, E.E. Dymek, E.F. Smith, T. Hennessey, E. Joachimiak, P. Urbanska, D. Wloga, W. Dentler, D. Nicastro, and J. Gaertig. 2015b. FAP206 is a microtubule-docking adapter for ciliary radial spoke 2 and dynein c. *Mol Biol Cell*. 26:696-710.

Wang, W., T. Wu, and M.W. Kirschner. 2014. The master cell cycle regulator APC-Cdc20 regulates ciliary length and disassembly of the primary cilium. *eLife*. 3:e03083.

Wloga, D., A. Camba, K. Rogowski, G. Manning, M. Jerka-Dziadosz, and J. Gaertig. 2006. Members of the NIMA-related kinase family promote disassembly of cilia by multiple mechanisms. *Molecular biology of the cell*. 17:2799-2810.

Wren, K.N., J.M. Craft, D. Tritschler, A. Schauer, D.K. Patel, E.F. Smith, M.E. Porter, P. Kner, and K.F. Lechtreck. 2013. A differential cargo-loading model of ciliary length regulation by IFT. *Current biology : CB*. 23:2463-2471.

Zhang, S., and B.J. Mitchell. 2015. Centriole biogenesis and function in multiciliated cells. *Methods Cell Biol*. 129:103-127.